UNIVERSITAT POLITÈCNICA DE CATALUNYA
BARCELONATECH
Departament d'Enginyeria Electrònica

Radiated Transient Interferences
in Digital Communication Systems

Author
Marc Pous Solà

Director
Ferran Silva Martínez

Thesis submitted in partial fulfillment of the requirement for the PhD Degree issued by the Universitat Politècnica de Catalunya, in its Electronic Engineering Program.

March 2015

"It doesn't matter how beautiful your theory is, it doesn't matter how smart you are. If it doesn't agree with experiment, it's wrong."

Richard P. Feynman

Abstract

In the Electromagnetic Compatibility research area, an unsolved interference problem is the measurement and evaluation of the distortion produced by radiated transient disturbances on digital communication systems. Measuring this type of man-made impulsive noise is exceptionally challenging due to its random and broadband intrinsic characteristics. With the aim of protecting sensitive communication receivers, measurements beyond EMC standards must be meticulously defined and carried out.

In this thesis, novel acquisition procedures are developed to overcome the limitations of the current EMC standards, allowing us to obtain the time-domain and the statistical information of the impulsive noise. Furthermore, combining transient interference measurements with digital communication analysis methodologies, we can predict with an excellent confidence level the bit-error-probability suffered by any digital communication system. Throughout all the thesis an exhaustive validation is performed capturing different types of radiated interferences and evaluating its impact on different communication systems such as RFID or GSM.

Acknowledgements

The acknowledgements are written in the native language of the author (in Catalan).

Agraïments

Finalment puc fer els agraïments, cosa que em fa especialment feliç perquè vol dir que ja he acabat la tesi. Per fi deixaré de tenir aquest pes damunt meu, i més d'un i d'una s'alegrarà de no haver-me d'escoltar parlant de la tesi. Sobretot tots aquells a qui el tema de la tesi els sona més estrany que el xinès i que posen els ulls en blanc i bufen quan senten a parlar de transitoris radiats, soroll impulsiu, interferències, ones electromagnètiques, i tots aquests termes tan apassionants. Encara que sembli un tòpic, és molt agradable asseure's a escriure aquestes poques línies per agrair a totes les persones que m'han ajudat des de molts i diversos punts de vista al llarg de tots aquests anys.

En primer lloc, vull agrair molt sincerament el suport tant tècnic com personal del meu cap i director de tesi, el Ferran. Al Ferran li agraeixo els consells i la perspectiva que em transmet a l'hora d'encarar la compatibilitat electromagnètica. Sempre és capaç de plasmar en un paper amb uns quants gargots un full de ruta per resoldre un problema d'EMC, que són implícitament complicats d'afrontar. A més a més, gràcies al GCEM, del qual ell és el director, he pogut tenir els recursos necessaris per fer la meva recerca, assistir a congressos i participar en projectes de recerca internacionals durant tots aquests anys. D'altra banda, també li vull donar el meu agraïment a la Mireya, que ha deixat que no m'allunyés de la compatibilitat

electromagnètica i m'ha donat temps per poder dedicar a la tesi doctoral, sobretot quan estava lligat a altres projectes d'investigació. També aprofito per donar les gràcies al Marcos Quílez, que va ser la persona que em va explicar què era això de la compatibilitat electromagnètica per primera vegada i, és clar, si no m'hagués transmès l'interès per l'EMC ara fa més d'una dècada mai hauria acabat fent aquest doctorat.

També m'agradaria agrair profundament el seu suport als meus companys del GCEM. Als meus companys i sobretot amics, l'Andreu, el Marc i el Ricardo. Tot i que el Ricardo va marxar fa un temps encara el considerem un dels nostres i el posem al mateix sac, només li falta parlar català. Des que vaig entrar al GCEM el desembre del 2008 hem compartit esmorzars, sopars amb les parelles, viatges, aniversaris de 30 anys (ja us queden lluny), el meu comiat de solter i, és clar, també discussions referents a la tesi. Intentant tirar les meves teories per terra o parlant de com de bé estan els resultats obtinguts o que aquests no serveixen per a res o que els resultats no s'assemblen una... En fi, l'únic que sé del cert és que treballant amb vosaltres afrontar la tesi ha estat més fàcil i motivador. Aprofito per agrair també als becaris i exbecaris del GCEM la seva companyia i el seu suport. En especial al Víctor i al Rubén, tot i que aquest últim sigui del Madrid. Amb el Víctor i el Rubén hem passat també molt bones estones i espero que mantinguem el contacte, ja que encara estan dins del món de la compatibilitat electromagnètica. No vull oblidar-me d'altres becaris, com el Lluís, l'Oriol, els Gerards o la Irene. Per últim, també recordar-me del Marco, tot i que fa poc temps que és al GCEM fent la tesi, ja hem pogut tenir converses molt interessants d'EMC.

Les persones a les quals vull estar agraït a la universitat no s'acaben al GCEM. Al laboratori de la tercera planta he tingut la sort de conviure amb l'Alfonso, el Benja i el Fede. L'Alfonso sempre ha estat disponible quan l'he necessitat, ja sigui per ajudar-me amb algun tema de hardware, arreglar-me alguna destrossa que hagi pogut fer al PC o parlar del Barça. El Benja sense dubte ha estat un amic al laboratori amb qui, a més a més, he pogut parlar i discutir moltes vegades sobre com fer mesures.

La realització de la tesi m'ha permès també conèixer altres persones fora de la universitat amb les quals he pogut parlar i aprendre, per tal d'aplicar els coneixements adquirits als objectius de la tesi. M'agradaria destacar l'Iñigo, que em va oferir la possibilitat de participar en un projecte de recerca estretament relacionat amb l'objectiu de la meva tesi. També voldria afegir el meu agraïment a la Kia

Wiklundh i al Peter Stenumgaard, que van venir des de Suècia interessant-se pel treball realitzat a la tesi, i amb els quals he tingut unes quantes xerrades molt interessants sobre interferències i sistemes de comunicació digitals.

Més enllà de la gent relacionada estrictament amb l'entorn laboral, vull tenir un record en primer lloc pels meus amics, l'Alberto José, l'Anna, el David, el Ferran, el Jose, la Meri, etc. Tinc la sort que uns quants dels meus amics de tota la vida també són enginyers de telecos. Com el Xavi, amb qui ens vam conèixer abans de tenir ús de raó i encara ens seguim veient gairebé cada setmana i aprofitem per parlar de com interferir o analitzar sistemes RFID o, com dirien l'Anna i l'Eli, de coses friquis.

Vull aprofitar també per donar-los moltes gràcies als meus pares per tot el seu suport, no només aquests darrers anys de la tesi, sinó al llarg de tota la vida. És una obvietat però s'ha de dir, sense la vostra ajuda mai hagués estat possible arribar fins aquí. Sempre heu tingut un grau d'interès i d'implicació molt alt amb tot el que ha envoltat la meva vida i, com és natural, també amb la tesi. És més, fins i tot el meu pare em va ajudar amb la fotografia de la portada de la tesi. Gràcies també a la meva germana, l'Ariadna. Sempre s'ha mostrat disposada a ajudar-me, tot i que cada vegada que li insinuo que m'hauria de donar un cop de mà amb alguna cosa de la feina en temes lingüístics posa una certa cara de pànic. Moltes gràcies per estar sempre al meu costat, nena!

I és clar, sobretot gràcies a l'única família que he pogut triar, els altres familiars et toquen amb més o menys desgràcia. Moltes gràcies a la meva dona, l'Eli, gràcies de tot cor i per molts i molts motius. Per on començar... m'imagino que ha de ser difícil conviure amb mi, i més si la tesi doctoral està pel mig. La pobra ha hagut d'aguantar els meus maldecaps per la tesi, fer-me dinars i sopars els dies que estava abduït per la feina o aguantar les xerrades amb els friquis de l'EMC. És més, et vas oferir voluntària a llegir-te tota la tesi per revisar l'anglès... sense dubte això és una incomparable demostració d'amor i sobretot de paciència... t'has guanyat el cel!! Així que moltes gràcies per compartir la teva vida amb mi, princess, amb tu tot és molt més fàcil i millor.

Per últim, moltes gràcies a tots, incloent els amics i familiars que no he anomenat. Una abraçada molt i molt forta!

Marc Pous i Solà

Contents

List of Figures

List of Tables

Abbreviations

AC	**A**lternating **C**urrent
ADM	**A**mplitude **D**ifference **M**easure
APD	**A**mplitude **P**robability **D**istribution
AWGN	**A**dditive **W**hite **G**aussian **N**oise
BBC	**B**ritish **B**roadcasting **C**orporation
BEP	**B**it **E**rror **P**robability
BER	**B**it **E**rror **R**ate
BPSK	**B**inary **P**hase-**S**hift **K**eying
BTM	**B**alise **T**ransmission **M**odule
BTS	**B**ase **T**ransceiver **S**tation
CAD	**C**omputer-**A**ided **D**esign
CCDF	**C**omplementary **C**umulative **D**istribution **F**unction
CDF	**C**umulative **D**istribution **F**unction
CDMA	**C**ode **D**ivision **M**ultiple **A**ccess
CISPR	**C**omité **I**nternational **S**pécial des **P**erturbations **R**adioélectriques
CRC	**C**yclic **R**edundancy **C**ode
DAB	**D**igital **A**udio **B**roadcasting
DC	**D**irect **C**urrent
DCS	**D**igital **C**ommunication **S**ystem
DFT	**D**iscrete **F**ourier **T**ransform
DTT	**D**igital **T**elevision **T**errestrial
DVB	**D**igital **V**ideo **B**roadcasting

DVB-T	**D**igital **V**ideo **B**roadcasting-**T**errestrial
EM	**E**lectro**M**agnetic
EMC	**E**lectro**M**agnetic **C**ompatibility
EMI	**E**lectro**M**agnetic **I**nterference
ESD	**E**lectro-**S**tatic **D**ischarge
ETSI	**E**uropean **T**elecommunications **S**tandard **I**nstitute
EUT	**E**quipment **U**nder **T**est
FDM	**F**eature **D**ifference **M**easure
FDMA	**F**requency **D**ivision **M**ultiple **A**ccess
FDTD	**F**inite **D**ifference **T**ime **D**omain
FFT	**F**ast **F**ourier **T**ransform
FSK	**F**requency **S**hift **K**eying
FSV	**F**eature **S**elective **V**alidation
GDM	**G**lobal **D**ifference **M**easure
GMSK	**G**aussian **M**inimum **S**hift **K**eying
GSM	**G**lobal **S**ystem for **M**obile
GSM-R	**G**lobal **S**ystem for **M**obile-**R**ailway
IEC	**I**nternational **E**lectrotechnical **C**ommission
IEEE	**I**nstitute of **E**lectrical and **E**lectronics **E**ngineers
IF	**I**ntermediate **F**requency
IQ	**I**n-phase and the **Q**uadrature
ISI	**I**nter-**S**ymbol **I**nterference
ISO	**I**nternational **O**rganization for **S**tandardization
ITU-T	**I**nternational **T**elecommunication **U**nion - **T**elecommunication Standardization Sector
ITU-R	**I**nternational **T**elecommunication **U**nion - **R**adio-communications Sector
MS	**M**obile **S**tation
OFDM	**O**rthogonal **F**requency **D**ivision **M**ultiplexing
OSC	**O**scilloscope
PCB	**P**rinted **C**ircuit **B**oard

PDF	**P**robability **D**ensity **F**unction
PEC	**P**erfect **E**lectric **C**onductor
PRF	**P**ulse **R**epetition **F**requency
PSK	**P**hase **S**hift **K**eying
QAM	**Q**uadrature **A**mplitude **M**odulation
QoS	**Q**uality **o**f **S**ervice
QP	**Q**uasi-**P**ic
QPSK	**Q**uadri**P**hase-**S**hift **K**eying
RBW	**R**esolution **B**and**W**idth
RCT	**R**adio **C**ommunication **T**ester
RFID	**R**adio **F**requency **ID**entification
RTC	**R**eal **T**ime **C**ommunication
R&S	**R**ohde & **S**chwarz
SHR	**S**parks **H**igh **R**ate
SLR	**S**parks **L**ow **R**ate
SNR	**S**ignal to **N**oise **R**atio
STFFT	**S**hort **T**ime **F**ast **F**ourier **T**ransform
TD	**T**ime **D**omain
TDMA	**T**ime **D**ivision **M**ultiple **A**ccess
TETRA	**TE**rrestrial **T**runked **RA**dio
UHF	**U**ltra **H**igh **F**requency
VoIP	**V**oice over **I**nternet **P**rotocol
WFSV	**W**eighted-**F**eature **S**elective **V**alidation
WGN	**W**hite **G**aussian **N**oise

Chapter 1

Introduction, Objectives & State of the art

1.1 Introduction

1.1.1 Impact of transient interferences on digital communication systems

Transient interferences are one of the most common sources of noise which the Electromagnetic Compatibility (EMC) has to deal with. A transient generated by a spark or a switching power supply could be propagated as a electromagnetic radiated interference reaching sensitive equipment, such as the antenna of a digital communication device [77]. Radiated transients are broadband noise which generates interference within the communication bandwidth slot, therefore they are perceived as useful signal by the communication system. The signal of interest and the impulsive noise are in the same frequency band; consequently, the interference cannot be filtered to prevent the transient influence. There are many examples of this EMC problem in the literature [1, 7, 16, 116, 148]. A typical example is the Digital Video Broadcasting (DVB) image degradation by the presence of impulsive interference [7, 39, 44, 47, 86]. The origin of these transient interferences is diverse, but even daily life actions, such as switching lights in the home, car loads switching or sparks can be responsible for them [3, 13, 17–19, 21, 23, 45, 90, 96, 97, 100, 114, 121].

Transient signals are especially detrimental in Real Time Communication (RTC) systems because retransmissions are not possible. In this type of communication, when a transient phenomenon occurs, the corrupted data cannot be recovered. Regardless a digital communication system becomes or not an RTC often depends on the specific service provided rather than the physical layer over which it is implemented. For example, a wireless network can carry e-mail packets and Voice over Internet Protocol (VoIP) packets. For the latter, Telecommunication Standardization Sector (ITU-T) defines a maximum delay of 150 ms for an end to end communication [59], consequently retransmissions become impossible in practice. If a transient interferes in the wireless network physical layer, both services will be affected, but only VoIP will experience a significant degradation. E-mail packets can be easily retransmitted and the delay is not detected by the users. Therefore, it is important to evaluate the error that impulsive noise could produce in RTC systems.

Communication systems that may have an impact on people safety, such as in-vehicle communication, are also RTC and can be easily affected by transient interferences produced by motors or switches close to them [20, 42, 52, 78]. The errors produced by the man-made impulsive noise could cause problems to critical driving systems, hence to passengers' safety, so it is vitally important to study this kind of phenomena.

To illustrate real transient interferences problems some examples are explained below.

1.1.1.1 DVB-T interferences

As it has been mentioned before, in the literature there are many examples explaining the degradation produced in a DVB receiver when transient interferences are present [75, 138, 144]. A transient interference capable to disturb the digital communication system can be generated by different household equipment. One example is the switching lights; commutation generates transients along the mains cables producing radiated interferences which propagate away reaching the antenna of a DVB-Terrestrial system. The interference at the frequency system band is managed as useful signal by the receiver and cannot be filtered. The degradation produced in digital television is observed as freezing images phenomena or 'pixeling'. DVB-T is a broadcasting communication system, so retransmissions are

not allowed and the information affected by the transient interference will never be recovered. Moreover, if the degradation produced by the transient interference is compared with the degradation suffered by old analogue communication systems, the degradation perceived by the end user is more severe with the new digital systems. In the analogue systems transient phenomena were closely to be unobserved as the duration of transient is short and only affect one or two lines in the analogue television transmission systems. On the other hand, with DVB-T several bits of information are affected by the transient and the image cannot be plotted. Although many devices fulfill standards requirements, the interference effect of common electronic devices over DVB-T is continuously under study as many equipments interfere with digital television [75].

1.1.1.2 GSM-Railway failure

Another example that is in the literature and has a huge effect in the proper behaviour of the railway system is the transient coupled to the GSM-Railway system [31, 32, 41, 51]. This GSM-R interference case is a critical example due to the system is related to the safety of the passengers [24, 27]. GSM-R system provides information about rolling stock position, etc. When the communication between the rolling stock and the Base Transceiver Station (BTS) is lost, a failure state is produced and the rolling stock changes its state to a safe mode. This produces speed reduction or that the high-speed train stops, causing huge problems to the railway. Nowadays, there is not a solution for this problem and it is been studied in European research projects [42, 107].

In high-speed railway, arching effect is caused by the discontinuity produced between the pantograph and the catenary [25, 26]. This arching effect produces radiated transient interferences that reach the antenna of the GSM-R communication system which is installed at the roof of the rolling stock as it is illustrated in Figure 1.1.

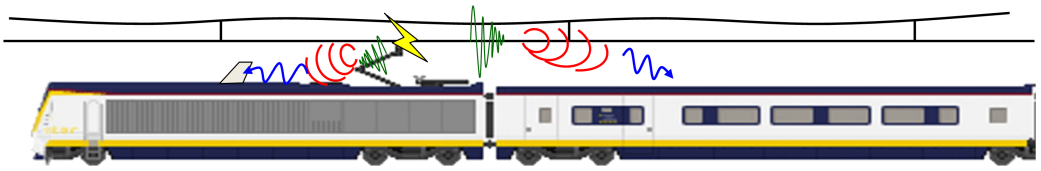

FIGURE 1.1: GSM-R radiated transient interference illustration. Picture from [42]

Regarding some details about the GSM-R system, it works between 876 MHz and 880 MHz at the uplink channel and between 921 MHz and 925 MHz at the downlink channel. The most sensitive channel to the radiated transient interference is the downlink as the transient is produced close to the antenna situated at the rolling stock; the GSM-R signal coming from the base station is received with a weak level by the GSM-R antenna. Typical coverage levels of the GSM-R system vary from -40 dBm, when the rolling stock is close to the base station, to -100 dBm when the base station is far away. Consequently, the transient produced by the arching between the pantograph and the rolling stock has spectral components from DC till several gigahertz, therefore the radiated impulsive noise will have components at the very sensitive GSM-R downlink frequency band.

1.1.1.3 Spot signalling system failure in railway

Another example related to railway is the transient interference produced between the rolling stock and the spot signalling system. Eurobalise is a safe spot transmission based system carrying safety related information between the track and the rolling stock [37]. The information that is transmitted is associated with signalling data, geographical information, speed restrictions, etc. The signalling system consists on an antenna installed on-board at the bottom of the rolling stock and a track-side balise, which is a passive resonant circuit. In the uplink of the communication the integrated loop antenna in the balise generates the magnetic field data received by the rolling stock antenna when it is over the balise. Data is frequency modulated with $\pm$282.5 kHz employing a data rate of 565 kbps and the carrier is at 4.2365 MHz.

As in the GSM-R example the transient interferences are produced by the discontinuity between the pantograph and the catenary [42]. In this case we can find several causes: discontinuity could be attributed at circuit breaker operations; pantograph operations, to vertical movements of the pantograph and the line or can be created by the ice between the line and the pantograph. In this occasion there is not a direct coupling between the spark or the pantograph to the receiving antenna as the BTM antenna is placed at the bottom of the vehicle; transient is coupled conducted to the train structure and also to the tracks, where a magnetic field is generated reaching the BTM antenna and the transient interference associated with the communication bandwidth is considered as useful signal.

Transient coupled to the communication system cause different types of errors; the system could stop receiving valid messages or system detects a 'ghost' balise when it was not any real balise present. When a ghost balise is detected, the vehicle is switched to a safety mode braking the rolling stock. The main problem in this kind of railway interferences to mitigate its effect to the communication system is that cannot be identified by the EMC tests according to the standards EN 50121-3-2, EN 50121-3-1 or CLC/TS 50232-2. Therefore, EMI problems with the systems cannot be identified until the validation process of the new rolling stock is complete and it is not referred to by any mandatory standard or specification.

1.1.2 Digital communication system evaluation in front of transient interferences

In analogue communication systems, the Signal to Noise Ratio (SNR) is the main figure of merit to evaluate their performance; analogue radio systems require SNR of as much as 40 dB for satisfactory operation. Digital Communication Systems (DCS) usually work with very low level signals at the receiver end, so a relative low level transient could easily interfere the system in the communication band if it has enough energy, in general, digital radio communication systems allow error-free operation down to SNR of 10 dB. However, the transition region from error-free operation to malfunction is small [59]; digital communication systems cannot be evaluated using only the SNR ratio [2, 67, 117, 133, 137]. In addition, parameters like the repetition rate or the burst duration must also be taken into account. In order to evaluate the errors produced by transient interferences in digital communication systems, it is necessary to consider more parameters, like the constellation diagram, the vector diagram, the Bit Error Rate (BER) or the Complementary Cumulative Distribution Function of the signal (CCDF), among others. For this reason time domain analysis must be carried out, it is not valid to examine the spectrum and measure the SNR; time-domain captures at the frequency band of the communications have to be done to get the time domain signal that will affect the communication system.

Additionally, another possibility is to carry out measurements to obtain the statistical parameters of the interference. In CISPR 16-1-1 new detectors have been defined to deal with transient interferences that can interfere critically to digital communication systems. Amplitude Probability Detector (APD) has been defined

and provides statistical information of the interference measured. Furthermore, there is a discussion on relating the APD measurement with the Bit Error Rate, but it has been demonstrate by Wiklundh the relation of APD and its impact on coherent digital radio receivers [84, 141]. So APD is highly accepted as the best tool to measure statically interference and in a second step study the effect over a digital communication system.

1.1.3 Transient interferences and EMC standards

Commonly, transient interferences are poorly measured following currently Electromagnetic Compatibility (EMC) standards. Man-made noise transient interferences are greatly present on the equipment evaluated inside EMC standards. In the EMC Directive 2004/108/EC the essential requirements that any apparatus and fixed installations must comply are described in Annex I.

'1. Protection requirements equipment shall be so designed and manufactured, having regard to the state of the art, as to ensure that:

(a) *the electromagnetic disturbance generated does not exceed the level above which radio and telecommunications equipment or other equipment cannot operate as intended;*

(b) *it has a level of immunity to the electromagnetic disturbance to be expected in its intended use which allows it to operate without unacceptable degradation of its intended use.'*

The main problem is that the accomplishment of the harmonized standards does not fully ensure the *(a)* point when transients are involved. Measurements methodologies following standards do not include a proper measurement for radiated transient interferences. As an example, quasi-peak detector defined in CISPR 16-1-1 [28] was developed to protect analogue communication systems, relating the output of the detector to the human perception when an analogue system was interfered.

Therefore, further measurement and evaluation is needed to acquire transient interferences and determine if they are critical, from an interference point of view, to the digital communication systems. Consequently, standard frequency sweep measurement techniques are not suitable and novel time-domain meas must be considered [54, 140].

1.2 Objectives

The main goal of this thesis is to demonstrate that it is possible to estimate the error that will be introduced into a digital communication system based on the radiated transient interference measurement. To reach this objective, first of all, the interference must be measured providing us all the significant parameters of the transient perturbation to evaluate properly the impact on a digital communication system. As it has been mentioned in the introduction, it is necessary to develop a time-domain measurement procedure to acquire the transient that will interfere directly with the communication frequency band. Once this measurement has been obtained, it will be used as an input to evaluate the impact of the transient on a digital communication system using digital communication software simulation. Moreover, transient interferences will be measured developing methodologies which employ new statistical detectors within the EMC standards. These measurements will solve standard measurements limitations and, at the end, the relation between statistical detector measurements and the degradation produced by the transient interferences to the DCS will be found. These three stages are described below like secondary thesis objectives.

1.2.1 Time-domian radiated transient interferences measurement

In the first stage of this thesis radiated transient interferences will be measured to evaluate their impact over real time digital communication systems. The main idea of this measurement is to acquire the interference just in the frequency band of the communication system that is going to be evaluated. As transient interferences are spread spectrum, usually starting at DC and ending at several hundreds of megahertz or some gigahertz, only the slot of the transient interference that overlap the communications system band will be measured. This frequency slot of the radiated transient is the profitable part for us as it cannot be filtered by the communication system and it will be considered as useful signal.

The foremost task to do is to analyse the intrinsic problems that transient interference presents when these radiated impulsive interferences are measured. The random characteristics of amplitude, duration, frequency rate and interval of this type of interference make it a challenge to measure properly transient interferences.

Related to this transient study, the next step is to identify the measurement equipment limitations and the measurement procedures, defined in EMC standards, weaknesses that imply an unsuitable measurement of the transient interferences. To illustrate this point, the resolution bandwidth (RBW) is a limitation of the instrumentation employed as it can only be set to a restricted number of frequency bands. Furthermore, from the EMC measurement procedures defined in standards point of view, an unique RBW of 120 kHz is employed to measure the frequency range from 30 MHz till 1 GHz.

In the next stage, the capture of the in-phase and quadrature components of the radiated transient interference will be the objective. To reach this goal, different novel techniques will be employed to measure properly the two components of the radiated interference. Firstly, measurements will be obtained using standard instrumentation such as an EMI receiver dealing with the random characteristics of the impulsive interferences to be measured. Afterwards, measurements are going to be carried out employing a combination of instrumentation using the high sensitivity of an EMI receiver and also the time-domain capabilities of an oscilloscope.

In this section, electromagnetic simulation will also be employed to manage specific interference scenarios when it is not possible to perform some measurement without interfering the scenario or for instance when we want to evaluate unreachable receivers such as implants. FDTD simulation software will be used in combination with post-processing to achieve, as before, the in-phase and quadrature components of radiated transients received by a certain digital communication system.

The last stage of this section is to carry out a measurement campaign employing all the different techniques described previously.

1.2.2 Evaluating real time communications against transient interferences employing time-domain captures

The aim of this secondary objective is to estimate the degradation that radiated transient interference produces to digital communication systems. This objective is strongly related to the previous goal where transient interferences were captured, using it as an input of the DCS evaluation.

Digital communication descriptors like BER, constellation diagram, vector diagram, etc. are used to quantify and analyse the degradation produced in digital communication systems. In this section, the most suitable descriptors to estimate the behaviour of a real time digital communication system will be identified analysing the information that such descriptor provides to the digital communication performance. Once the different possible descriptors that analyse properly the interference are identified, the next stage will be to carry out digital communication system simulations in baseband to get a tool capable of model properly digital communication systems in presence of transient interferences. Interferences previously measured will be added to the DCS simulation using the in-phase and quadrature components. The results of these simulations that evaluate real digital communication systems will give us information about the degradation produced on each descriptor of the DCS induced by all the main parameters of the transient interference (amplitude, frequency, duration and interval). The relation within the DCS descriptors and the main parameters of transient interferences could give novel guidelines to relate transient interferences and system degradation.

Finally, a validation procedure will be conducted using a rising new DCS that has not been evaluated before in front of transient interferences. A dummy communication device will be interfered by different types of radiated transient interference varying its main parameters. The simulation results will be compared to the degradation suffered by the real communication device; analysing the agreement between the methodology developed and the errors produced at the real equipment.

1.2.3 Statistical detectors to evaluate DCS

In this section, statistical detectors will be analysed to determine if statistical measurements of transient interferences can prodvide enough information to estimate the degradation produced in a digital communication system; and if it is necessary to develop new measurement techniques.

The first step is to analyse the advantages of the statistical detectors in front of traditionally detectors described in the EMC standards. Moreover, the relation between APD detector and the BER will be studied as the BER is one of the most accepted DCS descriptors to estimate the degradation produced in a digital communication.

APD measurements have limitations to be carried out during standard compliance electromagnetic emissions test at EMC laboratories. These measurement methods have strong inconveniences to define a test method to protect digital communication systems in all the frequency range. The main problem is that APD measurements are defined at a certain frequency with a bandwidth, which is also defined. There are many systems at different frequencies and also with different bandwidth, consequently it is nearly impossible to use instruments or methods capable to measure the whole spectrum to protect either digital communication system. The objective and, at the same time the challenge, is to develop a new methodology capable to measure the APD of transient interferences in any frequency band. If the new methodology to obtain the APD is achieved, an exhausting validation procedure must be made to ensure the accurate behaviour when different types of interferences are being measured. Different kind of noise, like White Gaussian Noise and impulsive interferences, must be considered and compared with standard EMI receivers capable to measure at certain frequency bands.

1.3 State of the art

1.3.1 Transient interferences measurements

Measuring time-domain transient interferences is a hard work according to its random amplitude, duration, frequency; due to the high number of different radiated transient interferences sources [9, 98, 102, 103]. Nevertheless, it is an important source of interference and it has to been characterized properly.

One of the first studies that characterize in time-domain different type of transient interferences was the measurement carried out by Spaulding and Disney [127]. In this study, results from many years of man-made radio noise were presented. The data base used in this report consists on some 300 hours data collected over the period from 1966 to 1971. The measurements were made on six different states; Colorado, Maryland, Texas, Virginia, Washington and Wyoming. The measurements were made in 103 areas; the area's size was ranging from a few square blocks in a business area to several square miles in some of the rural locations. The period of measurement for each location varied from approximately 15 minutes to over an hour, additionally, few stationary measurements were made for a 24 hours period. As an example, Figure 1.2 shows a time-domain measurement done in Colorado at 250 MHz.

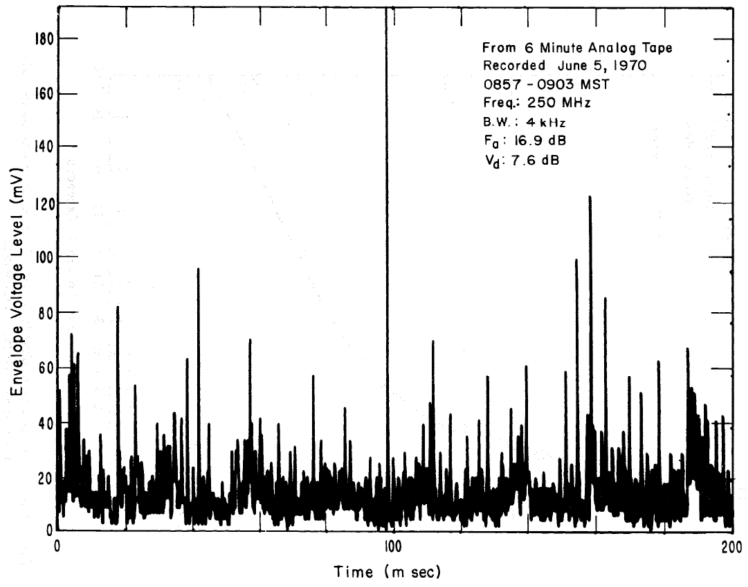

Figure 38. Randomly selected 200 ms sample of noise envelope from a 6-minute, 250 MHz central Colorado Springs recording.

FIGURE 1.2: Time-domain measurement result figure extracted from Man-made radio noise OT REPORT 74-38.

These measurements were carried out in order to estimate the behavior of a telecommunications system at some future time. The estimate of the interference involves a prediction process to estimate the characteristics of the environment. For this reason, statistical curves where obtained from the measurements carried out between 1966 and 1971. In Figure 1.3, statistical measurements of the impulsive noise are shown according to amplitude probability distribution.

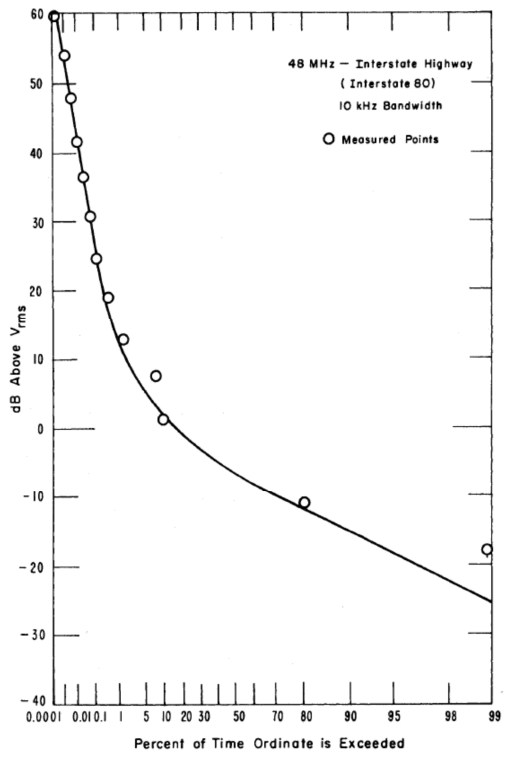

Figure 37. Amplitude probability distribution of man-made noise at 48 MHz, 10 kHz bandwidth.

FIGURE 1.3: Statistical noise result figure extracted from Man-made radio noise OT REPORT 74-38.

These probability results are one of the most used tools to represent time-domain measurement from transient interferences. D. Middleton published many studies where analytically and experimentally models of man-made electromagnetic interferences statistical-physical models were developed [91, 92]. The aim of these studies was to construct analytically tractable statistical models of man-made electromagnetic interference encountered in urban environments, generally and in transportation communication systems particularly, and ultimately, to develop and extend these models to a full interpretation and prediction of experimental observations.

Middleton proposed a statistical-physical approach to model the non-Gaussian noise produced by natural and man-made interferences creating a three categories classification of electromagnetic noise for a narrow-band receiver. The additive noise is classified into three broad categories, Class A, Class B and Class C [91, 92]. Class A noise was originally defined as noise which is typically narrower spectrally than the receiver in question, later it was redefined as the noise which produces ignorable transients in the typical receiver [93]. On the other hand, Class B noise was characterized by significant transients or ringing of the receiver which generally occurs when the noise bandwidth is wider than the receiver bandwidth. Finally, Class C noise was defined as a mixture of Class A and Class B noise; otherwise, it can be reduced to a Class B for practical analysis.

Once man-made interferences were classified properly there are many examples in the literature measuring in time-domain impulsive interference that made reference to Middleton classification. The most common transient characterization is the measurement done in the automotive sector [40, 122, 123]. Combustion engines produce transient interferences [95, 113, 128] that have been measured by automotive manufacturers, for instance, these studies demonstrate that during the ignition process many transient interferences are produced.

As it has been described in the introduction, one of the digital communication systems interfered by radiated transient interference is DVB-T. From October 2001 to October 2002 a working group led by British Broadcasting Corporation (BBC) and formed by Sony, Philips, Rohde & Schwarz, Zarlink and ST Microelectronics carried out transient interference measurements because it was noticed that impulsive noise was interfering DVB-T [75]. The goal of this study was to propose a set of test waveforms and methods which could be used to faithfully represent the effect of impulsive interferences on digital television. In the first stage, the idea was to perform a large number of measurements to get the statistical of impulsive interferences in different common scenarios. More than two hundreds captures were carried out at several households and different locations where traffic distortion was present.

The measurement system was set to capture only the part of the transient interference that falls into the Digital Television Terrestrial (DTT) communication band. The capture system consist in a 200 ms snapshots of 8 MHz DTT channel filtered and down converted to second intermediate frequency (central frequency 4.57 MHz and 7.61 MHz bandwidth). The data was sampled at 40 MHz with

a resolution of 12-bit analogue to digital converter. Captures were performed at UHF channels, and with the measurement system the radiated transient noise was captured. The baseband captures were like the results observed in Figure 1.4.

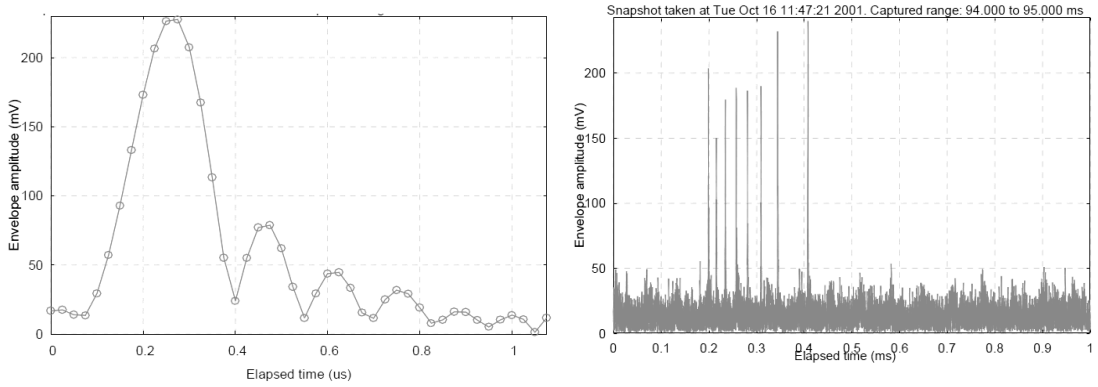

FIGURE 1.4: Time-domain transient interferences measurements BBC (picture from [75]).

The main sources of disturbance that they considered were central heating, cooker ignitions, dishwasher, light switches and traffic interferences. At the end of the measurements campaign they classified the transient interference and extract the main parameters of the transient interference as it can be seen in table extracted from [75] in Figure 1.5.

Type of capture	Pulse Spacing (μs)	Burst Duration (μs)	Burst Duration (pulses/burst)	Burst Spacing (ms)	Event Duration (ms)	Event Duration (bursts/event)
Central Heating 1	0 → 3 (0.5) / 0.9	< 500 (200) / 310	< 3000 (100) / 250	0.14 → 0.28 / 0.21	< 2.5 / 0.5	1 or 2 (1) / 1.4
Central Heating 2	10 → 45 (20) / 30	50 → 300 / 150	1 → 12 (2) / 6	—	1 burst/event	1
Central Heating 3	1.5 → 3 (1.6, 2.7) / 2.1	< 10 (1) / 19	< 10 (3) / 10	0.16 → 0.34 / 0.025	< 0.16 / 0.05	1 → 4 (1) / 1.7
Cooker ignition	1 → 3 (1.5) / 1.7	< 100 (40) / 40	< 80 (2) / 24	—	< 0.1 (0.04) / 0.04	1
Dishwasher 1A	0.3 → 3 (0.85, 1.1, 1.55) / 0.9	< 750 (150) / 360	< 1300 (300) / 330	0.2 → 0.5 / 0.3	< 1 (0.2) / 0.5	1 → 3 (1) / 1.31
Dishwasher 1B	0.5 → 3 (0.6, 0.85, 0.9, 1.1, 1.25, 1.5, 2) / 1.5	< 500 (100) / 190	1 → 500 (25) / 110	< 1.5 (0.75) / 0.73	< 30 (2.5) / 6.3	1 → 35 (3) / 9.6
Dishwasher 2	2 → 50 (11, 19.5) / 24	< 500 / 330	1 → 25 (3, 6) / 14.5	0.4 → 1.6 / 0.9	< 2.5 (0.5) / 1	1 → 3 (1) / 1.8
Dishwasher 3	0.8 → 20 (1.25, 2.5, 3.25) / 4.4	< 3000 / 1600	1 → 600 (50) / 350	0.187 / 0.187	< 3 (2) / 2	1 or 2 (1) / 1.2
Lights off 1	1 → 3 (1.45, 1.8, 2.45) / 1.7	< 800 (1 b/e) 2000 → 4000 (> 1 b/e) / 1630	< 500 (250) 1250→ 2250 (1700) / 820	— 2 → 11 (10) / 8.8	< 1 < 25 / 6	1 → 5 (1) / 1.9
Lights off 2	< 100 (5) / 14	< 500 (20) / 141	< 40 (1, 3, 8,14, 20) / 11.3	< 10 (1) / 2.1	< 10 / 4.4	1 → 4 (uniform) / 3
Fluorescent lights on	< 200 (10) / 45	< 400 (10) / 105	1 → 15 (1, 2, 4) / 3.3	0.3 → 1.1 (0.75) / 0.55	< 1.6 (0.1) / 0.52	1 → 4 (1) / 1.8
Incandescent lights on	< 30 (2) / 4.6	< 300 (2) / 210	1 → 250 (1) / 40	0.3 → 0.4 (uniform) / 0.35	< 0.6 (0.01) / 0.36	1 or 2 (1) / 1.3
Traffic 1	< 100 (5) / 24	< 300 (25) / 92	1 → 17 (2) / 5	0.3 → 0.8 (uniform) / 0.54	< 0.8 (0.05) / 0.22	1 or 2 (1) / 1.2
Traffic 2	< 20 (5) / 9.7	< 600 (80) / 200	1 → 60 (7) / 22	—	< 0.6 (0.08) / 0.2	1
Traffic 3	5 → 10 (7) / 9.2	0 → 20 (1) / 2.8	1 → 3 (1) / 1.25	10 → 15 (10) / 14.7	> 200 / 77	1 → 15 (1) / 6.2

FIGURE 1.5: Estimation of main transient interferences parameters (picture from [75]).

The results of this campaign measurements were used in a following stage to analyze the impact of the transient interference to DVB-T (in next section the model employed for BBC is presented).

Concerning radiated transient measurement, other studies have dealt with the difficulty of capturing transient interferences. Another communication system that is interfered by transient interferences has been explained before at the introduction; GSM-R is disturbed by radiated transient coming from the arching discontinuities between the pantograph and the line. Several measurement campaigns have been carried out to identify transient interferences [6]. In these references the measurements are performed without following the standards, they were developed to protect the equipment near the railway, not on the train. Transient interferences induced on the GSM-R antennas on board trains, were characterized in the following parameters: rise time, time duration, repetition rate and amplitude. Measurement campaigns were carried out in France to collect a large number of induced EM interferences on GSM-R antennas fixed on the train roof. With the ultimate goal of generating transient noise scenarios, representative of those detected by the antennas, and performing immunity tests in laboratory. Measurements were conducted in France between Saint Pierre des Corps near the city of Tours and Nantes. The cruising speed of the train was about 160 km/h and the maximal speed was 200 km/h. In order to record the EM noise observed on the roof of the train, the measurements were performed with a digital oscilloscope connected to a GSM-R antenna fixed at approximately 80 m from the pantograph. Experiments to characterize in time-domain the EM transient events, were carried out using a digital oscilloscope with a 20 GHz sampling frequency recorded in a 200 ns time window. Approximately, during 100 minutes of measurement, the oscilloscope collected the about 25,700 transient signals. Figure 1.6 shows some of the results published.

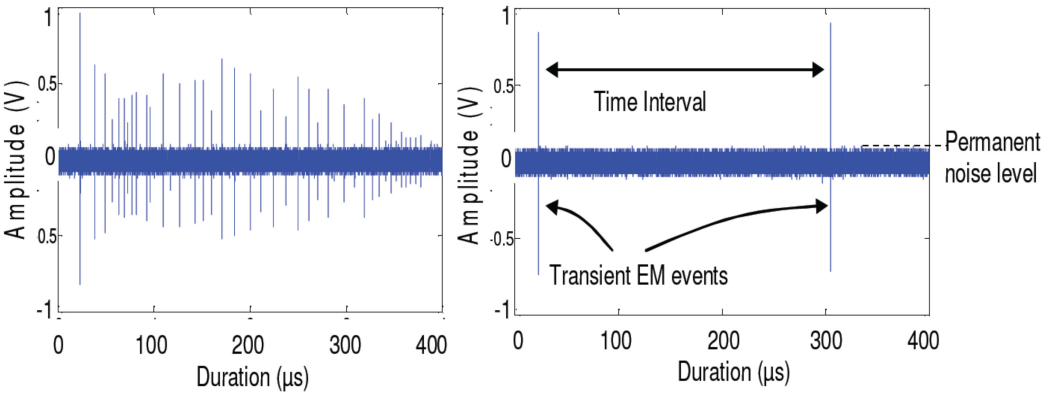

FIGURE 1.6: Time-domain radiated transient measurements carried out with an oscilloscope for GSM-R (picture from [6]).

From the measurement results it was concluded that statistically the rise time of the transient interference was defined to 0.4 ns, the duration of the pulse to 5 ns and the interval to 25 s. Each transient produces interferences whose level can reach up to -35 dBm in the GSM-R frequency band, whereas the GSM-R signals level can decrease to a minimal value of -95 dBm.

1.3.2 Evaluating real time communications against transient interferences

Classical measurement methods for emission standards were developed to protect analogue communication systems. The detectors used in the standards are the peak detector, quasi-peak detector and average detector. These detectors try to emulate the human perception of analogue systems against interferences weighting the different types of interferences. CISPR and ITU-R are working on the matter of weighting detectors to determine interference effect over digital communication systems. Generally, a weighted measurement of impulsive disturbance serves the purpose of minimizing the cost of disturbance suppression, while keeping an agreed level of radio protection. The weighting of a disturbance for its effect on modern digital radio communication services is important for the definition of emission limits that will protect these services [126, 130–134].

Amendment 1 of CISPR 16-1-1 defines classical detectors and a new one that is a combination of an r.m.s. and an average detector. The selection of the type of detector and the type of the transition between these detector functions is based on measurements and theoretical investigations to protect digital communication systems. In Report ITU-R SM.2002-1 [120] it was shown the first steps towards the weighting of interference to digital modulation services; a concept for the definition of weighting curves has been defined and experimental results were obtained for two examples. An interference source with certain characteristics will produce a certain BER, e.g. 10^{-3} in a digital radio communication system, when the interfering signal is received in addition to the radio signal. The BER depends on the pulse repetition frequency (PRF) and the level of the interfering signal. In order to keep the BER constant, the level of the interfering signal will have to be readjusted while the PRF is varied. This level variation vs. PRF determines the weighting characteristics. There are result examples of evaluation of the interference effect of transient interferences described in IEC TR CISPR 16-3

subclause 4.8. In this document, studies analyzing Digital Video Broadcasting Terrestrial (DVB-T), Digital Audio Broadcasting (DAB), TETRA, GSM, etc. are explained; the results were obtained adding pulse noise with different widths to a radio-channel, producing impulsive interferences. Figure 1.7 shows the results for a TETRA system of weighting detectors for a reference 2% of BER; when the PRF is increased, the level needed to interfere TETRA downlink is reduced.

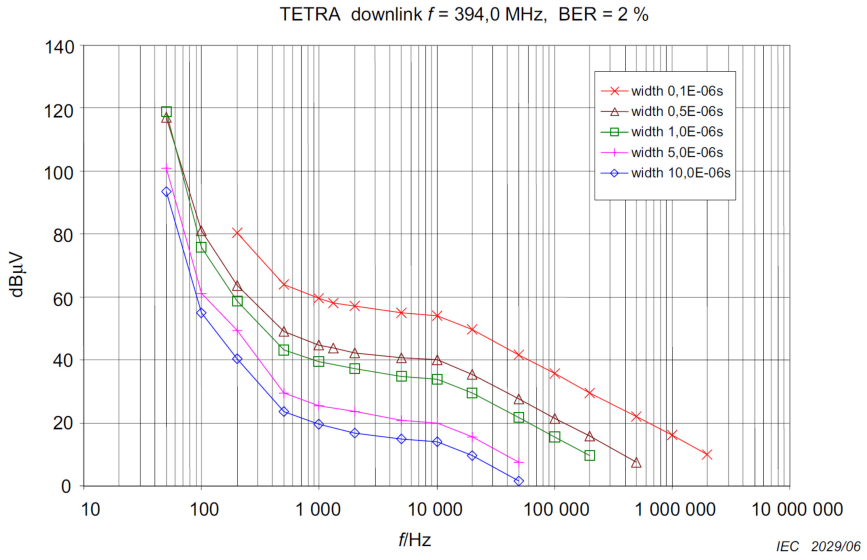

FIGURE 1.7: Weighting detector example defined in CISPR 16 (picture from CISPR 16-3 subclause 4.8).

Another approximation to study the impact of the transient interferences to DCS is to model the impulsive noise adding it to the communication system [79, 80]. Regarding the study described before evaluating the disturbance produced to DVB-T by impulsive noise, two types of test were performed by BBC to analyse the effect of radiated transient interference to the DVB-T [75]. When the communication system is considered as narrow band in front of the wide spectrum transient interference, the period of time that the impulsive noise is present can be modelled as white Gaussian noise. In the first approach, a train of pulses to gate an Additive White Gaussian Noise (AWGN) source is considered. The generation of an AWGN signal can be provided by several digital signal generators available in the market with an I/Q arbitrary waveform generation option; that allows the setting of the bandwidth and the output power level. Impulsive interference is generated instead as gated Gaussian noise; pulses are grouped in bursts as it can be observed in Figure 1.8, where the resulting signal can be seen as if gating is performed twice: the first gating defines the burst duration and the time spacing between consecutive

bursts, while in the second one Gaussian noise constituting a burst is gated to shape the pulses.

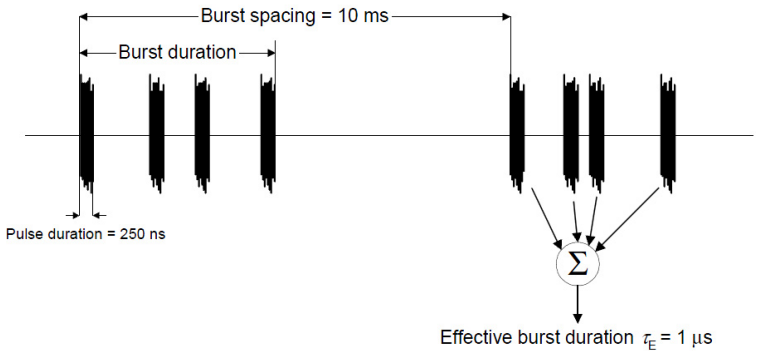

FIGURE 1.8: Double gated AWGN generated to interfere DVB-T according to previous measurements (picture from [75]).

In the second approach used to evaluate the transient interference (Figure 1.9), previous captures of radiated transient interferences are employed. A vector signal generator model SMIQ from Rohde & Schwarz was used to download the captured waveforms (I/Q signals).

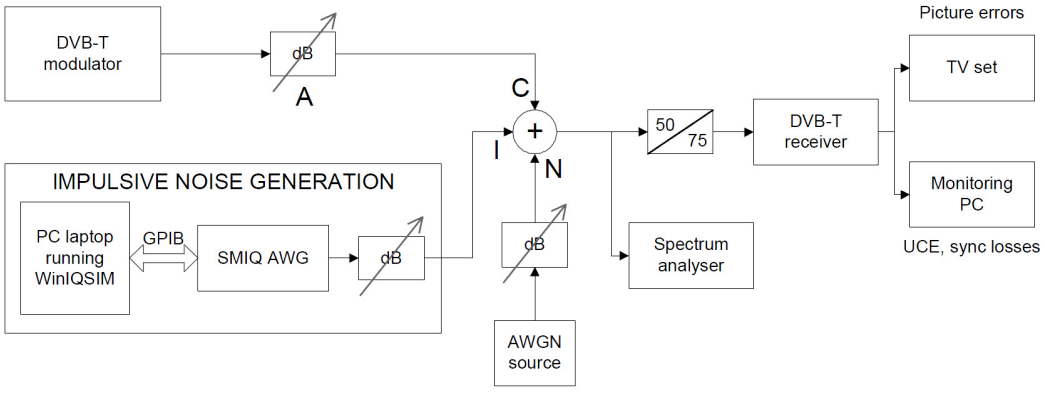

FIGURE 1.9: Interference setup employing captured waveforms from impulsive noise (picture from [75]).

At the end of both noise coupling techniques, the degradation produced at the pictures of the DVB-T transmission can be evaluated; linking the different type of impulsive noise interference with the effect on the RTC system.

Another technique developed to analyse the degradation produced by transient interferences is the test bench constructed to simulate transient burst in a GSM-R system [26, 31]. Statistical characteristics of the transient interferences present in a real scenario were obtained from the measurement explained in the last section.

The pulse duration, rise time and the amplitude was estimated to reproduce the source of interference in a test laboratory. To analyse the impact of the impulsive noise the immunity test bench observed in Figure 1.10 was developed.

The BER, Rxqual, and Rxlevel are descriptors that indicate the quality of the GSM-R link. Descriptors measurements require the use of a GSM-R mobile and a Signal Universal Radio Communication Tester (RCT). The RCT is a measurement apparatus that can send downlink signals, such as a BTS, and receive signals coming from the mobile to which it is connected. It can also make measurements, notably BER ones. The useful signal is interfered by adding sequences of transient disturbances. To generate the sequences, an arbitrary generator was connected to the combiner and configured with the pulse obtained from measurements campaign. The rise time of the pulse is 0.4 ns, the duration is 5 ns and the frequency of the sinus exponential model is 923 MHz, which coincide with the downlink centre frequency of the GSM-R standard.

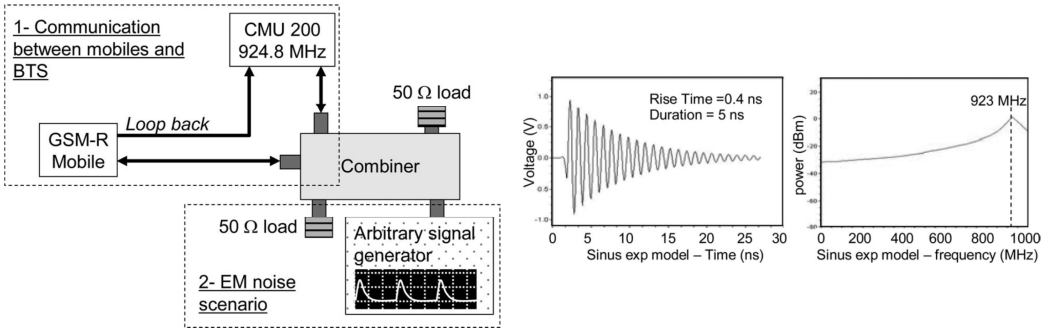

FIGURE 1.10: Interference test bench developed to evaluate transient interference against GSM-R (picture from [31]).

At the end of these tests the degradation produced by the artificial impulsive interference generated was evaluated. On the other hand, not all the transient interferences measured on-board during the campaign measurements were analysed. Nevertheless, the approximation of the immunity tests that we carried out have shown that the transient model is a well representative of the impact of real transient disturbances existing in the railway environment.

1.3.3 Statistical detectors measurements and evaluation

Obtaining the statistical of transient interferences is a key point to characterize, classify and model the impulsive noise. Amplitude probability distribution (APD)

is a frequently used term for random signals, which was originally used to categorize electromagnetic interference and is defined by the exceeding probability the envelope amplitude.

Some of the pioneer research of the Amplitude Probability Detector APD can be found in papers by Shepherd and Spaulding [122, 123, 127]. In these studies, APD measurements were employed as it was the best measurement method for their automotive application; the aim of their measurements was to get the statistical of the interferences and compare several vehicle and configurations to distinguish the worst case. APD measurements were carried out considering differences between power of vehicles, engine speeds, and different freeway locations. Figure 1.11 is an example of the measurements performed, where different engine speed produce differences in the APD diagram.

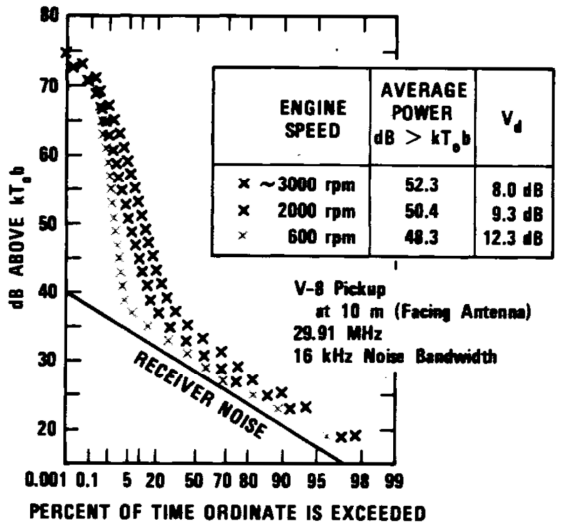

FIGURE 1.11: APD measurements performed for different engine speed (picture from [123]).

Next step with the APD detector was to relate these APD measurements with the degradation produced on communication systems. For the computation of the interference effect on a radio channel, the APD is a suitable basis [46, 139], however is not a weighting detector because it does not give one measurement result per frequency but it gives the probability of occurrence of certain amplitudes as a function of the amplitude. The APD has been proposed for standardization in CISPR recently, in CISPR 16-2-3 is explained how the APD measurement can be carried out. As it is described in the standards, a product committee may choose the APD measurement as the method for final emission testing. Currently, this

measurement method is still not used in product standards. On the other hand, different studies have evaluated the communication system behavior when it is interfered by transient noise.

APD was originally used to categorize electromagnetic interference, but recently it has attracted attention as an EMI test method since it was found to have strong correlation with the bit error probability (BEP) of a digital communication system subjected to the interference; it has been demonstrate the relation between APD measurements and their impact on digital radio receivers [38, 141–143]. In particular, the relation between the APD and the impact of microwave ovens on the performance of a certain digital receiver has previously been presented in [68, 145]. This correlation is mainly demonstrated by measurement, but in [145], a theoretical relation between a microwave oven and a differential quadriphase-shift keying (QPSK) receiver is shown.

Wiklundh presented how the relation between the maximum BEP and the information provided by the APD of the envelope applies to emission requirements. A practical method for performance estimation of digital coherent radio receivers in terms of BEP by using the APD in non-Gaussian interference was studied. The relation of APD and Bit Error Probability is presented by different modulation schemes in Figure 1.12.

TABLE I
BOUNDS DERIVED FOR DIFFERENT MODULATION SCHEMES

Mod.	β	Pr[bit error] $\approx$	Relation $P_{b,max}$ vs. APD
2-PSK	1	Pr[symbol error]	$P_{b,max} \approx \mathrm{APD}_R(\sqrt{E_b})$
4-PSK	1	1/2 Pr[symbol error]	$P_{b,max} \approx 1/2\,\mathrm{APD}_R(\sqrt{E_b})$
8-PSK	0.66	1/3 Pr[symbol error]	$P_{b,max} \approx 1/3\,\mathrm{APD}_R(0.66\sqrt{E_b})$
16-PSK	0.39	1/4 Pr[symbol error]	$P_{b,max} \approx 1/4\,\mathrm{APD}_R(0.39\sqrt{E_b})$
4-PAM	0.63	1/2 Pr[symbol error]	$P_{b,max} \approx 1/2\,\mathrm{APD}_R(0.63\sqrt{E_b})$
8-PAM	0.37	1/3 Pr[symbol error]	$P_{b,max} \approx 1/3\,\mathrm{APD}_R(0.37\sqrt{E_b})$
16-QAM	0.63	1/4 Pr[symbol error]	$P_{b,max} \approx 1/4\,\mathrm{APD}_R(0.63\sqrt{E_b})$
64-QAM	0.38	1/6 Pr[symbol error]	$P_{b,max} \approx 1/6\,\mathrm{APD}_R(0.38\sqrt{E_b})$
2-FSK	0.71	Pr[symbol error]	$P_{b,max} \approx \mathrm{APD}_R(0.71\sqrt{E_b})$
4-FSK	1	1/3 Pr[symbol error]	$P_{b,max} \approx 1/3\,\mathrm{APD}_R(\sqrt{E_b})$

FIGURE 1.12: Table relating modulation schemes bit error probability and APD (picture from [141]).

To ensure that the error rate of a receiver does not exceed a certain BER, the measured APD must be below the circle points, as illustrated in Figure 1.13. The

circles defines the limit conditions which the digital communications systems operates assuming a sufficient BER. The circle limits defines the minimum amplitude that must have an interference and its repetition rate (probability); if the circle is within the APD shape, the DCS will be interfered by a BER higher than the one fixed in the limit.

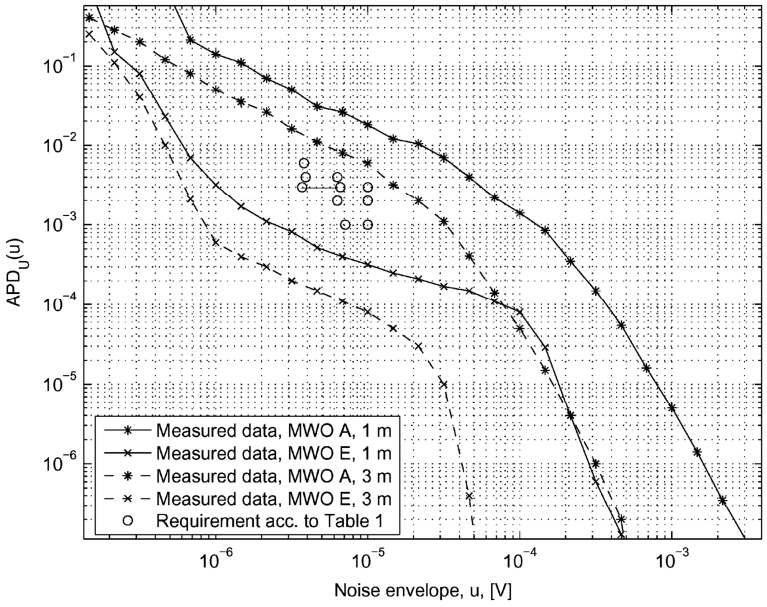

FIGURE 1.13: APD microwave oven measurements results including limits (picture from [141]).

The problem of APD measurements is that conventional receivers have a one fixed frequency, without frequency scanning. This is a substantial limitation for analyzing wideband and fluctuating interference [85]. Matsumoto had to develop a tailor made APD measurement system to evaluate the degradation produced in digital television. As an example, one of the main advantages compared to standard EMI receivers, is that the measured bandwidth is equal to the bandwidth defined in digital television standards, which is not equal to the bandwidth that can be found in the standard EMI receivers.

Chapter 2

Time-Domain Measurement and Characterization of Radiated Transients

2.1 Introduction

Radiated transient interference must be measured beyond EMC standards as the defined methodologies are not suitable to protect digital communication systems. If an impulsive noise is measured using the instrumentation and following the methodology according to the standards, the electric field obtained is not sufficient to predict the impact of transient interference over DCS. Unfortunately, the resulting data is only provided at the frequency domain, missing all the time domain information.

Firstly, to exemplify the measurement problematic, in Figure 2.1 the peak measurement of a radiated transient is shown. Although radiated transient are broadband interferences, the result shown do not clarify this type of interference. The plot of the electric field captured seems to be composed by several narrowband interferences instead of a broadband noise. That is why the measurement only gets the interference when the transient perturbation is synchronized with the sweep on the EMI receiver. Due to the short duration of the burst, most of the frequency spectrum captured will be background noise.

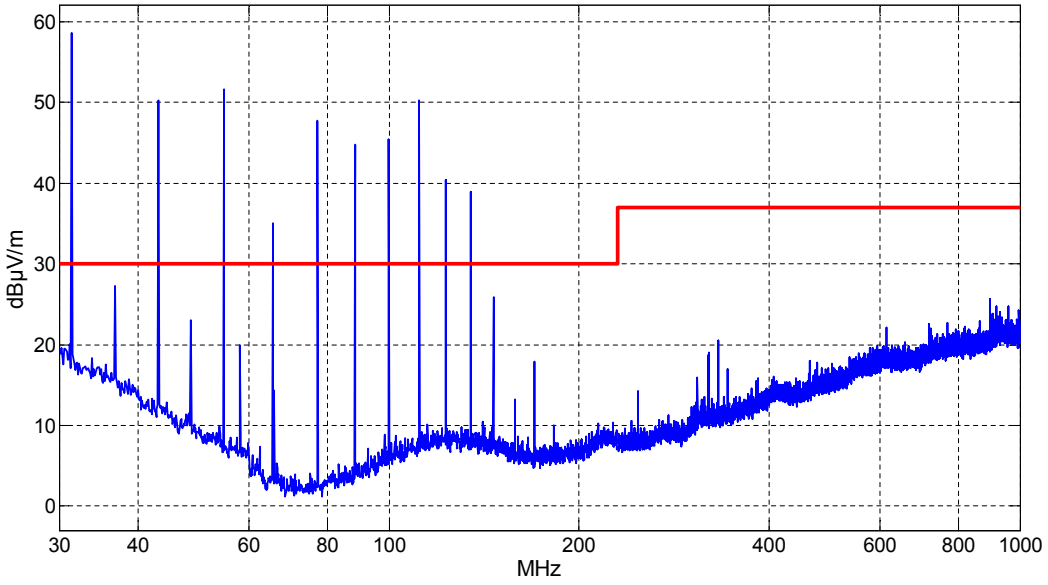

FIGURE 2.1: Radiated transient measurement according to EMC standards.

Secondly, the transient interference must be evaluated employing the detector that it is defined in the EMC standards. The Quasi-Pic (QP) detector is set between the 30 MHz and 1 GHz frequency band measurement. Measurements of different repetition rate interference cases have been carried out employing the QP detector at 54.2 MHz of centre frequency and using the 120 kHz resolution bandwidth which is defined for the full radiated spectrum range (Table 2.1). Contrarily, at the spectrum there are many reserved frequency bands to protect different communication systems. The results obtained show large differences when the quasi-pic detector is employed. However, it is not clear if the differences on the QP measurements are related to the impact that the interference will produce to a digital communication system.

Evaluate the degradation of the communication systems due to transient interference is the goal of the thesis. Therefore, new measurement methodologies out of the EMC standards must be developed. In the next section the basic requirements to carry out a useful measurement of a radiated transient interference are explained in detail.

TABLE 2.1: Peak and Quasi-Peak measurements obtained at 54.2 MHz using a RBW of 120 kHz

Burst frequency	Burst duration	Peak meas (dBuV/m)	QP meas (dBuV/m)
125 kHz	4 ms	52.5	49.2
5 kHz	4 ms	52.4	39.3
1 kHz	4 ms	52.4	29.7

2.2 Requirements to measure transient interferences

There are some shared requirements that all measurements must accomplish to find the degradation that impulsive noise will cause to the communication system. These essential requirements are connected with the intrinsic characteristics of the impulsive noise and also with the final aim of protecting the communication systems. In Figure 2.2 a resume of the essential requirements to perform a proper measurement of the impulsive noise is presented.

2.2.1 Event detection to acquire transient interference

Firstly, if we consider the main parameters of the transient interference, we will achieve some crucial measurement parameters. As it has been discussed in previous chapter, one of the main characteristics of the transient noise is its short duration, which can be some nanoseconds or milliseconds. However, there can be long periods of time between transient events. These long periods of inactivity can be quite short, meaning some hundreds of milliseconds or in other cases several seconds or minutes. This implies the necessity to develop a measurement methodology capable to detect when a transient interference takes place and acquire the short transient interference. Otherwise, the large amount of non-useful data captured will collapse the acquisition system without recording significant data. Standard receivers are based on frequency sweep instrumentation, meaning that the way to get the maximum of the interference is to set the receiver at certain frequency and perform a "maxhold" measurement. Unfortunately, the "maxhold" detection will be non-useful for analysing the effect over digital communication systems. As it has been explained before, the maximum value of the

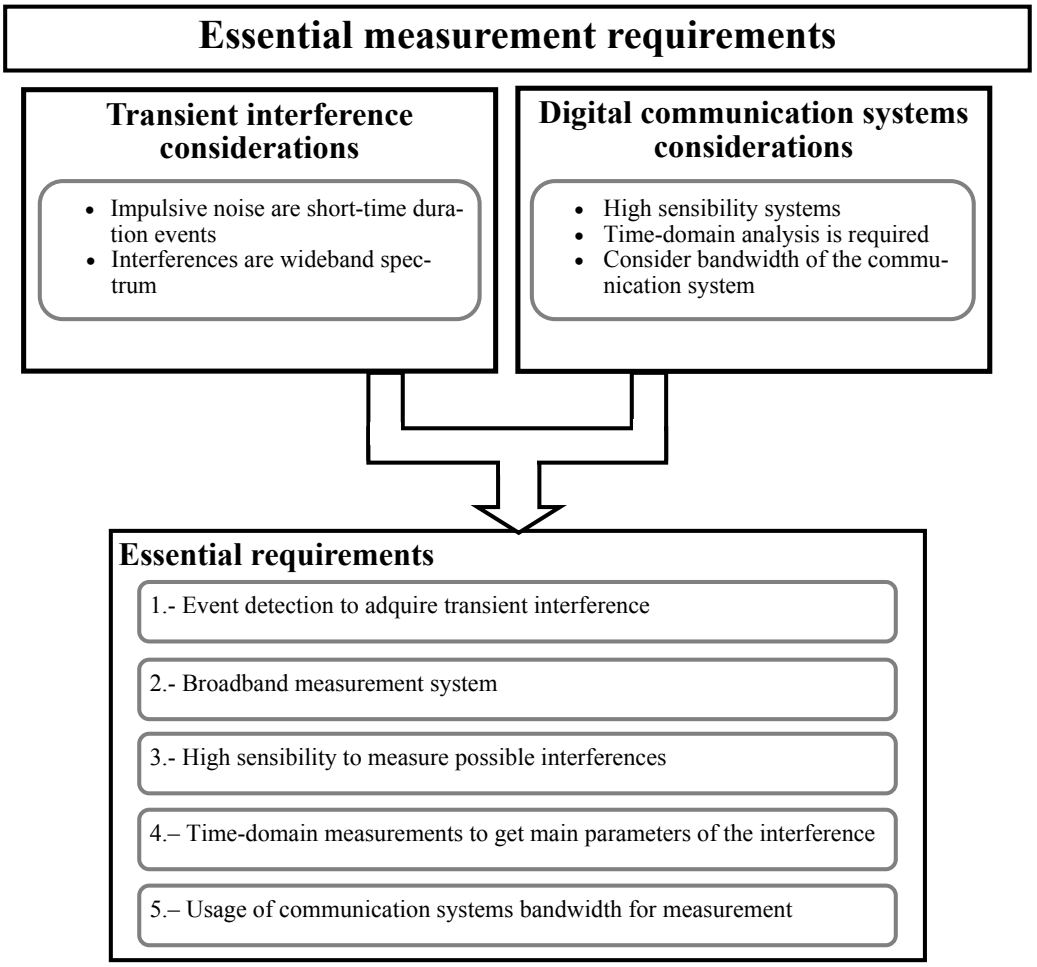

FIGURE 2.2: Schematic of the requirements needed for the measurement methodology considering the transient interfere characteristics and the communication systems parameters.

interference is not enough to estimate if a DCS will be degraded, other parameters of the interference related with time-domain must be measured. To overcome this limitation of event detection some strategy of triggering will be essential, the combination of frequency domain instrumentation such as the EMI receiver and also an oscilloscope could be the way to solve the challenge of event detection.

2.2.2 Broadband measurement system

Regarding the fact that transient interferences are broadband, a single pulse can interfere from DC to several hundreds of megahertz or even some gigahertz. As it has been described in previous chapter, impulsive interferences are classified as Class B noise based on the Middleton approach for non-Gaussian noise. Class

B noise was categorised as interferences that produce significant transients. In generally occurs when the impulsive noise is wider in terms of bandwidth than the receiver bandwidth. This is the case of transient interferences which we want to evaluate. To illustrate the vast occupation of the spectrum produced by impulsive noise, an example can be found below in Figure 2.3.

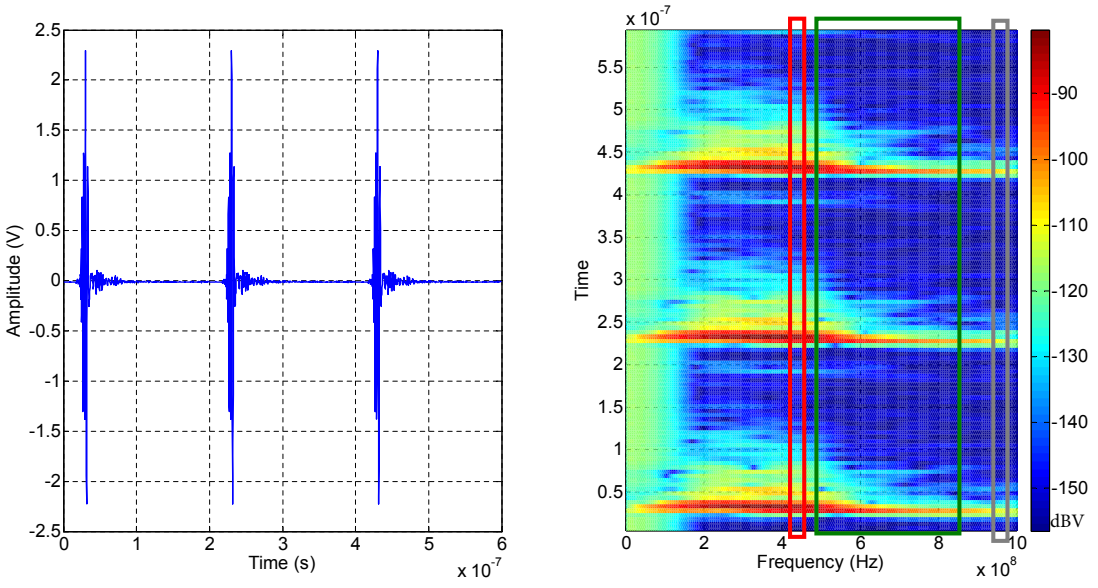

FIGURE 2.3: Time domain transient interference and its computed spectrogram.

In Figure 2.3, the measurement of three pulses in time domain carried out with an oscilloscope are represented. Taking these data as an input, a spectrogram has been computed employing Matlab to highlight how a single pulse can interfere most of the spectrum. The energy of the impulse interference is distributed along the entire spectrum till several hundred of megahertz covering many reserved frequency bands. For instance, in Figure 2.3 some frequency bands have been remarked; in red colour the frequency band of TETRA, in blue the spectrum reserved to Digital Video Broadcasting Terrestrial and finally in grey the reserved frequency band for GSM-R. Regarding this broadband characteristic of the transient interference, another requirement for the measurement system can be established. The measurement system developed must be capable of obtaining the interference impulsive noise at the whole spectrum. If traditional frequency sweep instrumentation is used, as the energy of the impulse noise is distributed along the entire spectrum, the receiver has to be tuned at each desired frequency band. Considering this full-spectrum interference, the radiated transient must be measured at different times when employing the EMI receiver. However, radiated interferences are non-continuous and large time periods can appear between

different transient phenomena. This can be a huge problem when the transient interference is produced randomly and sometimes with many minutes between events. Therefore, the measurement of the full-spectrum will not be performed with the EMI receiver due to time limitations.

2.2.3 Time-domain measurements

In addition to the level of the impulsive interference, other parameters like the repetition rate or the burst duration of the interference have to be measured to quantify the degradation of a DCS. In the past, in analogue communication systems, the Signal to Noise Ratio has been the main figure to evaluate its performance. Therefore, EMC standards limits where related to this SNR and also to human perception degradation quality to establish limits and detectors. To accomplish with this requisite, standard frequency-domain measurements are not suitable because more information is required to protect digital communication. Otherwise, time-domain measurement must be carried out in order to get all the main parameters of the transient interference. As it will be detailed in the next chapter, to perform an accurate analysis of the degradation produced by a transient interference over a digital communication system, it is necessary to measure in time-domain the in-phase (I) and the quadrature (Q) components of the interference. Although the IQ measurement is not implemented in any standard measurement, it will provide the necessary data to evaluate the degradation produced to communication systems in next stages. Consequently, the IQ time-domain measurement of the impulsive noise is included as one of the essential requirements for the developed methodology. Regarding the measurements procedures defined at the EMC standards, there is not any definition outside frequency domain. The advantage to overcome this limitation is that new instrumentation is capable to provide the IQ data to the user. However, some limitations appear associated with the sampling rate offered by receivers and the available memory to store the IQ data. As it is an internal procedure of the instrumentation, it will suppose a strong limitation of the capabilities of the developed methodology. To deal with the memory limitation, it will be necessary as before to perform a triggering technique and also employ time-domain instrumentation to record the transient interference. It will be studied the employment of an oscilloscope used as the receiver of the interference. Otherwise, new capturing procedures will be developed in order to deal with the limitations and to give us more flexibility. Finally, some simulation techniques

can be also considered to reach better results without receiver instrumentation limitations.

2.2.4 Usage of communication system bandwidth for measurements

Another important consideration that it must be noticed is the measured bandwidth. Transient interferences are broadband impulsive noise and the portion of the disturbance falling in the communication bandwidth slot is received by the system as it was useful signal. Therefore, as the signal and the transient interference are in the same frequency band, the interference cannot be filtered to avoid the degradation of the communication system. If a different bandwidth is set, compared with the communication system bandwidth, at the measurement stage an erroneous interference will be acquired. For that reason, another requirement of the developed methodology must be to measure using exactly the same bandwidth as the communication system bandwidth. However, standard instrumentation have only available some resolution bandwidth to be employed at the measurement. For instance, in EMI receivers, the bandwidth available and the defined in standards between 30 MHz and 1 GHz is 120 kHz. Consequently, the receiver must be used in spectrum receiver mode, where more resolution bandwidths can be set. Otherwise, when a resolution bandwidth is far away from the ones available at the instrumentation compared with the communication bandwidth, some post-processing technique must be employed to obtain the measurement. As an example, whereas the bandwidth defined in the DVB-T standard for each channel is 7.2 MHz, the closest resolution bandwidth available at the standard instrumentation is 3 MHz or 10 MHz. Using directly one of the RBW configurable at the instrumentation, would lead to a huge error because the receiver filters are far away from the DCS bandwidth. Therefore, to solve this limitation a post-processing filter stage will be necessary to reduce the amplitude errors produced by measuring with different bandwidths from the communication system specification.

2.2.5 High sensitivity

Continuing with the requirements that must be accomplished by the measurement system, it is time to establish the necessities regarding the concerns that must be

studied to protect the digital communication systems. Firstly, as it is well known, novel digital communication systems work with really weak signals, which can operate properly with signal levels lower than -100 dBm. Consequently, the developed methodology has to reach this level of sensitivity in order to determine when a faint transient interference can produce communication failures. Considering the instrumentation available to carry out EMC standard measurements, it is sufficient to reach the sensitivity requirements set by the digital communication systems. On the other hand, as it has been recently proposed [69–71, 74, 94, 161], time-domain instrumentation will be used to perform an accurate time analysis of the interference. The common used oscilloscopes employ 8 bits A/D converter, which means that sensitivity problems may appear. Therefore, some technique must be employed to manage the sensitivity problem and capture properly the time-domain interference.

2.3 Developed measurement methodologies

Once all requirements to carry out an accurate measurement of transient interferences and its limitations have been identified, it is time to propose a methodology to measure radiated transient interferences.

The goal of the developed time-domain measurement methodology is to obtain the in-phase and quadrature components of the radiated transient interference. In this section, two different measurement techniques have been developed depending on the difficulty of obtaining the IQ data. Both developed procedures fulfill the requirements defined, handling with the limitations perceived.

2.3.1 Basic Methodology

The first methodology to acquire the data coming from the radiated transient interference is based on the procedure described in Figure 2.4. The picture describes how is the interconnection between the different instrumentation to obtain at the end the in-phase and quadrature components of the interference. Regarding the instrumentation needed, an EMI receiver and an oscilloscope are used. The oscilloscope is used to produce a trigger signal to start the measurement recording data by the EMI receiver. Below the methodology is described in detail.

The first element of the measurement system to capture a transient interference which is propagated as an electromagnetic wave is the antenna. Whenever is possible, an antenna identical or equivalent to the current antenna used by the communication system under analysis must be used. In that case, antenna parameters like antenna factor, directivity, impedance, etc. are not relevant since we will be obtaining the same voltage as the communication system would get in the presence of the interference. If a substitutive antenna is employed instead, the measurement obtained could have a large uncertainty due to near field and mutual coupling effects [3, 135]. Consequently, it is highly recommended using only a substitutive antenna when we are measuring the transient interference in far field conditions [15].

In order to make an efficient usage of the instruments acquisition memory, it is indispensable to execute the capture only when a transient reaches the antenna. In a real situation, transients occur randomly and have short duration. If the

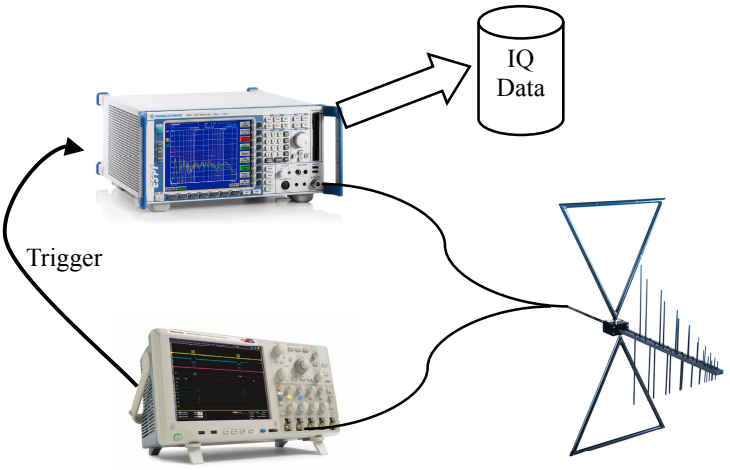

FIGURE 2.4: Schematic of the basic methodology to obtain the IQ data of the transient interference.

instrument used has no trigger circuitry (as usually occurs in Spectrum Analysers or EMI receivers) it would record all the time and most of the acquired data would contain non-useful information about the transient. To overcome this problem, we propose using an oscilloscope that detects when a transient is produced and sends a trigger signal to the measuring instrument. In this way, only useful information will be recorded [140]. Although an oscilloscope can be used for triggering purposes, this instrument cannot be employed for acquisition purposes. The main factors are the low sensitivity and the frequency range of this time-domain instrumentation. However, the lower frequency and higher energy components of the transient will usually be suitable for them to produce a trigger signal by the oscilloscope.

Regarding the sensitivity needed to carry the measurement, the main characteristic of EMI receivers or spectrum analysers is their high sensitivity across the whole frequency range. This measuring performance is important because the communication systems can work properly with very weak signals, so a weak interference in the useful bandwidth could produce significant errors. These instruments also carry out the needed functions of filtering, sampling and demodulation the in-phase and quadrature components as it is shown in Figure 2.5.

The electromagnetic field generated by a transient interference is received by the antenna which is connected directly to EMI receiver and also to the oscilloscope. Following the flow of the interference inside the EMI receiver, the first step is the pre-selection filter where impulse noise is filtered around the centre frequency.

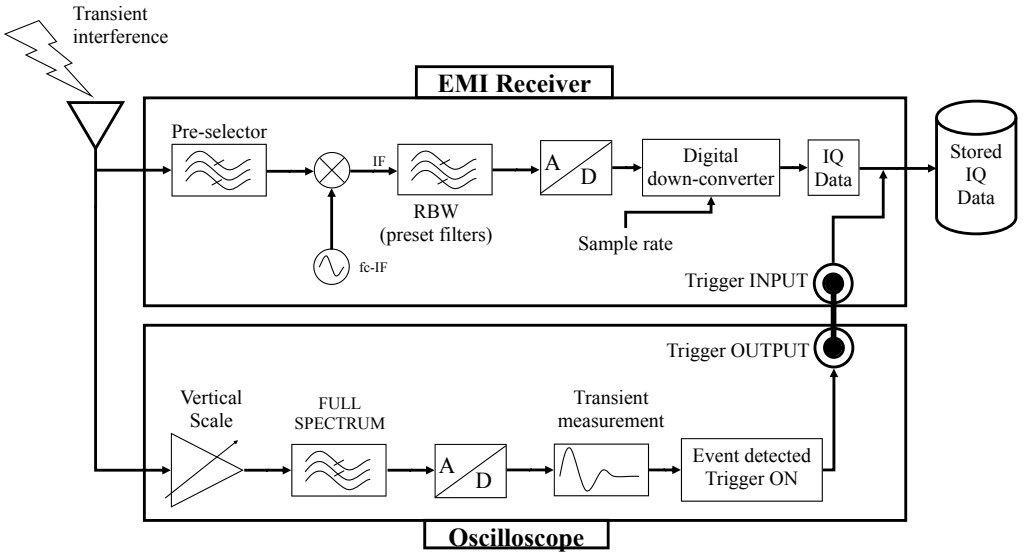

FIGURE 2.5: Schematic of EMI receiver and oscilloscope functions to obtain the IQ data with the basic methodology.

Afterwards, the transient interference is down-converted to the intermediate frequency and filtered by the resolution bandwidth. In this stage of the IQ demodulation procedure, the interference has been filtered at the frequency band of the communication system. The next stage, is to convert the analogue signal to digital in order to get at the final of this procedure the IQ components of the measurement. It is important to notice that this final procedure is really non-configurable by the user. One of the unique parameters that the user can set is when to start to record the IQ signal, which is a key point as it is needed to record only when transient events takes place.

Regarding the path that the transient interference follows at the oscilloscope according to Figure 2.5, first the vertical scale of the oscilloscope is adjusted to capture properly the transient interference. Once the vertical scale is adjusted and the transient is properly seen, the trigger of the oscilloscope must be set to generate a trigger event each time that a transient phenomenon appears. The trigger output of the oscilloscope will produce an input signal to the EMI receiver to start storing the IQ data.

The methodology proposed is a good alternative to measure correctly transient interferences according to the requirement defined. Unfortunately, some problems described below must be solved with the aim of improving the developed methodology to capture the impulsive noise.

The main problems of the presented methodology are the following ones. The number of bandwidth filters is limited by the EMI receiver, for instance, it is not possible to set filters such as 200 kHz employed by GSM-R system or 7.2 MHz bandwidth used by DVB-T. If a larger filter than the communication system is selected, the level of the amplitude will be higher than the interference that would be received by a digital communication system. Otherwise, if the filter is smaller than the bandwidth of the communication system, a better case for the communication system will be evaluated, the level of the interference measured will be lower than in a real equipment situation.

Another important restriction detected is the limited number of sample rates that can be set by the user. It is necessary to sample with a sufficient rate to properly obtain the transient interference to evaluate afterwards the communication system with a simulation. If the sample rate selected is too low, the impulsive noise will be measured partially causing a non-accurate evaluation of the interference impact [99]. Otherwise, if a high sample rate is selected, the memory of the instrumentation will be filled quickly and will not be sufficient to measure the entire transient interference. Therefore, it can be said that the memory of the instrumentation can be an important handicap.

Finally, another undesired effect that appears with this methodology is the mismatch between the antenna and the receiver due to the parallel connection of the oscilloscope. The mismatch effect will produce amplitude measurement errors and also undesired propagation reflections. One way to overcome this problem is to use various antennas; if another antenna is available, it can be used to detect the transient events. This antenna will be connected directly to the oscilloscope just to generate the trigger signal for the EMI receiver.

2.3.2 Advanced Methodology

The second methodology, which has been denoted as the advanced methodology, has the aim to solve the problems detected with the basic methodology previously explained. The procedure of the new approach uses the analogue input stage of the EMI receiver, and the oscilloscope to detect and capture the transient interference. Finally some data processing to obtain the IQ components (Figure 2.6).

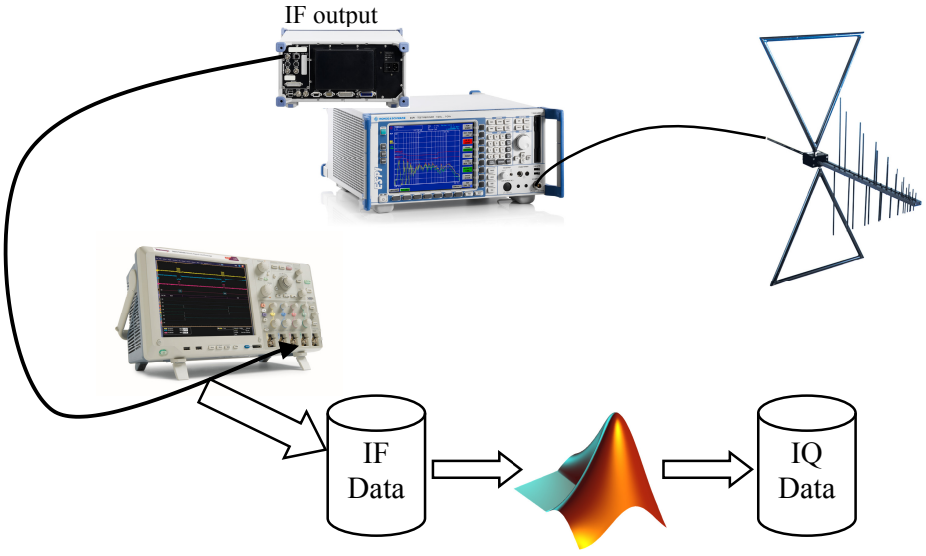

FIGURE 2.6: Schematic of the advanced methodology to obtain the IQ data of the transient interference.

As the above mentioned case, the transient interference is received by an antenna, which can be the same antenna as the communication system or a broadband antenna. While in the previous methodology the antenna was connected to the EMI receiver and also to the oscilloscope, with the new methodology the antenna is connected only to the EMI receiver. Connecting the antenna exclusively to the EMI receiver, the mismatching problematic disappears reducing the possible amplitude errors. Employing the EMI receiver at the first stage of the transient acquisition makes the most of the high sensitivity capabilities of the receiver. The analogue input stage is used to filter the transient interference at the communication frequency band and down-convert it to the intermediate frequency IF. This IF signal is available for the user since there is an output at the rear of EMI receivers and spectrum analysers. The IF output of the EMI receiver is connected to the input of the oscilloscope; which performs the tasks to detect transient events and also to store the IF transient interference. Afterwards, this IF data is post-processed using a mathematical software running in a computer. In this final stage, a post-processing is carried out to obtain the IQ components of the measured impulse noise. In Figure 2.7 a schematic explaining all the different stages is shown.

Regarding the flow of the interference in the advanced methodology, some important differences appear compared with the previous methodology giving to the user more options to implement an accurate measurement of the transient interference. As it has been mentioned before, in this measurement setup, the antenna

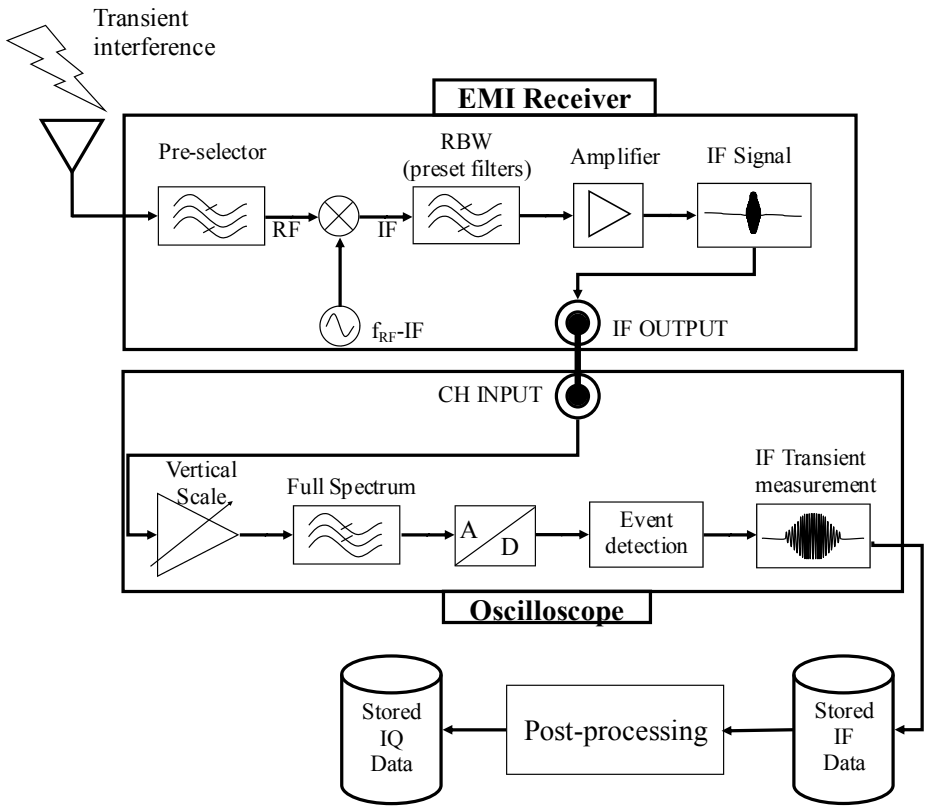

FIGURE 2.7: Schematic of EMI receiver and oscilloscope functions to obtain the IQ data with the advanced methodology.

is connected only to the EMI receiver instead of connecting it also to the oscilloscope for transient event detection. With the new procedure, the event detection is also obtained with the oscilloscope but it is done directly with the IF signal coming from the EMI receiver. The IF signal is reached by filtering the transient noise at the desired frequency band, with the centre frequency set by the user, and employing one the most accurate RBW from the available ones at the EMI receiver. In this occasion, the RBW selected by the user must be larger than the bandwidth of the real time communication systems that is going to be evaluated. For instance, if DVB-T system is the system to be evaluated, at least, a 10 MHz resolution bandwidth has to be configured at the EMI receiver. Regarding the IF signal provided by the receiver, it is amplified and the output level is related to the reference level set at the measurement. Consequently, the sensitivity of the measurement system will be extremely high although the employment of an oscilloscope.

The IF signal coming from the EMI receiver is connected to the oscilloscope to

digitalize it and also to detect when a transient interference is present with the trigger. From the user point of view, many advantages appear using the oscilloscope to deal with the IF signal. Employing the oscilloscope makes easier to digitalize the transient signal at the IF frequency band. The reasons are that the sample rate can be configured between many more options compared with the sample rates available at the EMI receiver; and the oscilloscope also permits to store higher record length compared with EMI receivers. The oscilloscope used in the application described in section 2.4 allows to store 250 million samples, while the EMI receiver only records as long as 130560 samples.

The intermediate frequency of the receiver used in the thesis measurements is centred at 20.4 MHz. Meaning that the output signal is modulated at 20.4 MHz and the bandwidth will be varied by the user selecting the appropriate RBW. The output modulated IF signal is connected directly to the oscilloscope input. Considering that the IF signal is centred at several decades of megahertz it is not necessary to use a high performance oscilloscope. To illustrate the signals that will be produced from a transient interference, a measured impulsive noise is acquired. In Figure 2.8, the impulsive noise which will be received by the antenna is shown.

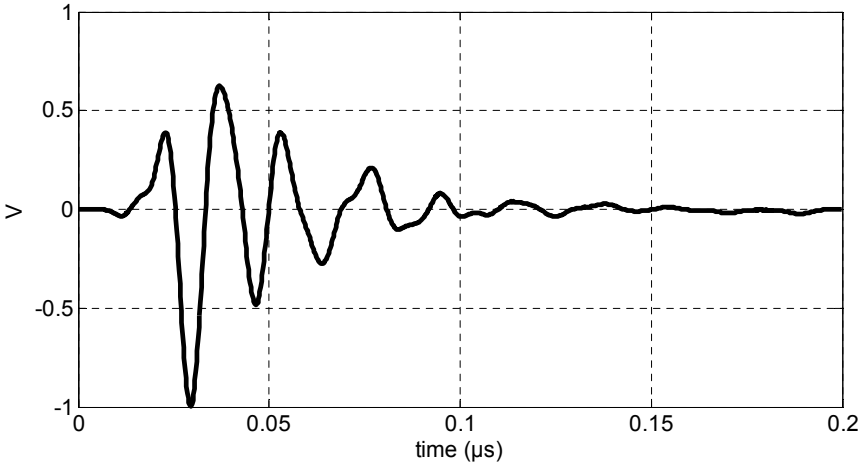

FIGURE 2.8: Time-domain measurement of the transient interference received by the antenna.

The amplitude of the interference is 1.5 Vpp, the duration is less than 1 s and the rise time of the transient is several decades of nanoseconds. If the FFT of the transient interference is computed, the resulting spectrum can be seen in black colour in Figure 2.9. In the spectrum graph, it is observed that the interference has wide-spectrum energy till several hundreds of megahertz. To show and understand the applicability of the methodology, two different frequency bands of the

interference will be analysed. One of the frequency bands is centred at 50 MHz and the bandwidth is set to 3 MHz; the second frequency band is at 70 MHz and employing a lower bandwidth, in this case 1 MHz. In Figure 2.9, in blue colour, it is highlighted the portion of the interference that is filtered by the receiver when it is configured at 50 MHz and with red colour when the receiver is set at 70 MHz.

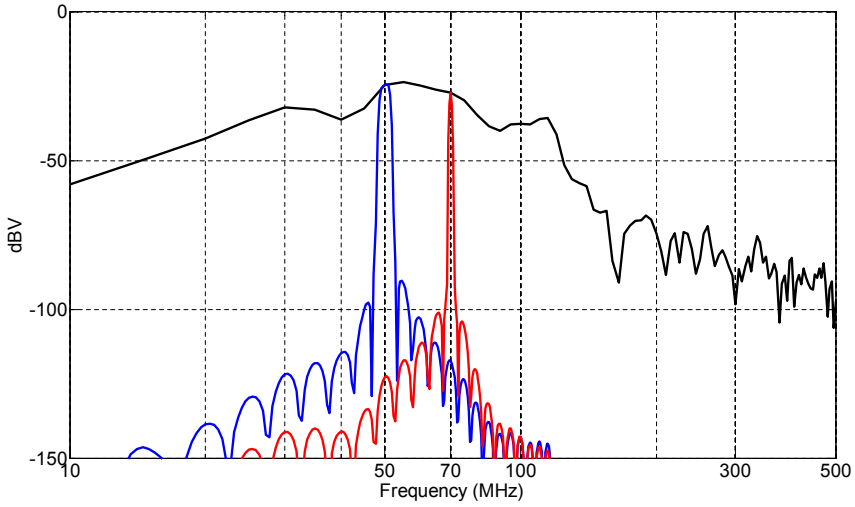

FIGURE 2.9: Spectrum of the transient interference received by the antenna indicating the 50 and 70 MHz components.

Following the schematic described in Figure 2.7, after the broadband interference is filtered in the first stage of the EMI receiver, it is down-converted to the intermediate frequency. In Figure 2.10, the modulated IF signal of each case is shown, in blue the IF output signal that the receiver gives to the oscilloscope for the centre frequency of 50 MHz with a resolution bandwidth of 3 MHz and in red the corresponding IF signal when the receiver has been set at 70 MHz with a RBW of 1 MHz.

The IF signals in time-domain show some important facts that can be emphasized. Firstly, as the input signal has been filtered by a 3 MHz and a 1 MHz bandwidth, the pulse has get wider. If the duration of the input pulse shown in Figure 2.8 is quantified, the interference duration was less than 200 nanoseconds, alternatively when the interference has been filtered its duration has been increased to 2 or 3 s. Moreover, the signal is clearly modulated with the same intermediate frequency for both cases. Considering the spectrum of the signal delivered from the EMI receiver to the oscilloscope, this signal is modulated at 20.4 MHz with different bandwidth. In Figure 2.11, the FFT is computed, emphasising that the spectrum

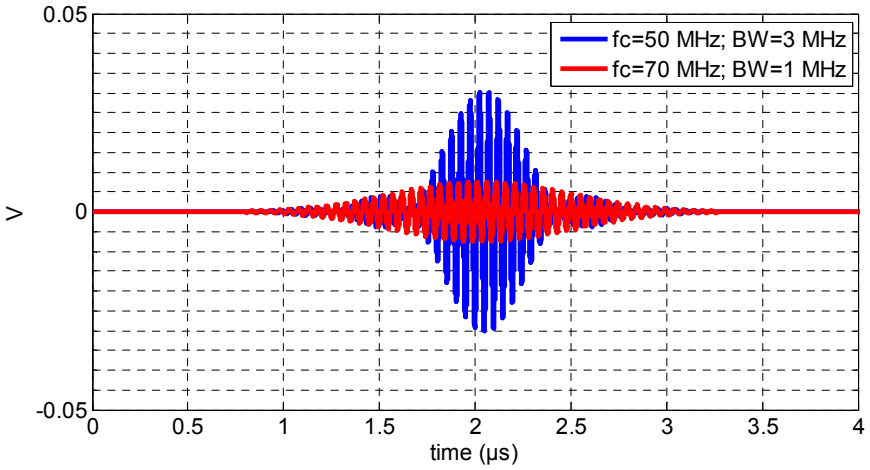

FIGURE 2.10: Time-domain IF signals of the 50 and 70 MHz components.

is centred at 20.4 MHz but the bandwidth for the signal coming from the 50 MHz is 3 MHz and the bandwidth of the 70 MHz signal narrower (1 MHz).

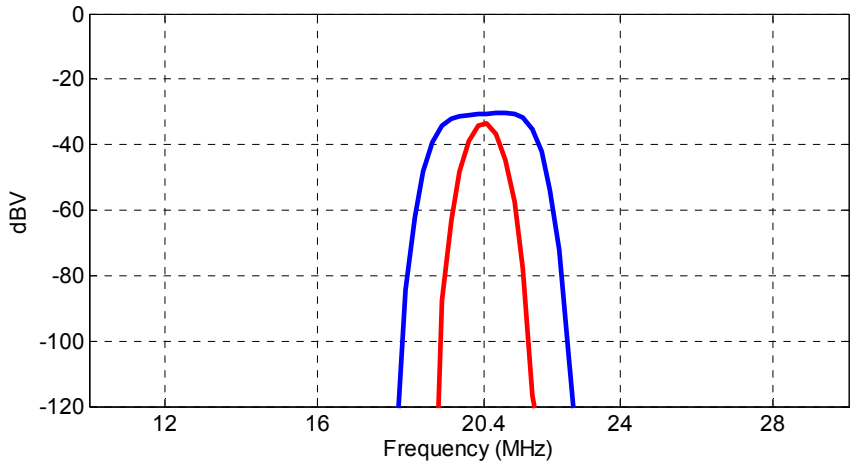

FIGURE 2.11: Spectrum of the IF signals of the 50 and 70 MHz components.

It is important to notice that the oscilloscope will always receive the signal modulated at the intermediate frequency. However, the input IF signal will have different bandwidths according to the RBW set at the EMI receiver. Despite this bandwidth variation, the oscilloscope capture can be easily optimized to reach and store properly the IF signal because the unique parameter that will be changed is the bandwidth of the modulated signal.

Once the IF signal has been acquired, the measurement methodology is able to compute and to obtain the in-phase and quadrature components of the interference. The schematic shown in Figure 2.12 details the post-processing procedure carried out with the IF signal.

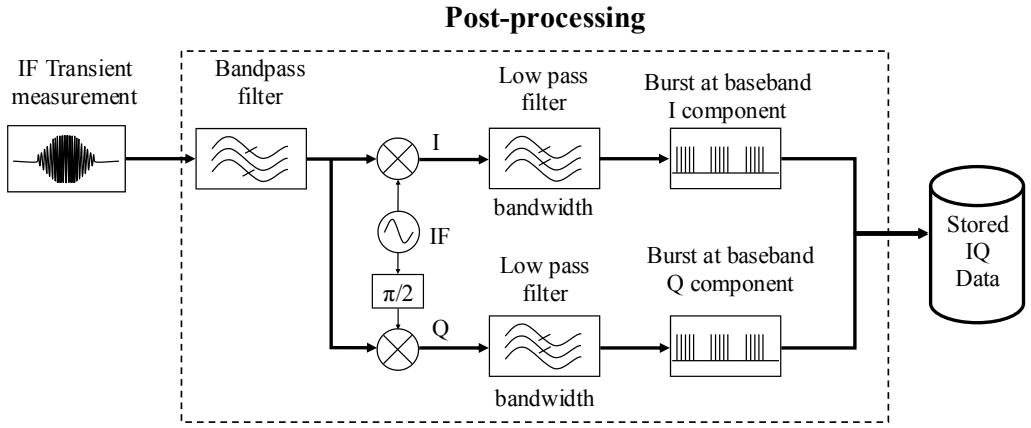

FIGURE 2.12: Schematic of the post-processing to obtain the IQ components of the transient interference.

Firstly, the data is band-pass filtered at the IF centre frequency to filter undesired spurious components. Secondly, the signal is demodulated obtaining the in-phase and quadrature components according to the following equations:

$$i(n) = x(n)cos(2\pi f_{IF}(n)) \tag{2.1}$$

$$q(n) = x(n)sin(2\pi f_{IF}(n)) \tag{2.2}$$

where $x(n)$ is the discrete input signal modulated at the f_{IF} frequency. As an example, the intermediate frequency of the EMI receiver employed in the measurements is 20.4 MHz.

Afterwards, the $i(n)$ and $q(n)$ components of the interference are filtered with a low-pass filter equal to the resolution bandwidth. This is one of the main advantages that offer the advanced methodology, where the bandwidth can be equal to the bandwidth of the communication system. The low-pass filter is adjusted to obtain the portion of the interference that will be received by the DCS. The last stage of the post-processing is to store in a file the IQ data. Furthermore, in order to reduce the file size it could be interesting to resample the data with a lower sample rate. This sample reduction can be done because at the input of the post-processing we had the data modulated at 20.4 MHz and at the end the data is at baseband.

If the post-processing procedure is applied to the example, using the IF input data that can be seen in Figure 2.10, the following IQ components are obtained. For the

dataset of the IF signal related with the frequency-band at 50 MHz, the output IQ components can be seen in Figure 2.13. Otherwise, when the data according to the centre frequency of 70 MHz with a bandwidth of 1 MHz is demodulated, the results are shown in Figure 2.14.

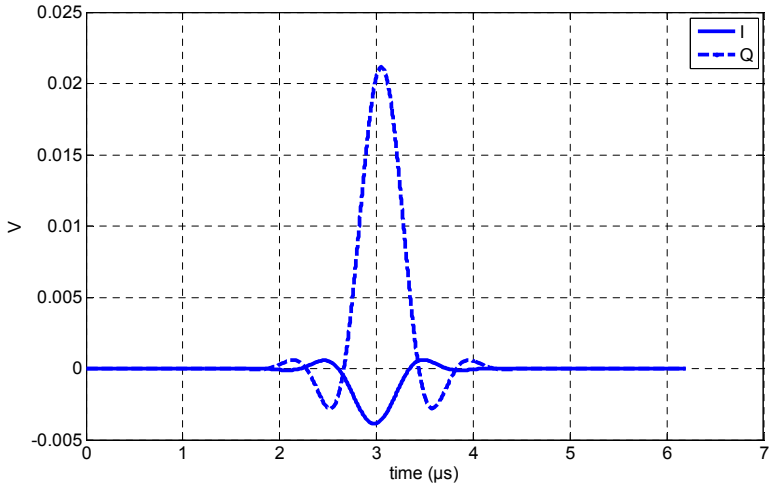

FIGURE 2.13: IQ components of the transient interference at 50 MHz when 3 MHz bandwidth is considered.

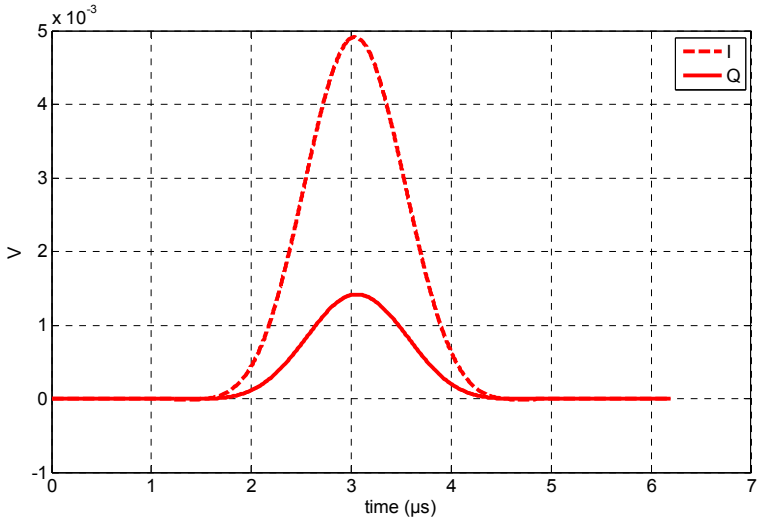

FIGURE 2.14: IQ components of the transient interference at 70 MHz when 1 MHz bandwidth is considered.

2.4 Methodology application

In this section, the methodology developed is applied to measure radiated transient interferences. The aim of the measurements performed below is to obtain the in-phase and quadrature components of the impulsive noise at certain desired frequency bands. The IQ data will be used in the following chapter to predict the impact of the transient interference on a communication system.

2.4.1 Radiated transient measurement

As it has been previously described, one of the main sources of transient interferences are the impulsive noise produced by switching devices. These switching devices are connected along the mains power network and generate transients that are propagated through the wires. Therefore, this radiated impulsive noise reaches the antennas of digital systems which could cause communication malfunctions. In order to evaluate these common scenarios, a test scenario has been built to examine the applicability of the method developed in Figure 2.15.

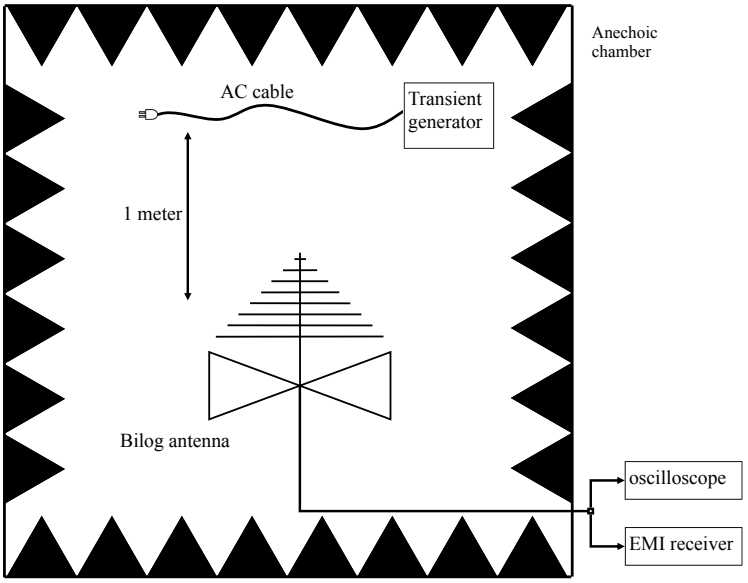

FIGURE 2.15: Transient scenario built to measure radiated transient interferences.

The test scenario built is placed inside an anechoic chamber to ensure that it is only measured the transient noise. The equipment used to generate the burst interference is a Schölder burst generator model SFT 1400, which is used to perform

fast-transient tests defined in the standard EN 61000-4-4 [36]. The fast-transient test is intended to demonstrate the immunity of electrical and electronic equipment subjected to types of transient disturbances such as those originated from switching transients (interruption of inductive loads, relay contact bounce, etc.). Consequently, the transient interference employed in this validation stage of the developed methodologies is a realistic source of interference in a real scenario.

Regarding the main parameters of the transient interference defined in the standard, each pulse of the burst has the shape shown in Figure 2.16, where it is important to highlight the pulse duration 50 ns and the rise time of 5 ns. Indeed, this rise time implies that the spectrum of the pulse interference reaches at least 200 MHz.

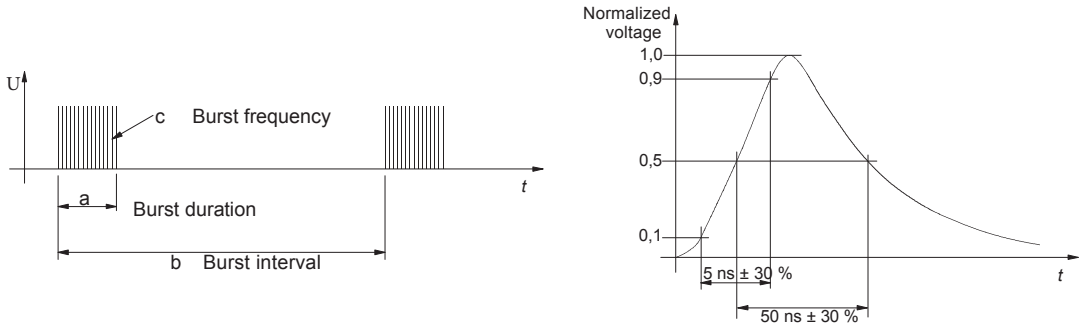

FIGURE 2.16: Transient interference according to EN 61000-4-4 (U: burst level; c: burst frequency; b: burst interval; a: burst duration).

Considering the parameters of the transient interference that must be set according to the standard, the burst frequency is 5 kHz, the duration of the burst is 15 ms and the burst interval is 300 ms. These main parameters defined at the standard will be used in this validation stage to obtain the IQ components at an arbitrary frequency band. The frequency band selected to carry out the measurement is centred at 50 MHz with 3 MHz of bandwidth.

To conduct the transient interference measurements, using both methodologies described in section 2.3, the following instrumentation and setup has been employed. To receive the electromagnetic fields of the radiated interference a Bilog antenna has been placed inside the anechoic chamber. The antenna is connected to the Rohde & Schwarz ESPI3 EMI receiver and the oscilloscope employed is Tektronix DPO7104.

For the setup of the basic methodology, the antenna is connected to the EMI receiver and also to the oscilloscope, the auxiliary output of the oscilloscope is

connected to the external trigger input of the EMI receiver in order to identify transient interference events. The IQ measured data is obtained by means of the IQWizard software [118] developed by R&S. It is really important to emphasize that the EMI receiver can record only 130560 samples and the sample rates are limited.

Regarding the measurements carried out with the advanced methodology, the antenna is connected to the EMI receiver. The intermediate-frequency output of the EMI receiver is connected directly to one of the input channels of the DPO7104 oscilloscope. As it has been discussed before, the oscilloscope permits to record 250 MSamples and the sample-rate can be selected from a larger number compared with the EMI receiver. As an example, if the sample rate is set to 100 MSamples/s the oscilloscope permits to save 2.5 seconds.

2.4.1.1 Measurement employing the basic methodology

When the basic methodology is employed to measure the impulsive noise, the result of the in-phase and quadrature components data is the presented in Figure 2.17. The Sample rate employed in this measurement is 4 MSamples which permits to capture at least the 15 ms burst duration considering that the available samples record length at the EMI receiver is 130560 samples.

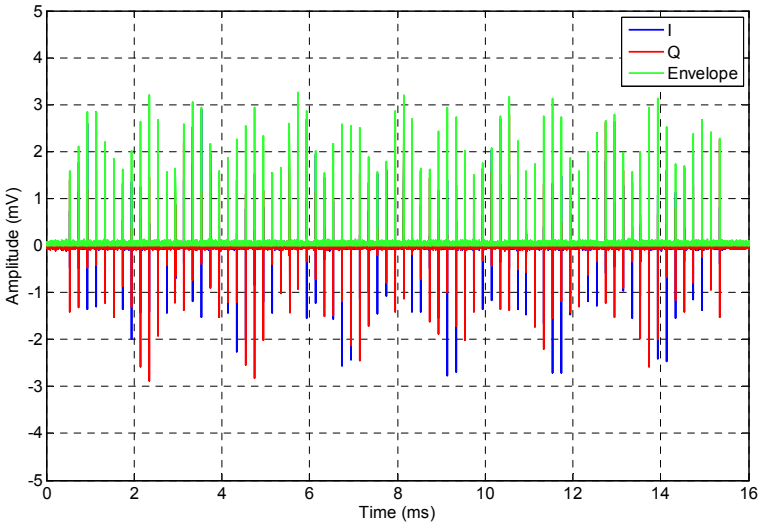

FIGURE 2.17: IQ components measured at 50 MHz, with a 3 MHz RBW obtained with the basic methodology sampling at 4 MSamples/s.

From the results obtained with the basic methodology, it can be shown that the duration of the transient interference is 15 ms and the burst frequency is 5 kHz.

Considering the amplitude measured, the envelope of the interference captured with the basic methodology is not the same for each pulse. This effect on the measurement is directly related with the sample rate that has been selected to capture the entire transient interference. As it has been indicated, the measurement is performed at 50 MHz using a RBW of 3 MHz, therefore the bandwidth of the baseband signal is 3 MHz. Unfortunately, the IQ components are sampled at 4 MSamples/s as we want to capture the full burst, however there is a undersampling effect. Figure 2.18 demonstrate that the IQ components are sampled poorly when the basic methodology is applied.

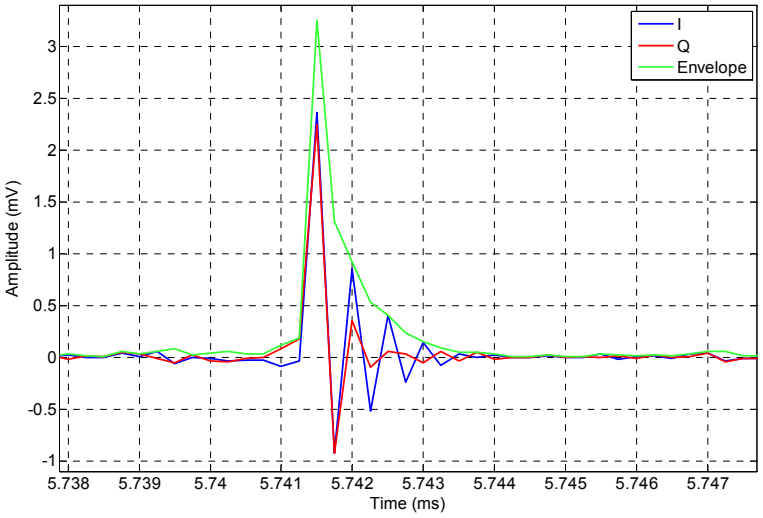

FIGURE 2.18: Zoom view of the IQ components measured at 50 MHz, with a 3 MHz RBW obtained with the basic methodology sampling at 4 MSamples/s.

When the sample rate is reduced to measure a larger time, the IQ components resulting seem to have lower amplitude. We can conclude from the measurement that the available memory to store the transient interference is critical to capture the full transient interference. Sometimes the available memory will be sufficient to capture the interference. However, as we have seen in this example when transient interference has long durations, the EMI receiver memory is not sufficient to capture the entire interference. Therefore, the basic procedure is suitable to carry out an accurate measurement of the interfering noise when it is necessary to record only some milliseconds to evaluate the DCS.

2.4.1.2 Measurement employing the advanced methodology

In the second measurement, the acquisition of the radiated transient shows the advantages that implies the use of the advance methodology in comparison with the basic one. The main limitations of the basic methodology are the sample rate and the total number of samples available at the EMI receiver. Despite the quite good results obtained before, the advanced methodology will show the improvement on the measurement.

As it has been described, with the advanced methodology the captured signal is the output of the IF signal coming from the EMI receiver. The IF signal has been sampled at 100 MSamp/s. The sample rate is selected at 100 MSamp/s because the IF signal is modulated at 20.4 MHz. Therefore, we are sampling at 5 times the bandwidth of the signal. Below it is shown in Figure 2.19 the capture of the IF signal when the EMI receiver is set at 50 MHz of centre frequency with a RBW of 3 MHz.

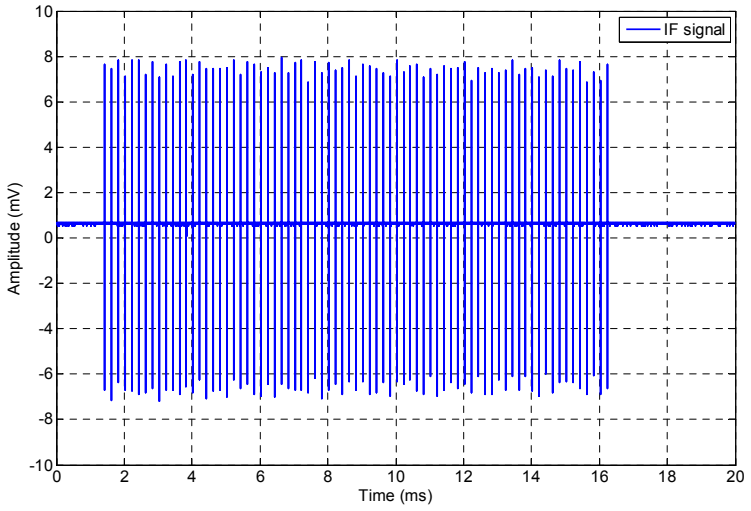

FIGURE 2.19: IF signal measured at 50 MHz employing the advanced methodology.

The total time that can be acquired with this methodology is equal to 2.5 seconds, which is sufficient to view all the transient interference. From the acquisition it can be clearly observed the duration of 15 ms of the radiated transient interference. As it can be seen in Figure 2.20, which is a zoom image of the entire measurement, the captured signal is modulated with the intermediate frequency (20.4 MHz). As it has been sampled at 100 MSamp/s the signal is captured accurately and precise amplitude results will be expected.

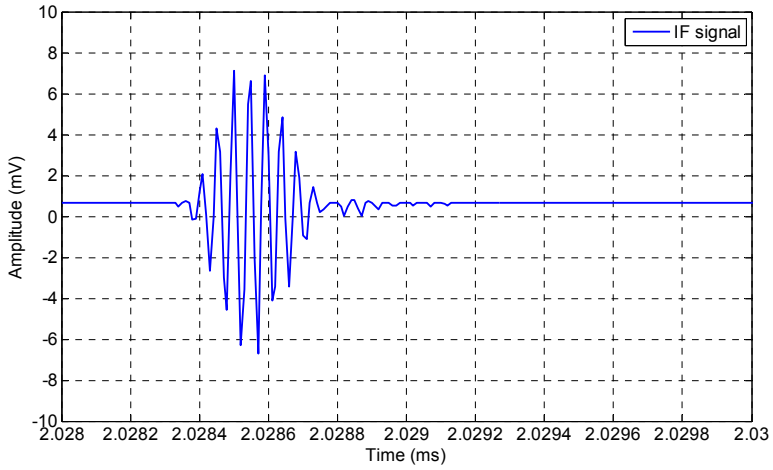

FIGURE 2.20: Zoom of the IF signal of 50 MHz sampling at 100 MSamples/s.

Once the IF signal has been recorded, it is post-processed in a computer using Matlab to finally obtain the in-phase and quadrature components of the radiated transient interference. Next figures (Figure 2.21 and Figure 2.22) show the IQ components demodulated using the advanced methodology, in the figures is clearly observed the high resolution reached at the end of the post-processing.

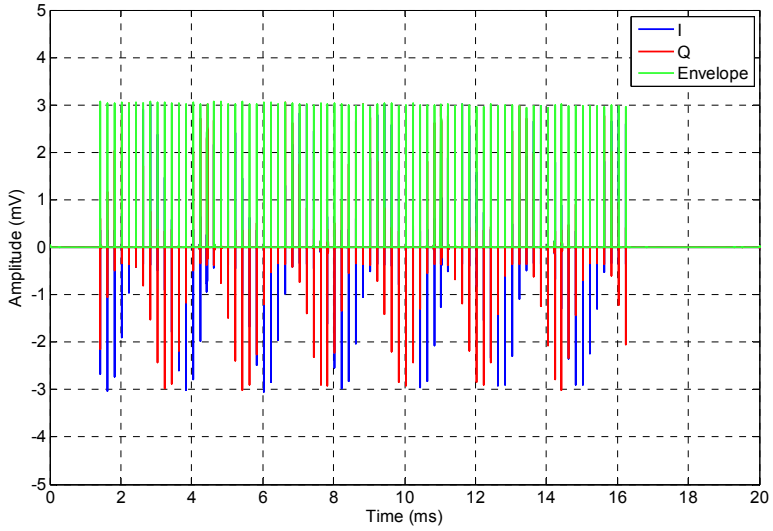

FIGURE 2.21: IQ components measured at 50 MHz obtained with the advanced methodology.

Compared with the results obtained with the basic methodology Figure 2.17, alike previous case the burst frequency of 5 kHz can be easily identified and the duration of 15 ms of the transient interference can be also estimate. However, with the advanced methodology the amplitude of each pulse is equal to 3 mV. A zoom picture of the measurement is shown in Figure 2.22 in order to highlight the quality of the IQ components obtained following the advanced procedure.

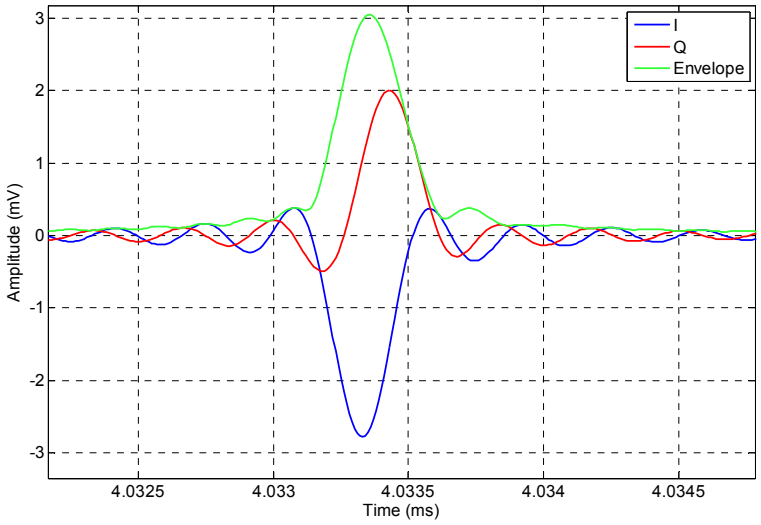

FIGURE 2.22: Zoom view of the IQ components measured at 50 MHz obtained with the advanced methodology.

Finally, another advantage of the advanced methodology is that employing the post-processing procedure the bandwidth can be selected by the user outside the limitations imposed by the EMI receiver. To illustrate the differences that can appear using different bandwidth, the previous measured interference has been filtered employing three different bandwidth filters. The filters selected are 3 MHz, 2 MHz and 1 MHz; it is important to emphasize that the 2 MHz filter is not available at the EMI receivers and cannot be set with the basic methodology. In Figure 2.23 the differences of the resulting envelope is shown using three filters.

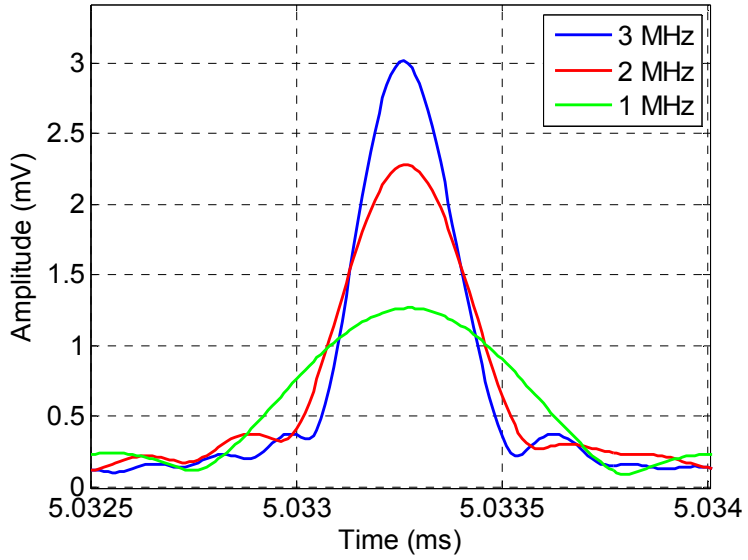

FIGURE 2.23: Amplitude differences observed when 3 MHz, 2MHz and 1 MHz filters are used.

In connection with the amplitude of the measured impulsive noise, when the 3 MHz filter is set the amplitude is approximately the double compared with the 1 MHz filter. Otherwise, the 1 MHz output is is approximately 1 mV lower compared with the 2 MHz filter. Hence, important error difference can appear if the bandwidth set is different from the bandwidth defined by the digital communication system. Additionally, the shape of the transient interference is also modified in time-domain, as the filter is narrower in frequency-domain, the resulting pulse in time-domain will be wider. This is another reason to conclude that it is necessary to measure with the appropiate filter the radiated transient interference. Consequently, the advanced methodology offers an important improvement to capture the interference noise that will interfere the digital communication system.

2.4.2 Measurements related with a RFID system

Once the previous measurement of radiated transient has been done, it is time to carry out measurements to protect a certain real time communication system. The communication system evaluated is an RFID system according to the standard ISO/IEC 14443B [57, 58]. The data obtained with time-domain measurements methodologies will be used in next chapter in order to predict the impact on the RFID system.

The main characteristics of the RFID system communication are the following: the carrier frequency is 13.56 MHz, the modulation is a Binary Phase-Shift Keying (BPSK) and the bit rate and symbol rate is 847.5 kbit/s, so the bandwidth of the communication system is 1.7 MHz.

A real interfering scenario has been built in the lab to observe the response of this RFID system when it is perturbed by a radiated transient. The setup built emulates a real interference situation; many times an RFID system works in close vicinity to many AC main wires. At these power wires there could be a lot of electrical devices connected at some point of the electrical network, producing transient noise that could go through the wires and be propagated reaching the communication systems antenna. The transient noise used as an impulsive source is the burst defined in standard EN 61000-4-4 [36]. The rise time of the pulses generated, according to the standard, is 5 ns; this means that the transient noise has noticeable energy from DC till 200 MHz. For validation purposes different

bursts have been defined; changing the frequency of the burst, the duration and the amplitude of the pulses according to Table 2.2.

TABLE 2.2: Different transient interference applied in the scenario

Level	Burst Frequency (1/c)	Burst interval (b)	Burst duration (a)	Reference
3000 V	125 kHz	200 ms	4 ms	A
3000 V	1 kHz	200 ms	0.01 ms	B
3000 V	5 kHz	200 ms	4 ms	C
3000 V	1 kHz	200 ms	4 ms	D
2000 V	125 kHz	200 ms	4 ms	E

The interferences are coupled to a cable which is not terminated and is 2 m long. The interfered cable is located at the same height as the RFID system antenna; which is 80 cm far away from the middle of it (Figure 2.24). The antenna used to capture the transient signal in this step is identical to the antenna used by an current RFID communication system, so the impedance, the gain and the antenna factor are the same. Therefore, it is not necessary to make any corrections in the measurements regarding these parameters.

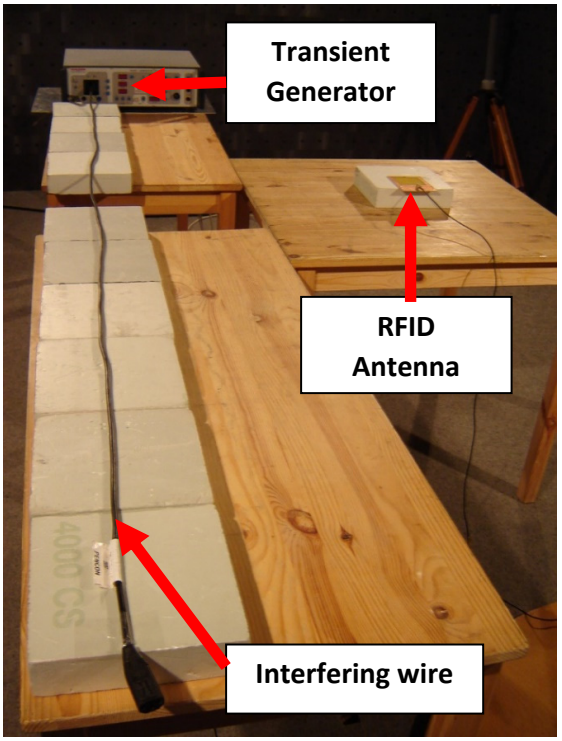

FIGURE 2.24: Interference scenario composed by a generator coupling transients to a wire close to an RFID antenna.

Regarding the methodologies used to carry out the measurements, the basic and advanced methodologies have been used. For the basic procedure, the antenna is connected to the Tektronix DPO7104 oscilloscope and the Rohde & Schwarz ESPI3 EMI receiver and for the advanced one the antenna is coupled only to the receiver. The centre frequency of the EMI receiver is set at 13.56 MHz and the measurement bandwidth must be set according to the communication system. The RBW selected is 3 MHz as it is the closest upper filter to the 1.7 MHz bandwidth. The results obtained with the developed methodology are presented offering an excellent precision.

To start with, measurements employing the basic procedure are illustrate (Figure 2.25). When the basic method is employed quite good results are reached. However some errors on the amplitude appear as the sample rate needed to measure the full burst interference is 4 MSamples.

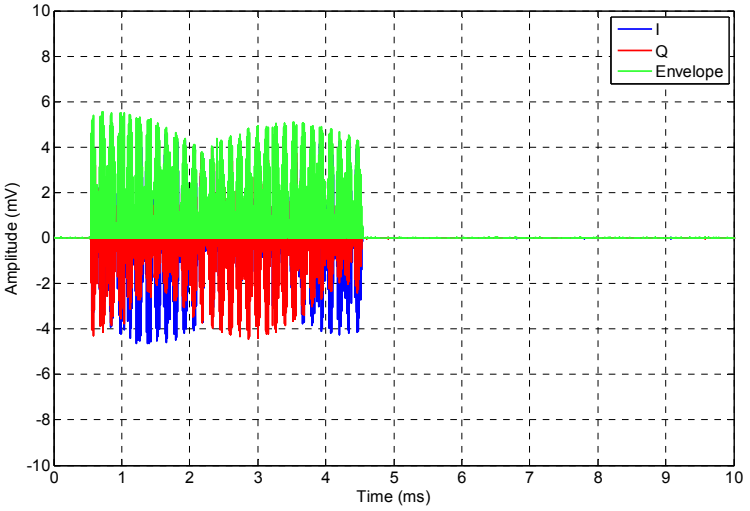

FIGURE 2.25: IQ components measured at 13.56 MHz obtained with the basic methodology.

If a closer look is made to one pulse of the burst interference in Figure 2.26, it is clearly observed that the sample rate is not sufficient to capture properly the IQ components. Moreover, the bandwidth used with the basic methodology was set to 1 MHz as it is the closest to the bandwidth of the RFID communication system. This difference at the selection of the bandwidth also incurs in amplitude error as the bandwidth of the ISO/IEC 14443 type B system is equal to 1.7 MHz.

Measurements employing the advanced methodology has been also performed in order to see the differences with the basic measurement methodology. The first

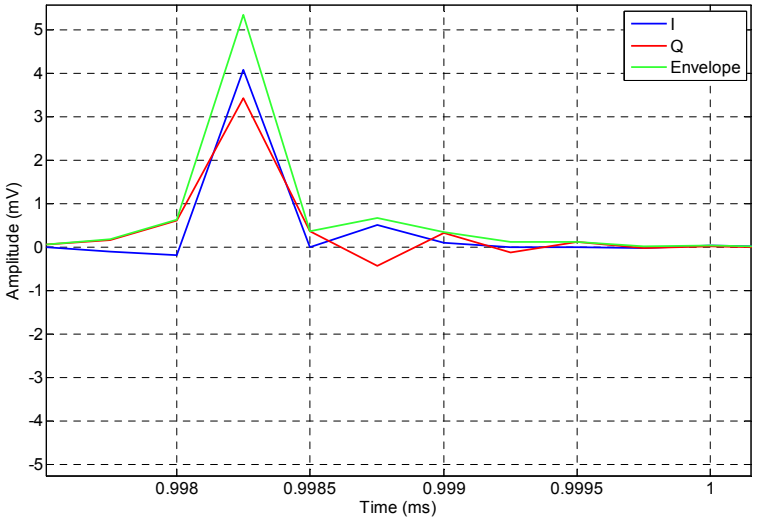

FIGURE 2.26: Zoom of the IQ components measured at 13.56 MHz obtained with the basic methodology.

results shown in Figure 2.27 are the IF signal captured with the oscilloscope when type A interference was coupled to the RFID antenna.

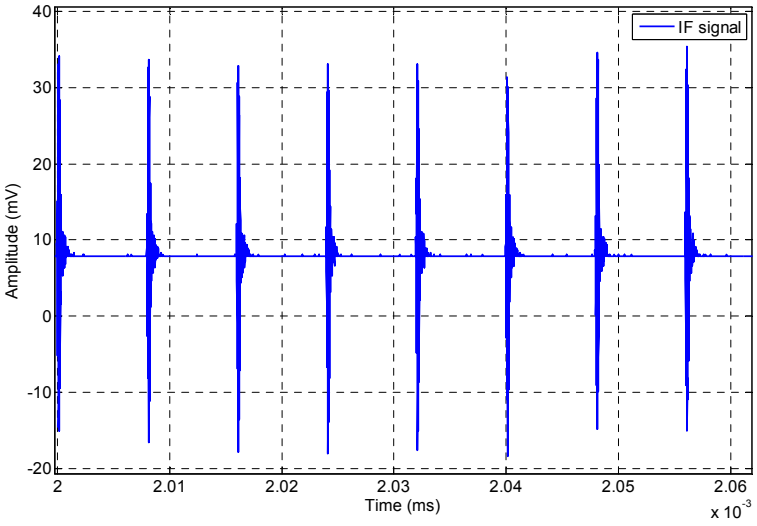

FIGURE 2.27: IF signal measured at 13.56 MHz employing the advanced methodology.

A closer view of one of the IF signal pulses is shown in Figure 2.28, where the 20.4 MHz modulated pulse is observed. The sampled rate used to capture the IF signal has been set to 100 MSamples/s to measure properly the modulated signal.

Afterwards, using the IF signal as the input signal of the post-processing stage, the IQ demodulation of the interference is carried out employing the bandwidth of the communication system. The final results obtained at the end of the advanced

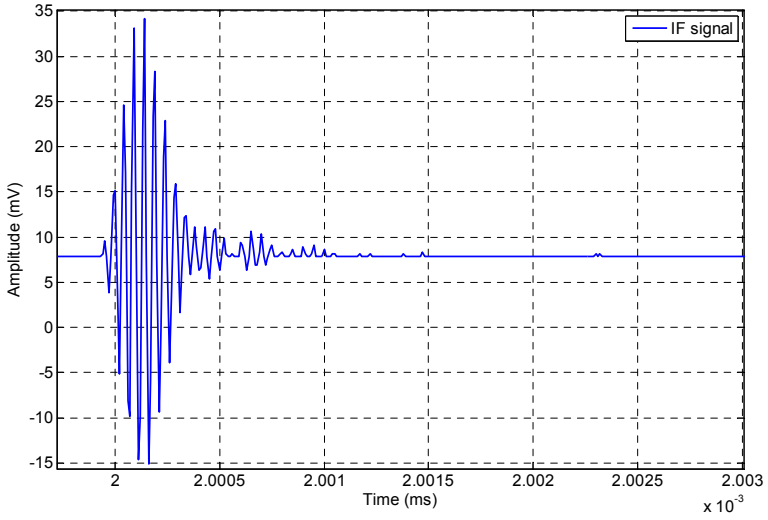

FIGURE 2.28: Zoom of the IF signal at 13.56 MHz sampling at 100 MSamples/s.

methodology are shown in Figure 2.29. The IQ components of the transient interference permits to identify the burst frequency of 125 kHz and the amplitude of all the pulses, which have the same value as expected.

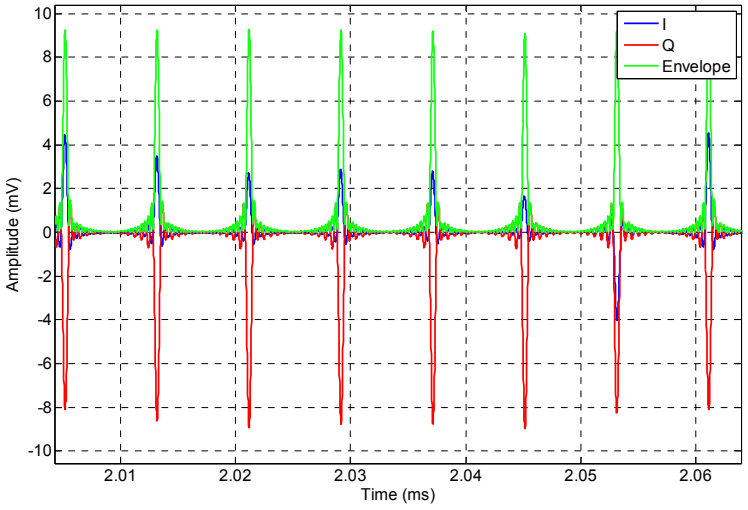

FIGURE 2.29: IQ components measured at 13.56 MHz obtained with the advanced methodology.

In Figure 2.30, a detailed picture of the IQ components demodulated is plotted to show the excellent resolution obtained when the advanced methodology is employed. In the figure, the IQ components and also the amplitude of the interference noise are represented.

With the purpose of using the measured data in the next chapter to evaluate the degradation that it is produced by the radiated transient to the DCS, the

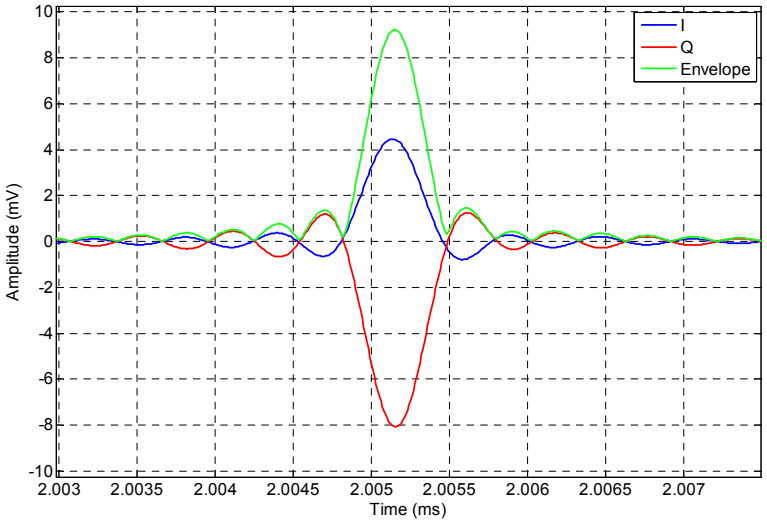

FIGURE 2.30: Zoom of the IQ components measured at 13.56 MHz obtained with the advanced methodology.

advanced methodology has been used to acquire the interferences defined in Table 2.2. In Figure 2.31, it is shown the IQ components of the radiated transients when interferences A, B, C and D are applied to the AC wire. From the results shown, it is easy to interpret that the worst interfering radiated transient noise will be interference A. Moreover, it is observed that in type A, C and D interferences the duration of the burst is 4 ms. Otherwise in type B interference a unique pulse is present. From results it can also be appreciated the different number of pulses that will interfere the communication system; type A interference will be the worst case, the best case will be type B interference and type C interference will be harder than type D noise.

The time-domain information reached is essential to determine the degradation that will produce impulsive noise to digital communication systems. Comparing these results with the frequency domain results given by the standard EMC measurement methodology, the time-domain measurement method developed permits to have much more data to estimate if a digital communication system will be interfered. It is also remarkable that all the transient interference measurement requirements are fulfilled when the advanced methodology is used to carry out the measurements.

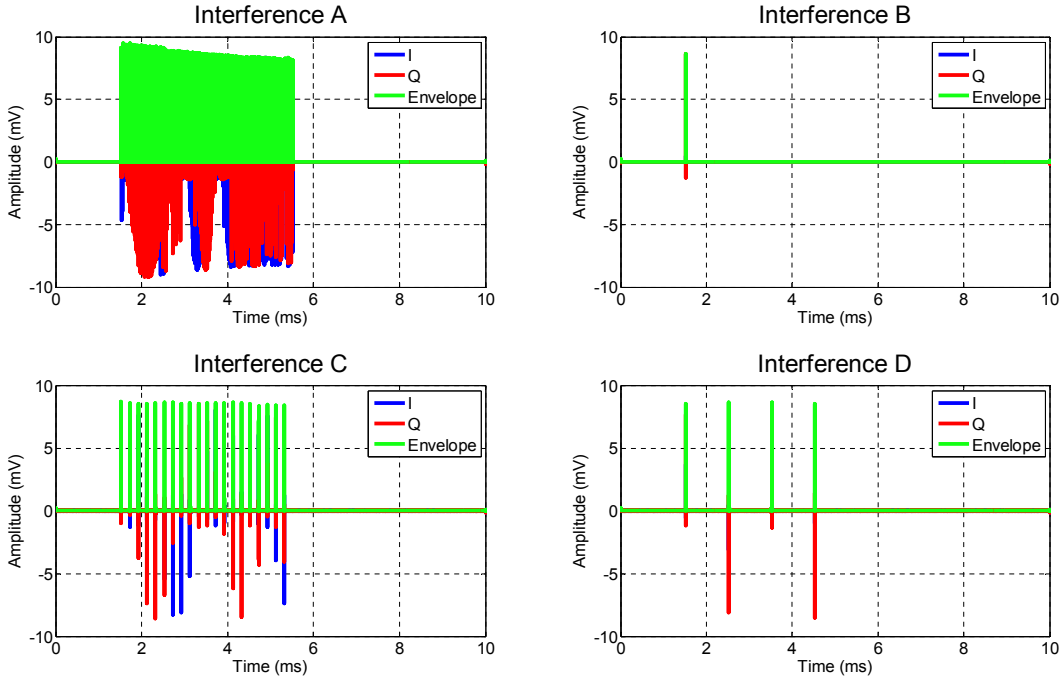

FIGURE 2.31: IQ components measured at 13.56 MHz obtained with the advanced methodology of type A,B,C and D interferences.

Chapter 3

DCS performance evaluation employing TD measurements

3.1 Impact of transient interferences over digital communication systems

As it has been discussed in previous chapters, real-time digital communication systems can be interfered by impulsive noise. With the purpose of quantifying the degradation that may be produced by radiated transient interferences, an evaluation considering previous impulsive noise measurements must be performed.

In digital communication systems, the basic transmission and receiver diagrams are the ones specified in Figure 3.1. The data is modulated in-phase and quadrature at a certain frequency band before it is transmitted. In the information transmission stage, channel impairments could appear produced by different types of noise and propagation effects. The aim of this thesis is to evaluate the degradation caused by impulsive noise when it is present at the channel. From the receiver point of view, the communication system will receive the signal and also the contribution of the transient interference. As it has been described largely in this thesis, transient interference is a broadband noise that covers hundreds or thousands of megahertz. Consequently, the portion of the transient interference that coincides with the communication system band will be considered as useful signal. Both, the signal and the interference will be demodulated by the digital receiver in-phase

and quadrature. Therefore, it is necessary to identify if the superposition of the radiated transient will produce an increase of the number of errors at the digital communication system.

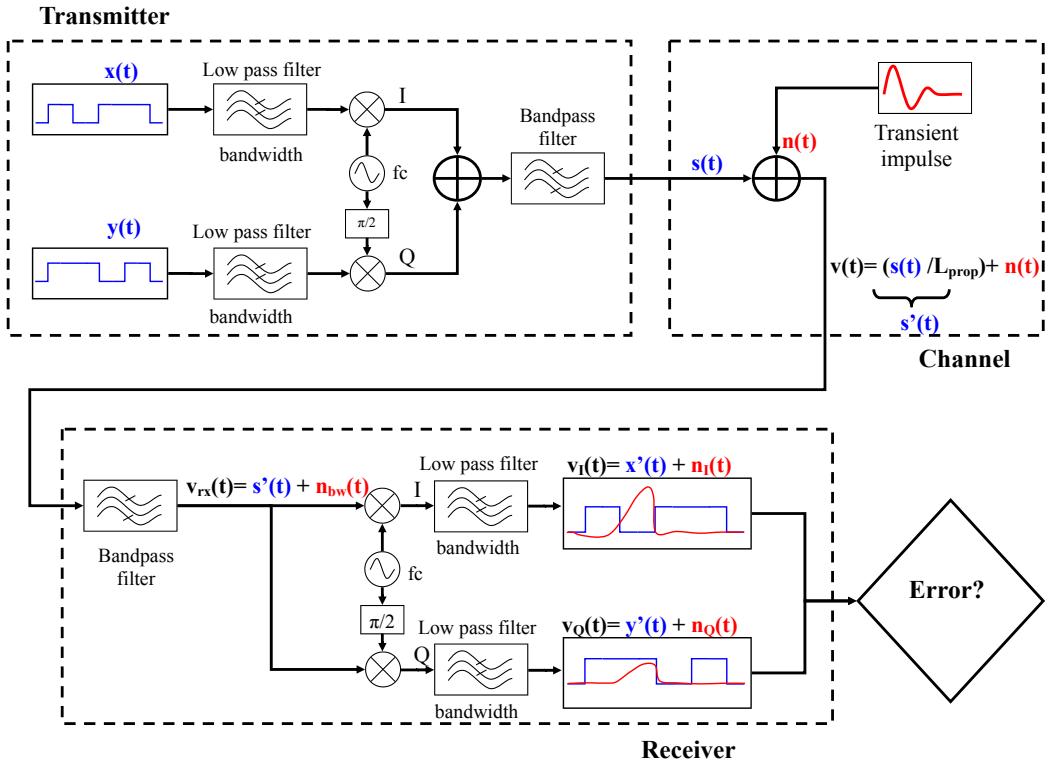

FIGURE 3.1: Transmitting and receiving simplified block diagram including transient interferences.

Regarding the flow of the signal and the interference in Figure 3.1, the main stages are described next. Firstly, the information is split into the in-phase and quadrature components for the digital transmission. The signal transmitted is $s(t)$, which is described in equation 3.1.

$$s(t) = x(t)cos(\omega_c t) - y(t)sin(\omega_c t) \tag{3.1}$$

where ω_c is 2π the carrier frequency of the transmission. When the signal is propagated through the channel, which is the air in radiated communication systems, propagation losses appear. In the case of study the impulsive noise is added as a source of interference. The received signal is formulated according to the following expression:

$$v(t) = \frac{s(t)}{L_{prop}} + n(t) \tag{3.2}$$

Where L_{prop} are the propagation losses and $n(t)$ is the transient interference noise present in the communication channel. Consequently, the signal $v(t)$ will be demodulated in-phase and quadrature at the receiver, and the noise contribution is superposed to the signal. The impulsive noise will be filtered at the frequency band of the communication system, remaining only the spectrum components coexisting with the signal.

$$v_{rx}(t) = \frac{s(t)}{L_{prop}} + n_{bw}(t) \tag{3.3}$$

where $n_{bw}(t)$ is the impulsive noise filtered at the frequency band of the digital communication system. In the next stage, the signal v_{rx} will be demodulated, and the IQ components will be obtained. Therefore the in-phase and quadrature components of the noise will contribute directly to the degradation of the communication system. As it has been mentioned before, to predict the impact of the transient interference, the measurement procedure defined in the previous chapter is employed. Those measurements performed provide us the in-phase and quadrature components of the impulsive noise at the base-band. Hence, the evaluation of the transient interference could be carried out considering the transient interference. Tools extendedly used for digital communication evaluation will be employed to quantify the degradation suffered by the communication system. In the below section 3.2 these tools are explained to show the essential information that can be used in order to estimate with high accuracy the behaviour of the communication system in presence of radiated transients.

3.2 Evaluate the degradation of the communication system

Regarding the harmonized standard according to the EMC Directive, the measurements methodologies do not offer outputs to evaluate properly the degradation of a DCS. It is not possible to predict the impact suffered by a certain communication system when radiated transients are present. Transient interferences are by definition random noise with large periods of inactivity; thus all the measurement methodologies based in continuous interferences are not suitable [120]. Although several studies have unsuccessfully tried to establish a relationship between the

performance of the communication system and some standard measurement detectors, the results were obtained for only some communication systems and just considering a controlled noise.

The main goal of this chapter is to find a methodology that could estimate the degradation produced by any kind of radiated transient interference over any digital communication system. Consequently, to reach this objective other descriptors different from the standard detectors must be identified to determine if a failure of the communication system will occur.

To estimate the performance of digital communication systems computer assisted techniques has been employed since 70's [63]. The bit error rate (or bit error probability) remains like the most common figure of merit for a digital communication system. Computer simulations are often used to estimate the bit error probability in cases where the detection and/or decoding algorithms are too complex to admit useful mathematical expressions. If we consider that the channel needs also to be modeled, the bare mathematical approach becomes unmanageable due to the random characteristics in terms of amplitude, duration, frequency rate and interval of the impulsive noise [5, 22, 48, 66, 76, 89, 110, 112, 146]. The usual approach to overcome the none-model scenarios is to generate N bits, simulate the processing required to transmit and detect these bits. Then, the number of erroneous bit decisions at the output can be counted and the bit error rate is commonly estimated using the following equation 3.4.

$$BER = \frac{\text{number of errors}}{N} \tag{3.4}$$

where N is the total number of bits transmitted. The applicability of the previous method depends in general on the particularities of the modulation scheme and the coding defined by the digital communication system to be evaluated. Decisions are made on a bit-by-bit basis by observing a base-band waveform within each bit interval and comparing the observation to the decision regions (threshold limit). We can consider the simplified relevant block diagram of the binary communications receiver shown in Figure 3.2(a). The decision process can be described in terms of the probability density functions (pdf), $f_0(v,T)$ and $f_1(v,T)$, of the input voltage at the sampling instant T, given that a 'zero' or a 'one' was sent, respectively. These probability densities are plot in Figure 3.2(b), where for a simple threshold-limit, an error will occur when a 'zero' is sent and there is an

interference sufficient to exceed the threshold V_T. Otherwise, an error will also take place when a 'one' is sent and disturbances induce the voltage below V_T. The probability of these occurrences is described with the following equations 3.5 and 3.6.

$$Prob\,[error/one] \triangleq p_1 = \int_{-\infty}^{V_T} f_1(v)dv = F_1(V_T) \tag{3.5}$$

$$Prob\,[error/zero] \triangleq p_0 = \int_{V_T}^{\infty} f_0(v)dv = 1 - F_0(V_T) \tag{3.6}$$

where the functions $F_0(V_T)$ and $F_1(V_T)$ are the cumulative distribution functions (CDF) corresponding to $f_0(v,T)$ and $f_1(v,T)$, respectively. Clearly, all of the necessary information is contained in the distribution functions. It is important to highlight that the significant information of the pdf is inside the 'tails', which are responsible of the erroneous bits. Moreover, heavy-tailed distributions are characteristic pdfs of impulsive interferences [88].

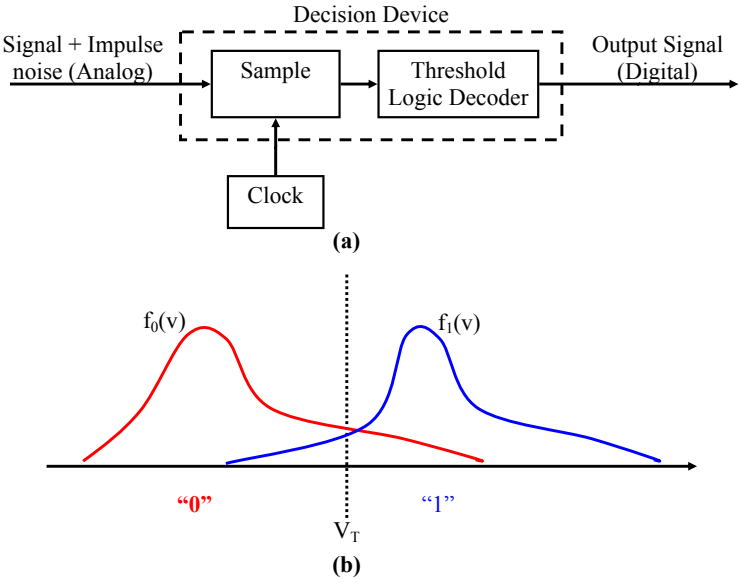

FIGURE 3.2: Illustration of (a) typical decision mechanism and (b) hypothetical pdfs and threshold.

As it has been explained, for a digital radio receiver the bit error probability (BEP) is used to show the impact on the receiver performance when the disturbing noise is present in the channel. The BEP caused by a certain EM disturbance can be

estimated and must be compared to satisfactory requirements. The BEP requirements are strongly related with the service offered by the digital communication system and the Quality of Service (QoS) defined in the standards. Examples of BEP typical requirements are 10^{-3} for speech communication and 10^{-6} for data transfer [136]. Consequently, when the requirements are not fulfilled, a failure of the communication system is considered.

Moreover, if we want to evaluate accurately if a failure of the system can occur, the coding capabilities of the system under evaluation must be also reflected. Modelling the coding capacity of correcting errors must be contemplate on the transmitter-receiver simulation as the data stream includes redundancy to detect and correct errors produced by interferences.

3.3 Methodology employing base-band simulation

The process of the methodology, to quantify the degradation produced by the EMI, is the one described in Figure 3.3. A measured impulsive noise is added in the communication system base-band simulation to evaluate its impact. The data is coded and modulated before the impulsive noise is superposed simulating the effect that it is produced at the communication channel. Once the signal and the interference have been combined, the resulting signal is demodulated and decoded also by means of the base-band simulation. At the last stage of the simulation, the received data which is interfered by the impulsive noise is obtained. Finally, a comparison of the transmitted and received data is carried out in order to establish the degradation that it is produced by the radiated transient interference. If the degradation is above the specifications defined by the communication system, a failure of the system will be considered. On the other hand, if non-error is present or the BEP is within the specifications defined by the communication system standard, it will be concluded that the impulsive interference previously measured is not sufficient to disturb the digital system. Furthermore, the simulation permits us to observe different useful tools such as the BER, the cdf, or constellation diagram in order to understand the impact of the radiated interference over the digital communication system.

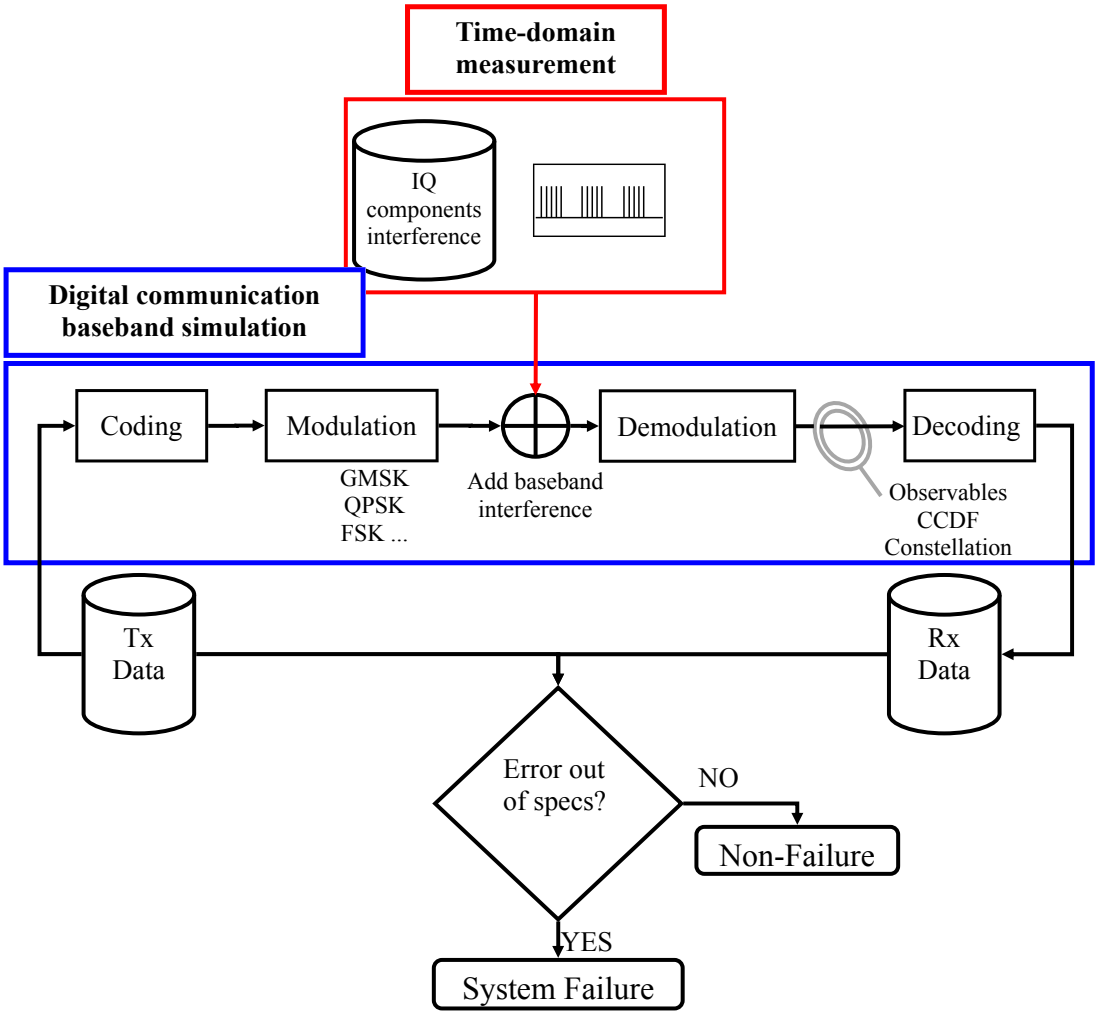

FIGURE 3.3: Block diagram of the methodology developed to predict the impact of impulsive noise.

3.3.1 Measured impulsive interference

From the first stage of the methodology it can be concluded that a properly measurement of the transient interference is a crucial fact to reach satisfactory results. Additionally, the measurement must be obtained in base-band with the purpose to simulate the effect that is produced inside the receiver where the signal and the interference are band-pass filtered and down-converted. Fortunately, in the previous chapter, the methodology defined and employed has shown excellent results capturing several radiated transient interferences. Measurement examples can be found in Figure 2.31 plotted in the previous chapter. Therefore, the in-phase and quadrature components of the impulsive noise are available to use it at the base-band communication system simulation.

3.3.2 Base-band simulation

Regarding the base-band simulation, several stages and parameters must be carefully modelled to obtain suitable results at the end of the procedure. It is necessary to study the parameters of the RTC system in order to perform a proper simulation and achieve successful results. Communication parameters such as modulation type, symbol rate, codification and sensitivity are necessary in this stage. Concerning the modulation, the data can be modulated onto a carrier by changing the amplitude or the phase according to different modulation techniques applied (i.e., QPSK, MSK, GMSK). Moreover, each of these modulations could use TDMA, FDMA, CDMA or OFDM multiplexing techniques. As it has been mentioned before, modelling the communication system through all of its parameters is essential, for instance, OFDM systems are robust against short-time pulsed interference 3.4.

To carry out the simulations of the communication system at base-band, commercial applications like WinIQSIM [119], Advanced Design System (ADS) [65] or *Simulink*® [83] can be used. The interference degradation is evaluated modelling the communication signal and introducing the data of the transient captured beforehand. Besides, these software tools allow us to analyse the most common communications parameters such as BER, CDF, the constellation, the vector diagram, eye diagram, etc. Using results observation we are able to estimate any error that may be produced in the communication system.

As it has been described in the previous section to quantify the degradation produced, the BER is the main figure. Additionally, when a simulation of the digital communication system is carried out, the user has the capability to observe different communication analysis tools which provide really useful information. As an example, the constellation diagram tool permits us to distinguish the received symbols that are outside the theoretical transmitted symbols. If the represented points of the constellation diagram fall in another decision zone, a decision error will be produced. Another useful tool is the vector diagram that shows us if transitions between symbols go further than the decision zone limit. This tool is essential to know if a transient interference has enough energy to change the value of a symbol and produce errors. For instance, a transient interference will add a new path over the vector diagram different from the theoretical transitions. Going on with the tools available, the eye diagram displays the signal superimposed on

itself many times providing qualitative information. An open eye pattern (the eye width and eye height as large as possible) corresponds to a minimal signal distortion. The distortion of the signal waveform due to inter-symbol interference and other type of interference appears as a closure of the eye pattern. Moreover, it is also possible to observe if the amplitude of the transient signal is high enough to interfere the communication system.

Finally, the BER performance of communication systems can be directly obtained from the CDF [141] as it has been mentioned in section 3.2. Therefore, the cumulative distribution function diagrams are really useful to detect and quantify interference scenarios [50].

3.4 Application of the methodology to evaluate the degradation on the RFID system

The methodology described in this chapter is applied to the scenario defined previously at the measurement chapter (Chapter 2). In section 2.4.2 an interference setup was built in order to emulate the radiated interference produced in a power supply cable that could disturb a RFID system.

3.4.1 Base-band simulation employing transient measurements

Regarding the interferences that should be added in the base-band simulation to predict the degradation that will suffer the RFID system, time-domain measurement have been carried out previously. Measurements were performed applying the developed advanced methodology explained in section 2.3.2, to acquire properly the radiated transient interference. The acquisitions of the different impulsive noise generated can be seen in Figure 2.21 of the previous chapter. As it is explained in section 2.4.2 the results are obtained for five different type of interferences defined in Table 2.2.

Once the interference portion of the transient has been obtained, the next step is to conduct the base-band simulation of the communication system. The main characteristics of the RFID system communication are: the modulation is a Binary

Phase-Shift Keying (BPSK) and the bit rate and symbol rate are 847.5 kbit/s so the bandwidth of the communication system is 1.7 MHz. BPSK is the simplest form of Phase-Shift Keying (PSK), it uses two phases which are separated by 180 °. The distortion produced by the five different types of considered bursts is evaluated using WinIQSIM software. To simulate a worse case, the level of the signal is equal to the sensitivity of the communication system, which is 5 mV. Finally, the following essential communication tools are employed to quantify and understand the degradation produced by the different radiated transient interferences: the constellation in Figure 3.4, the in-phase and quadrature signals in Figure 3.5, the eye diagram in Figure 3.6 and also the vector diagram in Figure 3.7.

Figure 3.4 shows the constellation diagram for an interference free system and the five type of burst, when a 5,000 symbol transmission is simulated. As it can be clearly seen from Figure 3.4, when the frequency of the radiated noise is increased, a higher degradation is produced on the constellation diagram. Additionally, it is observed that interfered symbols are capable to change from BPSK "1" symbol decision zone to the "-1" zone causing bit errors.

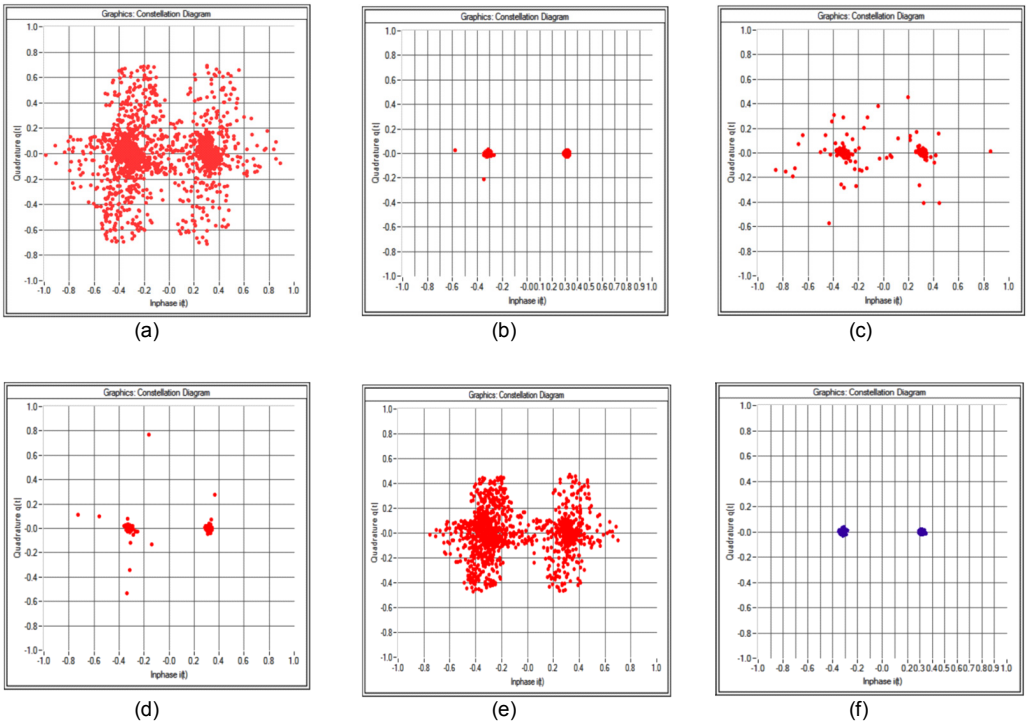

FIGURE 3.4: Constellation diagram for the five interfering signals: A (4a), B (4b), C (4c), D (4d), and E (4e) and interference free system (5f).

In Figure 3.5, symbols are represented in time-domain to view and identify the impulsive noise. The in-phase and quadrature signals are represented when the

system is free from interference and when three of the interfering signals are applied. The plotted interferences are type A, B and C. In Figure 3.5, the magnitude and the frequency of the transient interference can be observed. When the burst frequency is increased more bits of the digital communication system are interfered generating a higher BER. Moreover, it is also important to emphasize that the level of the transient interference will produce errors because it has enough energy to disturb the transmitted bits.

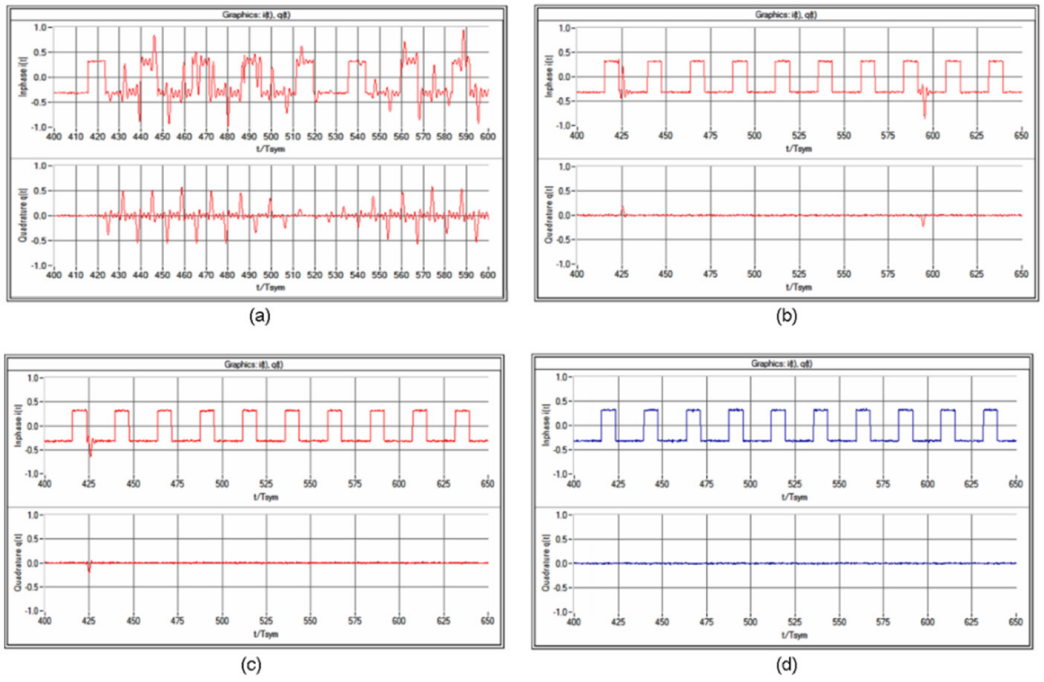

FIGURE 3.5: I(t) q(t) signal when transient type A (a) , type B (c) and type C (b) are analysed with the communication software. I(t) Q(t) signal for interference free system (d).

In Figure 3.6 the eye diagrams for the interferences type A, B and C are represented. As an example, the superimposed signals show that when the burst repetition is equal to 125 kHz the eye pattern is extremely closed involving a relevant distortion of the digital communication system (Figure 3.6(a)).

Finally, in Figure 3.7 the vector diagram is shown. When non-interference is present, the transitions between the two symbols of the communication system is a straight line. Otherwise, when interferences with high burst frequency are evaluated, the signal is affected creating erroneous trajectories between symbols that will cause errors in the communication link.

Below, a more accurate analysis of each of the interferences is carried out to explain and quantify the degradation produced at the communication system.

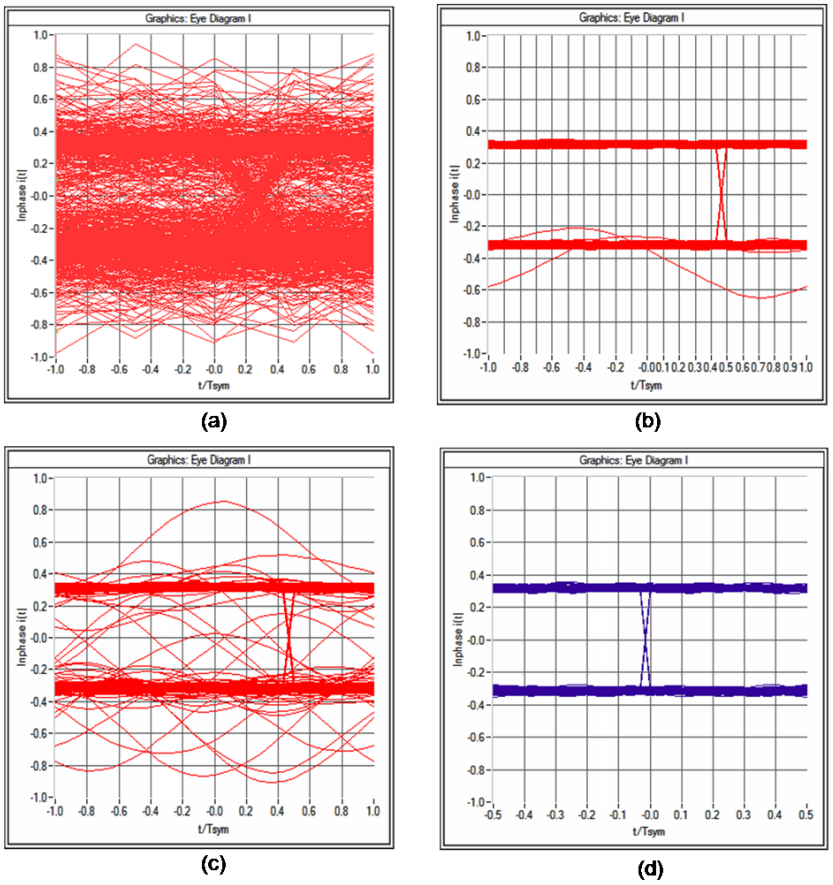

FIGURE 3.6: Eye diagram when transient type A (a) , type B (b) and type C (c) are analysed with the communication software. I(t) q(t) signal for interference free system (d).

3.4.1.1 Type A interference evaluation

The first interference analysed is type A, according to Table 2.2 in Chapter 2, which has a level of 3 kV, a frequency of 125 kHz, a duration of 4 ms and an interval of 200 ms. This measured interference is added to study the influence of this transient on the useful signal. A 5,000 symbol transmission is simulated to check if the interference produces degradation by the constellation diagram. As shown in Figure 3.4a, the constellation suffers an obvious large degradation. Therefore it can be concluded that this transient would produce errors at the system reception. In the constellation diagram we observe that many points are in the region near the decision frontier which will cause decision errors. The effect of the burst in the communication signal can also be analysed by observing the in-phase and the quadrature signal. Each transient pulse produce changes in the amplitude value of both components thus modifying the digital value (Figure 3.5a). In Figure 3.6a it is shown that the eye width and the eye height are almost nonexistent in presence

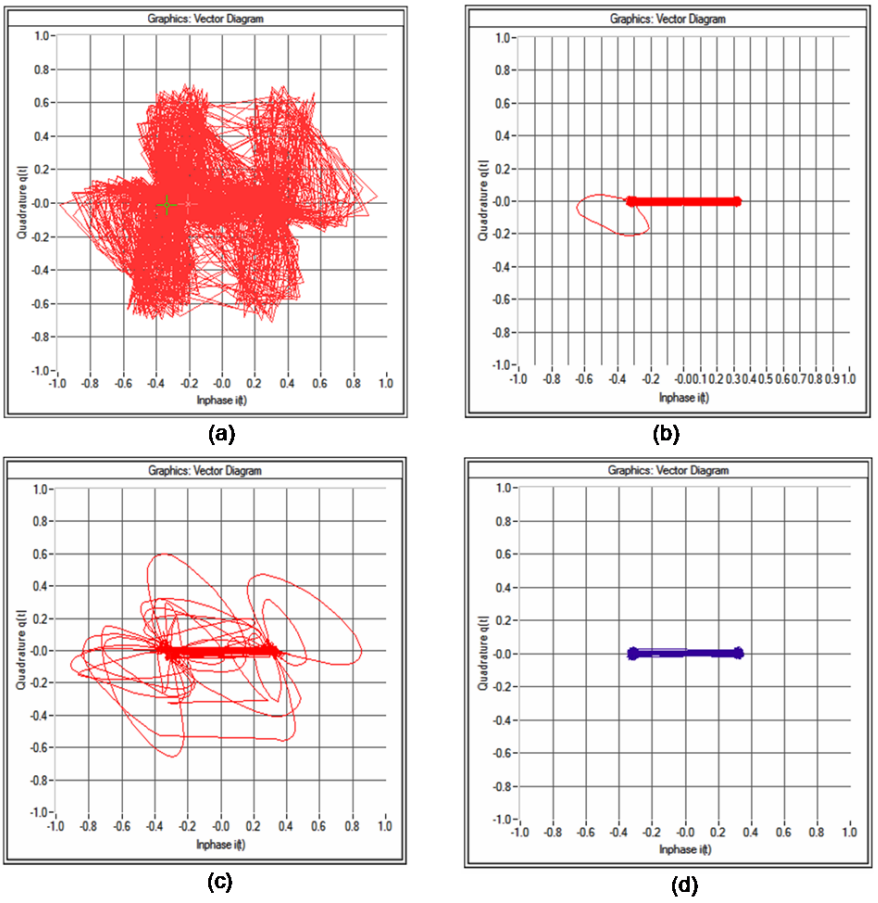

FIGURE 3.7: Vector diagram when transient type A (a) , type B (b) and type C (c) are analysed with the communication software. I(t) q(t) signal for interference free system (d).

of interference so we can conclude that this kind of transient will produce severe errors in the communication. Regarding the BER obtained with the transition of the signal, when 5000 symbols are transmitted type A interference produces a BER of 14%.

3.4.1.2 Type B interference evaluation

Comparing the parameters of type B interference with the type A interference, the level of the burst is the same (3 kV) but the burst has lower duration (0.01 ms) and also lower frequency (1 kHz). The same simulation than before has been carried out evaluating 5,000 symbols.

If we analyse the communication system in presence of the transient interference, we observe in the constellation diagram (Figure 3.4b) that just two decision errors could be produced by type B interference. Consequently, the BER obtained when transient B is added to the channel is 0.04%. This means that most of the communications data are received without any error. Regarding the in-phase signal and the quadrature signal, we observe only small changes. In a range of 250 transmitted symbols, we distinguish only a single transient (Figure 3.5b).

The eye diagram shown in Figure 3.6 corroborates the low influence that the type B transient has in the communication system. We can see that the diagram obtained when type B interference is present (Figure 3.6b) is similar to the interference free situation (Figure 3.6d). Also, the information provided by the vector diagram (Figure 3.7b) shows that the interfering burst produces only one path different from theoretical transitions between symbols. Therefore, it can be concluded that the degradation introduced by the transient type B is very low due to the short burst duration and the low burst frequency of the pulses.

3.4.1.3 Type C interference evaluation

Type C transient has the same level than the previous cases but in this case the frequency is set to 5 kHz and the duration is 4 ms. Burst duration is the same than in type A interference and the burst frequency is between type A and type B interference burst frequency.

In the constellation diagram (Figure 3.4c), it can be seen that many points of the constellation appear outside of the theoretical points of the BPSK modulation (Figure 3.4f). In addition, many points are close to decision zones limit, so decision errors will appear. The BER produced by type B interference determined by observing the 5,000 symbols simulation is 1.08%. The eye diagram of the type C case (Figure 3.6c) shows the transient signal clearly, where it is noted that the transient implies an exchange between the low and the high levels. These jumps produce decision errors as it has been appreciated from the BER results. The transitions between all the simulated symbols can be observed in the vector diagram (Figure 3.7c), when a transient phenomenon occurs it can be easily detected because it produce curved lines.

3.4.1.4 Type D interference evaluation

Type D interference has 1 kHz burst frequency and a burst duration of 4 ms. The same procedure as in the previous interference types is performed to obtain the errors produced by type D transient interference. From the constellation diagram, Figure 3.4d, it is concluded that the interference affects the RFID system. This time, the interfered symbols are less than type A and type C transients and the bit error rate is reduced to 0.14%.

3.4.1.5 Type E interference evaluation

Finally, type E interference is evaluated. In this case the level of the transient signal is set at 2 kV, maintaining the same burst frequency and burst duration of the worst case (type A interference). By observing the constellation diagram (Figure 3.4e) it can be shown that many symbols change their level. However, comparing the constellation diagram with the constellation diagram of type A interference (Figure 3.4a) the interference produces less symbols that jump at the opposite decision zone. By analysing the transmitted and received symbols, a BER of 0.19% is measured when E interference is present in the channel.

3.4.1.6 Interference results resume obtained employing the base-band simulation

A resume of the impact of the five different type of interference over the RFID communication system is shown in Table 3.1. From the table it is observed the different bit error rate that will take place for each of the transient interferences applied at the power wire. The worst interference for the communication system will be type A interference, causing a really high BER. Otherwise the interference that registers the weakest impact over the RFID system is interference type B.

TABLE 3.1: Errors caused by transient interference base-band

Level	Burst Frequency (1/c)	Burst interval (b)	Burst duration (a)	Ref.	Expected BER
3000 V	125 kHz	200 ms	4 ms	A	14%
3000 V	1 kHz	200 ms	0.01 ms	B	0.04%
3000 V	5 kHz	200 ms	4 ms	C	1.08%
3000 V	1 kHz	200 ms	4 ms	D	0.14%
2000 V	125 kHz	200 ms	4 ms	E	0.19%

3.4.2 Verification of the methodology employing a RFID equipment

3.4.2.1 Real-equipment evaluation against transient interferences

In this section, the interference scenario has been built employing a real RFID equipment to ensure that the results previously achieved with the simulation methodology are valid. The RFID system used is according to the standard ISO14443-B. This system uses a carrier frequency at 13.56 MHz and the modulation used at reception is a BPSK with an 848 kbps rate. Moreover, this RFID system is capable of detecting errors but cannot correct them.

In order to validate the proposed method, the real RFID system is interfered by the same transients analysed in the previous section and also using the same scenario previously described. The RFID antenna used before is replaced by a complete RFID system: a STMicroelectronics Reader USB CRX14 and a STMicroelectronics SRIX4K tag with 128 addresses of 32 bits, which is compliant with the standard ISO/IEC 14443B. The performance of the RFID system is monitored with a specific software provided by the RFID manufacturer that enables us to detect and read the RFID tag placed in the readers neighbourhood (Figure 3.8 and Figure 3.9). The tag is placed 2 cm away from the RFID reader, which is the maximum reading distance without errors. Consequently, the RFID system is working at the sensitivity level that is the same level that the base-band simulation has been performed.

The results reached by placing the RFID device in presence of the five different type of interferences are shown in Table 3.2. It describes if the tag can be read or if the system is not capable to detect it. The results show that when type A interference and type C interference are applied, the reader cannot detect any

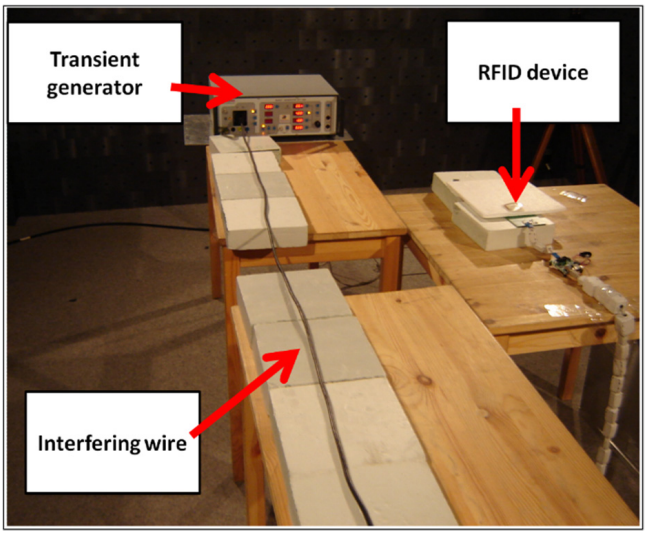

FIGURE 3.8: Interference scenario composed by a generator coupling transients to a wire close to an RFID system

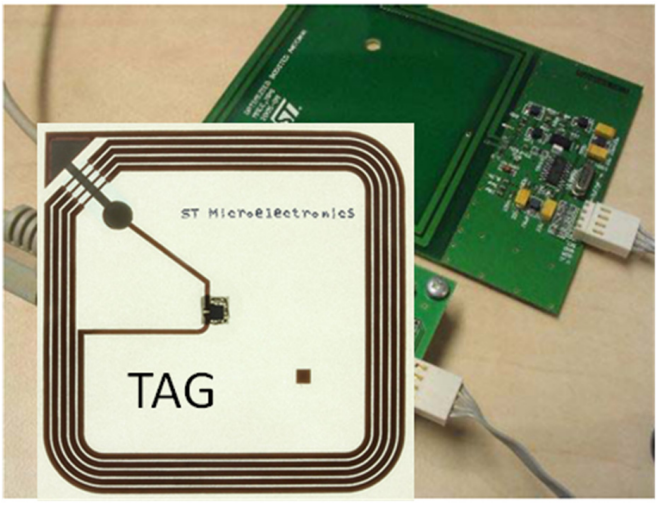

FIGURE 3.9: RFID device composed by a tag and a reader.

tag at its neighbourhood. Otherwise, when type B, D or E interferences are applied to the mains wire, the tag is detected by the RFID reader. However some reading errors appear when the device tries to read tags 4 bytes addresses. For instance, when type D interference is applied, 4 of the 128 addresses cannot be read implying that the frame error probability is 3.12%. On the other hand, with type E interference the frame error probability is 3.91% and with type B interference the error is 0.78%.

TABLE 3.2: Errors caused by transient interference when the real equipment is placed

Interference	Measurement		
Reference	*Tag detection*	*Number of errors reading tag addresses*	*Frame error detected*
A	NO	-	No TAG
B	YES	1/128	0.78%
C	NO	-	No TAG
D	YES	4/128	3.12%
E	YES	5/128	3.91%

3.4.2.2 Comparison between the results obtained with the base-band simulation and the real equipment

In order to compare if the developed methodology has achieved the same results than the results obtained directly from the RFID device, the BER has to be related with the tag detection and the frame error probability. A different BER will produce different degradation at the communication systems. Although in this RFID application it is important to detect the cases where the reader will not be able to identify the tag. Several studies of the ISO/IEC 14443 RFID standard relate the BER with the incapacity to recognize the tags over the reader and the frame error [106].

TABLE 3.3: Probability that a frame arrives with no bit errors (without any error-correction)

Frame length	BER			
	1 %	*0.1 %*	*0.01%*	*0.001 %*
4 byte	72.5 % *	96.6 %	99.7 %	100 %
16 byte	27.6 % *	88.0 %	98.7 %	99.9 %
64 byte	0.6 % *	59.9 % *	95.0 %	99.5 %
256 byte	0 % *	12.9 % *	81. 5 %	98.0 %

* No tag detection

Table 3.3 shows the probability of an error-free detected frame in dependence of BER and frame length. According to Table 3.3, a BER of 1% is not sufficient for a reliable error-free detection of a 4, 16, 64 or 256 byte frame. In the system

under study the frames used in each of the 128 addresses have 32 bits (4 bytes). Therefore, we also include a BER of 0.01% in our study that allows an error-free detection of a 4 byte long frame in 99.7% of all attempts and a BER of 0.1% which permits a frame error-free detection of 96.6%.

For each transient signal, the error produced in the communication system is classified according to Table 3.3. Once the BER has been related with the tag detection and the frame probability error, the comparison can be carried out. In Table 3.4, the results obtained by the base-band simulation methodology and the direct measurement of the RFID device are presented.

TABLE 3.4: Errors caused by transient interference when the real equipment is placed and when the proposed method is used

Interference	Real equipment measurement			Base-band method developed	
Reference	*tag detection*	*Number of errors reading Tag addresses*	*Frame error detected*	*BER*	*Frame error expected according to specs defined*
A	NO	-	No TAG	14%	No TAG (BER>1%)
B	YES	1/128	0.78%	0.04%	0.3% (BER>0.01%)
C	NO	-	No TAG	1.08%	No TAG (BER>1%)
D	YES	4/128	3.12%	0.14%	3.4% (BER>0.1%)
E	YES	5/128	3.91%	0.19%	3.4% (BER>0.1%)

The correlation between the results obtained with the developed methodology and the measurements of the real RFID device is extremely high. When it is crosschecked the BER with the specifications defined, it is possible to predict the behaviour of the RFID communication system in presence of transient interference. Employing the developed methodology it is concluded that in type A and C interference scenarios, the RFID system will not be capable to identify any tag in the proximity. Otherwise, when interferences type B, D and E interferences are evaluated, the developed system and the equipment measurements conclude a properly recognition of the tag, however some frame errors will take place.

Finally, in general terms, concerning the methodologies employed to evaluate the degradation produced by transient interference over digital communication systems the next items are remarkable. Both methods confirm that measuring only the level of the interference is not sufficient to assess the communication system performance in presence of transients. In this study, although the first four transient interferences types have the same amplitude, the types of errors produced are completely different. Other parameters such as the repetition rate and the

duration of the transients, must be taken into account to fully analyse the performance of the RTC system when it is perturbed by a transient. Consequently, it is essential to perform the time-domain evaluation to know if a digital communication system will be interfered instead of using the frequency-domain analysis, which is established at the EMC standards.

3.5 Full-simulation procedure

In this section, a full-simulation procedure is described to evaluate the distortion produced by radiated transient interferences. In this simulation procedure, EM simulation is employed instead of using the measurement methodology to obtain the in-phase and quadrature components of the transient interference. Although the measurement methodology presented in Chapter 2 enables us to obtain the IQ components of transient interference, some limitations can still remain when impulse noise is tried to be measured. One of the unsolved main disadvantages is the fact that the full-spectrum of the transient interference cannot be measured with a single measurement. In the methodology developed, the EMI receiver has to be tuned at each frequency band where the user wants to perform a measurement. As it has been discussed before, radiated transient interferences are not continuous interferences and large periods of time can appear between different transient phenomena. This can be an obstacle when the interference is random and with many minutes between events. Another problem where simulation can show its benefits is when it is not possible to make a measurement at the receiver point. For instance, in-humans implemented devices, such as pacemakers or RFID implants, it is not feasible to measure the interference inside the patient.

Regarding the full-simulation methodology followed to reach the degradation produced over the digital communication system, in Figure 3.10 the basic structure to obtain at the output the BER is illustrated. Firstly, the EM simulation is carried out to simulate a single pulse at the antenna of the digital communication system. Afterwards, the post-processing stage is done to obtain the in-phase and quadrature components of the full transient noise in base-band. Finally, this computed interference is added at the base-band communication system simulation to evaluate the degradation produced by the transient interference.

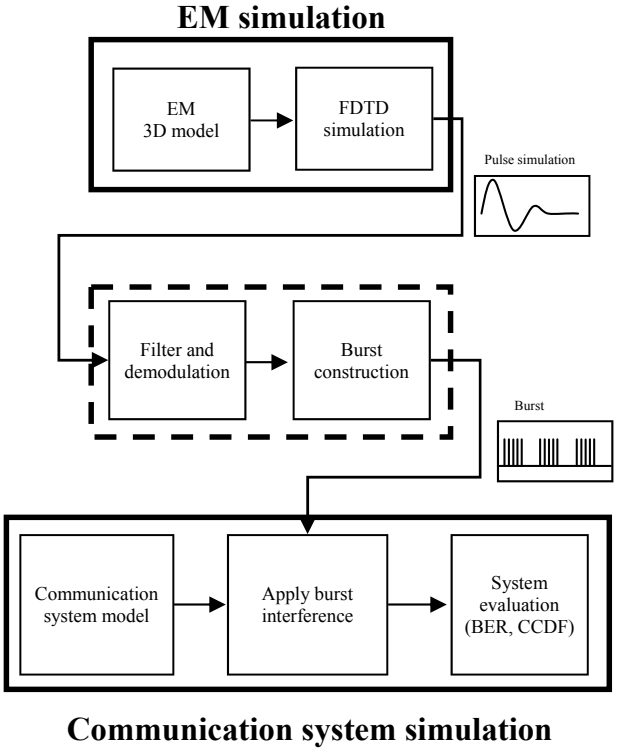

FIGURE 3.10: Block diagram of the methodology to predict the impact of impulsive noise with the full-simulation methodology.

3.5.1 EM simulation to obtain transient interference coupled to the receiver employing FDTD

It is proposed a method employing electromagnetic simulation tools to deal with the limitations mentioned above. In the simulation, the electromagnetic model of the transient interference scenario has to be built to predict the impulsive noise that would be coupled to the digital communication system. A 3D numerical method capable of calculating the magnetic and electric field that will reach the input of the receiving antenna must be employed. The elements that must be modeled properly in a simulation are the source, the coupling wires, the structures and the receiver antennas. Considering the different simulation methods, those based in time-domain electromagnetic simulation are the most suitable to study the effect of each pulse of the transient interference. Therefore, the numerical method selected to determine the interference coupled to the system antenna is Finite-Difference Time-Domain (FDTD). This numerical method is one of the most used in EMC applications as FDTD gives us broadband results [43, 53, 60, 104, 105, 108, 109, 111].

The Finite-Difference Time-Domain method proposed by Yee in 1966 is a direct solution of Maxwell's curl equations in the time-domain. The electric and magnetic field components are allocated in space on a discrete mesh of a Cartesian coordinate system (Figure 3.11). The E-field and H-field components are computed each time-step using the finite-difference by means of the second order approximation of Maxwell equations (3.7) and (3.8). When the space conditions and the source are known, the electromagnetic fields caused by transient interferences can be computed with this space and time discretization methodology.

$$\frac{\partial F(i,j,k,n)}{\partial x} = \frac{F^n(i+1/2,j,k) - F^n(i-1/2,j,k)}{\Delta x} + O\left[(\Delta x)^2\right] \tag{3.7}$$

$$\frac{\partial F(i,j,k,n)}{\partial t} = \frac{F^{n+1/2}(i,j,k) - F^{n-1/2}(i,j,k)}{\Delta t} + O\left[(\Delta t)^2\right] \tag{3.8}$$

where F^n is the electric (E) or magnetic field (H) at the instant $n\Delta t$. $i, j\&k$ are the spatial index, and $O[(\Delta x)^2]$ and $O[(\Delta t)^2]$ are the error terms.

$$\nabla \times H = \frac{\partial}{\partial t}\epsilon E + \sigma_E E \tag{3.9}$$

$$\nabla \times E = -\frac{\partial}{\partial t}\mu H - \sigma_H H \tag{3.10}$$

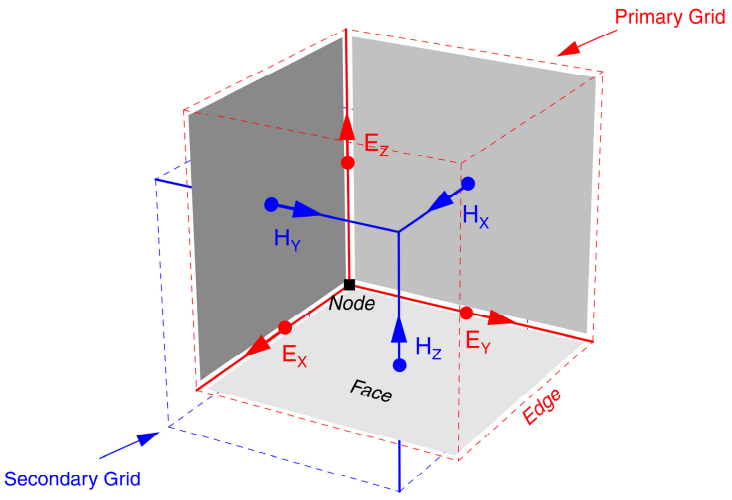

FIGURE 3.11: 3D Yee cell indicating the electric and magnetic field components.

Regarding the discretization of the space it is strongly important to compute a proper mesh. The mesh has to be sufficiently fine in order to not lose any detail of the geometry to simulate. However, the mesh cannot be extremely fine to avoid over sizing the resources to carry out the simulation. In relation, the minimum time-step of the simulation is defined by the following equation to ensure the stability:

$$\Delta t \leq \frac{1}{c\sqrt{\frac{1}{\Delta x^2} + \frac{1}{\Delta y^2} + \frac{1}{\Delta z^2}}} \tag{3.11}$$

where Δx, Δy & Δz are the minimum dimensions used in the mesh for each component of the Cartesian system and C is the velocity of light.

From the equation it can be deduced that if one of the components of the cell dimensions is reduced to the half, the time to obtain the simulation result will increase by a factor of sixteen and the storage memory needed will be increased by 8 times.

Returning to the goal of the FDTD simulation, which is to obtain the level of the burst that will be coupled to the receiver antenna, we have to keep in mind that usually transients are not generated as isolated pulses. Instead of that, a group of transients, or bursts, is more present in the reality. Although this multiple pulses interferences, a unique pulse of the transient interference will be simulated due to FDTD computer resources limitations. Later, the complete burst will be composed mathematically. Besides, simulating more than one pulse will not provide further information because the transient propagation of each pulse is the same.

Regarding the methodology developed to employ the electromagnetic simulation, the basic schematic of the simulation methodology is illustrated in Figure 3.12.

The procedure to obtain at the end the in-phase and quadrature components of the transient interference is divided into two stages. In the first stage, the electromagnetic simulation is carried out, where an accurate model of the electromagnetic scenario must be done considering the relevant elements at the CAD model. Additionally, concerning the source of the EM simulation, a measurement of a pulse can be used or instead it could be obtained also from theoretical analysis. However, as it has been mentioned before, the simulation will only be done for one pulse of the

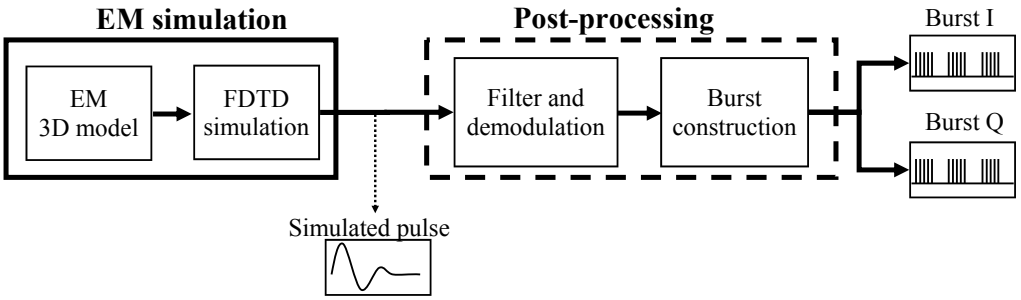

FIGURE 3.12: Schematic of the methodology used to perform the simulation strategy.

transient interference as it is not possible to simulate the hole transient interference due to computer limitations. Afterwards, in the second stage, the computed pulse that the communication system will receive is post-processed to reach the IQ components of the full burst interference.

The post-processing stage to obtain the portion of the transient that will interfere with the communication system is shown in Figure 3.13.

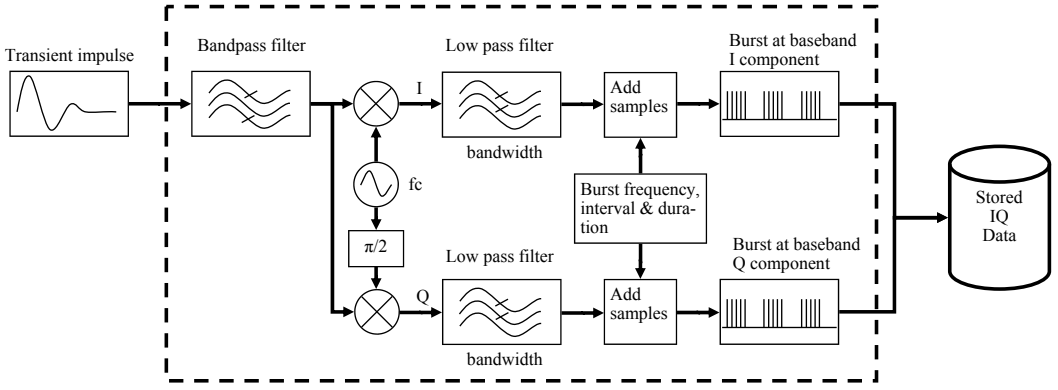

FIGURE 3.13: Schematic of the post-processing to adjust the signal coming from FDTD simulation to the input of communication system simulation.

As it has been discussed, impulsive interferences are broadband noise that begin at DC and usually end at several hundreds of megahertz or some gigahertz. The EM simulation gives us the information in the whole spectrum; nevertheless, the interesting part of the spectrum is to the frequency band of the communication system. To reach the IQ components, the first step involves the usage of the pulse resulting from the FDTD simulation and demodulates it in-phase and quadrature (IQ). Then, the demodulated signal is filtered in base-band, using the same bandwidth as the communication system; at this point of the post-processing procedure, the interference noise has been down-converted to base-band and filtered.

Consequently, the portion of the interference of a unique pulse that can affect the communication system has been obtained.

The next step of the method is to construct a burst according to its main parameters and the results from the EM model. The main parameters of transient interferences are the frequency, time duration and the level. The isolated pulse samples, after being filtered and demodulated, are combined with zero value samples that are added between pulses according to the burst frequency, duration and interval. These built IQ components of the entire radiated interference are the final data stored.

3.5.2 Full-simulation applied to the RFID system

3.5.2.1 EM simulation to obtain the the transient interference coupled at the RFID antenna

In this section, the simulation procedure is applied to the RFID interference scenario presented in section 2.4.2. The first stage is to model the scenario and simulate the pulse propagation using the electromagnetic (EM) numerical simulation. To carry out the simulation, the numerical method employed is FDTD and the software used is SEMCAD [129]. From the EM model point of view, the following considerations have been taken into account; the cable and the ground plane under the burst source are modeled as Perfect Electric Conductor (PEC) and the cable is modeled as a unique wire with a thickness of 1 mm. Finally the PCB antenna is modeled also with PEC material and the dielectric is defined as air. Detailed information of the EM model and mesh is shown in Figure 3.14. Concerning the source used, it is defined as a soft voltage source between the beginning of the wire and the ground plane. The signal source used to excite the EM model is a unique pulse of the burst according to the EN 61000-4-4 standard. As the performance of the burst is equal for each pulse, simulating only one pulse is enough to predict the behaviour of the full burst. Finally, a 50 ohms load (lumped element) is placed at the RFID antenna, which will record the voltage coupled to the RFID antenna in time domain.

To ensure that the system has been properly modelled and to validate the results, it is necessary to compare the simulation results with a measurement of the real system, performed in the lab (Figure 3.15). To perform the measurement an RFID

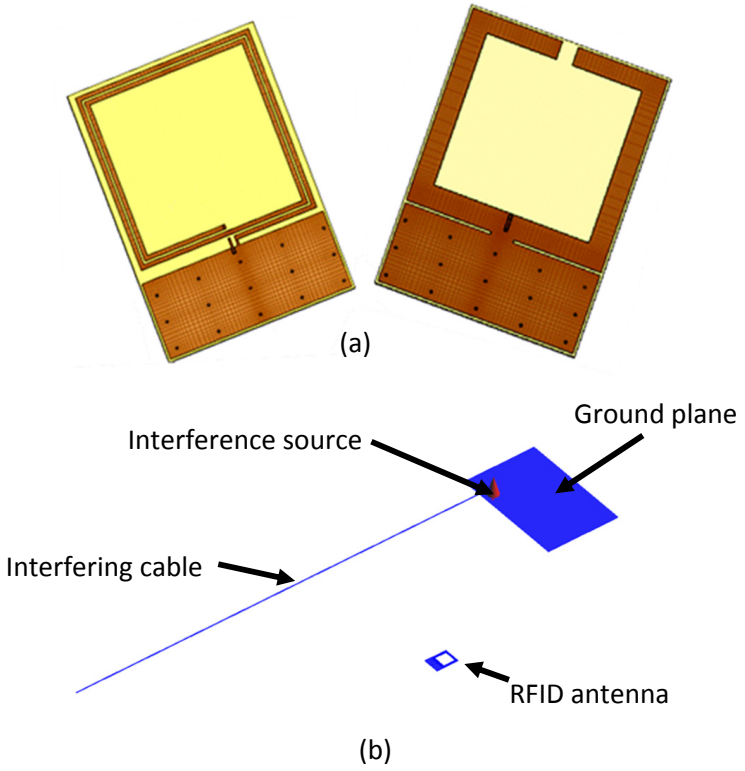

FIGURE 3.14: EM modelling of the RFID interference scenario to be evaluated.

antenna is placed and connected to a Tektronix oscilloscope model DPO7104 which has a bandwidth of 1 GHz. In this case the radiated transient is generated using a Schölder transient generator model SFT 1400 coupling the noise to a unique main wire. Furthermore, to prevent coupling effect to the measurement cable connected to the RFID antenna, a clamp is placed over it.

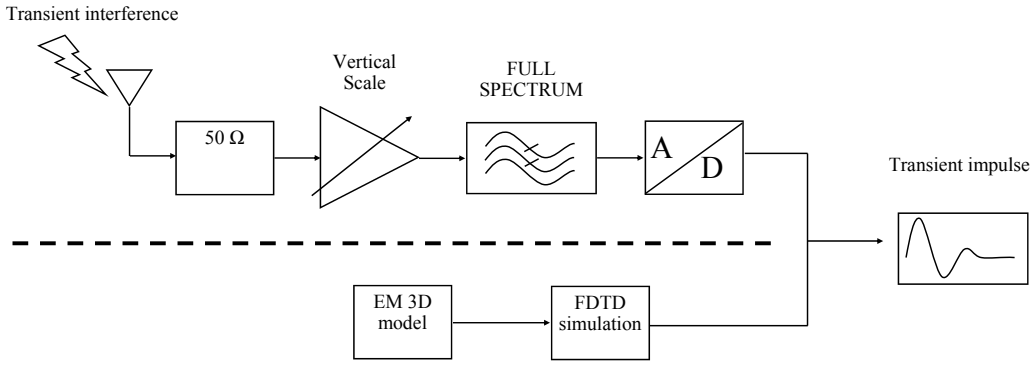

FIGURE 3.15: Schematic of the measurement procedure to compare results reached with simulation and captured from the measurements.

The results obtained by means of simulation and the results coming from the measurements are compared to ensure that the EM model has been performed

properly. Figure 3.16 shows the voltage signal coupled to the RFID antenna in time domain and Figure 3.17 shows the signal coupled in the frequency-domain.

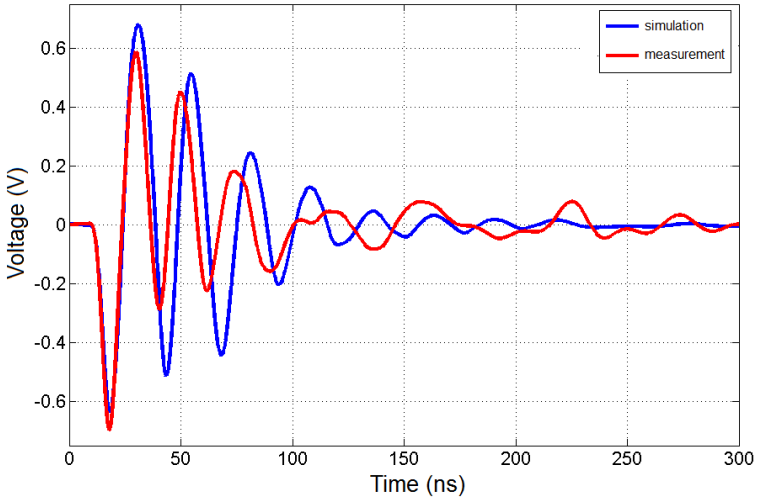

FIGURE 3.16: Comparison between measured pulse and simulated pulse coupled to the RFID antenna in time domain.

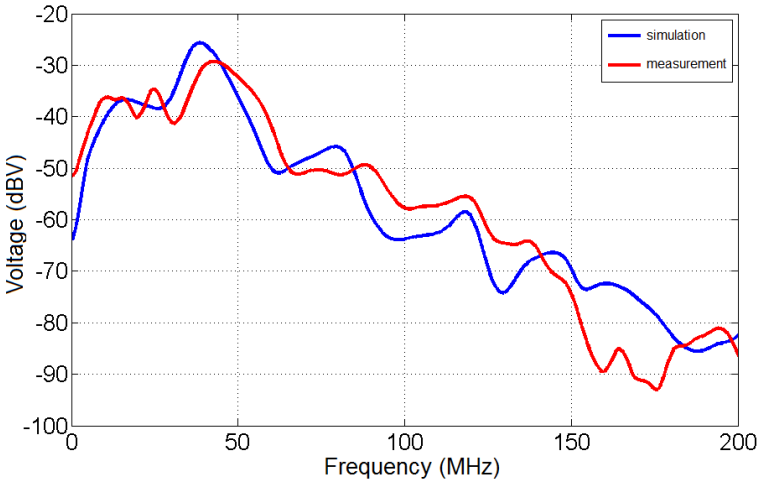

FIGURE 3.17: IQ components and envelope of the simulated pulse at the base-band of the RFID system.

When results obtained by the FDTD simulation and the results captured by oscilloscope measurements are compared, a very good agreement of the data is reached. The matching in terms of amplitude and shape seems to be really good. To quantify objectively the agreement between the simulation and the measurement it is necessary to apply a validation method like the Feature Selective Validation (FSV). In Appendix A there is detailed information regarding the FSV validation method. If we want to quantify the agreement between the results obtained in time-domain (Figure 3.16), a particular formulation of the FSV method must be

used [61, 62]. The results reached are ADM indicator of 0.3, FDM equal to 0.32 and the GDM indicator is 0.49, which means a very good agreement in qualitative terms.

Once the pulse simulation has been validated, the post-processing is carried out according to the methodology described in the last section (Figure 3.13). The pulse is filtered at 13.56 MHz with the 1.7 MHz bandwidth filter and it is demodulated in-phase and quadrature. The results obtained are shown in Figure 3.18.

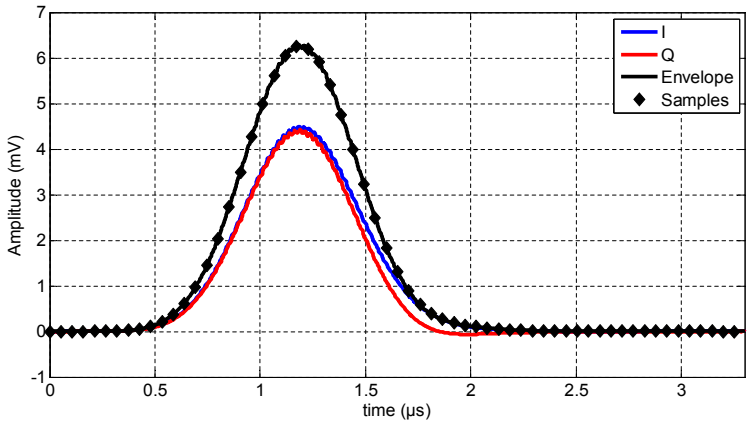

FIGURE 3.18: Comparison between measured pulse and simulated pulse coupled to the RFID antenna in frequency domain.

The IQ components of the simulated pulse reached following the electromagnetic simulation and the post-processing are really confident if they are compared with the measurement previously obtained. Consequently, we can move on to the next stage of the post-processing, which is to build the full burst that will interfere the communication system. In order to reduce the amount of data, a resample is done according to the dots viewed in the Figure 3.18. Considering the type A interference parameters defined in 2.2, where the burst frequency is 125 kHz, the duration is 4 ms and an interval is 200 ms, the full burst interference is built. The transient interference is computed using Matlab adding zero samples between pulses and bursts. The resulting interference that will be used in the next chapter to evaluate its impact over the RFID system is detailed in Figures 3.19, 3.20 and 3.19.

Regarding the results obtained with the simulation procedure, we can conclude that the IQ components of the interference reached are suitable to determine if a digital communication system could be interfered. In the next chapter, the results obtained with the electromagnetic simulation will be employed to evaluate the impact produced by the radiated transient interference on the RFID system.

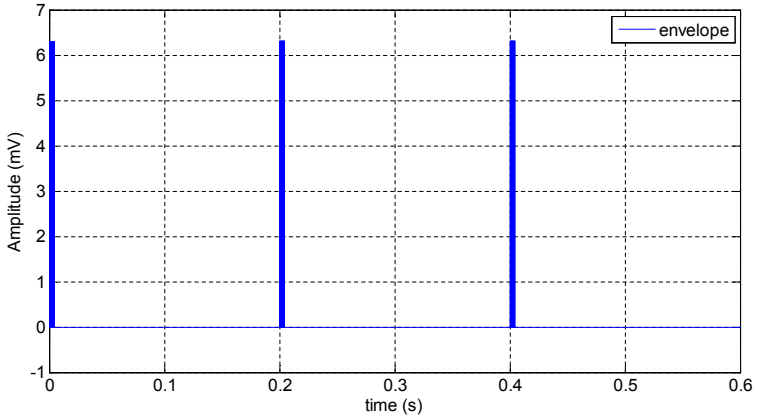

FIGURE 3.19: Envelope view of the full burst interference demodulated at the RFID frequency band.

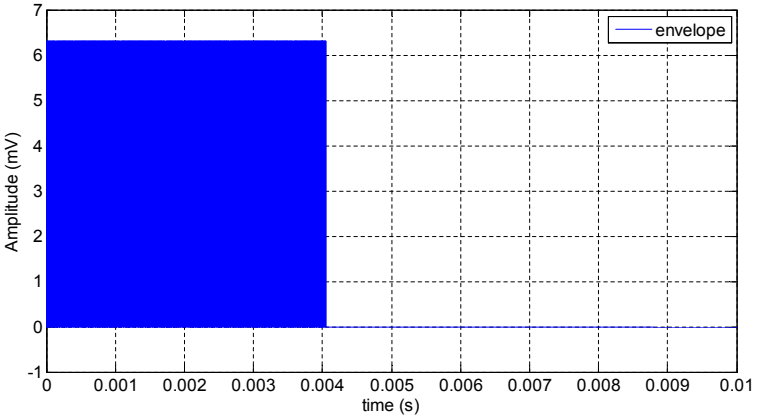

FIGURE 3.20: Zoom Envelope view of the interference demodulated at the RFID frequency band highlighting the burst duration.

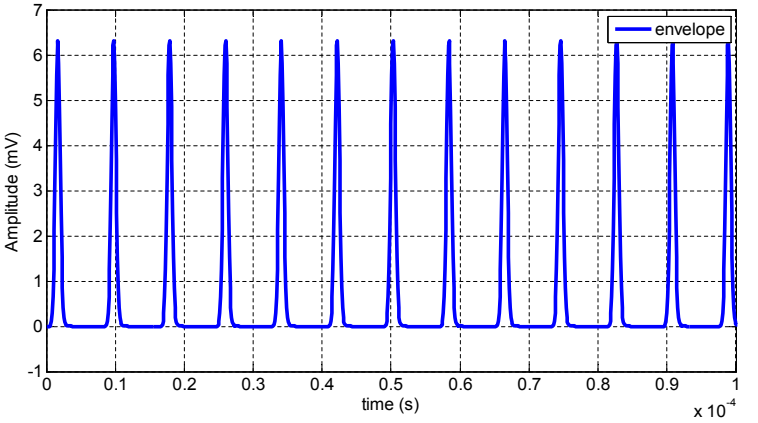

FIGURE 3.21: Zoom Envelope view of the interference demodulated at the RFID frequency band highlighting the burst frequency.

3.5.2.2 Full-simulation results for the RFID interference scenario

Results presented in Figures 3.18, 3.19, 3.20 and 3.21 are used for the input of the base-band simulation in order to determine the degradation produced by the transient interference over the RFID system. As the previous case, where the measurement of the impulsive interference was applied to the base-band simulation, it is necessary to generate the signal of the communication system. As before, the communication is according to standard ISO/IEC 14443B, using a Binary Phase-Shift Keying (BPSK) modulation with a bit rate of 847.5 kbit/s. After generating the useful signal, the burst created by means of simulation and post-processing is added to the RFID signal as they share the channel and the frequency band.

The tools employed in this analysis are the constellation, the eye diagram, the vector diagram and the cumulative complementary distribution function (CCDF). As it has been mentioned before, one of the most useful tools provided by the base-band simulation is the Cumulative Complementary Distribution Function (CCDF). This function shows the probability to have a peak of amplitude over the average amplitude. As BPSK only have two possible symbols, the amplitude of these symbols has to be always the same. Otherwise, if in a BPSK modulation system a peak signal is 6 dB higher than the average signal, a decision error can occur. These deviations from one decision zone to the other will be only caused by impulsive noise because white Gaussian noise will only produce small effect on probability values. To illustrate it, the WGN effect is represented by the black lines in Figure 3.22 and Figure 3.23.

Employing the full-simulation methodology, two of the interferences have been modelled. Interference type A and interference type D are the interferences selected to employ the full-simulation methodology. These interferences have the same level, duration and interval. However the frequency of the burst is 125 kHz for type A interference and 1 kHz considering type D interference. In Figure 3.22 the frequency of the burst is 125 kHz while in Figure 3.23 the frequency is 1 kHz. In both figures, the blue line represents the CCDF when the full-simulation methodology is applied and in red colour the results obtained when the impulsive measurement was used at the base-band simulation. As it can be clearly seen from the distributions, the shape is described by a heavy tailed distribution which is characteristic for impulsive interferences.

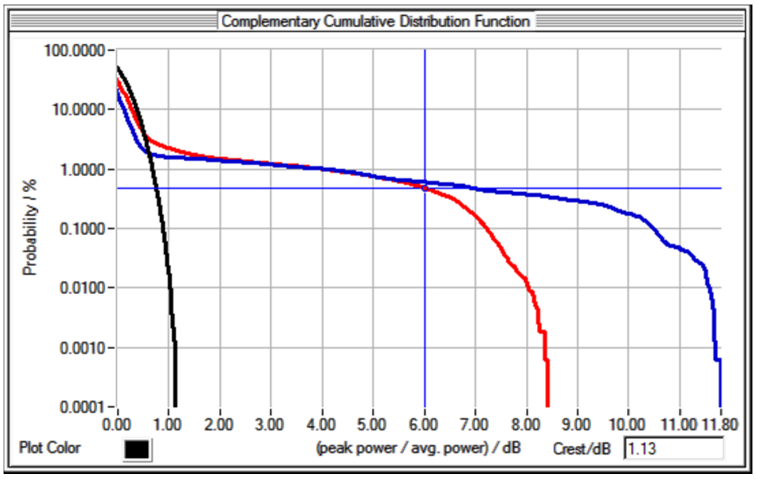

FIGURE 3.22: CCDF obtained with the measurement of the interference (red), using the simulation procedure (blue) and without an interference (black) when the frequency interference is 125 KHz.

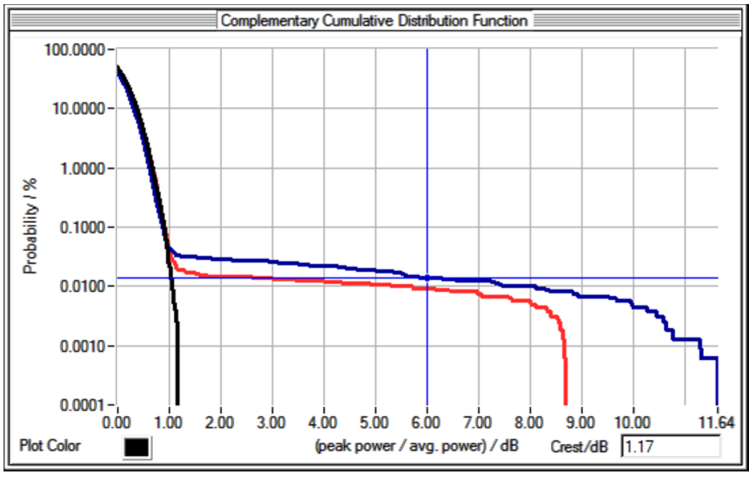

FIGURE 3.23: CCDF obtained with the measurement of the interference (red), using the simulation procedure (blue) and without an interference (black) when the frequency interference is 1 KHz.

Observing the plots, the effect over the RFID system could be clearly observed. As the repetition rate of the transient signal is increased, the error probability also increases. The agreement between the results reached by the simulation and the results obtained by the measurement of the transient interference is really good. When the frequency of the interference is 125 kHz, the probability to have an interference signal capable to interfere the BPSK system (when peak power is 6 dB over the average power) starts around 1%. Otherwise, when the frequency of the interference is 1 kHz the probability to have an interference strong enough to produce degradation at the communication systems is around 0.01 %.

Regarding the results reached when the real RFID equipment is interfered by the propagated transient, two different effects were observed when both transients were applied. When the transient interference of 125 kHz is applied, the RFID reader cannot identify the tag that it is placed over it. On the other hand, when the 1 kHz burst interference is coupled to the AC mains wire, the tag is detected by the communication system, although the tag information cannot be fully read.

3.5.2.3 Redesign by means of simulation

In this section, it is proved that the full-simulation methodology could be also a useful tool to find solutions to reduce the interference between the communication system and the transient interference source. The main advantage of the simulation is that it provides a large cost reduction compared with traditional redesign strategies because no extra measurements with real equipment are necessary.

As an example, a solution based on the idea of reducing the coupling between the interfering wire and the antenna of the RFID system is proposed. It consists of placing a finite conductive shielding plane between the interfering wire and the RFID system, it is observed in Figure 3.24. Therefore, to check if the solution proposed is good enough to ensure the proper behaviour of the RFID system, the full-simulation methodology is employed.

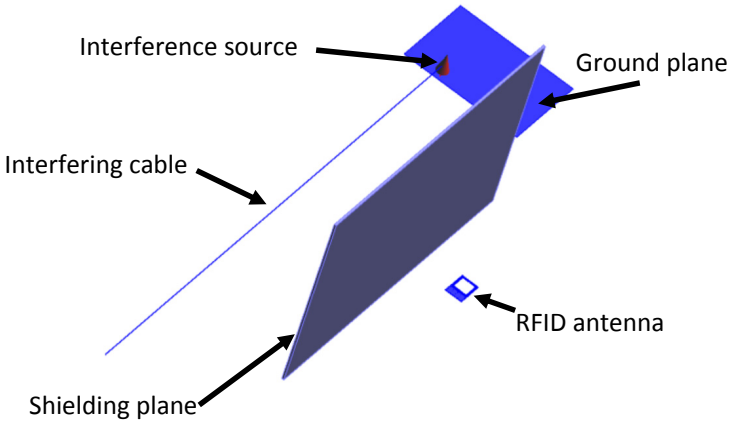

FIGURE 3.24: EM model of the solution proposed to avoid interference between the interfering wire and the RFID system.

In Figure 3.25 the result of the pulse time-domain simulation is compared with the scenario test case when the shielding metallic plane is introduced in the EM model. In Figure 3.25, in red colour it is plotted the redesign strategy result.

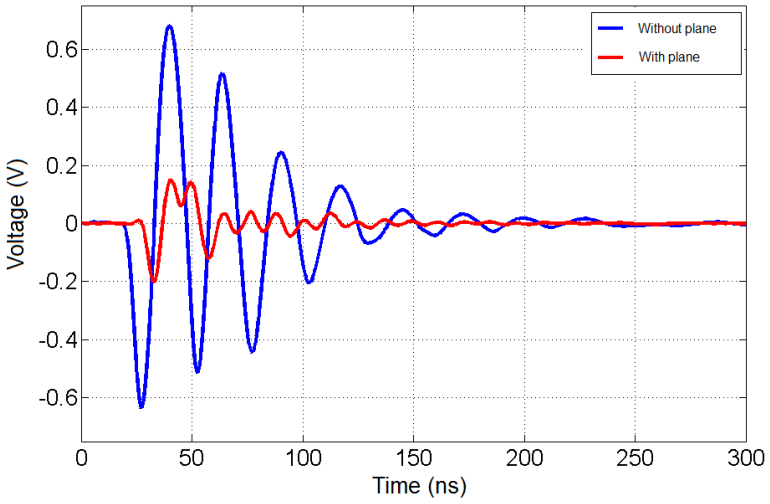

FIGURE 3.25: Time-domain comparison between simulated pulse with and without the conductive plane.

Observing Figure 3.25, in time-domain the reduction of the transient signal does not seem so strong. Otherwise, in the frequency domain it could be observed that a reduction of 15 dB is produced by the conductive plane at the frequency band of the RFID system (Figure 3.26).

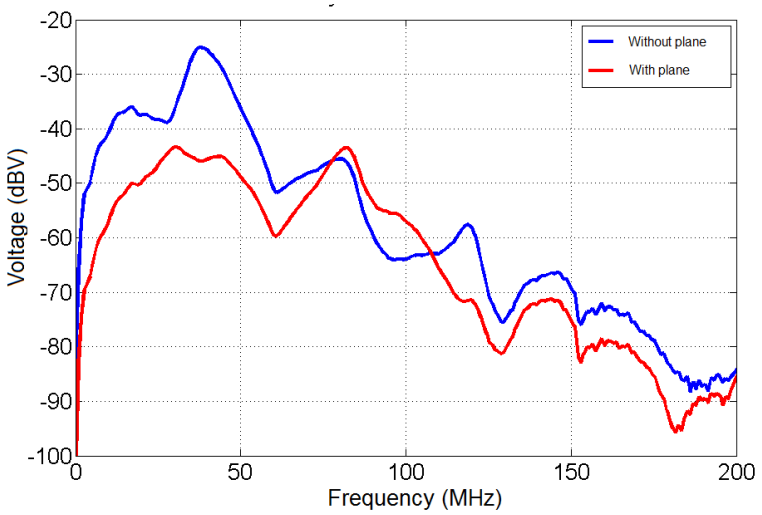

FIGURE 3.26: Frequency-domain comparison between simulated pulse with and without the conductive plane.

Additionally, observing the previous results it seems that it could be a solution to put the metallic plane between the transient source and the RFID antenna. As it has been demonstrated before, to fully ensure the correct behaviour of the RFID system, it is necessary to construct the burst and evaluate the effect of the transient interference over the RFID system using the base-band simulation. Subsequently,

the burst obtained is added to the simulation software and the CCDF is obtained when the shielding plane is placed.

The CCDF in Figure 3.27 shows us that the effect of the transient interference is not so strong to produce decision errors when the plane is placed between the interfering wire and the receiver antenna. The red line in Figure 3.27 does not cross the 6 dB limit that implies error-free on the RFID system.

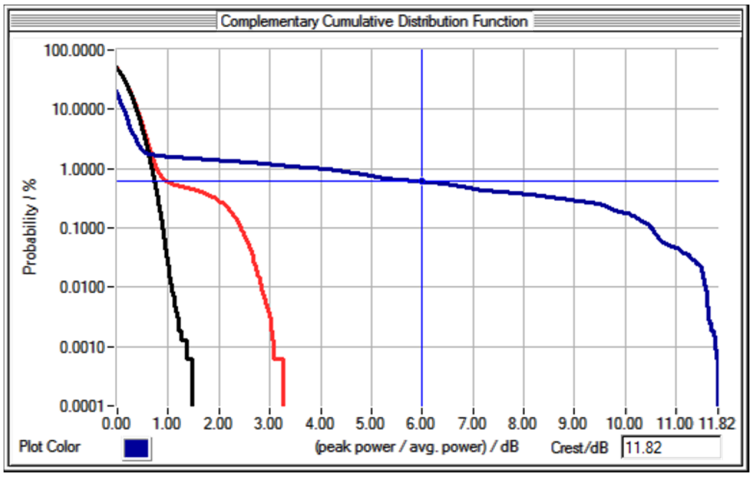

FIGURE 3.27: CCDF obtained analysing the interference when the plane is placed (red), without the plane (blue) and without transient interference (black).

Consequently, the redesign solution proposed to avoid the interference between the RFID system and the transient is effective after analysing the degradation produced at the communication system. Therefore, using the methodology described in this thesis it can be concluded that the proposed shielding is effective enough to protect the communication system.

Chapter 4

Novel APD measurement methodology

4.1 Introduction & motivation

As it has been discussed before, measuring beyond the conventional standards is necessary to evaluate properly the effect on digital communication systems. Detectors and methods defined in the standards were developed to protect analogue communication systems from interferences. As an example, quasi-peak detector defined in CISPR 16-1-1 was developed to relate the output of the detector to the human perception when the receiver was interfered. For digital communication systems these methods and detectors are not sufficient to predict the impact of transient interferences; the correlation between their outputs and the errors produced to a digital communication system is not direct [132, 133].

Alternatively, carrying out measurements to obtain the statistical parameters of the interference is one of the current main research lines. In CISPR 16-1-1 new detectors such as Amplitude Probability Detector (APD) have been defined in order to deal with transient interferences that can interfere critically on digital communication systems. APD was originally used to categorize electromagnetic interference, but it has recently attracted attention as an EMI test method, since it was found to have strong correlation with the bit error probability (BEP) of a digital communication system subjected to the interference [141, 143]. Furthermore,

a method has been proposed for defining emission requirements by introducing a limit line that restricts the slope of the APD curve [49].

Therefore, APD is highly accepted as one of the best tools to measure transient interference and, in a second step, to study the effect on a digital communication system. In contrast, APD measurements have limitations to be carried out during standard electromagnetic emissions tests on an Equipment Under Test (EUT) at EMC laboratories. These methods of measurement have strong disadvantages to define a uniform test method to protect digital communication systems in all the frequency range. This is why APD is not currently employed in any product or generic standard for EMC.

The main problem is that APD standard measurements must be defined at a certain frequency with a specific bandwidth, and typical coherent EMI receivers have a limited number of resolution bandwidth filters available. As there are many systems at different frequencies and also with different bandwidths it is nearly impossible to use instruments or methods capable of measuring in the whole spectrum to protect every digital communication system. Moreover, the high cost based on time terms employed in an EMC laboratory does not permit to evaluate the whole spectrum with the APD detector. Only few communication systems could be evaluated using the APD detector, and tailor-made measurement systems must be developed to measure APD at the required frequency bands [85]. This disadvantage is emphasized due to the main characteristics of impulsive interferences, which cover the frequency range from DC to hundreds of megahertz or several gigahertz.

Another existing problem is the advance of the communication systems technologies. Nowadays the number of digital communication systems specifications is rising rapidly. This fact implies that an EUT measured in the past with an APD detector at several frequencies bands must be measured again considering the new communication systems frequency ranges.

Furthermore, it is necessary to develop a methodology based in time-domain that enables us to evaluate the worst case of the transient interference scenario. While the standard methodology takes several minutes to get the APD statistical measurement, it is needed a methodology that can get the transient interference APD

as fast as the duration of the transient interference. Otherwise, the transient interference worst case suffers some kind of averaging by the periods of time without interference.

In this chapter a time-domain measurement system is developed to deal with the APD measurement limitations. The developed method, based on captures obtained from a general purpose oscilloscope, makes it possible to obtain the APD detector results at any desired frequency band. Also, the post-processing tools using mathematical software produce the APD results rapidly, employing the same time-domain captures for all the desired frequency bandwidths. To ensure that the developed methodology produces as good results as an EMI receiver APD detector, a validation procedure was carried out. Different types of conducted and radiated noise were measured at many frequency bands. White Gaussian Noise (WGN), burst generator and ESD gun have been used as sources of noise. Numerous centre frequencies have been selected from 50 MHz till GSM-R band at 923 MHz varying also the bandwidth between several kilohertz to some megahertz. All the results have been generated using the developed methodology with the time-domain captures, and also employing an EMI receiver according to the standard in order to compare the results and establish if the new methodology produces the same results.

4.2 Full-Spectrum APD developed methodology

Considering the huge advantages that introduce the APD, one of the most important goals of this thesis is the methodology presented in this section to obtain the APD at any frequency-band. Firstly, an overview of the conventional measurement employing standard EMI receiver and its associated problems are explained. Finally, the time-domain method is explained and compared with the standard receiver remarking the improvements to deal with conventional method limitations.

4.2.1 Standard APD acquisition methodology

The standard APD EMI receiver measurement follows the simplified block diagram shown in Figure 4.1. The radiated interference is captured by an antenna connected directly to the EMI receiver. The first stage of the EMI receiver is the

preselector, there the transient signal is filtered around the frequency band where the EMI receiver is centered. After the preselector stage, the interference is mixed by the frequency set at the EMI receiver, down-converting it to the intermediate frequency (IF). The next stage of the EMI receiver is to filter the input signal through the Resolution BandWidth (RBW) filter, which could be set with different established values. After being filtered with the resolution bandwidth, the signal is digitalized through an A/D converter, and after that the signal comes into a digital down-converter to obtain the signal in baseband. The last stage of the receiver is the APD detector where the amplitude measurement is shown in terms of probability.

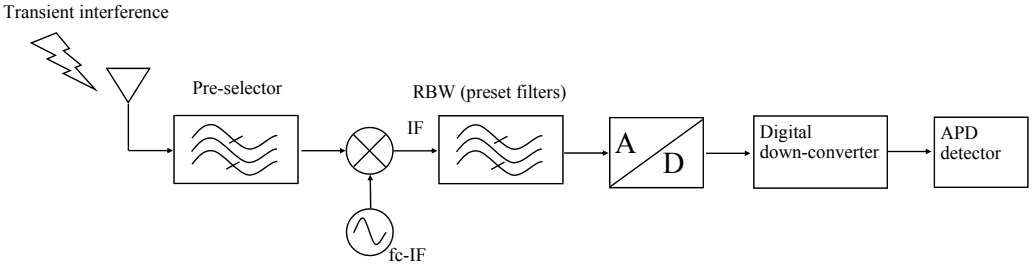

FIGURE 4.1: EMI receiver simplified APD measurement block diagram.

From the block diagram it is possible to observe that a different APD measurement must be carried out at each desired frequency band, setting appropriate centre frequency and resolution bandwidth. As an example, if we want to obtain the APD value at 50 different frequencies with 5 different resolution bandwidth filters in each frequency, we would have to carry out 250 APD measurements. Considering that an APD measurement properly performed to obtain the statistical shape of the interference might need 800 s (10 Msample at 12.5 ksamples/s), this implies a total elapsed time around 55.5 h. Regarding the time needed to carry out the APD measurements with the standard methodology, a noticeable inconvenience appears as transient interference will not be present during a large time. As it is well known, radiated transient interferences are not continuous interferences and large time idle periods can appear between different transient phenomenas. For instance, transient interferences associated with switching power supplies or generated by sparks can only be measured when the transitory event takes place. Therefore, measuring the impulsive interferences employing the APD standard methodology at the full frequency spectrum is not feasible. Alternatively, new time-domain measurement techniques based on the Short Time Fast Fourier Transform (STFFT) are improving APD measurement [10–12, 64, 72, 73, 115, 125]. However, receivers developed

employing these techniques are designed to measure the spectrum with a span up to 40 MHz. Consequently, if the objective, for instance, is to evaluate the DVB-T system, it is not possible to measure at the same time all the spectrum reserved to television channels.

Another limitation apart from the time-consumption measurement viability is the limitation associated with the resolution bandwidth that can be employed. For example, it is not possible to evaluate the APD measurement using a 200 kHz bandwidth that corresponds to GSM-R channel spacing; another example can be the 7.2 MHz bandwidth needed to evaluate a DVB-T channel. In these cases, the measurement must be carried out using the EMI receiver RBW filter closest to the communication system, for example 300 kHz and 10 MHz, unfortunately achieving different results as if the 200 kHz or 7.2 MHz were used. The validation section presents the differences obtained in APD measurements when several RBW are used for the same transient interference.

4.2.2 Developed methodology: full-spectrum APD using time-domain measurements

The method developed to obtain the APD measurement is divided into two different stages, see Figure 4.2. In the first stage, time domain captures are carried out using an oscilloscope to obtain the pulse shape, pulse level frequency and duration of the burst. This measurement carried out with the oscilloscope permits to evaluate the full-spectrum of the interference, only limited by the bandwidth of the oscilloscope. At the second stage, post-processing tools have been developed with mathematical software to obtain the APD of the transient measured at any desired frequency band defined by the user.

In the below sections the two stages of the developed methodology are explained in detail, describing the main parameters, limitations and advantages of each stage.

4.2.2.1 First stage: Time-domain transient capture

The first stage is the acquisition of the transient interference in time domain employing an oscilloscope. The oscilloscope is the adequate instrument to carry

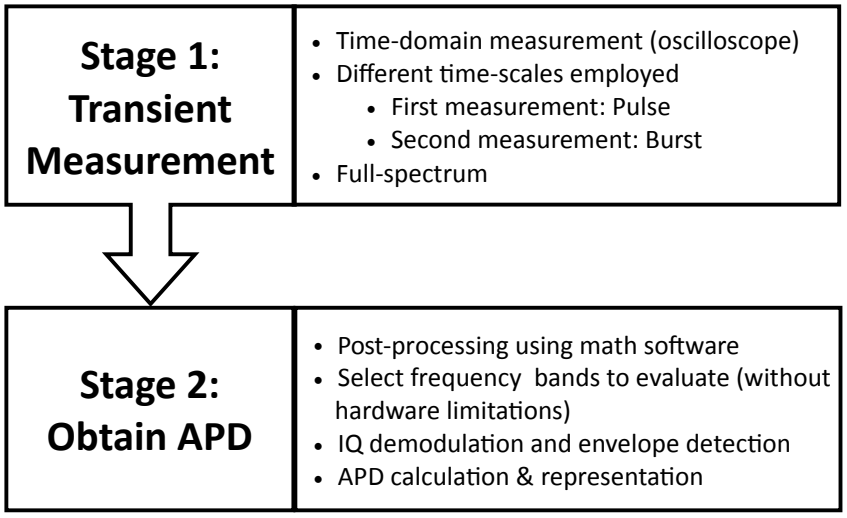

FIGURE 4.2: Schematic describing the two different stages of the developed methodology.

out the measurement for the following reasons. Firstly, the instrument is capable of measuring the whole spectrum in each acquisition. Secondly, time-domain measurements are necessary to obtain the statistical properties of the signal. Furthermore, the post-processing tools employed allow us to have enough sensitivity with an 8-bits oscilloscope dynamic range. There might appear an inconsistency between the use of an 8-bit A/D converter of the oscilloscope and the desire to view signal details that can be more than 100 dB below full scale. This inconsistency stems from the formula that relates A/D resolution to Signal to Noise Ratio (SNR).

$$SNR = 6.02N + 1.76dB \tag{4.1}$$

where N is the number of bits of resolution, achieving a best of approximately 50 dB for an 8-bit A/D converter. This would seem as if it is impossible to observe weak interferences. However, the noise predicted by this equation is broadband and typically spread uniformly across the bandwidth of the A/D converter. By reducing the bandwidth of the data processed, the noise floor is lowered, increasing the sensitivity. This effect is called the Process Gain and improves the SNR as follows:

$$ProcessGain = 10log_{10}\frac{f_s}{2 * RBW} \tag{4.2}$$

where f_s is the sample frequency and RBW the resolution bandwidth. As an example, if 5 GHz of sample frequency and 200 kHz of RBW are considered, the process gain obtained is up to 40 dB more of sensitivity. So with this example, the total SNR could achieve a value of 90 dB.

Another advantage that employing time-domain oscilloscope captures instead of traditional EMI receiver measurements is the possibility to acquire transient phenomena immediately. This is a crucial improvement if it is compared with the standard APD measurement, where long measurement times are needed to estimate the APD at each frequency band. These time-domain measurements allow us to evaluate the worst case of the transient interference scenario.

However, due to oscilloscope memory and sample rate limitations, it is not possible to measure the time domain signal with an infinite resolution and during various seconds or minutes to acquire the main parameters of the transient interferences. To solve these problems it is proposed to measure the transient with different time scales as it can be seen in Figure 4.3. At least two different configured acquisitions must be carried out, to perform these measurements an expert user can obtain easily the required information from the burst waveform. The first acquisition obtains the level and shape of the transient pulses while the second one acquires the main parameters of the transient interference.

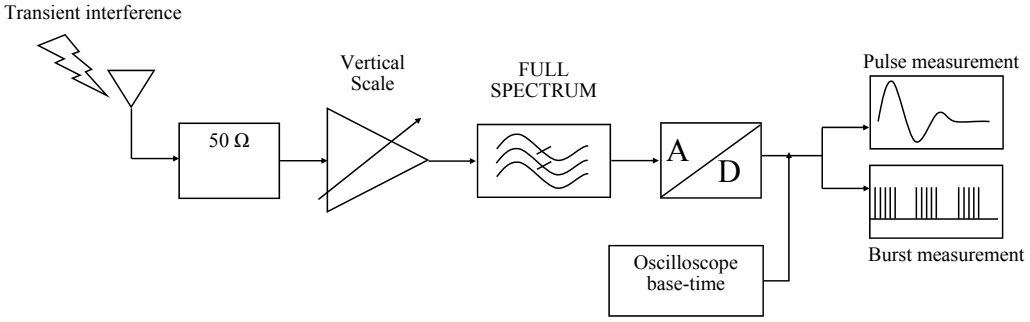

FIGURE 4.3: Time-domain oscilloscope captures block diagram.

For the pulse measurement, it is necessary to perform a measurement with a high sample rate but storing only the necessary time to capture properly the transient pulse. Employing high-sample rates, permits us to have a better SNR as it is described by equation 4.2 and evaluate higher frequencies achieving confident results. As an example, in Figure 4.4(a) a 1 s length transient pulse is measured employing a sample rate of five giga-samples per second. The measurement accuracy in terms of amplitude and shape has to be excellent to obtain good final APD results; the

measurement of the pulse in 4.4(a) is a good example of the resolution needed to obtain satisfactory results of the APD.

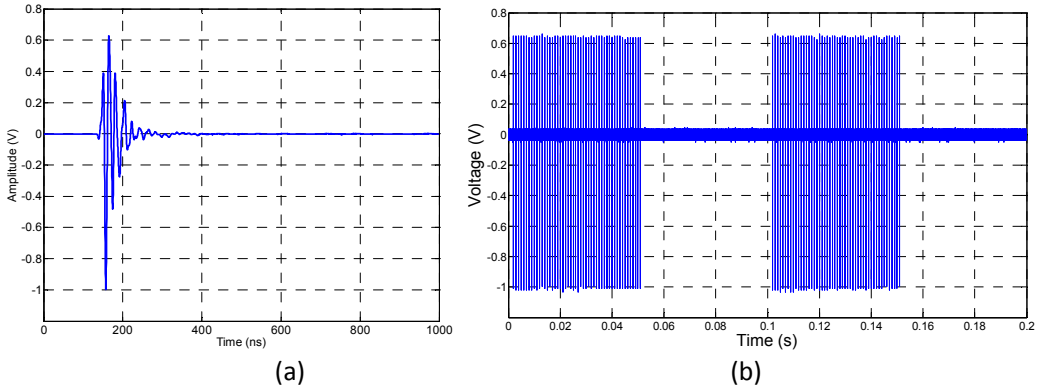

FIGURE 4.4: Time-domain transient interference, a pulse of the transient interference is shown in (a), and the burst frequency and duration is shown in (b).

Regarding the second measurement, the key point is to capture enough time to view the burst duration and interval but it is also necessary to measure with enough resolution to get all the pulses of the transient interference in order to measure its frequency. Figure 4.4(b) shows the measurement carried out to the same interference adjusting the configuration of the oscilloscope, now the sample rate is lower than before and the total time stored is 0.2 s. With the new configuration of the oscilloscope, the frequency, the duration and the interval of the transient interference could be identified. It is immediately clear from the measurement that the interference duration is 50 ms and the interval between bursts is also 50 ms. To identify the burst interference frequency, Fast Fourier Transform (FFT) of the transient measured is carried out.

Otherwise some oscilloscopes enable to work with a segmented memory architecture. One example is the FastFrame^{TM} available for example in Tektronix oscilloscopes, FastFrame^{TM} enables to divide the memory into a series of segments, permitting to capture only when a transient pulse is present. This technique permits to save memory, avoiding capturing the period between pulse events.

Finally, regarding the elapsed time employed by the oscilloscope to acquire the two time-domain measurements, it is negligible if we compare it to the acquisition time needed to reach the APD results with the EMI receiver at the full frequency range.

4.2.2.2 Second stage: Obtaining APD diagram from time-domain measurements

The second stage of the method is to obtain the APD values employing post-processing tools using the previous measurements carried out with the oscilloscope. The goal of this time-domain methodology is to analyze transient interferences to protect digital communication systems. Consequently, the results must be calculated at any frequency band where the communication systems is able to work. The APD detector output must be obtained at the frequency and with the resolution bandwidth that the user defines. The simplified block diagram is shown in Figure 4.5. describes the methodology to obtain the APD measurement from the pulse and the burst measurement.

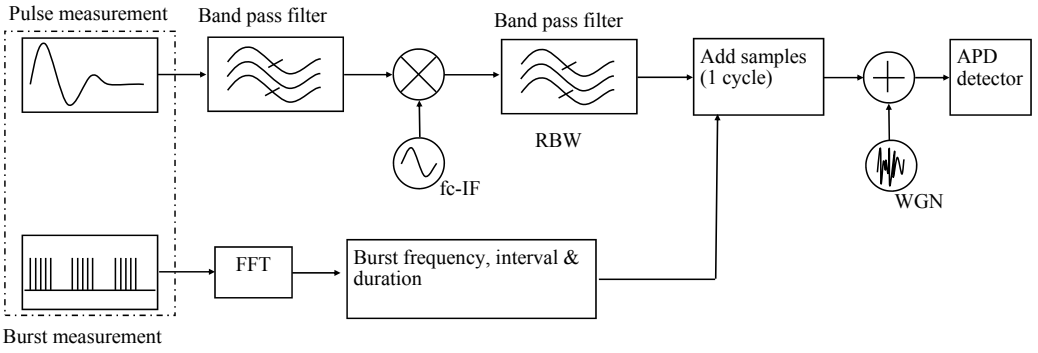

FIGURE 4.5: Post-processing simplified block diagram to obtain the APD results using the time-domain captures.

To obtain the APD data, the pulse interference is filtered by a pre-selection band-pass filter to avoid undesired spurious components. This band-pass filter is set at the centre frequency where the user desires to perform the evaluation and with a bandwidth equal to the communication channel spacing. At the output of this pre-selector filter, the pulse interference corresponding to the frequency band selected is reached. Figure 4.6 shown below contains the 7.2 MHz band-pass filter of a transient pulse measurement centre around 380 MHz.

The next step of the post-processing is to mix the time-domain pulse interference filtered and down-convert it to the intermediate frequency (IF); obtaining the in-phase and quadrature components of the transient interference.

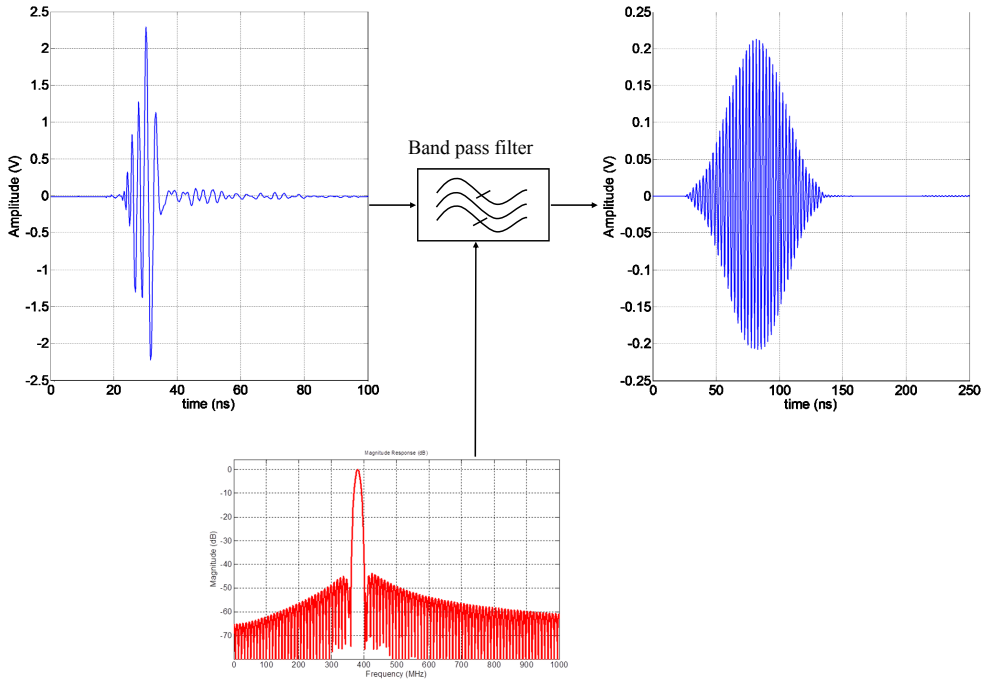

FIGURE 4.6: Band-pass filtering of the input signal.

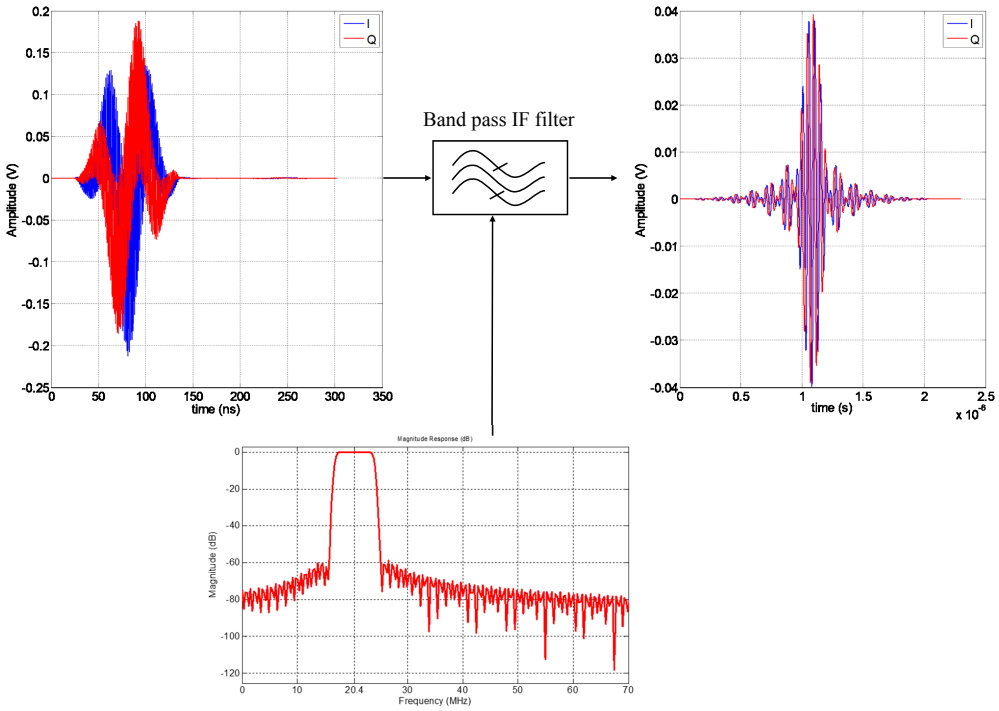

FIGURE 4.7: IQ demodulation and band-pass filtering at IF frequency using a 7.2 MHz RBW.

$$i(n) = x(n)cos(2\pi(f_{RF} - f_{IF})(n)) \tag{4.3}$$

$$q(n) = x(n)sin(2\pi(f_{RF} - f_{IF})(n)) \tag{4.4}$$

After being down-converted, the IQ components of the interference are filtered by a band-pass filter equivalent to the resolution bandwidth filter and centered at IF frequency. In Figure 4.7 the time-domain interference is demodulated and filtered employing a RBW of 7.2 MHz at 20.4 MHz. In this case the resolution bandwidth is the equivalent band used at DVB-T.

The APD gives information about the envelope statistics from the IF filter output, which corresponds to the required information for performance evaluation at the radio receiver. Therefore, it is necessary to carry out an envelope detection using the interference filtered by the RBW at the IF frequency-band. The envelope detection is reached by means of the Hilbert Transform, which is used extensively for analysis and signal processing in pass-band communication systems; in Figure 4.8 the envelope calculation using the Hilbert Transform is shown. The Discrete Hilbert Transform is designed to produce a discrete time analytic signal $z(n)$ [81]. For a discrete function $x(n)$, with a discrete Fourier transform (DFT), $X(m)$,

$$X(m) = T\sum_{n=0}^{N-1} x(n)e^{-i2\pi k/N} \tag{4.5}$$

The DFT of the analytical signal is created as it is described in equation 4.6.

$$Z(m) = \begin{cases} X(0) & \text{for } m = 0 \\ 2X(m) & \text{for } 1 \leq m \leq N/2 - 1 \\ X(N/2) & \text{for } m = N/2 \\ 0 & \text{for } N/2 + 1 \leq m \leq N - 1 \end{cases} \tag{4.6}$$

Then the envelope (analytical signal) is the N-point inverse

$$z(n) = \frac{1}{NT}\sum_{m=0}^{N-1} Z(m)e^{-i2\pi k/N} \tag{4.7}$$

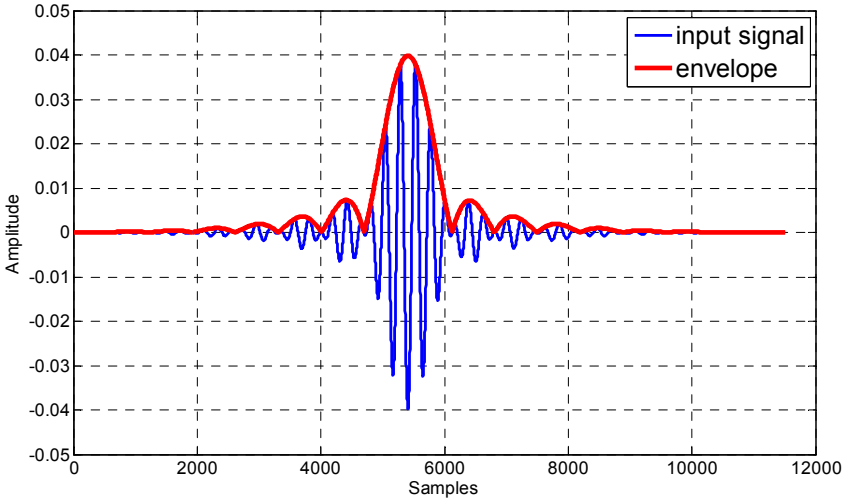

FIGURE 4.8: Envelope detector based on the Hilbert transform.

At this stage of the post-processing procedure, the portion of a transient pulse that will interfere to the digital communication system band has been obtained.

Afterwards, it is time to determine the complete burst interference that will be coupled to the communication band instead of considering only one of the burst pulses. The second measurement of the oscilloscope, the burst capture, is used to examine the burst and obtain its repetition frequency, duration and interval. The procedure consists in applying an FFT to the burst measurement to achieve the frequency repetition of the pulses. Otherwise, oscilloscope capabilities like $FastFrame^{TM}$ also permits to identify the pulse repetition rate. The single pulse interference at the communication band found before is combined with the burst frequency obtained from the second measure. Zero value samples are added at the end of the pulse signal after being filtered and mixed by the frequency band to complete one cycle of the burst period to achieve the statistical properties of the burst.

As an example, if we consider the interference in Figure 4.4, where the burst frequency is 5 kHz, the duration of the burst is 50 ms and the interval is also 50 ms, from an statistical point of view, is the same situation as having an equivalent burst frequency of 2.5 kHz (0.4 ms). In this case, zero value samples are added at the end of the pulse finishing at 0.4 ms. As seen in Figure 4.5. white noise is added to emulate the receiver noise level in order to emulate a real communication system receiver or, for instance, to compare measurements with the standard EMI receiver instrumentation, which is the case used in this study.

Once the whole period of the burst has been obtained, it is time to apply the APD detector. The APD is defined as the amount of time the measured envelope of an interfering signal exceeds a certain level [87]. The relation between the $APD_R(r)$ and the probability density function of the envelope R is

$$APD_R(r) = 1 - F_R(r) \tag{4.8}$$

and

$$f_R(r) = \frac{d}{dr} F_R(r) = -\frac{d}{dr} APD_R(r) \tag{4.9}$$

where $F_R(r)$ is the cumulative distribution function (cdf) and $f_R(r)$ is the probability density function (pdf). The cdf describes the probability that a value of the envelope variable R with a given pdf will be found to have a value less than or equal to r; the cdf function is given by the following equation where R is a discrete variable.

$$F_R(r) = F(R \leq r) = \sum_{r_i \leq r} F(R = r_i) = \sum_{r_i \leq r} f(r_i) \tag{4.10}$$

Every cumulative distribution function F is non-decreasing and right-continuous. Furthermore, the limit conditions of the cumulative distribution are the following:

$$\lim_{r \to -\infty} F(r) = 0, \quad \lim_{r \to \infty} F(r) = 1, \tag{4.11}$$

As it has been mentioned before, it is necessary to compute firstly the pdf of the interference to obtain afterwards the cdf. The pdf is reached by means of the histogram computation. The next Figure 4.9 shows a typical pdf of an impulsive noise obtained from the previous post-processing.

Last, the APD is directly obtained from the cdf using the expressions shown above. The APD is plotted with the percentage of time the ordinate is exceeded on the y-axis and the envelope values on the x-axis. These values are in accordance with the APD measurement function proposed by CISPR [56] to make use of the correlation between the BEP and the APD. In the APD results presented in the next section,

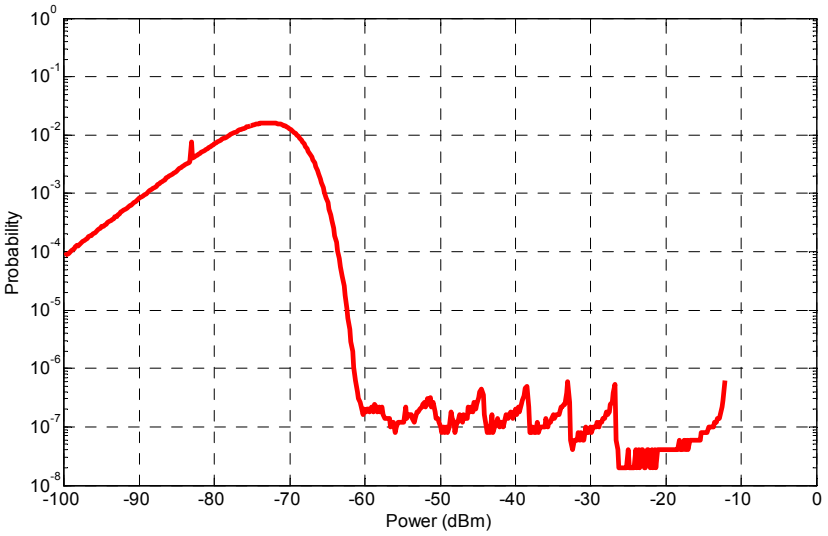

FIGURE 4.9: Example of the interference pdf obtained following the developed methodology.

plot units of the envelope (x-axis) have been set to power units referenced to one milliwatt (dBm). However, they can be converted to voltage values or electric-field applying the corresponding conversion or antenna factor.

The resultant APD diagram corresponding to the pdf shown before is the observed in Figure 4.10. This is a characteristic APD diagram coming from an impulsive interference. Transient interferences produce this APD diagram result with this type of heavy-tailed shape. At the following section this shape of the APD diagram is discussed.

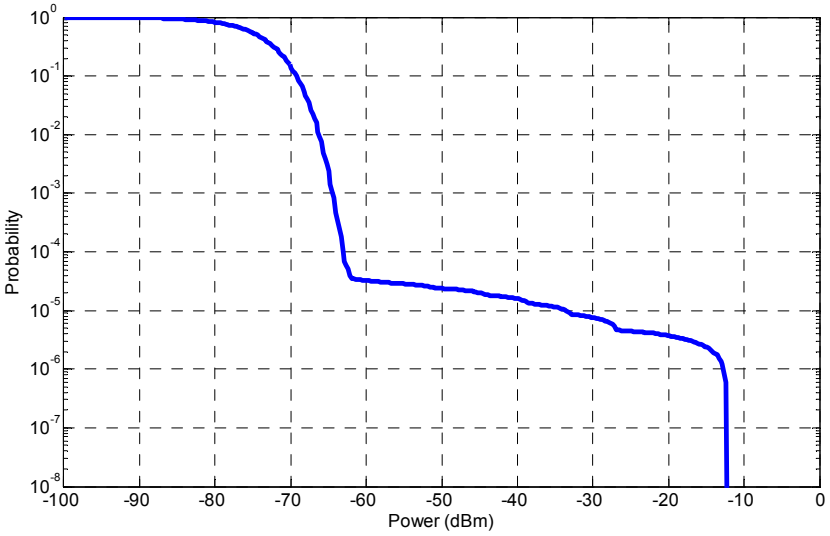

FIGURE 4.10: Example of the interference APD diagram obtained following the developed methodology.

4.3 Validation & Results of the developed procedure

In this section a validation procedure is carried out to ensure the quality of the APD results reached following the described methodology, as it can be seen in Figure 4.11. The APD results of four different interference test-cases are used to compare the results acquired directly with an EMI receiver and the data obtained employing the oscilloscope. The evaluation is performed comparing the agreement between the APD results in terms of the diagram shape fitting and the maximum amplitude values obtained. Furthermore, we have done the validation at many frequency bands for each test-case to ensure that the methodology works properly at the full spectrum.

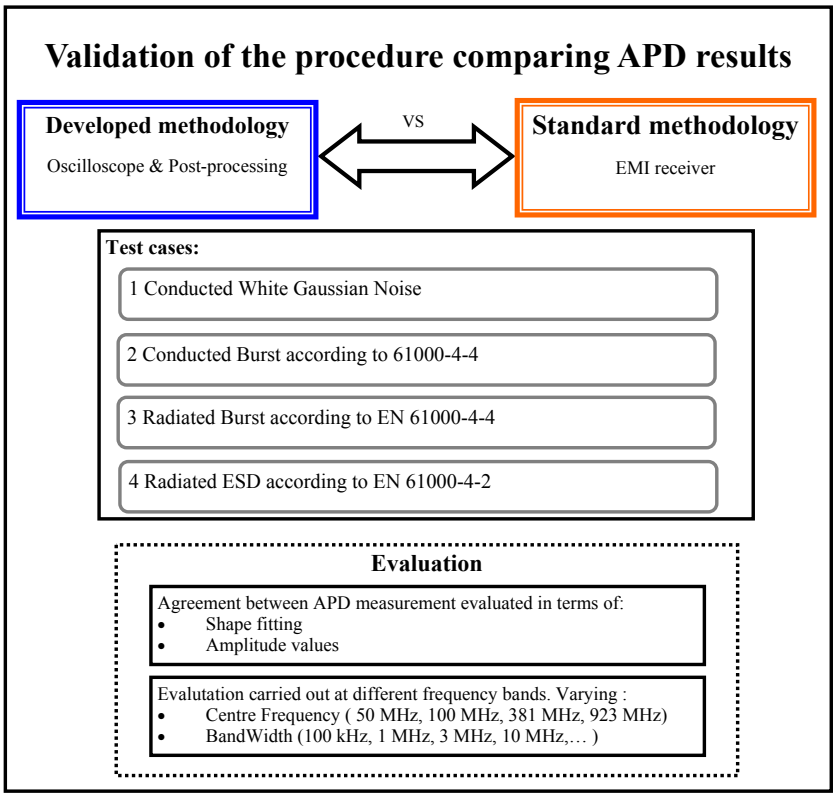

FIGURE 4.11: Validation procedure of the developed methodology to obtain the APD diagram.

Concerning the different test-cases, in the first one, conducted White Gaussian Noise (WGN) is set as the interference source; in the second test-case, the interference generated is a conducted pulse according to EN 61000-4-4 standard; in the third one, the same pulse is applied to a power line cable radiating electromagnetic

fields that are measured with a Bilog antenna; in the last test, an electromagnetic radiated field coming from an electrostatic discharge according to EN 61000-4-2 is produced.

Below, only some of the most significant results are plotted and discussed to show the applicability and the advantages that the developed methodology offers.

4.3.1 Conducted White Gaussian Noise

For the first validation procedure a conducted interference setup has been considered. The aim of these measurements is to compare the developed method measurements with the standard measurement obtained with an EMI receiver when WGN is acquired. The generated noise is coupled to two output channels of an arbitrary generator; one of these outputs is connected directly through a coaxial cable to the EMI receiver and the other output is connected to the oscilloscope (Figure 4.12). In this test case, WGN is generated by Agilent arbitrary generator (model 81160A) producing WGN from DC up to 500 MHz. The duty cycle of the noise will be varied from 20% to 80% employing a gated signal produced by a function generator connected to the arbitrary generator. With the variation of the duty cycle the pdf of the noise will be changed as it implies APD different results. Finally, the period of the generated noise was set to one millisecond (1 kHz).

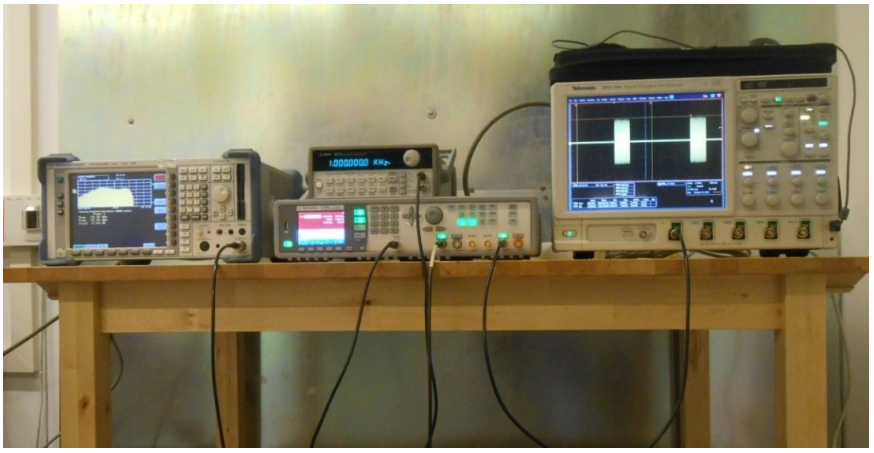

FIGURE 4.12: View of the setup to perform the validation.

The APD measurements carried out with the EMI receiver were done by measuring ten millions of samples to obtain the correct statistical properties of the WGN interference. Measurements with the EMI receiver were performed at 50

MHz, 100 MHz and at 381.5 MHz, which correspond to TErrestrial Trunked RAdio (TETRA) security services frequency band. At each centre frequency three different bandwidths were employed. The elapsed time for each measurement with the EMI receiver was around 800 seconds. For time domain measurements using the oscilloscope, the sample rate selected was 1 GSample as the maximum output frequency of the arbitrary generator was 500 MHz. It is significant to mention that the oscilloscope was configured with an input impedance of 50 Ω to have a matched system like in the EMI receiver. The total time measured with the oscilloscope is equal to one period of the generated signal (1 ms). Figure 4.13 shows the time-domain captures employed to obtain the APD results using the developed methodology.

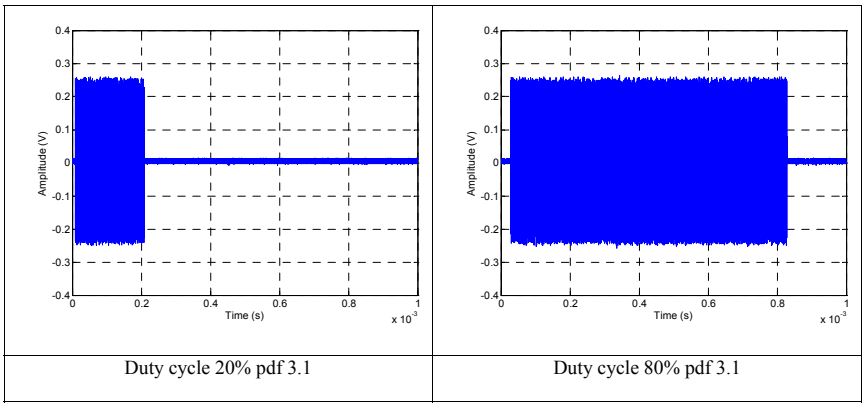

FIGURE 4.13: WGN time domain measurements carried out with the oscilloscope.

The first comparison analysed is related with the pdf measured at 100 MHz employing a resolution bandwidth of 3 MHz in two different cases of the WGN. The duty cycle of the WGN is set to 20%, and 80%. The results of the measurements conducted with the EMI receiver are plotted with a dot line in Figure 4.14. When white Gaussian noise signal is generated with a duty cycle of 20% the pdf shape result is according to the red line (Figure 4.14) and when it is set to 80% the line is displayed in blue.

The results of the pdf measurement show an excellent agreement between measurements carried out with the EMI receiver and the measurement employing the oscilloscope. The probabilities obtained at each level of amplitude are almost equal with both methodologies when pdf are compared. From the results it is observed that there are two peaks in each plot, these peaks correspond with the two levels of noise generated by the arbitrary generator. The peak at the right side of Figure

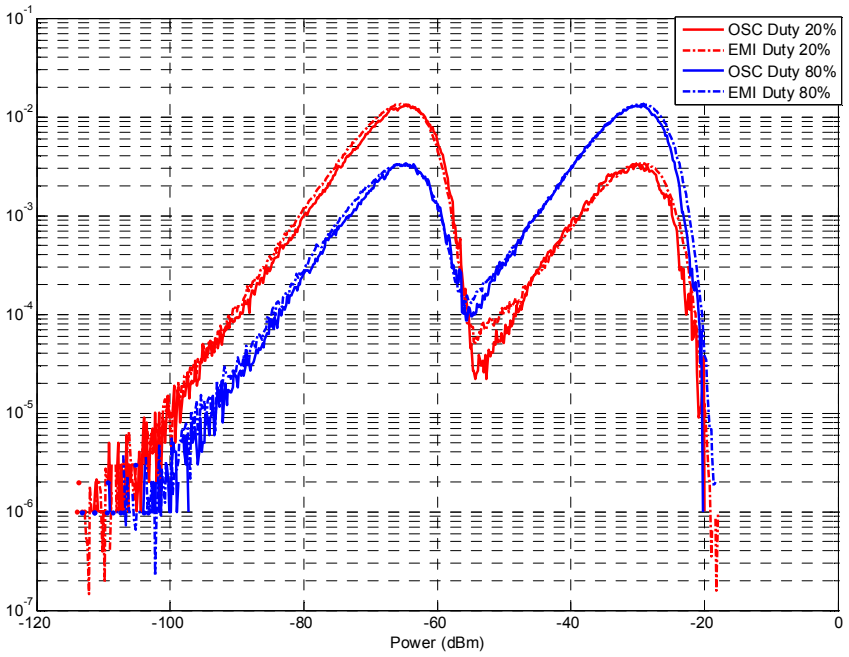

FIGURE 4.14: pdf result at 100 MHz of centre frequency and 3 MHz of bandwidth when WGN of pdf = 3.1 is applied.

4.14 is related to the highest level of the WGN (Figure 4.13), and the peak at the left side is associated with the lowest level. As the results obtained comparing the pdf were really good, we expected that the APD results show the same excellent agreement, which is the goal to achieve. Below, APD results obtained with both methodologies are shown. The plotted comparison is related to the APD measured at a centre frequency of 100 MHz employing a resolution bandwidth of 3 MHz in two different cases of the WGN, when the duty cycle of the WGN was set to 20% and 80%.

Regarding the similarity of the APD results, when oscilloscope results are compared with EMI receiver acquisitions, an excellent agreement is achieved. The fitting of the APD curve and the amplitude maximum values obtained with both methodologies is really remarkable. From the APD results in Figure 4.15, we can obviously see the impact of increasing the duty cycle of the WGN; the probability obtained at the lowest and highest values is the same. However, a huge variation in the probability is observed between -60 dBm and -30 dBm due to the duty cycle variation. The value of the probability in this amplitude range coincides with 0.8 when the duty cycle is 80% and 0.2 when the duty cycle is set at 20%.

Next, other APD results are shown, the 80% DC interference is evaluated at two different frequency bands. In Figure 4.16 the APD results are shown in blue

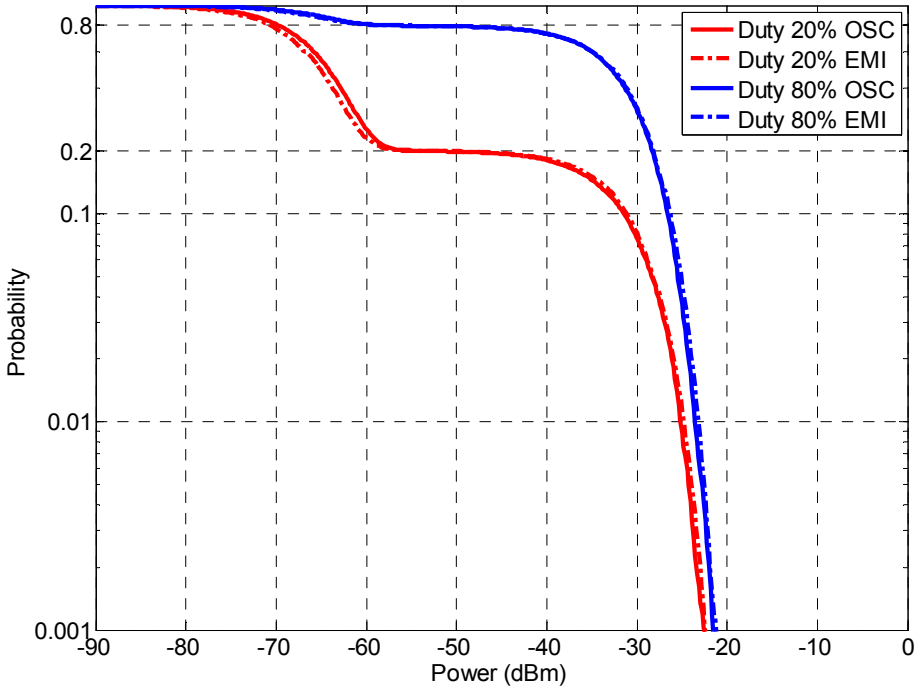

FIGURE 4.15: APD measured at 100 MHz employing a resolution bandwidth of 3 MHz in two different cases of the WGN; when the duty cycle of the WGN is set to 20% and 80%.

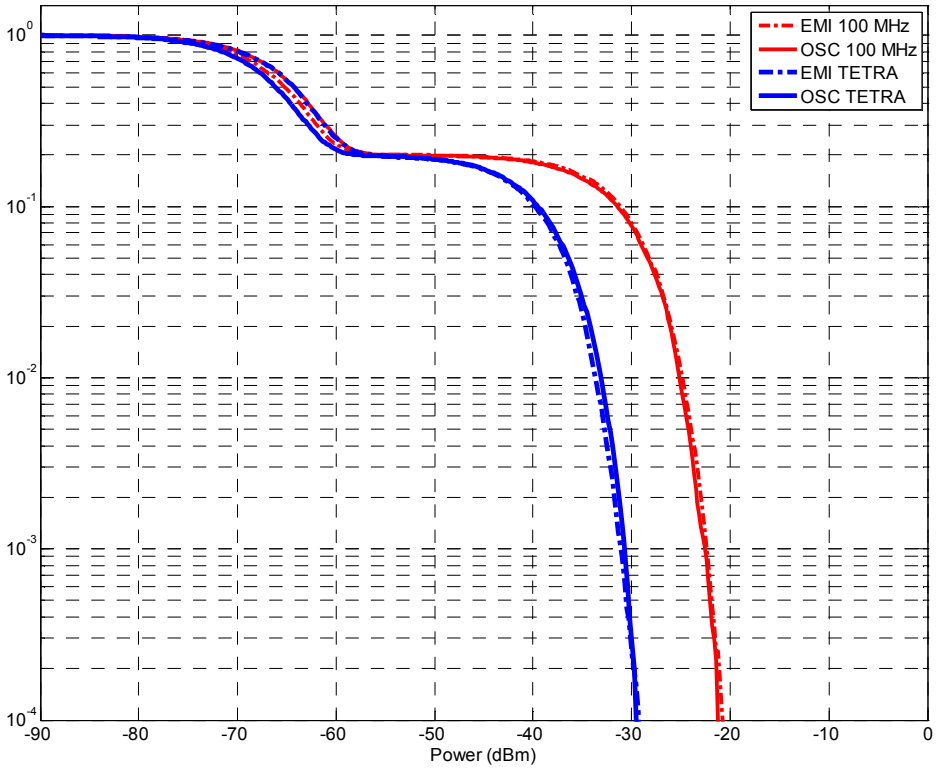

FIGURE 4.16: APD results at 100 MHz and 381.5 MHZ of centre frequency when 3 MHz bandwidth is set. The interference noise is WGN of pdf = 3.1 and a duty cycle of 80%.

when the centre frequency is 381.5 MHz (TETRA) and in red when the centre frequency is 100 MHz. In addition, in both cases the resolution bandwidth set is 3 MHz. In this occasion, the measurements with standard EMI receiver and the measurements reached with the oscilloscope time-domain captures are also compared.

The results found in Figure 4.16 are, as before, excellent. The fitting between the curve produced by the EMI receiver response and the curve coming from the oscilloscope captures are excellent. From the results it can be observed that the amplitude measured at 100 MHz is larger than the one measured at TETRA frequency band. This can be due to the non-perfect uniform distribution of the WGN arbitrary generator and higher attenuation on the coaxial cables when the frequency is increased.

4.3.2 Conducted Burst according to 61000-4-4

The goal of the second test case is to measure a different type of noise from WGN and also obtain the APD figures. In this case, an impulsive noise is generated by the pulse arbitrary generator (81160A) and measured employing the EMI receiver and the oscilloscope. The results are also compared in order to determine if the agreement between standard measurement and the APD obtained with the developed methodology is good enough when impulsive noise is measured. The same conducted setup as before is used to produce and measure the interference. Otherwise, in this test setup a burst of pulses according to standard EN 61000-4-4 is generated by the arbitrary generator. The pulse shape is produced by the formula of the ideal waveform described at section 6.2.2 of EN 61000-4-4:2012 standard.

$$v_{EFT}(t) = k_V \left[\frac{V_1}{k_{EFT}} \cdot \frac{(\frac{t}{\tau_1})^{n_{EFT}}}{1 + (\frac{t}{\tau_1})^{n_{EFT}}} \cdot e^{\frac{-t}{\tau_2}} \right] \tag{4.12}$$

where

$$k_{EFT} = e^{-\frac{\tau_1}{\tau_2} \cdot \left(\frac{n_{EFT} \cdot \tau_2}{\tau_1}\right)^{\frac{1}{n_{EFT}}}} \tag{4.13}$$

and

$V_1 = 0.92 \quad \tau_1 = 3.5ns \quad \tau_2 = 51ns \quad n_{EFT} = 1.8ns \quad k_V = 1$

The frequency of the burst generated is 100 kHz. Consequently, each 10 s a pulse is produced by the arbitrary generator. The pulse rise time is 5 ns and the pulse duration is near 400 ns, as described in the EMC standard mentioned before. Therefore, the maximum frequency spectrum component generated should be around 200 MHz.

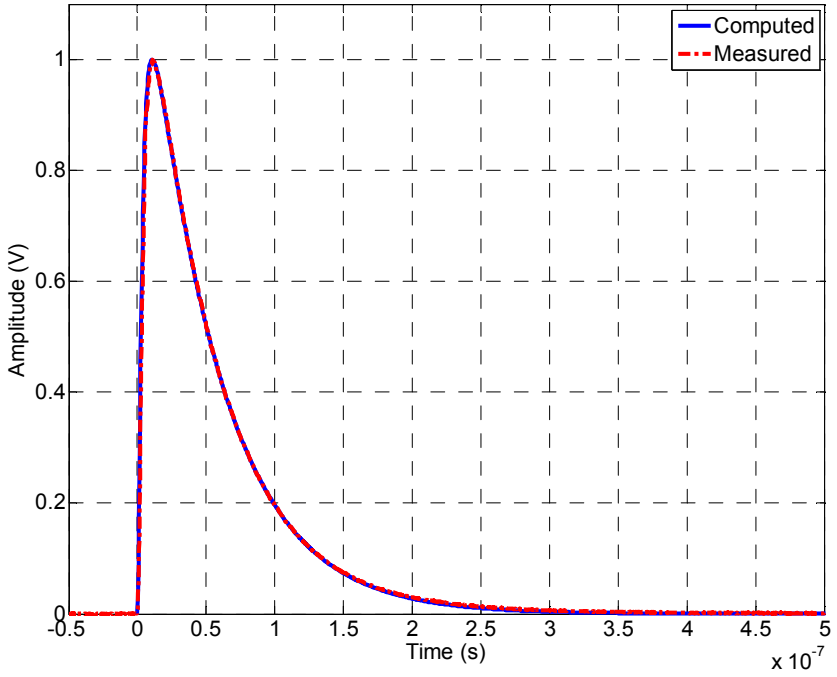

FIGURE 4.17: Time domain pulse generated by the arbitrary generator.

Regarding the APD results, different measures were done with the EMI receiver at different frequency bands. Otherwise, with the oscilloscope methodology developed, just a single measurement was needed to obtain the APD diagram at any frequency band using the post-processing tools. The results shown in Figure 4.18 are one example of the APD results obtained. In this figure, the comparison is carried out between the APD measurement coming from the EMI receiver and the developed method result when it was set the centre frequency at 100 MHz with a RBW of 3 MHz.

The agreement of the results related to both methodologies is excellent, as the case already mentioned when WGN was applied. No appreciable differences are observed at the probability curve and the difference at the highest level of amplitude is lower than 0.5 dB. Concerning the APD diagram obtained when transient interference is measured, the contribution of the WGN is observed at the left side

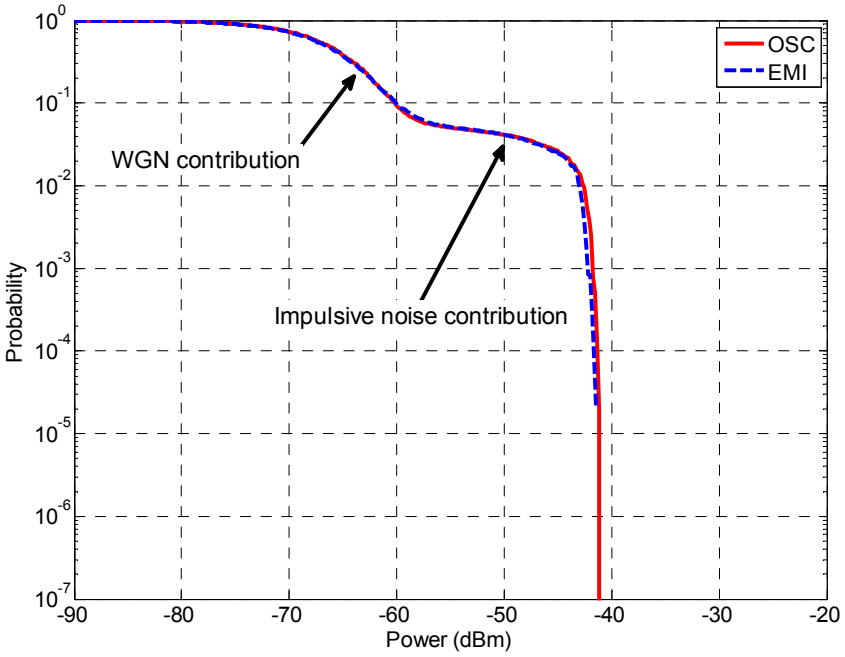

FIGURE 4.18: APD measured at 100 MHz employing a resolution bandwidth of 3 MHz, when conducted impulsive interference according to 61000-4-4 is applied.

of the APD result and the shape is changed at 0.05 probability value due to the transient contribution. A straight line appears finishing abruptly at the maximum value of amplitude measured; this straight line is directly related to the frequency and duration of the transient interference, while the maximum level of amplitude is related to the peak level of the impulsive interference. This type of distribution seen in the APD diagram is characteristic of impulsive interferences, therefore transient interference produce heavy-tailed distributions [8].

Once conducted WGN and impulsive interference have been validated, it is time to study radiated transients varying its parameters and study their impact over the APD diagram.

4.3.3 Radiated Burst according to EN 61000-4-4

In this section, radiated transient interferences are measured with the conventional acquisition instrumentation and the developed methodology. The test setup consists of a burst generator (Schölder SFT SFT1400) according to EN 61000-4-4 placed inside an anechoic chamber and an AC cable connected directly to the output of the transient generator. The validation procedure has been done inside a full anechoic chamber to ensure that only the desired radiated transient is measured,

avoiding uncontrolled external interferences and possible internal reflections disturbing the obtained results. A Bilog antenna is placed at 1 meter distance from the AC cable where the transient interference is coupled. The antenna employed is a Schaffner Bilog antenna model CBL6143 that covers the frequency range between 30 MHz and 3 GHz, so it can measure the radiated transient interference (Figure 4.19).

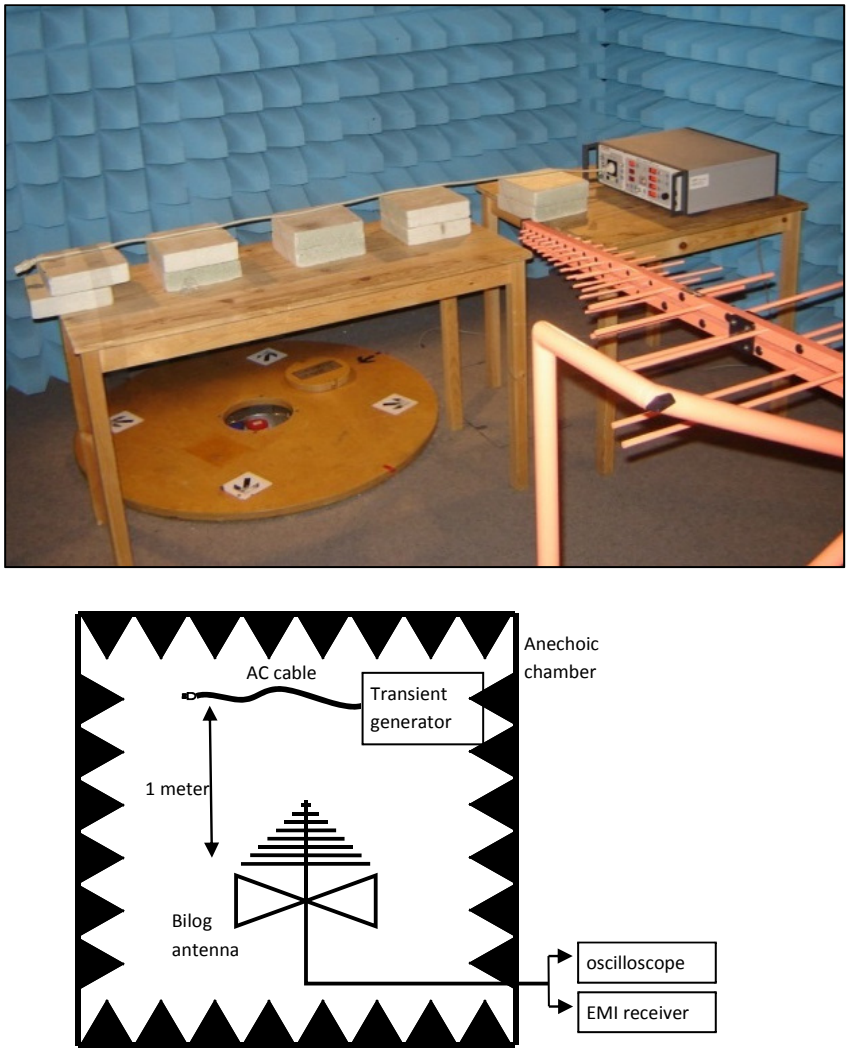

FIGURE 4.19: Measurement test setup built in order to obtain APD from radiated fast transients according to EN 61000-4-4.

The output of the antenna is connected directly to the oscilloscope (Tektronix DPO 7104) for APD measurements according to the new methodology, and it is also connected to the EMI (ESPI3 R&S) receiver to carry out standard APD measurements. The burst generator used has the capability to adjust the frequency, the duration, the interval and the amplitude of the transient interference. Several

interferences have been defined to validate the procedure and also to study the variation of APD measurements (Table 4.1).

TABLE 4.1: Burst interferences applied

Reference	Level (V)	Frequency (kHz)	Duration (ms)
Int1	400	10	50
Int2	200	0.1	50
Int3	200	1	50
Int4	200	10	5
Int5	200	10	50

For measurements carried out with the EMI receiver, different centre frequencies and resolution bandwidth filters are set to obtain the APD measurements. A large number of measurements were performed; the centre frequencies measured were 50 MHz, 70 MHz and 100 MHz; and in each frequency different resolution bandwidths were employed (1 MHz, 3 MHz and 10 MHz). To carry out measurements using the conventional methodology, a time consumption of 10 hours was needed to acquire all the different types of transients defined.

As it has been described before, the measurements are also carried out with the oscilloscope following the guidelines explained at the time-domain transient capture section. The time-domain measurement was done in less than a minute for each transient interference type. As an example, the data acquired with the oscilloscope is the time-domain graph shown in Figure 4.20 for the pulse measurement. The pulse measurement will be used to reach the interference level and the burst measurement will provide the statistical information of the interference. The post-processing time spend to reach an APD diagram at a certain frequency band is only a few seconds when the input signals have 5,000 samples for the pulse measurement and 500,000 samples for the burst capture. In order to obtain better interference measurements several acquisition options could be used; tools such as averaging the waveforms for pulse acquisition; using envelope detector when it is possible at the oscilloscope to get the burst and setting 50 Ω impedance of the oscilloscope to compare with EMI receiver results. These are essential parameters that should be considered.

All the different transients are post-processed using $MATLAB^{®}$ to compare the results obtained with the EMI receiver, but only the most significant results are plotted below to analyze the agreement between both methods. For instance,

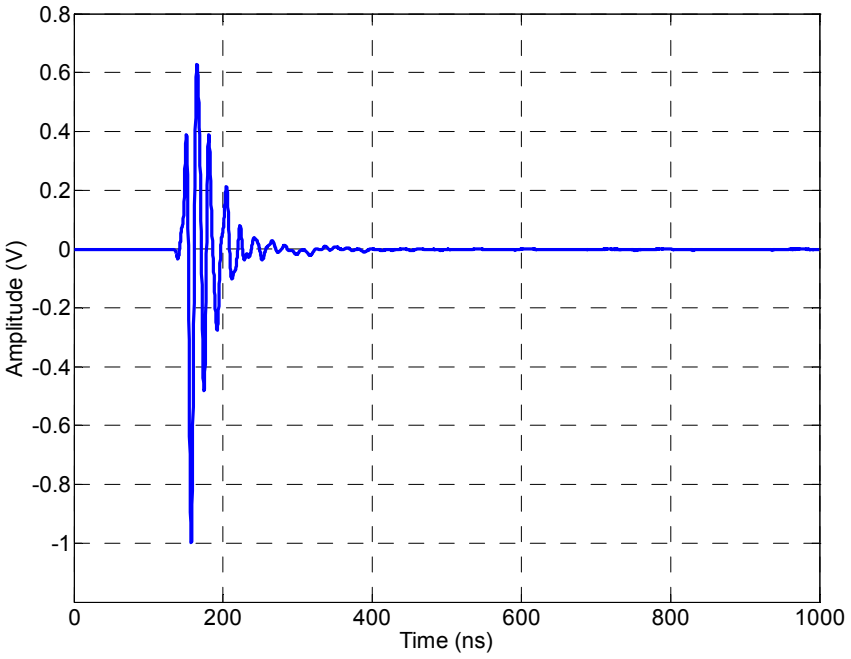

FIGURE 4.20: Time-domain oscilloscope capture of the radiated impulsive noise generated by the burst generator (Schölder SFT SFT1400).

results achieved from the EMI receiver are displayed as dashed lines in Figure 4.21. while solid lines correspond to the oscilloscope based APD proposed method. In this case, the interference measured was Int3 according to Table 4.1. This means that the amplitude of the burst was 200 V, the frequency 1 kHz and the duration 50 ms. The measurement with the EMI receiver was carried out at a centre frequency of 100 MHz using a RBW filter of 1MHz, 3 MHz and 10 MHz.

Regarding the matching of the data reached by both methodologies, again the fitting between APD curves is really good when the different bandwidths are set. Figure 4.21 shows significant differences when several resolution bandwidth filters are employed. The peak level reached has differences up to 10 dB when resolution bandwidth varies only from 1 MHz to 3 MHz and increasing these differences to 20 dB when 1 MHz RBW results are compared with the results produced by 10 MHz RBW. Therefore, it is crucial to measure the interference with the same bandwidth as the communication system that is going to be evaluated. This implies that only correct measurements will be provided by the EMI receiver when the bandwidth of the communication system coincides with the resolution bandwidths available on the instrument. Otherwise, with the new proposed time-domain methodology the bandwidth filter can be selected with no limitation.

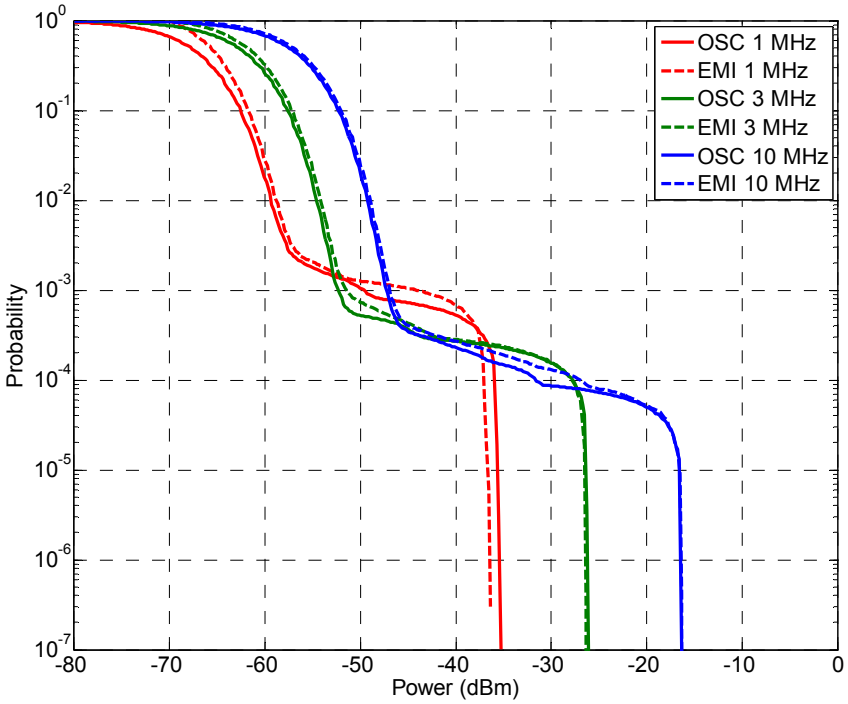

FIGURE 4.21: APD measured at 100 MHz employing a resolution bandwidth of 1, 3 and 10 MHz; when Int 3 radiated impulsive interference is applied.

From the APD measurements, the effect of varying the frequency of the burst interference can also be easily studied. For this reason, interferences Int2, Int3, Int5 defined in Table 4.1 are compared, where Int2 burst frequency is 0.1 kHz, Int3 frequency is 1 kHz and, finally, Int5 frequency is 10 kHz. All the other interference parameters, amplitude and duration are the same in those transient interferences. Similar to the previous cases, the results shown in Figure 4.22. display the APD diagram acquired directly from the receiver and the results achieved with the oscilloscope measurements after being post-processed. The APD measurements were carried out at 50 MHz centre frequency, with a resolution bandwidth of 3 MHz.

Observing the APD results, the agreement between the standard EMI receiver measurement and the developed method using the oscilloscope is good. In all the cases, the difference of the interference maximum amplitude is less than 1 dB and the probability of the highest amplitude matches perfectly. However, minor probability differences appear when the amplitude of the interference is between -50 dBm and -30 dBm.

If the behavior of the APD results is analyzed according to the variation of the burst frequency, a noticeable consequence is detected over the resultant diagram.

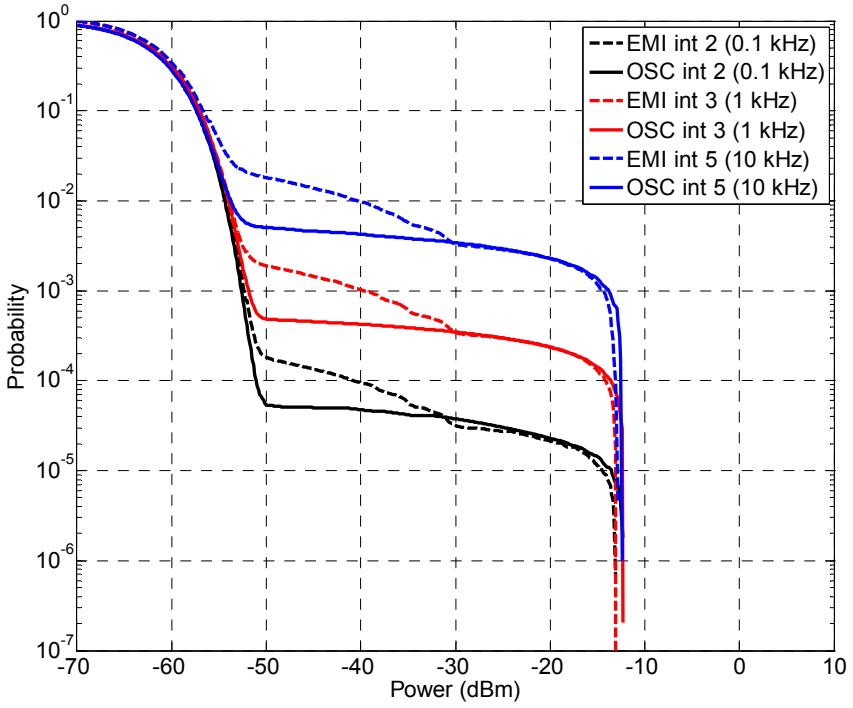

FIGURE 4.22: APD measured at 50 MHz employing a resolution bandwidth of 3 MHz; when Int 2, Int 3, Int 5 radiated impulsive interference are applied.

As the frequency is increased by a factor of 10, the probability curve and the probability at the maximum level of the APD diagram are also increasing by a factor of 10. This is a great example to show the powerful capabilities of the statistical analysis that APD provides compared to methodologies defined at the EMC standards, where all the measurement information come from peak, quasi-peak and average detectors.

4.3.4 Radiated ESD according to EN 61000-4-2

The last test-case validates the methodology employing a different type of impulsive interference. In this case, the interference source used is an ESD gun according to standard EN 61000-4-2. The ESD gun produces discharges of +1 kV to a conductive strip with a repetition rate of 20 Hz. Compared to burst generator, the ESD is capable of generating pulses with smaller rise time; the rise time defined in the standard is 0.8 ns. Hence, measurements of the radiated interference will end at frequencies up to 1 GHz [14].

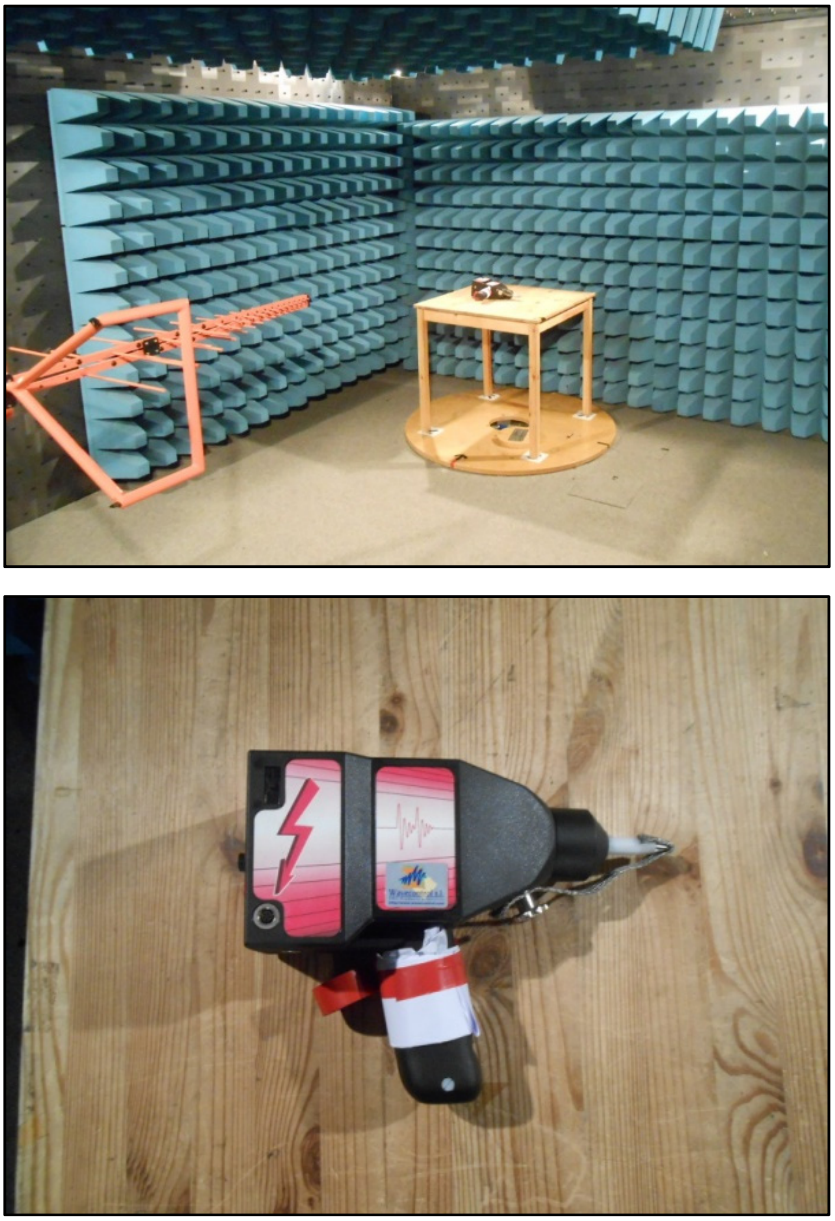

FIGURE 4.23: Measurement test setup built in order to obtain APD from ESD arching effect.

To measure the radiated transient interference, the Schaffner Bilog antenna model CBL6143 that covers the frequency range between 30 MHz and 3 GHz is employed. The output of the antenna is connected by means of a coaxial cable to the oscilloscope (Tektronix DPO 7104), for the new proposed time-domain APD measurements, and it is also connected to the EMI receiver (ESPI3 R&S) to carry out the standard APD measurements. The measurements have been performed inside a full anechoic chamber avoiding uncontrolled interferences (Figure 4.23).

Measurements were conducted with the EMI receiver at the following frequency

bands: the centre frequency was set to 381.5 MHz, which is reserved for TETRA security services; to 923 MHz, which coincides with the frequency reserved for the downlink GSM-R services; and it was also set to 100 MHz, as it is a frequency band distant from previous ones. At these different frequencies several resolution bandwidths were also set simulating the digital services to protect. Measurements performed using the oscilloscope were configured with the sample rate at 5 Gsample/s and the record length was 200 ns. As it is a controlled and repeatable source according to standards, the pulse measurement was averaged with 500 waveforms to reduce measurement noise. The pulse measurement is shown in Figure 4.24. Moreover, the same time-domain acquisitions make it possible to evaluate frequency bands far away between them like GSM-R downlink that is at 923 MHz and TETRA which was measured at 381.5 MHz.

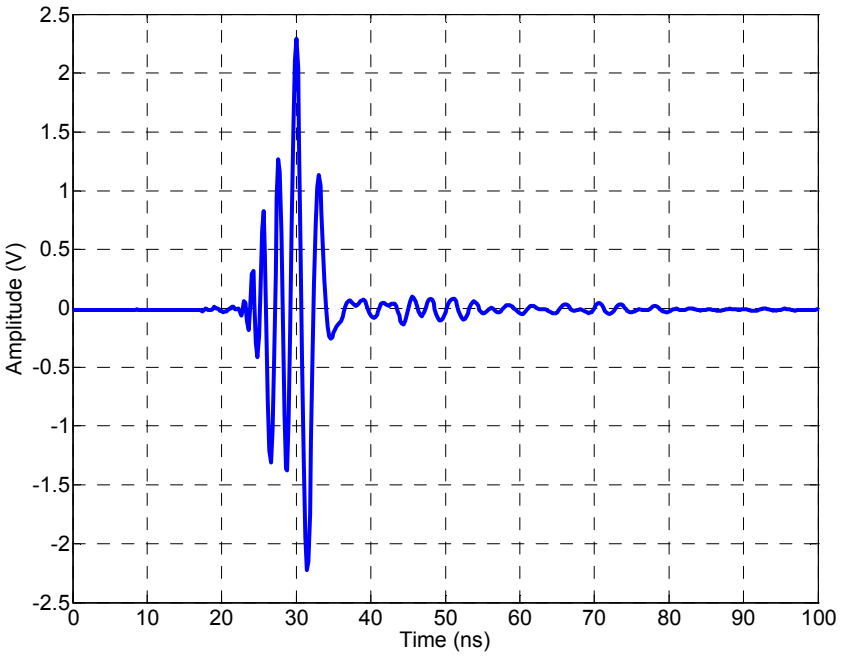

FIGURE 4.24: Time-domain oscilloscope capture of the radiated transient generated by the ESD gun.

The first results analyzed in this example are the ones obtained with a bandwidth of only 30 kHz. Measuring these frequency bands is a challenge for the proposed methodology as the level of amplitude coupled could be very low and a high sensitivity is needed. Figure 4.25 represents the results achieved with both measurement approaches.

Evaluating the similarity between the results obtained with the standard EMI receiver and the data found employing the TD captures and post-processing, the

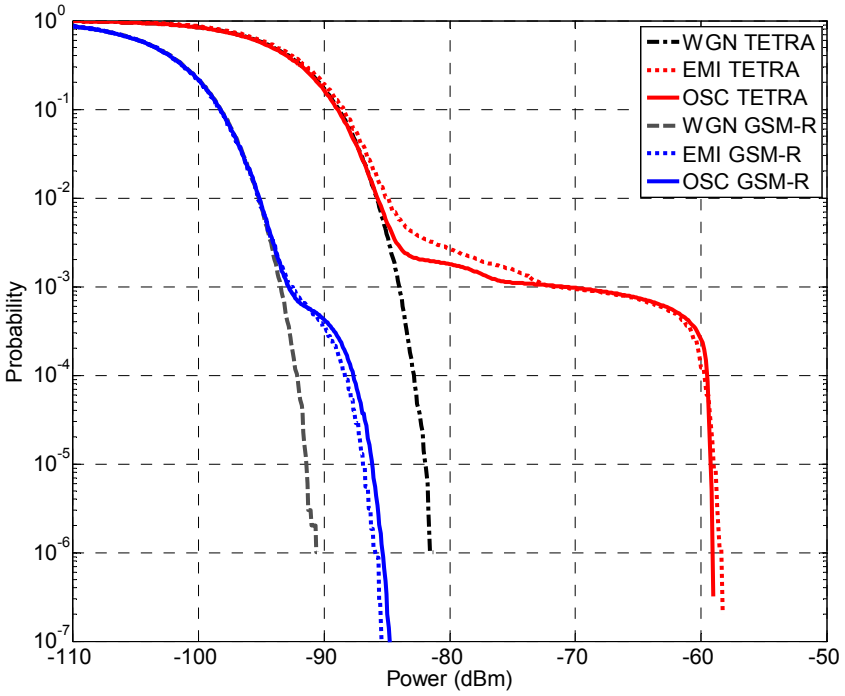

FIGURE 4.25: APD result comparing TETRA and GSM frequency bands employing a 30 kHz bandwidth when ESD radiated transient interference is measured.

outcome is an excellent concurrence. From Figure 4.25 it can be perceived that the shape of the APD diagram is almost equal in both evaluated cases; the probability and amplitude are fitting extremely close for the evaluation at 923 MHz when a 30 kHz bandwidth filter is employed and also when the evaluation is carried out at TETRA frequency band (381.5 MHz). Considering the deviations in amplitude, the maximum value of amplitude difference is less than 1 dB. When the transient noise is measured at TETRA frequency band, the maximum value of amplitude obtained is -58 dBm. Alternatively, the maximum level at the GSM-R frequency band is only -85 dBm. This implies that the coupling to the TETRA frequency band at 381.5 MHz is more severe than the portion of the ESD interference coupled to the frequency band corresponding to 923 MHz (GSM-R).

To illustrate the contribution due to the frequency band evaluated, the APD diagram has been computed at several frequency bands employing another resolution bandwidth. In this case, the bandwidth selected is 3 MHz and the centre frequencies chosen are 100 MHz, 381.5 MHz (TETRA) and 923 MHz (GSM-R). Figure 4.26. shows the results reached with the time-domain capture after post-processing it using Matlab.

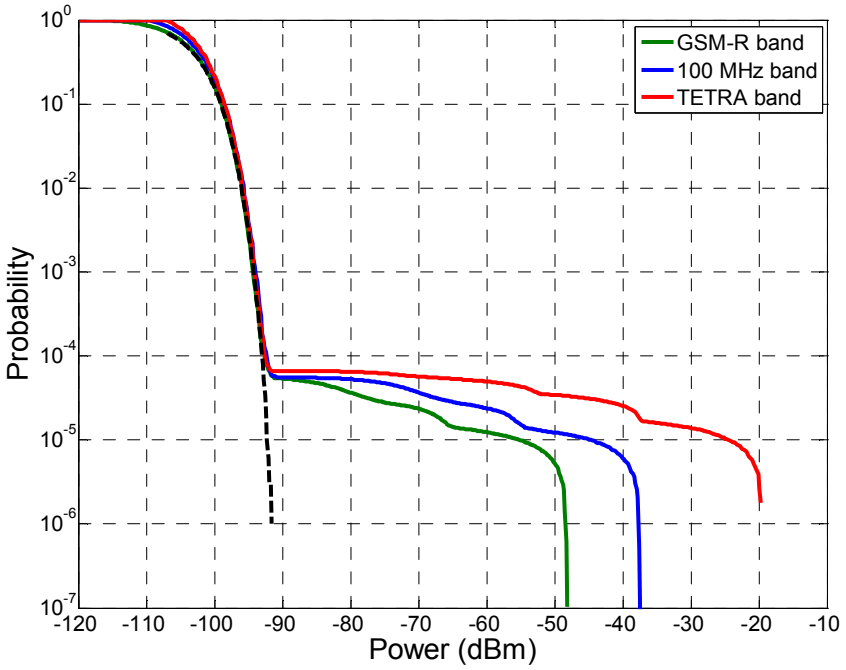

FIGURE 4.26: APD result comparing GSM-R, TETRA and 100 MHz frequency bands using a 3 MHz bandwidth.

The time-domain captures have been performed using 8 bits Tektronix DPO oscilloscope averaging 500 waveforms. It is really noticeable that due to the post-processing filtering, the sensitivity reached is extremely high; achieving values up to -100 dBm. Observing the results provided by Figure 4.26 it can be noted that the electromagnetic field generated by the electric spark coupled to the Bilog antenna varies in amplitude from -48 dBm to -20 dBm depending on the frequency band considered. The maximum value recorded was at 381.5 MHz, the second corresponds to 100 MHz and the last was at 923 MHz; this is associated to the metallic strip size, the antenna performance and also to the frequency domain characteristics of the interference pulse generated.

Additionally to the centre frequency, the bandwidth has also a strong influence over the APD graph. Results presented in Figure 4.27 show the influence of using different bandwidth at the GSM-R centre frequency (923 MHz). The plots refer to the data obtained with oscilloscope and EMI receiver when 30 kHz and 1 MHz bandwidths are set; and the 200 kHz GSM-R channel spacing is set only with the new time-domain method, as it is not available at the EMI receiver.

Considering the agreement between the data obtained with the EMI receiver and the oscilloscope captures, the similarity is excellent when amplitude values and

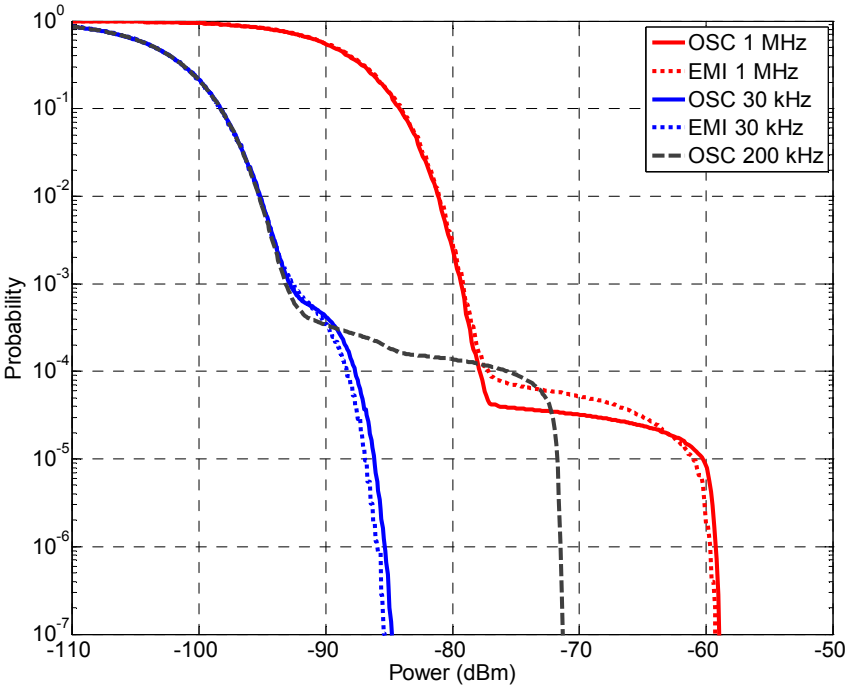

FIGURE 4.27: APD results at GSM-R centre frequency using 30 kHz, 200 kHz and 1 MHz bandwidths when ESD radiated transient interference is measured.

shape fitting are considered. The developed methodology using time-domain captures allows us to evaluate any frequency band with the post-processing. In Figure 4.27, the 200 kHz measurement is plotted, highlighting large differences obtained at the APD diagram when the other bandwidths are employed.

Differences are similar to the previous case, when TETRA and GSM-R bands were compared with the same resolution band. In this example, the centre frequency is equal but the bandwidth is varied from 30 kHz to 1 MHz appearing divergences around 25 dB. On the other hand, when the 200 kHz bandwidth is computed by the developed method, amplitude differences between 12 dB and 14 dB are observed compared with 1 MHz bandwidth and 30 kHz bandwidth. Therefore, this example clearly shows the importance of measuring the interference with the same bandwidth as the communication system. For GSM-R system the channel spacing is 200 kHz, so with EMI receivers the bandwidth equal to the channel spacing cannot be set. Otherwise, with the time-domain developed technique, there is not any inconvenience to set the bandwidth to 200 kHz because there is no hardware limitation.

Finally, it is important to emphasize that time-domain methodology presented in this work makes it possible to carry out quick measurements reducing the time

needed to provide satisfactory APD results, when the duration of the transient interference is really short. Otherwise, standard EMI receiver measurements will not be able to obtain all the statistical information of the short impulsive noise and produce satisfactory APD results.

Chapter 5

Application: GSM system interfered by radiated transients

5.1 Introduction

With the objective to demonstrate that the developed methodologies are suitable to achieve the thesis goals, in this chapter a transient interference scenario is evaluated. The different methodologies created are employed to estimate the error that will be introduced into a DCS using previous time-domain measurements of radiated transients. Although an extensive validation procedure has been performed along the thesis, a final application procedure is carried out to highlight the capabilities of the developed methodologies. As it is described in Figure 5.1, three different procedures to quantify the degradation produced by the impulsive noise are carried out.

The first way to obtain the degradation caused by the radiated transients is the direct evaluation. The methodology consists in placing an equipment of the DCS that we want to evaluate under the influence of radiated transient interference. The equipment will transmit and receive data in order to obtain the bit-error-probability. This methodology will be used as the reference for the other methodologies that have been developed in this research work. The second methodology to predict the degradation produced by the transient interference over the DCS

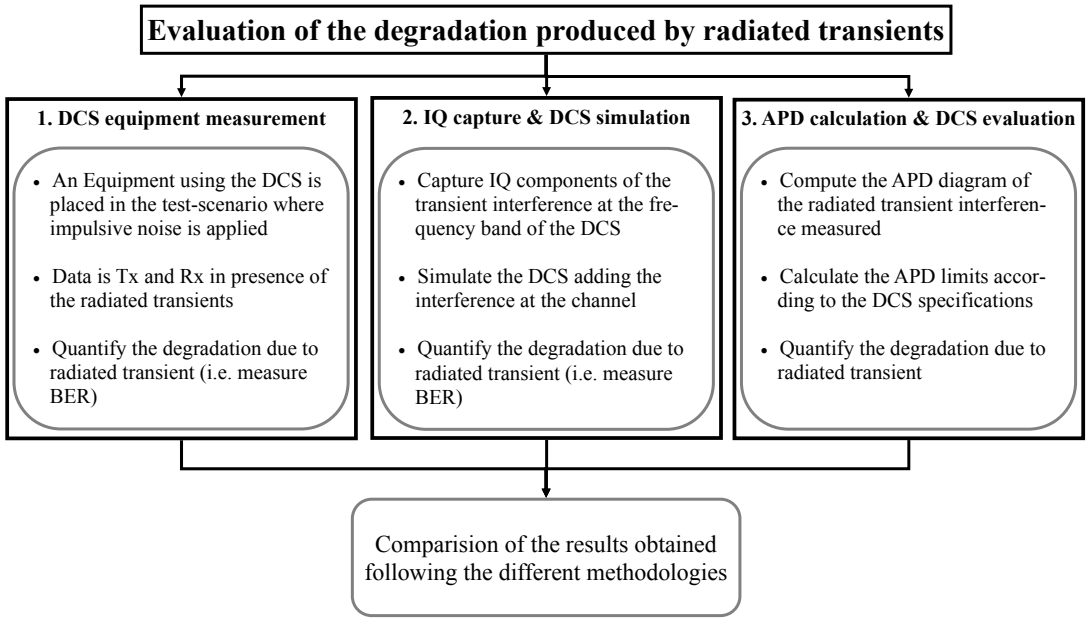

FIGURE 5.1: Schematic of the different methodologies employed to estimate the degradation produced to a digital communication system.

involves the time-domain acquisition of the interference. The in-phase and quadrature components are measured according to the developed methodology explained in Chapter 2 and afterwards, a simulation of the DCS adding the interference is performed. The simulation of the DCS considering the impulsive noise enables us to quantify the degradation produced by the radiated transient interferences as it is described in Chapter 3. Finally, the third methodology to estimate the degradation produced at the DCS consists in compute the APD diagram using the time-domain measurement of the radiated interference. As it is explained in Chapter 4, the methodology developed allows us to obtain the APD diagram of the interference. Therefore it is possible to calculate the APD limits related to the DCS specifications and estimate if the communication system is interfered.

Once all the results of the different methodologies have been obtained, they will be compared to show their agreement. Consequently, it will be concluded if the novel measurement and analysis methodologies enable us to estimate properly the degradation produced by transient interferences achieving the thesis goals.

5.2 Test Scenario

5.2.1 GSM system interfered by radiated transients produced by sparks

The communication system selected to evaluate its performance under the effect of transient interferences is the worldwide used GSM system, which will be interfered by radiated transients generated by sparks. The purpose of choosing this communication system is to reproduce in the laboratory the common interference scenario that has been described in the introduction section. The objective is to emulate the GSM-R system that it is interfered by the arching effect caused by the discontinuity between the pantograph and the catenary, shown in Figure 5.2. As it has been explained, the radiated transients reach the GSM-R antenna of the mobile station that is placed on the roof of the rolling stock producing irrecoverable errors at the downlink of the DCS, which can create problems related to passengers safety [24, 26, 30–32, 41, 51].

FIGURE 5.2: Arching effect caused by the discontinuity between the pantograph and the catenary.

5.2.2 Laboratory GSM interference scenario

The interfering scenario that has been built in a test lab to interfere and measure with the different methodologies the disturbance produced to the GSM system is described next. Firstly, it is important to mention that the test has been performed

in an anechoic chamber avoiding other interferences coming from uncontrolled sources. Inside the anechoic chamber the Schlöder ESD simulator model SESD 200 in conformity with EN 61000-4-2 has been used to generate the sparks to interfere the GSM system. The ESD gun emulates the sparks that are produced by the discontinuity between the pantograph and the catenary in the railway. The sparks generated by the ESD gun at the lab produce an electromagnetic field that reaches a Mobile Station (MS) and also a GSM antenna, which are placed close to the spark generator at 50 cm. In this study case, it has been used a mobile phone as a MS according to the GSM standard.

Regarding the mobile phone, it is used to execute the first methodology where a measurement of the equipment is performed when the radiated transient is present. Consequently, it is necessary to create a link between the mobile and an auxiliary equipment that enables to monitor the quality of the data transmission. In our application, a GSM Mobile Station Test Unit is employed to simulate a Base Transceiver Station (BTS) and quantify the error produced by the sparks close to the mobile. In addition, as the sparks are produced close to the mobile, the interfered GSM communication signal will be the associated with the downlink signal.

Concerning the other methodologies used to evaluate the performance of the GSM system when it is interfered by the sparks, the measurement system is composed by a GSM antenna, an EMI receiver and an oscilloscope. The GSM antenna is connected directly to the EMI receiver and the IF output is conducted to the oscilloscope input. The IF data is captured in time-domain to afterwards, by means of post-processing employing Matlab, obtain the IQ components of the sparks interference at the frequency band of the GSM downlink channel.

In the second methodology, the GSM system is simulated employing Simulink and the previous measure is added to the DCS simulation. The output of the simulation will let us to know the bit error rate of the communication system in presence of the sparks produced by the ESD gun.

Alternatively, to obtain the results of the third methodology, a different post-processing is employed to reach the APD diagram employing the same time-domain measurements used before. In the next sections a more detailed description is provided for each methodology. Otherwise, in Figure 5.3, the basic schematic that

has been described in this section concerning the scenario and the measurement methodologies is shown.

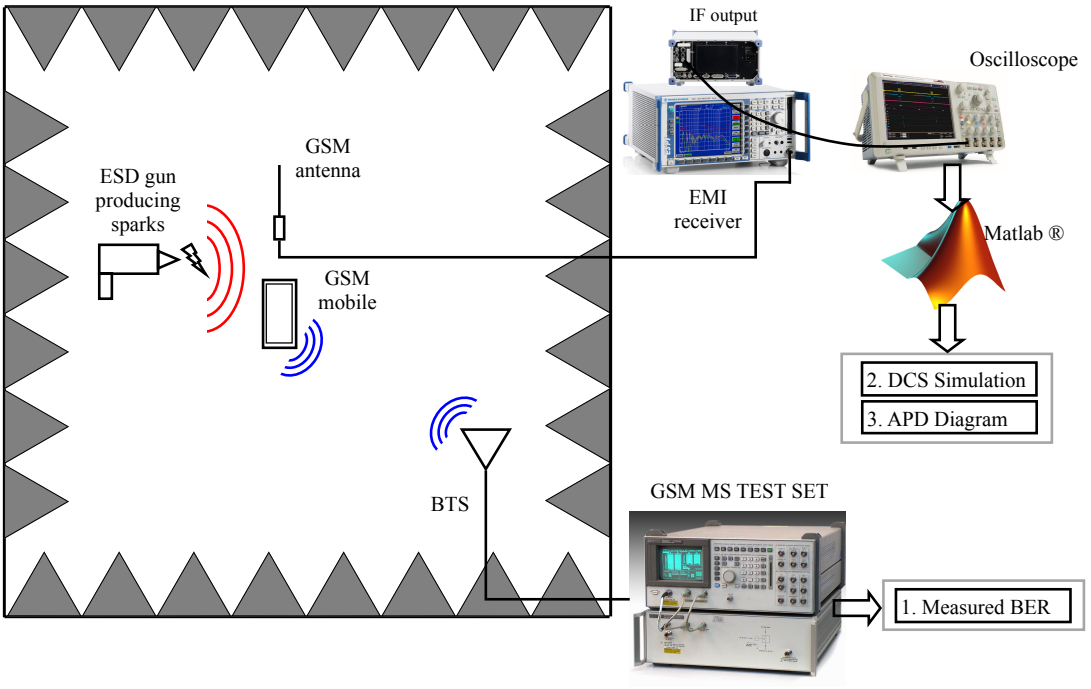

FIGURE 5.3: Measurement scenario of the GSM interfered system.

Regarding the sparks created to interfere the communication system, they are generated placing a metallic slice close to the air-discharge test electrode. The repetition frequency of the discharge pulses depends on the distance between the discharge electrodes and the metal where the discharge is produced. With the aim to study several cases of interference, the distance has been varied to produce different repetition rate of the sparks. In the thesis it has been largely discussed that the repetition rate of the transient interference is a key parameter to interfere a digital communication system. Therefore, two different distances have been selected to produce impulsive noise with different repetition rates. The first distance selected is the minimum distance that enables a spark to takes place. The minimum distance will allow us to evaluate the case with the highest repetition rate. Moreover, a larger distance equal to 1 mm has been also selected to view the incidence of a lower repetition rate over the degradation of the DCS. Regarding the amplitude set at the ESD gun, it has been set to +12 kV. However as the dielectric breakdown voltage is lower due to the proximity between the electrode and the metal this tension is not reached.

5.2.2.1 DCS equipment measurement procedure

The first evaluation method is used as the reference to determine if the developed methodologies results are in accordance. As it has been mentioned before, the measurement carried out involves an equipment (a mobile station) and a Base Transceiver Station (BTS), simulated by the Hewlett-Packard GSM Mobile Station Test Unit model HP8922M. The aim of the measurement is to evaluate the downlink of the GSM system which can be interfered by the sparks produced close to the mobile station. The downlink is the problematic link in the GSM-R system because the signal level received from the BTS is extremely weak.

The GSM technical specification ETSI GSM 05.08 [35], establishes that the mobile station shall report the received signal quality. In the technical specification it is detailed how the received signal quality shall be measured by the MS in a way that can be related to an equivalent average BER before channel decoding. The parameter that is used to record the quality of the received signal is the RXQUAL. The GSM technical specification defines eight levels of RXQUAL that must be mapped to the equivalent BER before channel decoding as it is detailed in Table 5.1.

TABLE 5.1: GSM technical specification to quantify the signal quality

Quality Band	Range of actual BER	Assumed value
RXQUAL_0	Less than 0.2 %	0.14 %
RXQUAL_1	0.2 % to 0.4 %	0.28 %
RXQUAL_2	0.4 % to 0.8 %	0.57 %
RXQUAL_3	0.8 % to 1.6 %	1.13 %
RXQUAL_4	1.6 % to 3.2 %	2.26 %
RXQUAL_5	3.2 % to 6.4 %	4.53 %
RXQUAL_6	6.4 % to 12.8 %	9.05 %
RXQUAL_7	Greater than 12.8 %	18.1 %

It is important to remark that the BER probabilities values used to define a quality band are the estimated error probabilities before channel decoding. After channel decoding the RXQUAL probability values are also specified but are different from the values described in Table 5.1. In our application, the RXQUAL value before the decoding is provided by the MS and it is shown at the screen of GSM MS Test unit. Additionally to the RXQUAL reported by the MS, BER measurement can be also carried out using the GSM MS Test unit providing more accurate measurements than the RXQUAL.

Once the quality parameters to quantify the degradation of the GSM communication system have been defined, the procedure to measure the influence of the radiated transient is explained following:

1. The GSM MS Test unit is set up to offer coverage to the MS. A single channel of the GSM frequency band is selected and the output power is defined to establish the communication. The power has to be defined to work with the wanted reception level at the MS and also to maximize the transmitted power of the MS to not influence the uplink channel with the radiated interference.

2. After the link has been set up an established between the MS and the GSM MS Test unit, a call is performed by the GSM MS Test unit to the MS in order to generate a link bit transfer between them.

3. Finally, during the call, the different radiated transient interferences are applied and the RXQUAL parameter is recorded. In addition to the reported RXQUAL by the MS, a BER measurement is also carried out using the GSM MS Test unit to obtain a more accurate BER.

Consequently, when the first methodology is applied for each of the transient interferences that we want to evaluate, the RXQUAL reported by the MS and the BER measured by the GSM MS Test unit are information available, which will be used as the reference for the other measurement and evaluation procedures.

5.2.2.2 IQ capture & DCS simulation procedure

The second methodology is based on the acquisition of the IQ components of the radiated interference developed in this work. Afterwards, a simulation of the DCS adding the interference previously measured is performed to determine the degradation produced by the impulsive noise.

Regarding the time-domain measurement of the transient interference, the acquisition is carried out following the advanced measurement methodology described in section 2.3.2. As it is explained in Chapter 2, to perform the time domain measurement, the receiver antenna is connected to the R&S EMI receiver ESPI3 centred at the working frequency of the DCS and the IF output of the EMI receiver is connected to the oscilloscope Tektronix DPO7104. This instrumentation

combination is used to join EMI receiver high sensitivity capability and the time-domain and event detection capabilities provided by the oscilloscope. Then, a final post-processing stage is carried out by mathematical software, where the IQ components of the radiated transient interference are obtained.

Regarding the scenario built to estimate if the GSM system is interfered by the sparks produced close to the MS, a GSM antenna is placed side-by-side to the MS and connected directly to the EMI receiver. When sparks begin to be generated, the oscilloscope detects the event and starts recording the IF signal coming from the EMI receiver. This signal is digitalized and stored properly as it was described in Chapter 2. Afterwards, the IF signal modulated at 20.4 MHz is down-converted to the base-band and filtered by the bandwidth of the GSM channel, which is equal to 200 kHz in the post-processing stage.

The second stage of the methodology is to employ the IQ base-band interference adding it into a base-band simulation of the GSM communication system. As it is described in section 3.3, the DCS simulation enables us to determine the BER of the communication system when the radiated transient interference is present at the environment. Considering the peculiarities imposed by the GSM system simulation, more details are described in section 5.4.2 of this chapter.

5.2.2.3 APD calculation & DCS evaluation

The last methodology to determine if the radiated transient interferences generated by the sparks cause malfunction to the GSM system is based on the APD diagram. In this occasion, the previous IF measured signal is used to compute the APD diagram of the transient interference. The statistical measurement enables us to know all the information regarding the measured interference. Moreover, as it has been mentioned before, it is possible to establish limits at the APD diagram to analyse if a certain interference will produce degradation on the DCS. Therefore, using the APD data obtained following the procedure described in Chapter 4 and calculating the limits referred to the GSM technical specification, we will be able to estimate the degradation produced by the sparks.

Regarding the limits that must be introduced to the APD diagram, in Appendix B an extended explanation is given to understand where they are coming from and how to calculate the limit points. However, in general terms those limits dots

are related to the probability required by the system specifications and also to the amplitude of the received signal. In our study case scenario, the BER requirements are related with the RXQUAL following the GSM specifications described in Table 5.1. Consequently, we will be able to compute and plot the APD limit points at the APD diagram following the equation described below.

$$(u_{limit}, \quad P_{limit}) \equiv \left(\frac{\beta_1 A}{\sqrt{m}}, \quad P_{req}\right) \tag{5.1}$$

where for a QPSK modulation scheme $\beta_1 = 1$, $m = 2$, A is the rms amplitude of the communication signal and P_{req} is the probability required by the communication system [88]. Therefore, in the GSM system evaluation we will compute a limit point for each RXQUAL value, meaning that if the APD curve is above the limit point, the GSM system will have a BER associated to the limit point. In Figure 5.17 an example of the APD diagram including the limit points can be observed.

5.3 Measurement of the interference

The radiated transient interferences are measured according to the developed advanced technique to use them in the second and the third methodologies. A detailed description of the instrumentation and the parameters configured to obtain, at the end of the procedure, the in-phase and quadrature components of the impulsive noise are explained in this section. Moreover, the time-domain results obtained for each of the radiated transient produced by the sparks are also shown.

As it has been mentioned before, two different radiated transient interferences have been generated to produce disturbances on the GSM downlink. When the electrode of the ESD generator is at the minimum distance to the metal, sparks with higher repetition rate are produced; we have named this interference as Sparks High Rate (SHR) interference. Otherwise, when the metal is placed at the distance of 1 mm, sparks with lower repetition rate are generated and the radiated transient has been named as Sparks Low Rate (SLR) interference. In Figure 5.4 pictures of the interferences SHR (a) and SLR (b) are shown.

For the time-domain acquisition, the GSM antenna is connected to the R&S ESPI3 EMI receiver. The EMI receiver is centred at the frequency band of the downlink

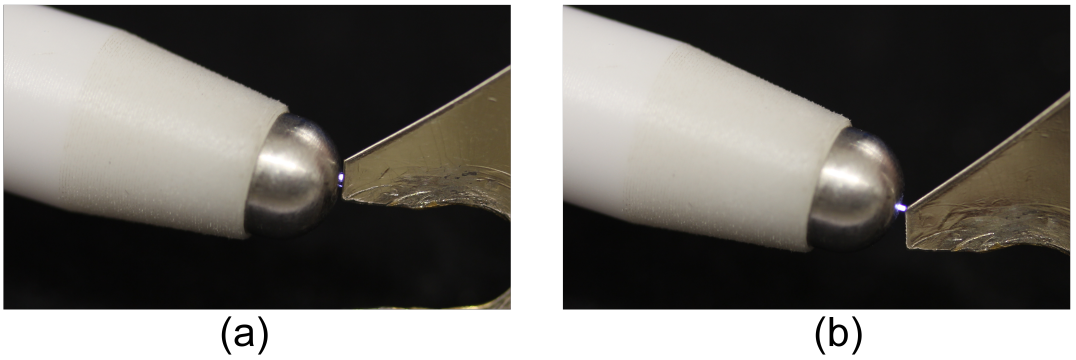

FIGURE 5.4: Pictures of SHR interference (a) and SLR interference (b)

GSM channel 20, which corresponds to 939 MHz. Regarding the resolution bandwidth employed at the EMI receiver, it is set at 3 MHz, which is larger than the 200 kHz of the GSM channel bandwidth. The reference level of the EMI receiver is also configured to maximize the dynamic range without saturating the instrument. The IF output signal is used as the input of the Tektronix DPO 7104 oscilloscope, which is sampling at 125 MSamples/s as the IF output of the EMI receiver is 20.4 MHz. The total record length set to carry out the measurements is 10^6 samples, as it has been sufficient to measure all the main parameters of the transient interference. This 10 millions of samples correspond to a total acquisition time of 80 ms.

Figure 5.5, shows the IF signal captured by the oscilloscope when the SHR interference is produced. The total time observed is equal to the 80 ms, where 104 pulses appear due to the high rate of the sparks produced by the breakdown of the air dielectric. Figure 5.6, shows the IF signal captured by the oscilloscope when SLR interference is applied.

Once the IF measurement has been carried out, it is time to apply the post-processing to obtain the in-phase and quadrature components of each type of interference. Furthermore, in this stage the interference is filtered by the GSM frequency bandwidth in order to know the exact interference that will be received by the MS.

In Figure 5.7 the in-phase component of the 104 transient pulses detected is represented after it has been filtered through the 200 kHz bandwidth. In Figure 5.8 the quadrature component is represented overlapping the 104 transient pulses that occur in the 80 ms. The maximum value measured for the SHR interference is around 150 V.

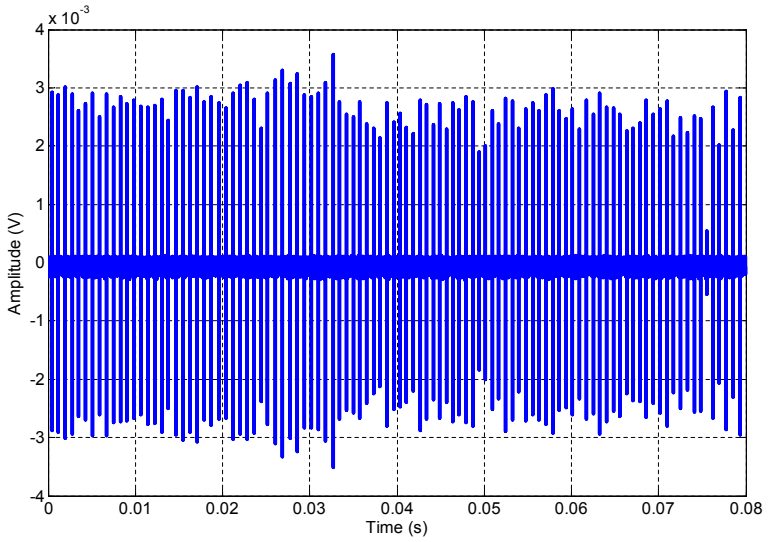

FIGURE 5.5: Time-domain measurement of the IF signal when the SHR interference is produced.

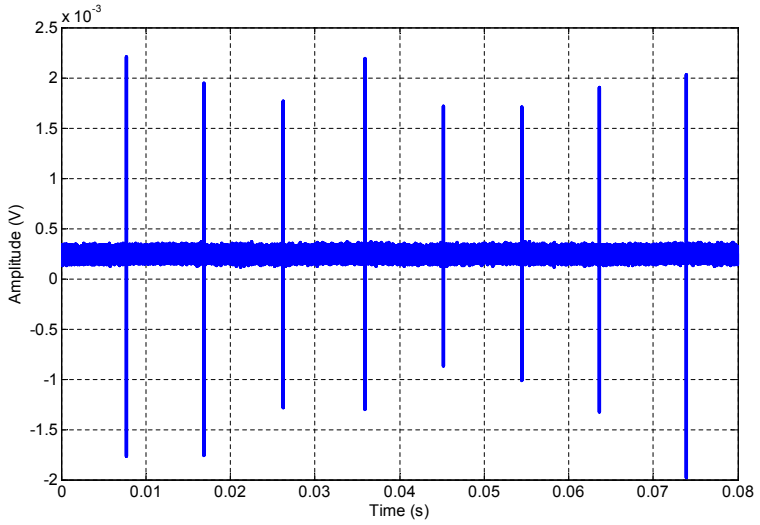

FIGURE 5.6: Time-domain measurement of the IF signal when the SLR interference is produced.

Finally, the in-phase and quadrature components are represented in Figure 5.9 and Figure 5.10 when the SLR interference is produced by the ESD gun. In comparison with the IQ components of the SHR interference, the amplitude has been reduced to 30 V and the number of pulses generated by the sparks has been reduced to just 8 pulses in 80 ms. Consequently, the repetition rate of the interference has been varied from a mean frequency of 1.3 kHz when the SHR interference is generated to 100 Hz when the SLR interference is applied.

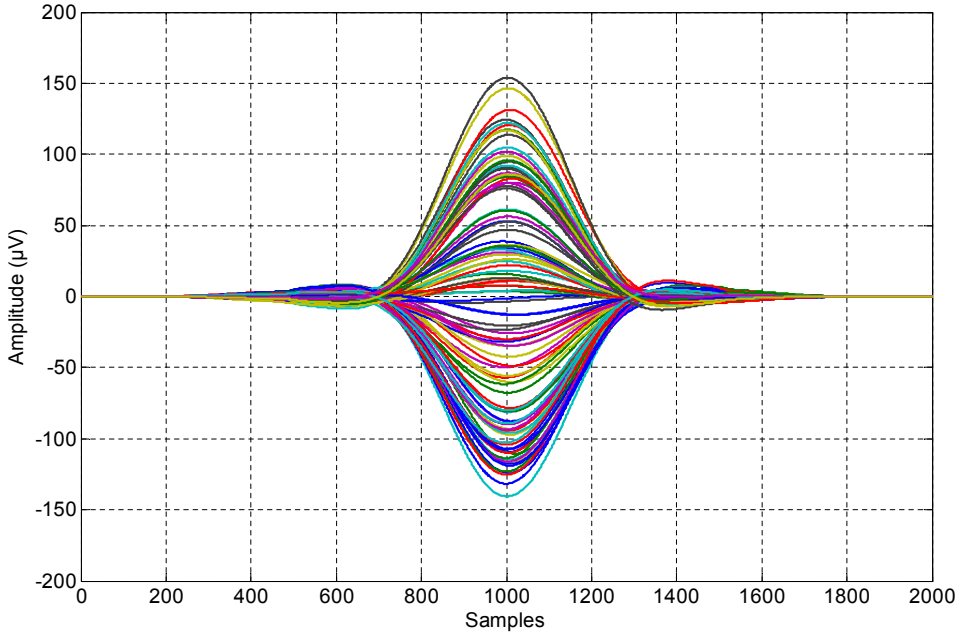

FIGURE 5.7: In-phase component of the transient interference when the SHR interference is produced.

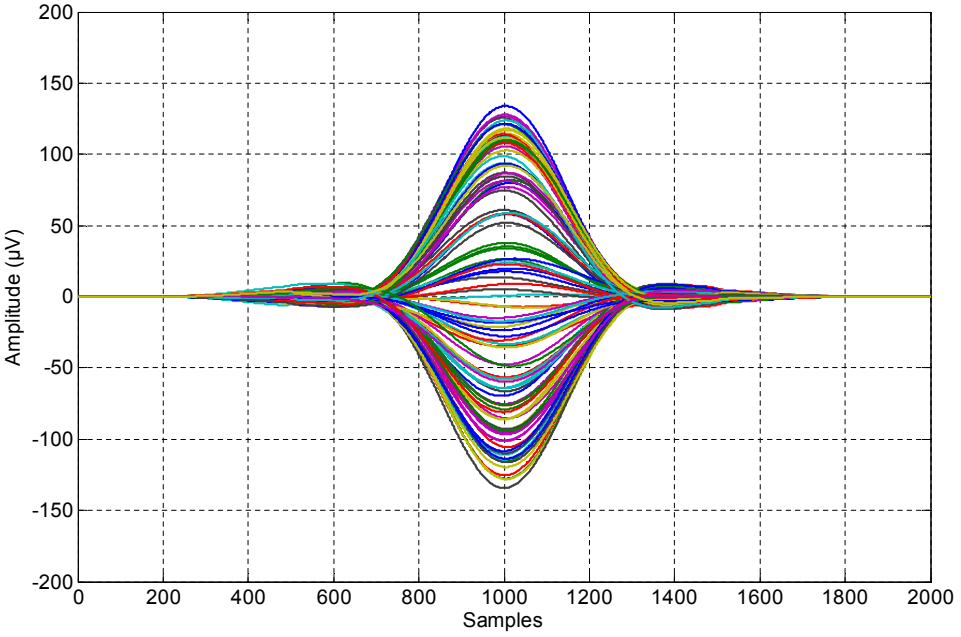

FIGURE 5.8: Quadrature component of the transient interference when the SHR interference is produced.

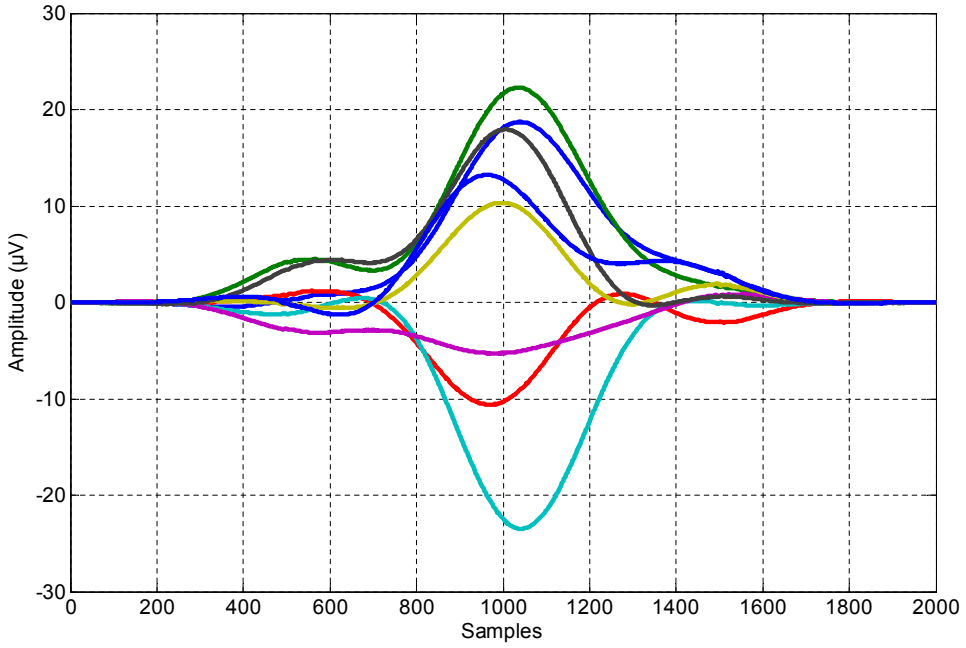

FIGURE 5.9: In-phase component of the transient interference when the SLR interference is produced.

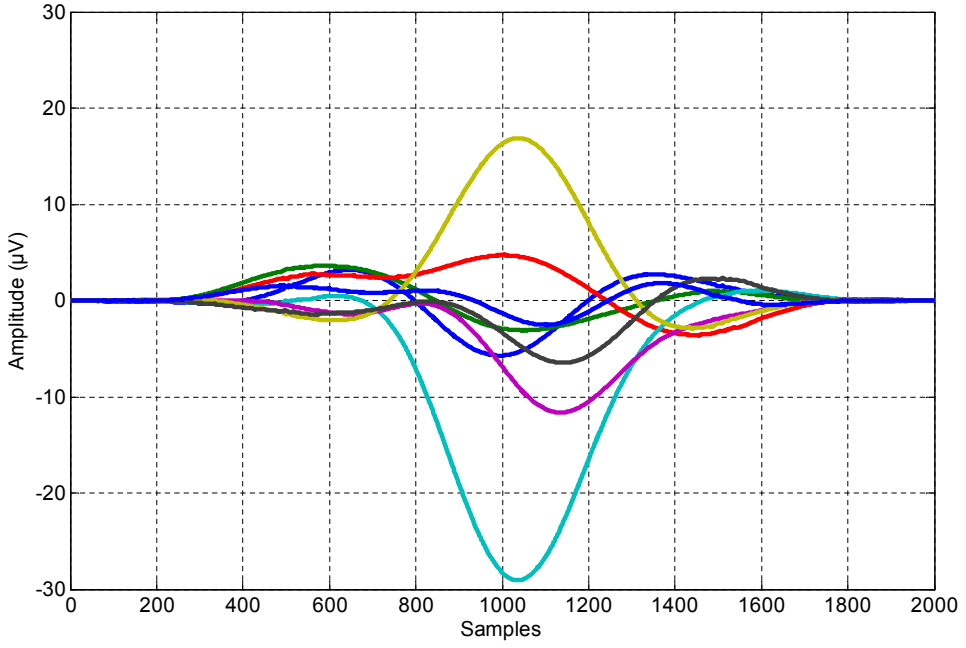

FIGURE 5.10: Quadrature component of the transient interference when the SLR interference is produced.

5.4 Evaluate the degradation produced to the GSM system

In this section, the results of the three procedures to determine the distortion produced by the two radiated transient interferences on the GSM system are presented.

5.4.1 BER measured with the GSM MS Test unit

In order to carry out the measurements, the link between the MS and the GSM MS Test unit is created. The GSM communication channel designated has been chosen arbitrary without any specific condition; the channel selected is 20 which corresponds to an uplink frequency of 894 MHz and a downlink frequency of 939 MHz. Regarding the output an input level set, the GSM MS Test unit has been configured providing the mobile a signal corresponding to an RXLevel equal to 25, which corresponds to a signal between -86 dBm and -85 dBm. If a lower level of the receiver signal is selected, it will imply that it will be easier to disturb the communication, on the other hand if the received signal level is higher, it will be more difficult to interfere the communication system. Therefore, the level of signal received has been selected in terms of a reliable situation, considering that usually the GSM-R communication system receives levels that vary from -40 dBm to -100 dBm.

Considering the measurement provided by the equipment, the MS reports the value of the RXQUAL level and the GSM MS Test unit performs a BER measurement of 10,140 bits for each of the transient radiated interferences. When SHR interference is applied at the proximity of the MS, the RXQUAL reported by the MS is RXQUAL_4, meaning that the BER reported by the mobile is between 1.6% and 3.2 %. Additionally, the measurement carried out by the GSM MS Test unit reports a BER of 2.07 % when 10,140 bits are considered.

The results provided when the interference with lower frequency is applied (SLR interference) are the following. The MS reports an RXQUAL_0, which means that the BER is lower than 0.2 %. In addition, when the BER measurement is done by the GSM MS Test unit, the BER measured is 0.01 % when 10,140 bits

are considered. A summary of the measurements reported when the two type of interferences are considered is shown in Table 5.2.

TABLE 5.2: GSM signal quality measurements by the MS and the GSM MS Test unit when the MS is interfered by SHR and SLR interferences.

Interference	Signal quality reported by MS		BER measured by GSM MS Test unit
	Quality Band	*Range of actual BER*	
SHR (High Rate)	RXQUAL_4	1.6 % to 3.2 %	2.07 %
SLR (Low Rate)	RXQUAL_0	Less than 0.2 %	0.01 %

From the results stated by the MS and the GSM MS Test unit we can observe that the influence of the radiated interferences generated by the sparks is harder when the interference with the highest spark rate is applied. When the interference with a mean rate of 100 Hz (interference SLR) is applied close to the MS, the degradation produced to the GSM system is negligible because the reported RXQUAL is zero. Otherwise, SHR interference produces a significant degradation to the quality of the GSM transmission, causing a BER around 2 %. Consequently, the interference with a mean repetition rate of 1.3 kHz is capable to interfere significantly the GSM system.

Once the reference procedure measurements have been done, it is time to proceed with the developed methodologies and to evaluate if the results reached are the same.

5.4.2 GSM simulation adding the measured interferences

The second procedure to evaluate the influence over the GSM system is based on the base-band simulation of the DCS, adding the IQ components previously measured. In Chapter 3, it has been explained that computer assisted methods are used to estimate the bit-error-probability when the detection and decoding algorithms are too complex to use mathematical expressions. Therefore, a transmission of N bits is carried out in base-band while the transient interference measurement is added at the channel, causing erroneous bit detection.

Regarding the evaluation of the GSM system in presence of the impulsive noise generated by the sparks, a simulation has been performed using Simulink. Firstly, the baseband has to be modelled properly with the objective to reach accurate results. A GSM transmitter and receiver are modelled according to the specifications

defined at the GSM standards, including also the impulsive noise channel. In Figure 5.11, the block diagrams built in Simulink are shown to simulate accurately the interference scenario. Referring to the transmitter and receiver, they are divided into two main blocks; one block is responsible of generating the codification while the other generates the modulation. In the coding block, the Cyclic Redundancy Code (CRC) is generated and also an interleaving of the bits is carried out. Afterwards at the modulation block, the Gaussian Minimum Shift Keying (GMSK) modulation is produced as the GSM specification call GMSK the physical layer modulation scheme. GMSK is a special case of MSK modulation where the phase of the transmitted signal is continuous and smoothed by a Gaussian filter. This results in more compact spectrum than MSK and enables a better utilization of the available frequency spectrum, at the expense of increased inter-symbol interference (ISI). The main definition parameter of the GMSK modulation is the BT, which is defined by the following equation:

$$BT = \frac{f_{-3dB}}{BitRate} \tag{5.2}$$

where B is the 3 dB bandwidth of the filter and T is the symbol duration. In the simulation the bit rate selected is 9.6 kbps and the BT parameter is assigned to 0.3.

Concerning the bit-error measurement, the simulation allow us to obtain the BER before and after the coding is applied to the transmission as it can be seen in Figure 5.11. It is essential to consider that the results reported at the previous section by the GSM MS Test unit are provided before the decoding is produced; consequently the BER computed before channel decoding will be the reference simulation data.

In relation to the interference that should be added to the channel, at the Simulink simulation the in-phase and quadrature components are added as it can be seen in the diagram of Figure 5.12. The IQ data of the measured impulsive noise is added as well as it is also possible to add white Gaussian noise.

From the channel diagram it can also be observed that the impulsive noise data must be normalized. A gain is included as the base band simulation is normalized to 1 V. Hence, if we want to evaluate the GSM system considering the received

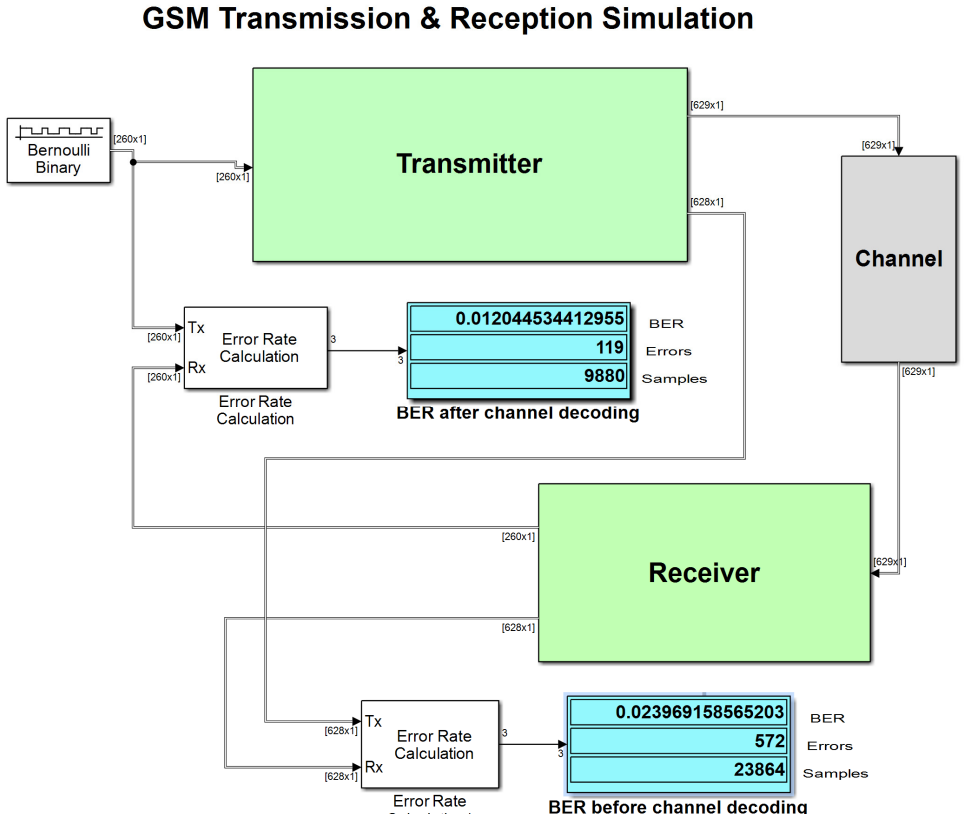

FIGURE 5.11: Simulink model of the GSM base-band transmission and reception.

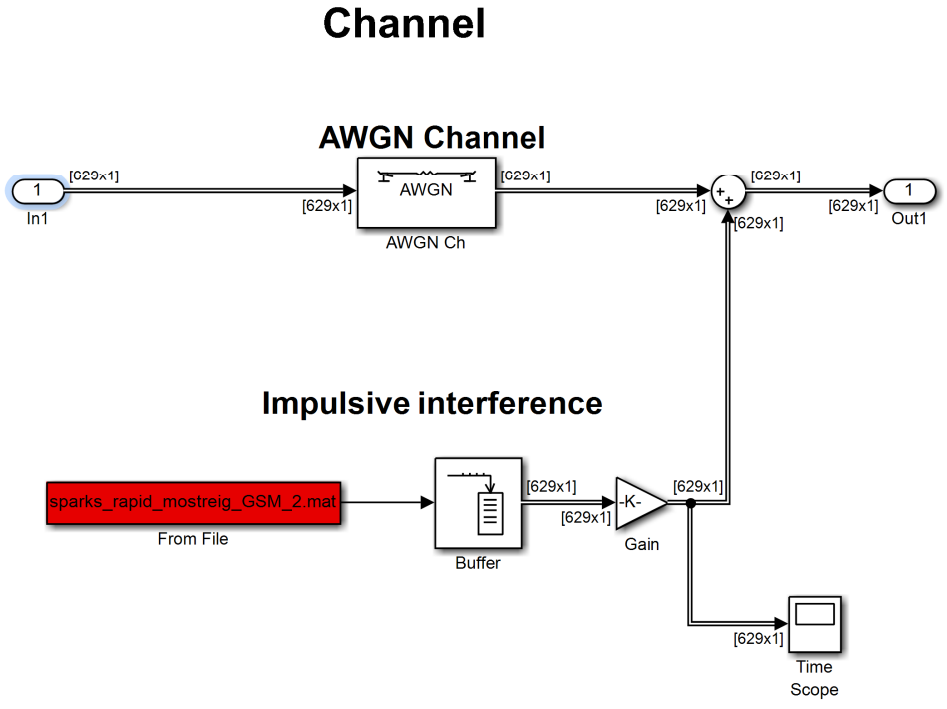

FIGURE 5.12: Simulink model of the GSM base-band channel. Where AWGN and the measured impulsive interference are added.

level by the MS, the interference must be multiplied by the factor to normalize the -86 dBm signal to 1 V.

Regarding the simulated time, it has been fixed to one second, in order to analyse a sufficient number of bits to achieve accurate results. During this period of time the interference coming from the spark generator will be always present. Therefore, we are simulating the interference scenario where the transient interference longs at least 1 s. However, the measurements presented in section 5.3 where only performed for 80 ms (Figure 5.5), consequently a concatenation of the 80 ms IQ measurements is done till reaching one second. This solution is the most optimized, with the 80 ms measurement the main characteristics of the transient interference have been measured properly. Additionally, it is not necessary to store a full second sampled at 125 MSamples/s which will have incurred in an unmanageable amount of data for the post-processing.

Once the interference is added to the channel, the simulation can be run providing us the corresponding results when both interferences are taken into account. Firstly, the case when the high repetition spark interference is generated is simulated to analyse its influence over the GSM system. In Figure 5.13, it is observed the in-phase and quadrature components added to the channel when the SHR interference is applied and simulated.

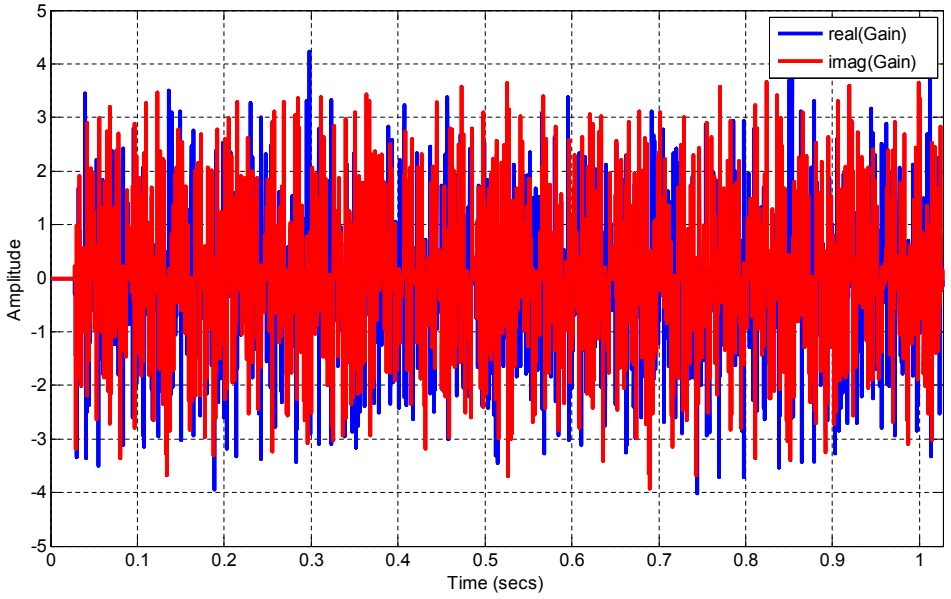

FIGURE 5.13: SHR impulsive interference added to the simulation after the amplitude normalization.

As it has been discussed in previous chapters, one of the advantages of the DCS simulation is that useful communication analysis tools can be employed to understand and rapidly view the impact of certain interference over the communication system. As an example, in Figure 5.14, the constellation diagram of the GSM communication system is represented when the SHR interference is applied. From the constellation diagram, it is rapidly and clearly observed the large impact of the radiated interference that will produce bit error decisions.

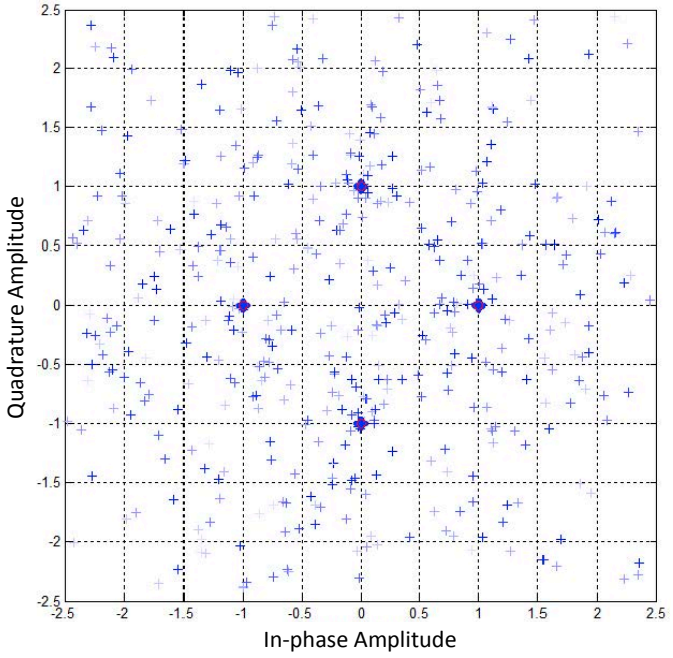

FIGURE 5.14: Constellation interfered by SHR impulsive interference added to the simulation after the amplitude normalization.

Regarding the BER produced by the interference, with the simulation it is easy to estimate the errors produced as the transmitted bits are known. Consequently, when the SHR interference is present at the channel simulation the BER obtained before decoding is 2.39 %, which corresponds to a RXQUAL_4.

Considering the distortion generated by the SLR interference, it is expected a reduction of the degradation produced to the communication system in comparison with the SHR interference. In Figure 5.16, the IQ components of the SLR interferences added to the channel for the simulation is shown. If Figure 5.16 is compared with Figure 5.13, it is noticed that the distortion produced to the GSM system caused by the short rate sparks interference will be reduced.

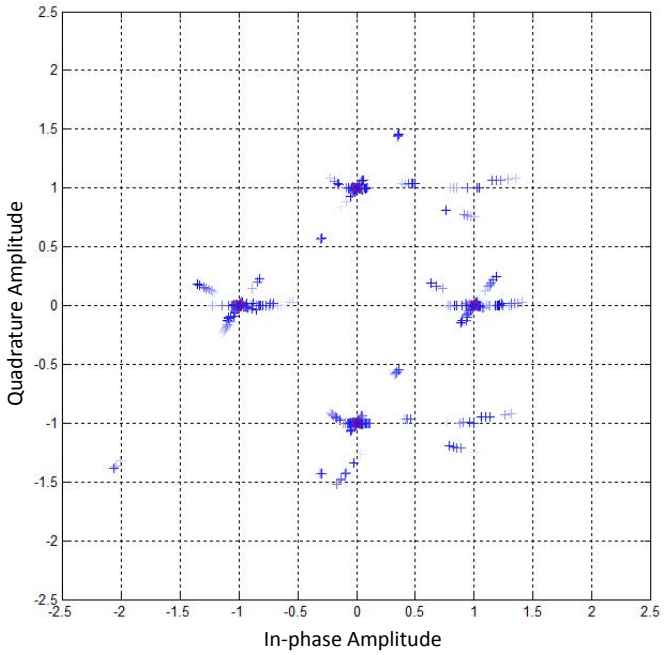

FIGURE 5.15: Constellation interfered by SLR impulsive interference added to the simulation after the amplitude normalization.

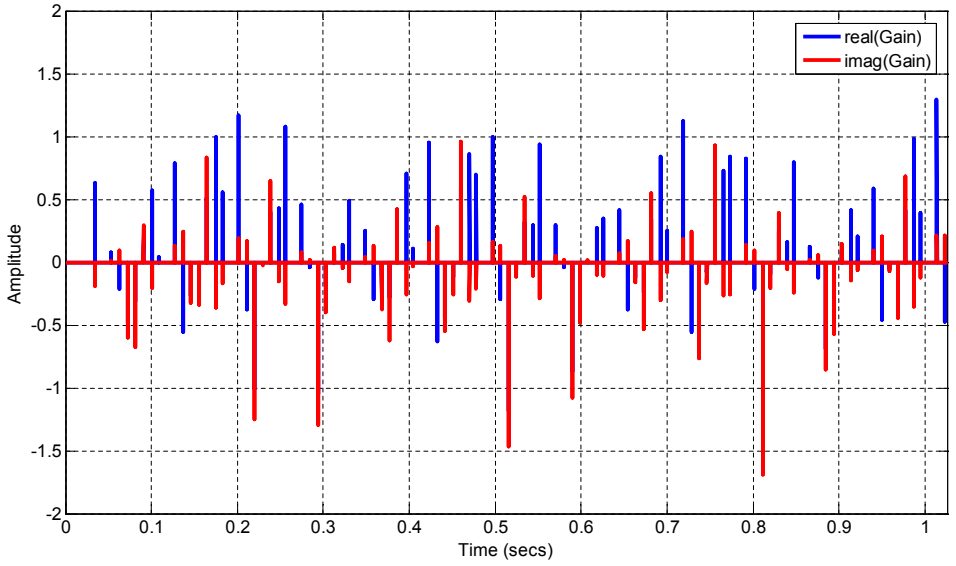

FIGURE 5.16: SLR impulsive interference added to the simulation after the amplitude normalization.

Once the simulation has been carried out, the BER results are available to quantify the degradation produced by the SLR interference. In Figure 5.15, the constellation diagram produced by the simulation enables us to qualitative predict that the degradation suffered by the GSM system will not be so strong compared with the SHR interference case (Figure 5.15). If the BER when the SLR interference is applied to the simulation is evaluated, the resulting BER before the decoding is 0.04 %, which is related to a RXQUAL_0, meaning that the interference produced to the GSM system is negligible. Moreover, if the BER is measured after the channel decoding, any bit is interfered due to the CRC capacity. Below a resume of the results employing the DCS simulation methodology for the two defined interferences is shown in Table 5.3.

TABLE 5.3: GSM signal quality when the GSM system is simulated and interfered by SHR and SLR radiated transients

Interference	DCS simulation methodology	
	BER	*RXQUAL*
SHR(High Rate)	2.39%	RXQUAL_4
SLR (Low Rate)	0.04 %	RXQUAL_0

5.4.3 APD results including GSM specification limits

The last methodology to determine the degradation produced by the SHR and SLR interference uses the APD diagram. As it has been mentioned, limit points can be established to the APD diagram to know the degradation produced to the GSM communication system.

The in-phase and quadrature components measured in section 5.3 of this chapter for both interferences are used as the input to compute the APD diagram and find the statistical properties of the radiated transient interferences. The APD diagram calculation has been obtained using Matlab mathematical software at the downlink 939 MHz channel of the GSM system and using the 200 kHz bandwidth. The results for the fast (SHR) and slow (SLR) interferences have been plotted in Figure 5.17 as well as the computed case when non-impulsive interference is considered. Besides, the limit point associated with each of the RXQUAL levels defined at the GSM specifications is also represented to quickly identify the RXQUAL resulting level. The RXQUAL limit points have been calculated in accordance with equation

5.1 considering the -86 dBm level received by the mobile and the corresponding module scheme for the GSM system. The resulting RXQUAL level will be determined considering the point below the line of the APD diagram. Additionally, if the APD diagram line is below all the limit points represented at the APD diagram, the RXQUAL value will be RXQUAL_0 which means a bit-error-rate lower than 0.2 %.

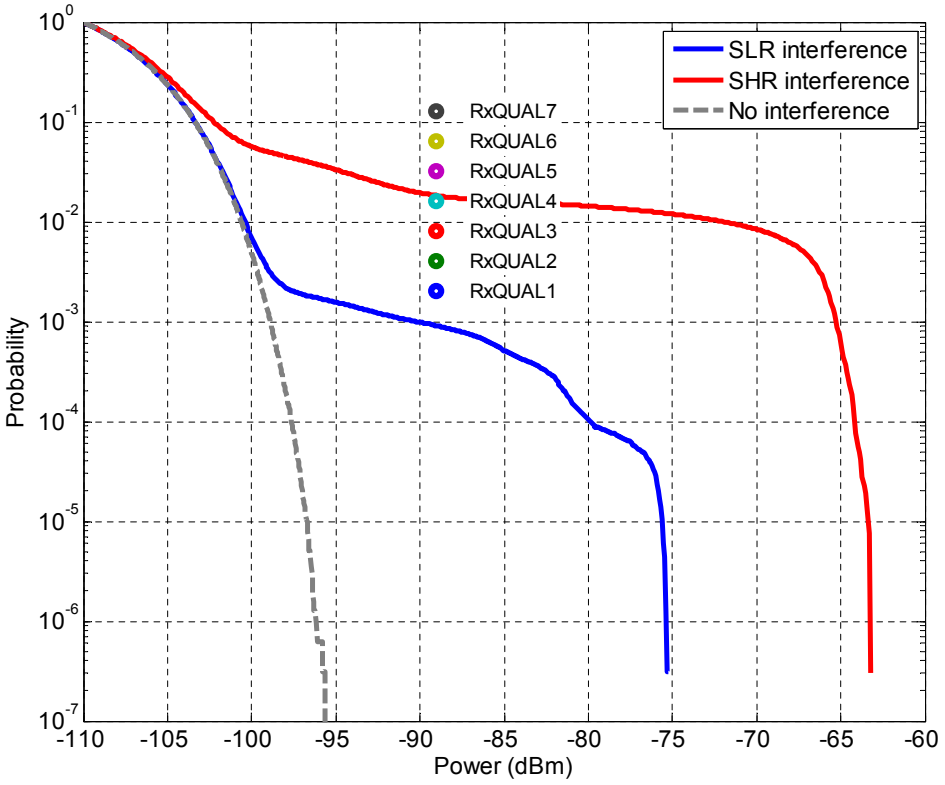

FIGURE 5.17: APD diagram of the SHR and SLR interferences including the RXQUAL limits.

From the results shown in Figure 5.17, the amplitude probability distribution (APD) curve for each of the transient interferences represents the exceeding probability of the interference envelope amplitude. Therefore, it is easy to interpret the different slopes produced by each of the impulsive interferences. The SHR interference has higher amplitude and also higher probability than SLR interference, which means that in impulsive interferences such as the radiated transients the repetition rate of the interference is also higher. Furthermore, the limit points enables us to delimit that the SHR interference will produce a signal quality of RXQUAL_4 when the disturbance is present at the environment. On the other hand, from the APD diagram it can be also concluded that the SLR interference will not cause any noticeable degradation to GSM system, as the APD resulting

curve is below all the RXQUAL levels. An enlarged view of the APD diagram is shown in Figure 5.18, to estimate properly the error probabilities caused by the radiated transient interferences.

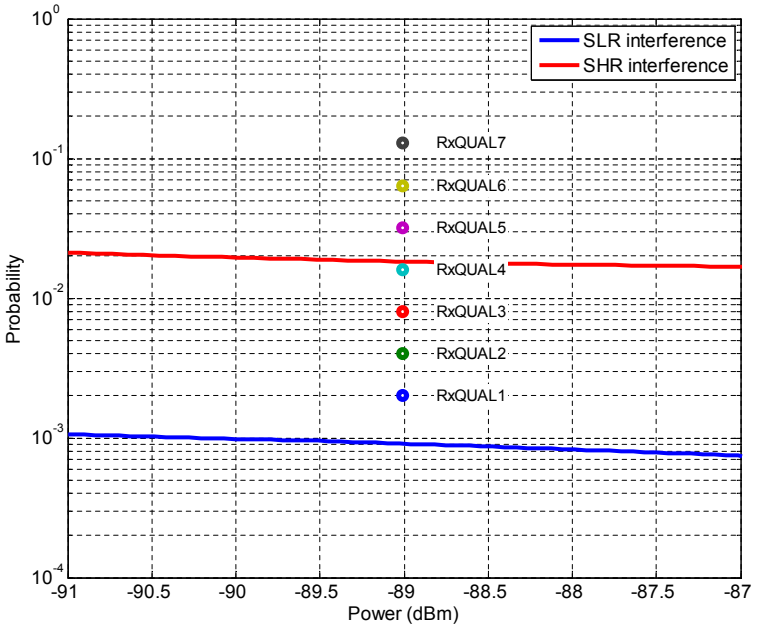

FIGURE 5.18: Zoom of the APD diagram of the SHR and SLR interferences including the RXQUAL limits.

Using the information provided by the enlarged figure and the equation 5.1, it is easy to estimate the BER that each transient interference will produce to the GSM system. From direct observation of the APD diagram it can be established that the SHR produced a bit error rate close to 1.8 %. Otherwise, when the slow repetition spark interference is generated, the error rate is around 0.09 %.

The APD diagram has shown that the interference statistical information provided is an extraordinary tool to analyse rapidly and properly the DCS performance in presence of radiated transient interferences. Considering the results obtained in this section, the APD shows its powerful capabilities to be the best methodology to measure and analyse radiated transient interferences. In addition, using the APD methodology with a single time-domain measurement, various GSM channels can be evaluated rapidly calculating the APD curve. For instance, with the measurements performed in section 5.3, where the 3 MHz RBW was set at the EMI receiver, the APD diagram can be computed for either 15 GSM downlink channels. Otherwise, if the RBW of the measurement is increased to 10 MHz, up to 50 GSM downlink channels can be analysed employing a single measurement. Consequently, if a full-spectrum measurement is performed as it is explained in

Chapter 4, all the GSM channels can be evaluated with a single time-domain measurement.

In Table 5.4 a summary of the results obtained by the observation of the APD diagram when SHR and SLR interference are considered.

TABLE 5.4: GSM signal quality when the GSM system is interfered by SHR and SLR radiated transients applying APD measurements

Interference	APD diagram error estimation	
	BER	*RXQUAL*
SHR(High Rate)	1.8 %	RXQUAL_4
SLR (Low Rate)	0.09 %	RXQUAL_0

5.4.4 Methodologies comparison

In this section the results obtained using the different methodologies to evaluate the influence of both radiated transient interferences over the GSM downlink system are compared. The measurements get from the GSM MS Test unit are the reference ones, as in that methodology an equipment transmitting information was placed under the radiated transient interferences. The measurement of the interferences and afterwards the performance of the GSM simulation and the APD diagram calculation are the methodologies developed to predict beforehand the behaviour of the DCS. A summary chart of the results reached by the different methodologies is displayed in Table 5.5.

TABLE 5.5: Comparison of the measured-simulated degradation produced by SHR and SLR interferences over the GSM system

Methodology	Interference	RXQUAL	BER
Measured signal quality by MS	SHR	4	2.07 %
	SLR	0	0.01 %
DCS simulation	SHR	4	2.39 %
	SLR	0	0.04 %
APD error estimation	SHR	4	1.8 %
	SLR	0	0.09 %

Firstly, it is important to highlight the excellent agreement reached between all the different methodologies. When the impact of the SHR interferences is evaluated with the DCS simulation methodology and the APD error estimation, the

RXQUAL_4 value anticipated is the same that it is reported by the GSM MS Test unit. Additionally, if the BER differences are considered, the variation is close to 0.3 % compared with the reference value, which is a minimum difference if it is assumed that RXQUAL_4 level varies from 1.6 % to 3.2 %. Furthermore, if the SLR interference is evaluated, the results of each methodology conclude that a negligible interference effect is produced between the radiated transients and the downlink of the GSM system. All the methodologies associate the SLR interference to a received signal quality equal to RXQUAL_0, which mean an insignificant interference scenario. Regarding the BER related to the sparks interferences generated around a repetition frequency of 100 Hz, all the results are below 0.1 %.

In conclusion, the methodologies developed have an excellent accuracy compared with the results obtained by the GSM MS Test unit. Consequently, we can predict with an excellent confidence level the degradation produced by a previously measured radiated transient interference to the digital communication systems. Furthermore, in this application chapter, where the developed measurement and analysis methodologies are applied, the advantages of performing a proper time-domain measurements and afterwards predict the distortion produced to a DCS have been clearly perceived. As an example, the APD diagram has been specially useful due to its fast capacity to interpret and quantify the degradation produced to the GSM system.

Conclusions

Radiated transient disturbances are a meaningful source of interferences for digital communication systems. This impulsive noise, which is generated by switching devices or by sparks, is a broadband interference that covers the spectrum from DC to several hundreds of megahertz or some gigahertz. Additionally, this man-made noise is characterized by its short and random burst parameters, which make really challenging to measure it correctly. During the thesis, we have explained that impulsive noise is not properly measured and evaluated to prevent interference scenarios, when the EMC standard methodologies are applied. Detectors, such as the quasi-peak, frequency sweep measurements or signal-to-noise limiting evaluation described in the harmonized standards of the electromagnetic compatibility do not enable to determine beforehand the influence of transient interferences.

Our strategy to overcome the non-profit measurement has been to perform novel measurement and evaluation techniques beyond EMC standards. The measurement techniques are based on carrying out time-domain acquisitions, to afterwards evaluate the disturbances produced to a digital communication system by means of base-band simulation. Additionally, a new measurement methodology to obtain the amplitude probability diagram (APD) has been developed, offering the possibility to determine the bit-error-rate. Following, the main contributions of the thesis including some recommendations for the future work are detailed.

Transient interference measurement

Regarding the challenge associated with the performance of the radiated transient interference measurement, this thesis has developed an acquisition methodology. Firstly, an identification of the measurement requirements has been established in accordance to the need to protect the sensitive digital communication systems and also to the impulsive noise main characteristics. The main requirements identified are the transient event detection, the fact that it is necessary to measure the full-spectrum range, the high sensitivity of the time-domain measurement system and the need to measure the interference with the same bandwidth as the digital communication system.

The measurement technique developed joins the capabilities of EMI receivers and oscilloscope instrumentations to capture accurately the radiated transient interference. To carry out the measurement, the input stage of the EMI receiver is used for filtering and pre-amplifying purposes, conducting the IF output towards the oscilloscope, which is used for triggering and storage. Furthermore, a final post-processing stage is needed to obtain in time-domain the in-phase and quadrature components of the transient interference. Hence, one of the main advantages of using the post-processing stage is that we can demodulate the in-phase and quadrature components of the interference with the exact bandwidth employed by the digital communication system. As the results of the thesis have shown, the IQ measurements obtained following the novel measurement procedure are extremely precise and enable us to capture effectively any transient interference. For instance, different radiated transient interferences produced by burst over a RFID system were acquired successfully following the developed methodology and the results were published in [150, 151, 156, 160].

Regarding future work recommendations, on-site measurements using the developed advanced methodology could be carried out to acquire transients in several interference scenarios. The developed methodology has been validated with measurements performed in controlled environments. Therefore, it will be interesting going on applying the new advantageous methodology measuring original interfering cases.

DCS evaluation employing TD captures

Once the radiated transient interference has been measured properly, an accurate evaluation of the distortion produced to a digital communication system can be estimated. To evaluate the impact of the transient interference, a combination of the time-domain measurement with base-band simulation has been proposed to fulfil the thesis goal. The IQ time-domain measurement enables us to characterize the impulsive-noise present at the communication channel and determine the distortion produced to the DCS by means of base-band simulation.

The traditional EMC evaluation methodology is based on the signal-to-noise ratio, considering that a system will not be interfered if the measurement is below a limit line. Additionally, this basic measurement and analysis procedure employ the QP detector that was developed to protect analogue communication systems from interferences. In the EMC standards, the QP detector is defined with 120 kHz bandwidth at the frequency range between 30 MHz and 1 GHz. Instead of this, we propose to use the bit-error-rate (BER) as the main figure of merit, in order to evaluate the disturbances produced to the digital communication system.

To reach this goal, we use computer simulations to estimate the bit error probability, as it is too complex to find useful mathematical expressions that model the random characteristics of the radiated transient interference channel. The approach to overcome the none-model scenarios is to generate N bits and simulate the processing required to transmit and detect these bits. In addition, the in-phase and quadrature components of the previously measured radiated transient interference are added to the channel simulation, in order to establish the degradation produced to the communication system. This implies that the developed measurement procedure is a key factor to obtain satisfactory results from the base-band simulation. The simulation enables us to observe several useful tools such as the BER, the cdf, or constellation diagram in order to understand and predict the impact of the radiated interference on the digital communication system.

The procedure to determine the BER using the base-band simulation has been validated with experimental results, comparing the results reached with the developed methodology with the ones obtained when a communication system device is placed under radiated transient disturbances. The excellent results obtained employing the developed methodology, considering the interference produced by radiated transient to RFID or GSM communication systems, have been published

in [150, 151, 157, 159, 160]. Therefore, the established measurement and analysis methodology enables us to take a huge qualitative leap forward, if we compare it with traditional evaluation carried out following EMC standards.

Limitations of the developed methodology

Although the developed measurement and evaluation methodology estimates properly an interference scenario, some limitations have been detected. For instance, from the measurement point of view, it is not possible to evaluate the entire spectrum with a single instantaneous acquisition. The methodology combining the EMI receiver and the oscilloscope needs to be tuned at each frequency band where we want to conduct the measurement. Moreover, considering the time-domain capture and the simulation needed to evaluate communication system, the methodology developed could be quite slow and time consuming. However, as it has been shown during this thesis, it is an extraordinary procedure to estimate possible interference scenarios for several communication systems. Nevertheless, in this thesis different solutions have been proposed to solve this full-spectrum time-domain measurement limitation with a single acquisition.

Full-simulation procedure

In Chapter 3 of this thesis, we recommend electromagnetic simulation performed by FDTD method. The EM simulation combined with designed post-processing stages enables us to obtain with a single simulation the contribution of the transient interference at any frequency band. Moreover, the EM simulation enables us to analyse interference cases where it is not possible to carry out measurements, such as in-humans implants.

The EM simulation consist in modelling the interference scenario, reaching the interference that will be coupled to the antenna of the digital communication system receiver. The simulation method selected to compute the electromagnetic field is the FDTD, as it is based in time-domain. As it has been explained along this thesis, the in-phase and quadrature components of the radiated transient interference can be estimated from the simulation using some post-processing techniques. Consequently, with a single EM simulation, we can obtain the interference at any frequency band and we are able to determine with exactitude the degradation

produced by the transient if the base-band simulation is combined with the EM simulation. Moreover, the EM simulation provides other advantages, such as the possibility of evaluating EMC redesign strategies to overcome interference scenarios without the need to perform other measurements. This income has been exemplified and the results have been published in [150, 157]. Consequently, these results show that the full-simulation procedure to evaluate and solve electromagnetic compatibility interference scenarios, where radiated transient interferences are disturbing digital communication systems, is a fruitful new methodology.

APD measurement & evaluation procedure

One of the most important contributions of the work developed in this thesis is the time-domain measurement procedure that has been created to obtain the APD diagram. As it has been explained, recently APD interference measurements have been directly associated with the BER of digital communication systems. However, measurement methodologies based on frequency sweep instrumentation make it not suitable to acquire the APD diagram at the entire spectrum. Fortunately, this novel measurement methodology has been developed to obtain the APD measurement of an interference at any frequency band. The successful APD measurement system created is able to obtain the full-spectrum statistical measurement, employing several time-domain captures which can be acquired in practice immediately. This is also a solution to the limitations of the IQ measurement and evaluation presented before.

This measurement method, based on captures obtained from a general purpose oscilloscope, makes it possible to obtain the APD measurement at any frequency band with the same accuracy provided by an EMI receiver reducing the required measurement time. Furthermore, the post-processing tools using mathematical software produce the APD results rapidly at any bandwidth, and this makes it more powerful than employing an EMI receiver. The successful results and the developed methodology have been published in several publications [149, 151, 158, 160].

Additionally, it is possible to establish limits at the APD diagram to analyse if a certain interference will produce degradation on the DCS. These limit points in the APD diagram are related to the probability required by the system specifications and also to the amplitude of the received signal. In the final chapter of this thesis,

the GSM system is interfered by radiated transients produced by sparks. The results provided by the APD diagram including the limit dots have been especially useful due to its fast capacity to interpret and quantify the degradation produced to the GSM system.

Therefore, the new methodology to obtain the APD measurement is a really powerful measurement and evaluation technique. It provides us the capability to estimate with an excellent confidence level the degradation produced to any communication system located at any frequency band, employing two single time-domain measurements. This is extremely interesting from the EMC perspective because the APD measurements captured instantaneously including some post-processing enables to know which digital communication systems will be interfered by radiated transient interferences.

Therefore, the main future line that needs to be explored is how to implement this measurement and evaluation procedure to the standard radiated and conducted emissions test. Moreover, the developed APD measurement technique has a broad application, including non-transient interferences produced by different equipment which can be also evaluated with the developed procedure. Consequently, it can be established as a new measurement procedure inside the EMC harmonized standards to protect the digital communication systems. Finally, it will be necessary to crosscheck the measurements with all the communication systems that must be protected from electromagnetic disturbances.

Appendix A

Feature Selective Validation method (FSV)

A.1 Introduction

Validation methods are necessary to objectively evaluate the similarity between different datasets in a qualitative way. Nowadays, several validation methods are available for test engineers to discuss if the data is confident with a requirement [29]. Validation is usually carried out through comparison of a pattern or reference model with the model under study [4]. These validation methods also offer the possibility to interpret the results given as an expert opinion [33].

Currently, one of the most used validation methods in the EMC field, because of its versatility and simplicity, is the Feature Selective Validation method (FSV) [34, 101]. FSV, which is incorporated into IEEE standard 1597.1 [55], has the advantage of analysing the two major aspects that are widely considered to be paramount in any validation: the magnitude levels and the shape of the dataset-graphs.

A.2 FSV

The method of Feature Selective Validation (FSV) was developed by Anthony Martin and Alistair Duffy in 1999 [82] and today is the most widely used because of its versatility and simplicity. Regarding the FSV method, the data is compared in two diverse ways: the difference in amplitude (Amplitude Difference Measure, ADM) and the difference between the shape characteristics of the signal (Feature Difference Measure, FDM). In addition, a Global Difference Measure (GDM) is obtained from the ADM and FDM indicators, providing a global measurement of the overall difference.

These three metrics are performed in a point-by-point analysis, hence, it is possible to know which areas of the datasets have the dominant differences. All indicators are calculated according to the following equations, where the subscript "i" is added to consider this point-by-point feature ($ADMi$, $FDMi$ and $GDMi$).

$ADMi$ is calculated using the following expression:

$$ADMi(n) = \frac{(|Lo_1(i)||Lo_2(i)|)}{\frac{1}{N}\sum_{j=1}^{N}|(|Lo_1(j)| + |Lo_2(j)|)|} + ODM(i)e^{ODM(i)} \tag{A.1}$$

with:

$$ODMi(n) = \frac{x(i)}{\delta} \tag{A.2}$$

$$x(i) = (|DC_1(i)| + |DC_2(i)|) \tag{A.3}$$

$$\delta = \frac{1}{N}\sum_{j=1}^{N}(|DC_1(j)| + |DC_2(j)|) \tag{A.4}$$

$FDMi$ is obtained from:

$$FDMi(n) = 2(|FDM_1(n) + FDM_2(n) + FDM_3(n)|) \tag{A.5}$$

with:

$$FDM_1(n) = \frac{(|Lo_{1'}(n)| - |Lo_{2'}(n)|)}{\frac{2}{N}\sum_{i=1}^{N}(|Lo_{1'}(i)| + |Lo_{2'}(i)|)} \tag{A.6}$$

$$FDM_2(n) = \frac{(|Hi_{1'}(n)| - |Hi_{2'}(n)|)}{\frac{6}{N}\sum_{i=1}^{N}(|Hi_{1'}(i)| + |Hi_{2'}(i)|)} \tag{A.7}$$

$$FDM_3(n) = \frac{(|Hi_{1''}(n)| - |Hi_{2''}(n)|)}{\frac{7.2}{N}\sum_{i=1}^{N}(|Hi_{1''}(i)| + |Hi_{2''}(i)|)} \tag{A.8}$$

and finally the $GDMi$ is obtained from:

$$GDMi(n) = \sqrt{ADMi(n)^2 + FDMi(n)^2} \tag{A.9}$$

where $DC - data$ are the first five points of the FFT (Fast Fourier Transform) of the original data, Lo-data is the low-frequency component of the original data and Hi-data is the high-frequency component of the original data.

Afterwards, the $XDMi$ (where $X = A$, F & G) values are calculated and it is possible to find the average values using equation A.10.

$$XDM_{tot} = \frac{\sum_{n=1}^{N} XDMi(n)}{N} \tag{A.10}$$

These $XDMi$ indicators are very useful as they allow us to quickly evaluate the quality of the results because a single number is provided. The indicators are usually represented by histograms that are sorted according to the quality of the results into the following comparison categories: Excellent, Very Good, Good, Fair, Poor and Very Poor. In Table A.1, the different categories are related with the XDM_c values.

A.3 FSV to evaluate with transient interferences in TD

A modified version of the FSV method was created by Jauregui [61, 62] considering that all the time-domain transient interferences can be divided into three

TABLE A.1: XDMc interpretation scale

XDMc value ($X = A,F,G$)	
$XDMc<0.1$	Excellent
$0.1 \leq XDMc \leq 0.2$	Very Good
$0.2 \leq XDMc \leq 0.4$	Good
$0.4 \leq XDMc \leq 0.8$	Fair
$0.8 \leq XDMc \leq 1.6$	Poor
$1.6<XDMc$	Very Poor

regions: "pre-event", "event" and "post-event". The FSV is computed for each region of the transient interference and it is weighted according to the significance of the information contained. In addition, the different regions are identified automatically; further information can be found in the following publications [61, 62]. Figure A.1 is an example of how a transient phenomena is divided into several regions to afterwards compute the weighted FSV (W-FSV).

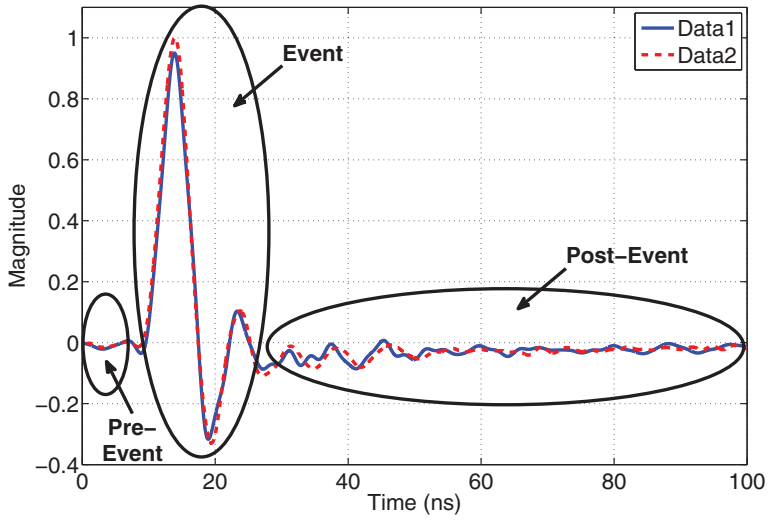

FIGURE A.1: Transient phenomena divided into the pre-event, event and post-event to weight the FSV calculation.

The division of the three regions follows the next rules; the first region ("pre-event"), is defined from $t_0 = 0$ to the time when each signal begins to rise significantly. The FSV is applied with a weight value of 0.05 in this region (equation A.11).

$$FSV_{pre} = FSV(Data_1(t), Data_2(t))|_{t=t_0}^{t_{pre}} \cdot 0.05 \tag{A.11}$$

The "event" region, is defined as the main component of the transient, which is the most important of the entire disturbance and the assigned weight is 0.7 A.12.

$$FSV_{event} = FSV(Data_1(t), Data_2(t))|_{t=t_{pre}}^{t_{event}} \cdot 0.7 \tag{A.12}$$

Finally, the "post-event" is defined from the end of "the event" to the end of the recorded signal. Usually, this is the region with the longest duration if it is compared with the other regions. The weight of the region is assigned to 0.25 A.13.

$$FSV_{post-event} = FSV(Data_1(t), Data_2(t))|_{t=t_{event}}^{t_{final}} \cdot 0.25 \tag{A.13}$$

Once the results of the FSV method have been weighted at each region, all the confidence XDMc results from the three regions are added, obtaining a total value for the comparison.

$$W - FSV_{XDMc} = XDMc_{pre-event} + XDMc_{event} + XDMc_{post-event} \tag{A.14}$$

A.4 Other FSV applications: Pattern recognition to identify Transients

In this section, a new vision of the capabilities offered by the FSV validation method is introduced. FSV can be used in the field of pattern recognition, proving the capacity to identify transient interferences from data-set [152]. Concerning the EMC measurement applications, the FSV pattern recognition can be applied to discard ambient noise and also to identify the time-domain disturbances produced by the equipment under test.

In the reference [152], the capture of radiated transient interferences produced by ESD discharge and the ones generated by a burst are measured and identified using the FSV pattern recognition. In Figure A.2 the generated transient interferences are shown and in Figure A.3 the recognition of the ESD pulses in a data-set, where burst and ESD transients are present, is shown.

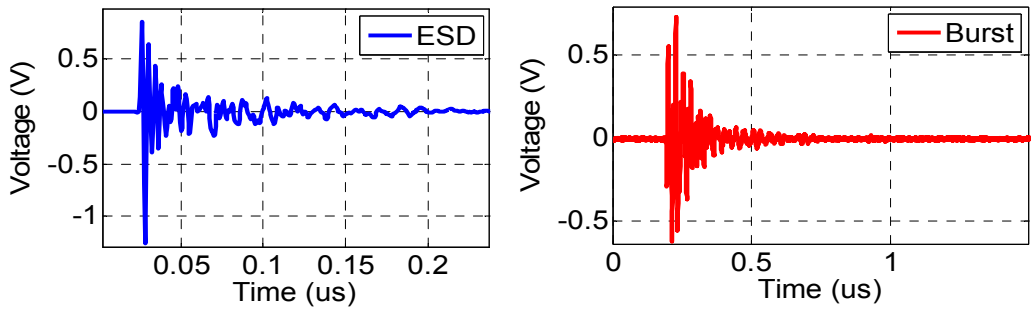

FIGURE A.2: ESD and burst transient interference identified by FSV pattern recognition.

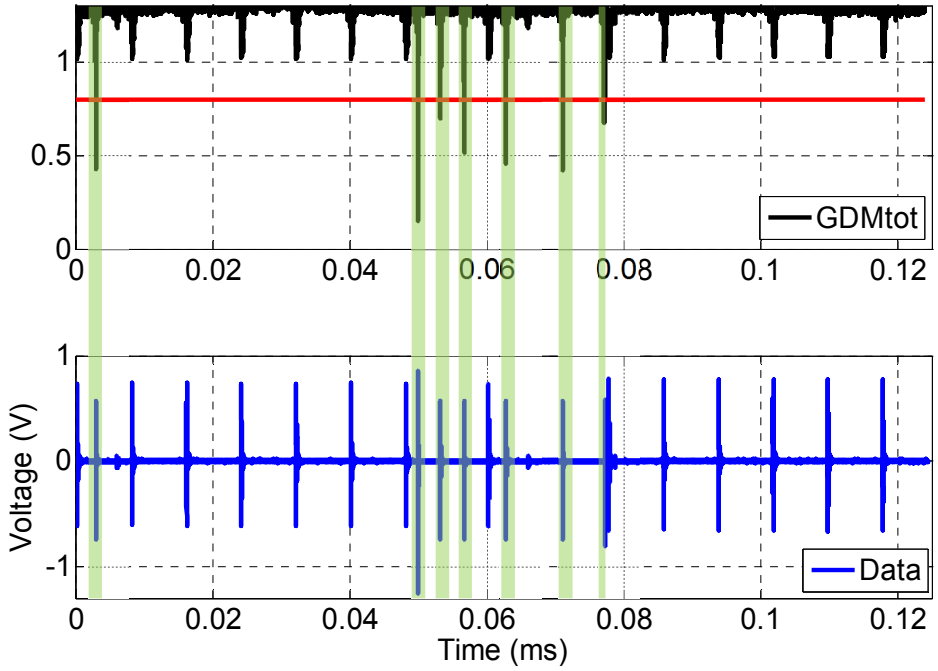

FIGURE A.3: (a) Value of GDMtot where pattern and signal are compared. (b) Signal under analysis and ESD events identified (shaded area).

To identify the expected pattern, which is defined as an N-point vector and the signal is an M-point vector (where $M > N$); the grade of similarity, which we will refer to as Feature Selective Validation Similarity Coefficient (FSV_{SC}), can be defined by the following equation:

$$FSV_{SC}(i) = FSV_{XDM_{tot}}(pattern, signal_i)|_{i=1}^{M-N+1} \tag{A.15}$$

with:

$$signal_i(j) = signal(i + j - 1)|_{j=1}^{N} \tag{A.16}$$

Further information can be obtained from the following publication [152].

Appendix B

APD limits

Several studies have been carried out with the aim to specify a limit value in the APD diagram. This limit represents a criterion for the measured interference that gives the maximum permissible bit-error-probability [84, 87, 88, 124, 141, 143, 147]. Wiklundh demonstrate the relation between the symbol error probability and the APD diagram for a coherent receiver [141], assuming that the measurement bandwidth is the same bandwidth as the communication receiver. The relation between the APD measurement and the symbol error probability is described by the equation below (B.1).

$$Pr[\text{symbol error}]_{max} = P_r\left[r > \frac{d_{min}}{2}\right] = APD_R\left(\frac{d_{min}}{2}\right) \tag{B.1}$$

where the APD is defined as the amount of time the measured envelope of an interfering signal exceeds a certain level. The relation between the $APD_R(r)$ and the probability density function of the envelope R is

$$APD_R(r) = 1 - F_R(r) \tag{B.2}$$

and

$$f_R(r) = \frac{d}{dr}F_R(r) = -\frac{d}{dr}APD_R(r) \tag{B.3}$$

where $F_R(r)$ is the cumulative distribution function (cdf) and $f_R(r)$ is the probability density function (pdf). The cdf describes the probability that a value of the envelope variable R with a given pdf will had a value lower or equal to r.

The d_{min} is referred to the minimum distance between symbols considering the distances between the symbols of a modulation scheme. From equation B.1, the symbol errors will only appear when the interference level exceeds half the minimum distance, $d_{min}/2$. To illustrate the concept of the minimum distance, in Figure B.1 a constellation diagram of a QPSK modulation is shown. In the Figure, d_1 and d_2 are the distances between the different symbols, and R is the envelope of the interference. The minimum distance between the symbols is d_1.

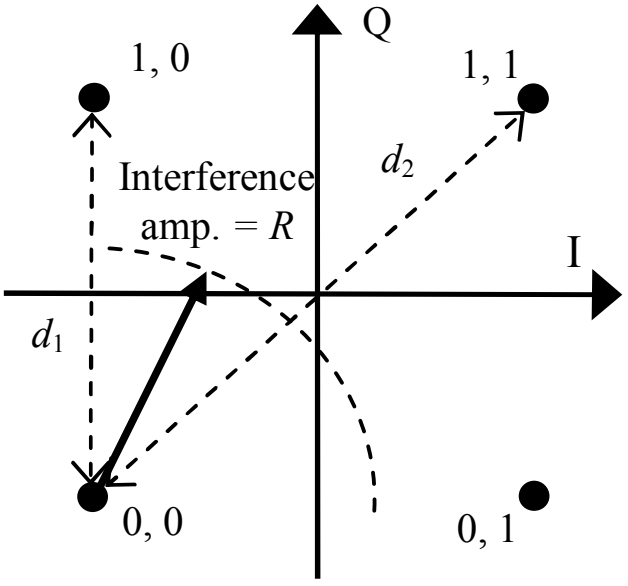

FIGURE B.1: Constellation of a QPSK signal and the distances between symbols, d_1 and d_2. Picture from [88].

It is not possible that no symbol errors can occur if the envelope amplitude does not exceed half the minimum distance, the maximum symbol error probability is expressed in terms of the APD as

$$Pr[\text{symbol error}]_{max} = APD_R\left(\beta\sqrt{E_b}\right) \tag{B.4}$$

where

$$\beta \equiv \frac{d_{min}}{2}\frac{1}{\sqrt{E_b}} \tag{B.5}$$

hence E_b is the bit energy. Therefore, the expression for approximated BEP can be obtained from the next expression:

$$P_b \cong \frac{1}{m} APD_R\left(\beta\sqrt{E_b}\right) \tag{B.6}$$

where m denotes the number of transmitted bits per symbol. In order to use these requirements in APD graphs expressed in envelope voltage U, the requirements can be rewritten as

$$P_b \cong \frac{1}{m} APD_U\left(\beta\sqrt{E_b\frac{Z_0}{T_s}}\right) = \frac{1}{m} APD_U\left(\frac{\beta A}{\sqrt{m}}\right) \tag{B.7}$$

where $APD_U()$ is the APD expressed in voltage, Z_0 is the input impedance of the receiver, T_s is the symbol time of the radio system and A is the rms amplitude of the communication signal.

As it has been described largely along the thesis, transient interferences produce heavy tailed APD distributions. In consequence, multiple bit-errors will be produced if $d > d_{min}$. Thus, the emission limit is defined by a single point as

$$(u_{limit}, \quad P_{limit}) \equiv \left(\frac{\beta_1 A}{\sqrt{m}}, \quad P_{req}\right) \tag{B.8}$$

where P_{req} is the required error probability by the communication system.

Although the proposed APD relation with the BEP expression is suitable for many communication systems, it should be noticed that it will underestimate the maximum BEP for multilevel modulation systems interfered by impulsive noise [88]. As an example, if a communication system with a 16 QAM modulation scheme is evaluated, multiple distance appear at the constellation diagram, producing different number of bit-error. In Figure B.2, a constellation diagram of a 16 QAM is represented indicating the distances.

If all the different distances are considered, the expression to define a limit on the APD diagram is described by the below expression, where a limit line is established by the following points:

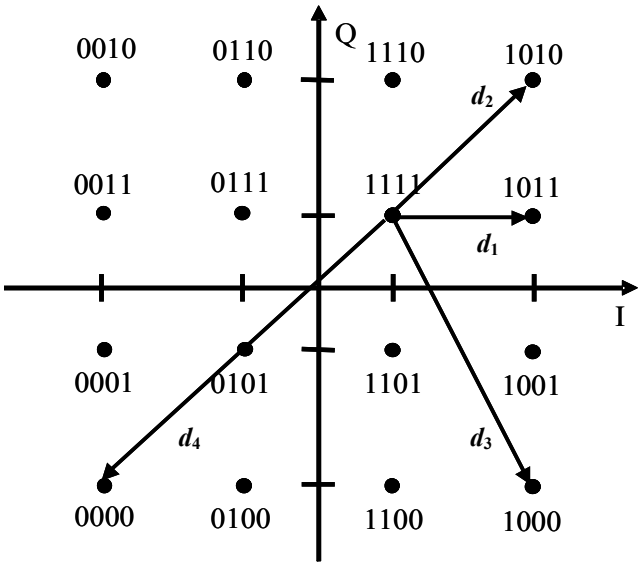

FIGURE B.2: Constellation of a 16QAM signal and the distances between symbols. Picture from [88].

$$\left(\frac{\beta_1 A}{\sqrt{m}}, \quad \frac{m}{\gamma} P_{req}\right) and \left(\frac{\beta_m A}{\sqrt{m}}, \quad \frac{m}{\gamma}\left(\frac{\beta_m}{\beta_1}\right)^L P_{req}\right) \tag{B.9}$$

where

$$\gamma \equiv \sum_{k=1}^{m}\left(\frac{\beta_k}{\beta_1}\right)^L \tag{B.10}$$

and L is the gradient of the APD curve.

For instance, in Figure B.3 and APD diagram including a limit point and a limit line are represented. Consequently, if the APD curve cuts the limit line or contains the limit point, a bit error probability higher than the required probability is assumed.

Further information can be found in the following publications [88].

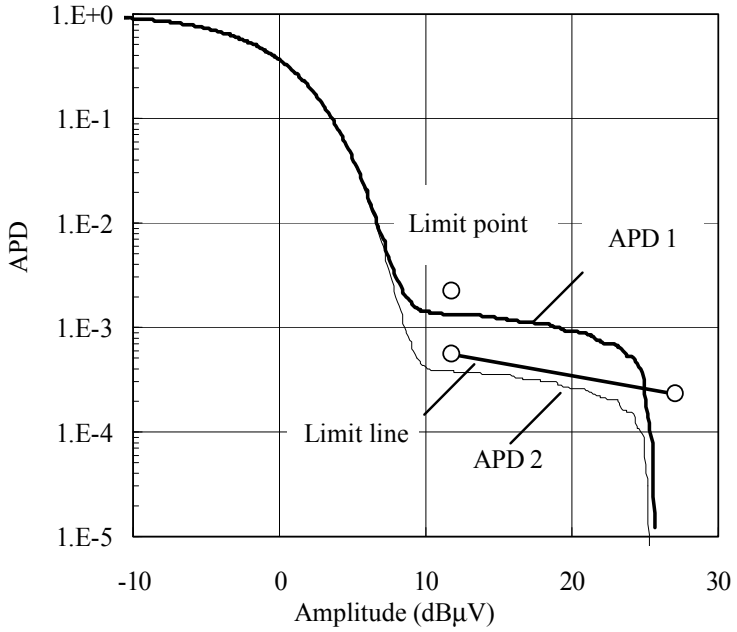

FIGURE B.3: Example of an APD diagram with the limits included. Picture from [88].

References

[1] R.R. Adriano, N. Ben Slimen, V. Deniau, M. Berbineau, and P. Massy. Prediction of the ber on the gsm-r communications provided by the em transient disturbances in the railway environment. In *Electromagnetic Compatibility - EMC Europe, 2008 International Symposium on*, pages 1–5, Sept 2008.

[2] R.G. Albano, L. Franchina, and S.A. Kosmopoulos. Bit error performance evaluation of double-differential QPSK in faded channels characterized by Gaussian plus impulsive noise and Doppler effects. *Vehicular Technology, IEEE Transactions on*, 49(1):148–158, Jan 2000.

[3] M.J. Alexander, M.J. Salter, D.G. Gentle, and K.P. Holland. Advances in measurement methods and reduction of measurement uncertainties associated with antenna calibration. *Science, Measurement and Technology, IEE Proceedings* -, 141(4):283–286, Jul 1994.

[4] B. Archambeault and S. Connor. Proper model validation is important for all EMI/EMC applications. In *Electromagnetic Compatibility, 2008. EMC 2008. IEEE International Symposium on*, pages 1–8, Aug 2008.

[5] P.A. Bello and R. Esposito. A New Method for Calculating Probabilities of Errors Due to Impulsive Noise. *Communication Technology, IEEE Transactions on*, 17(3):368–379, June 1969.

[6] N. Ben Slimen, V. Deniau, S. Baranowski, J. Rioult, N. Dubalen, B. Demoulin, and Consortium Railcom. On board measurements of the railway electromagnetic noise with moving train. In *Electromagnetic Compatibility, 2007. EMC Zurich 2007. 18th International Zurich Symposium on*, pages 365–368, Sept 2007.

[7] M. Bertocco, M. Farias, D. Fortin, and A. Sona. Cross-Layer Measurement for the Analysis of DVB-T System Performance. *Instrumentation and Measurement, IEEE Transactions on*, 57(7):1304–1312, July 2008.

[8] K.L. Blackard, T.S. Rappaport, and C.W. Bostian. Measurements and models of radio frequency impulsive noise for indoor wireless communications. *Selected Areas in Communications, IEEE Journal on*, 11(7):991–1001, Sep 1993.

[9] T.K. Blankenship and T.S. Rappaport. Characteristics of impulsive noise in the 450-MHz band in hospitals and clinics. *Antennas and Propagation, IEEE Transactions on*, 46(2):194–203, Feb 1998.

[10] S. Braun, A. Alt, and P. Russer. A novel multiresolution high-dynamic ultra-broadband time-domain EMI measurement system. In *Microwave Symposium Digest, 2005 IEEE MTT-S International*, pages 4 pp.–, June 2005.

[11] S. Braun, T. Donauer, and P. Russer. A Real-Time Time-Domain EMI Measurement System for Full-Compliance Measurements According to CISPR 16-1-1. *Electromagnetic Compatibility, IEEE Transactions on*, 50(2):259–267, May 2008.

[12] S. Braun and P. Russer. A low-noise multiresolution high-dynamic ultra-broad-band time-domain EMI measurement system. *Microwave Theory and Techniques, IEEE Transactions on*, 53(11):3354–3363, Nov 2005.

[13] M.A. Bridgwood. An Assessment of Impulsive Noise via a Double-Ringing Model. *Electromagnetic Compatibility, IEEE Transactions on*, EMC-27(3):126–130, Aug 1985.

[14] G. Cerri, S. Chiarandini, S. Costantini, R. De Leo, Valter Mariani Primiani, and P. Russo. Theoretical and experimental characterization of transient electromagnetic fields radiated by electrostatic discharge (ESD) currents. *Electromagnetic Compatibility, IEEE Transactions on*, 44(1):139–147, Feb 2002.

[15] Christos Christopoulos. Principles and Techniques of Electromagnetic Compatibility, Second Edition, 2007.

[16] J.F. Coll, J. Chilo, and B. Slimane. Radio-Frequency Electromagnetic Characterization in Factory Infrastructures. *Electromagnetic Compatibility, IEEE Transactions on*, 54(3):708–711, June 2012.

[17] V. Degardin, I. Junqua, M. Lienard, P. Degauque, S. Bertuol, J. Genoulaz, and M. Dunand. Predicted performances of power line communication in aircraft. In *Aerospace EMC, 2012 Proceedings ESA Workshop on*, pages 1–4, May 2012.

[18] V. Degardin, K. Kilani, P. Laly, M. Lienard, and P. Degauque. Power line communication between an inverter and a motor: Noise characterization in the time domain and in the frequency domain. In *General Assembly and Scientific Symposium, 2011 XXXth URSI*, pages 1–4, Aug 2011.

[19] V. Degardin, M. Lienard, P. Degauque, and P. Laly. Performances of the homeplug phy layer in the context of in-vehicle powerline communications. In *Power Line Communications and Its Applications, 2007. ISPLC '07. IEEE International Symposium on*, pages 93–97, March 2007.

[20] V. Degardin, M. Lienard, P. Degauque, E. Simon, and P. Laly. Impulsive Noise Characterization of In-Vehicle Power Line. *Electromagnetic Compatibility, IEEE Transactions on*, 50(4):861–868, Nov 2008.

[21] V. Degardin, M. Lienard, P. Degauque, A. Zeddam, and F. Gauthier. Impulsive noise on indoor power lines: characterization and mitigation of its effect on plc systems. In *Electromagnetic Compatibility, 2003. EMC '03. 2003 IEEE International Symposium on*, volume 1, pages 166–169 Vol.1, May 2003.

[22] V. Degardin, M. Lienard, A. Zeddam, F. Gauthier, and P. Degauque. Classification and characterization of impulsive noise on indoor powerline used for data communications. *Consumer Electronics, IEEE Transactions on*, 48(4):913–918, Nov 2002.

[23] P. Degauque, P. Laly, V. Degardin, and M. Lienard. Power line communication and compromising radiated emission. In *Software, Telecommunications and Computer Networks (SoftCOM), 2010 International Conference on*, pages 88–91, Sept 2010.

[24] V. Deniau, N. Ben Slimen, S. Baranowski, H. Ouaddi, J. Rioult, and N. Dubalen. Characterisation of the EM disturbances affecting the safety

of the railway communication systems. In *Reliability in Electromagnetic Systems, 2007 IET Colloquium on*, pages 1–5, May 2007.

[25] V. Deniau, S. Dudoyer, S. Ambellouis, M. Heddebaut, and A. Mariscotti. Research of observables adapted to the analysis of EM noise impacting the quality of GSM-Railway transmissions. In *Electromagnetic Compatibility (EMC EUROPE), 2012 International Symposium on*, pages 1–6, Sept 2012.

[26] V. Deniau, S. Dudoyer, M. Heddebaut, A. Mariscotti, A. Marrese, and N. Pasquino. Test bench for the evaluation of GSM-R operation in the presence of electric arc interference. In *Electrical Systems for Aircraft, Railway and Ship Propulsion (ESARS), 2012*, pages 1–6, Oct 2012.

[27] V. Deniau, H. Fridhi, M. Heddebaut, J. Rioult, I. Adin, and J. Rodriguez. Analysis and modelling of the EM interferences produced above a train associated to the contact between the catenary and the pantograph. In *Electromagnetic Compatibility (EMC EUROPE), 2013 International Symposium on*, pages 721–726, Sept 2013.

[28] Comité International Spécial des Perturbations Radioélectriques. CISPR 16-1-1: Specification for radio disturbance and immunity measuring apparatus and methods - Part 1-1: Radio disturbance and immunity measuring apparatus - Measuring apparatus.

[29] A.L. Drozd. Selected methods for validating computational electromagnetic modeling techniques. In *Electromagnetic Compatibility, 2005. EMC 2005. 2005 International Symposium on*, volume 1, pages 301–306 Vol. 1, Aug 2005.

[30] S. Dudoyer, R. Adriano, V. Deniau, N. Ben Slimen, and B. Meyniel. Testing of the GSM-R system against electromagnetic disturbances present in the railway environment. In *Intelligent Transport Systems Telecommunications,(ITST),2009 9th International Conference on*, pages 117–122, Oct 2009.

[31] S. Dudoyer, V. Deniau, R.R. Adriano, M.N.B. Slimen, J. Rioult, B. Meyniel, and M. Berbineau. Study of the Susceptibility of the GSM-R Communications Face to the Electromagnetic Interferences of the Rail Environment. *Electromagnetic Compatibility, IEEE Transactions on*, 54(3):667–676, June 2012.

[32] S. Dudoyer, V. Deniau, S. Ambellouis, M. Heddebaut, and A. Mariscotti. Classification of Transient EM Noises Depending on their Effect on the Quality of GSM-R Reception. *Electromagnetic Compatibility, IEEE Transactions on*, 55(5):867–874, Oct 2013.

[33] A. Duffy, D. Coleby, A. Martin, M. Woolfson, and T. Benson. Progress in quantifying validation data. In *Electromagnetic Compatibility, 2003 IEEE International Symposium on*, volume 1, pages 323–328 vol.1, Aug 2003.

[34] A.P. Duffy, A.J.M. Martin, A. Orlandi, G. Antonini, T.M. Benson, and Malcolm S. Woolfson. Feature selective validation (FSV) for validation of computational electromagnetics (CEM). part I-the FSV method. *Electromagnetic Compatibility, IEEE Transactions on*, 48(3):449–459, Aug 2006.

[35] European Telecommunications Standards Institute ETSI. GSM Technical Specification: Digital cellular telecommunications system (Phase 2+);Radio subsystem link control(GSM 05.08), 2008.

[36] European Committee for Electrotechnical Standardization CENELEC. EN 61000-4-4: Electromagnetic compatibility (EMC) - Part 4-4: Testing and measurement techniques - Electrical fast transient/burst immunity test.

[37] Directorate-General for Mobility and European Commission Transport. *Eurobalise sub-system*. 1996.

[38] K.M. Fors, K.C. Wiklundh, and P.F. Stenumgaard. A Simple Measurement Method to Derive the Impulsiveness Correction Factor for Communication Performance Estimation. *Electromagnetic Compatibility, IEEE Transactions on*, 55(5):834–841, Oct 2013.

[39] D. Fortin. *Performance assessment of DVB-T and wireless communication systems by means of cross-layer measurements*. PhD thesis, University of Padova, 2008.

[40] R.K. Frazier and S. Alles. Comparison of ISO 7637 transient waveforms to real world automotive transient phenomena. In *Electromagnetic Compatibility, 2005. EMC 2005. 2005 International Symposium on*, volume 3, pages 949–954 Vol. 3, Aug 2005.

[41] H. Fridhi, V. Deniau, J.P. Ghys, M. Heddebaut, J. Rodriguez, and I. Adin. Analysis of the coupling path between transient EM interferences produced

by the catenary-pantograph contact and on-board railway communication antennas. In *Electromagnetics in Advanced Applications (ICEAA), 2013 International Conference on*, pages 587–590, Sept 2013.

[42] The Seventh Framework Programme funded European Research and Technological Development. FP7- TRANSPORT-285259 TREND Test of Rolling Stock Electromagnetic Compatibility for cross-Domain interoperability.

[43] S.V. Georgakopoulos, C.A. Balanis, and C.R. Birtcher. Cosite interference between wire antennas on helicopter structures and rotor modulation effects: FDTD versus measurements. *Electromagnetic Compatibility, IEEE Transactions on*, 41(3):221–233, Aug 1999.

[44] K. Gotoh, S. Ishigami, Y. Matsumoto, M. Ryoshi, J. Nishio, and S. Yoshimura. Development and its application of FFT-based multi-channel APD measuring equipment. In *Proc. EMC Europe 2010, Wroclaw*, pages 46–51, Sept 2010.

[45] K. Gotoh, S. Ishigami, T. Shinozuka, and Y. Matsumoto. Interference study of microwave ovens emission with satellite broadcasting according to the emission limits in CISPR 11. In *Electromagnetic Compatibility (EMC EUROPE), 2013 International Symposium on*, pages 717–720, Sept 2013.

[46] K. Gotoh, Y. Matsumoto, S. Ishigami, T. Shinozuka, and M. Uchino. Development and Evaluation of a Prototype Multichannel APD Measuring Receiver. In *Electromagnetic Compatibility, 2007. EMC 2007. IEEE International Symposium on*, pages 1–6, July 2007.

[47] K. Gotoh, Y. Matsumoto, H. Tsutagaya, and S. Kazama. Evaluation of sensitivity of digital TV receiver subjected to intrasystem interference. In *Electromagnetic Compatibility - EMC Europe, 2008 International Symposium on*, pages 1–4, Sept 2008.

[48] K. Gotoh, T. Shinozuka, S. Ishigami, and Y. Matsumoto. Electromagnetic disturbance evaluation using pulse duration distribution. In *Electromagnetic Compatibility (EMC EUROPE), 2012 International Symposium on*, pages 1–5, Sept 2012.

[49] K. Gotoh, Ifong Wu, S. Ishigami, and Y. Matsumoto. Use of independent component analysis to separate noise sources in emissions radiated from LED

lamps. In *Electromagnetic Compatibility (EMC Europe), 2014 International Symposium on*, pages 1195–1198, Sept 2014.

[50] V.R. Gowda, K.H. Li, and K.C. Teh. BER analysis of selection diversity receivers over generalized-K fading environments. In *Information, Communications and Signal Processing, 2009. ICICS 2009. 7th International Conference on*, pages 1–5, Dec 2009.

[51] T. Hammi, N. Ben Slimen, V. Deniau, J. Rioult, and S. Dudoyer. Comparison between GSM-R coverage level and EM noise level in railway environment. In *Intelligent Transport Systems Telecommunications,(ITST),2009 9th International Conference on*, pages 123–128, Oct 2009.

[52] K. Hassan, R. Gautier, I. Dayoub, M. Berbineau, and E. Radoi. Multiple-Antenna-Based Blind Spectrum Sensing in the Presence of Impulsive Noise. *Vehicular Technology, IEEE Transactions on*, 63(5):2248–2257, Jun 2014.

[53] T. Hikage, S. Hiraiwa, T. Nojima, S. Futatsumori, A. Kohmura, and N. Yonemoto. Numerical estimation of the electric field distributions due to mobile radio in an aircraft cabin based on large scale FDTD analysis. In *EMC Europe 2011 York*, pages 523–526, Sept 2011.

[54] C. Hoffmann and P. Russer. A Real-Time Low-Noise Ultrabroadband Time-Domain EMI Measurement System up to 18 GHz. *Electromagnetic Compatibility, IEEE Transactions on*, 53(4):882–890, Nov 2011.

[55] IEEE Electromagnetic Compatibility Society. IEEE Recommended Practice for Validation of Computational Electromagnetics Computer Modeling and Simulations. *IEEE Std 1597.2-2010*, pages 1–124, Feb 2011.

[56] Special international committee on radio interference CISPR. CISPR 16-1-1 Ed.3 : Specification for radio disturbance and immunity measuring apparatus and methods Part 1-1: Radio disturbance and immunity measuring apparatus Measuring apparatus.

[57] ISO Standards. ISO/IEC 14443-2: Identification cards – Contactless integrated circuit(s) cards – Proximity cards – Part 2: Radio frequency power and signal interface, 2001.

[58] ISO Standards. ISO/IEC 14443-1: Identification cards – Contactless integrated circuit cards – Proximity cards – Part 1: Physical characteristics, 2008.

[59] ITU-T. International telephone connections and circuits - general recommendations on the transmission quality for an entire internation, 2003.

[60] R. Jauregui. *Comportamiento Electromagntico en el Dominio del Tiempo de Estructuras Complejas Mediante FDTD.* PhD thesis, Universitat Politècnica de Catalunya, 2010.

[61] R. Jauregui, F. Silva, A. Orlandi, H. Sasse, and A. Duffy. Factors influencing the successful validation of transient phenomenon modelling. In *Electromagnetic Compatibility (APEMC), 2010 Asia-Pacific Symposium on*, pages 338–341, April 2010.

[62] R. Jauregui, Gang Zhang, J. Rojas-Mora, O. Ventosa, F. Silva, A.P. Duffy, and H. Sasse. Analyzing Transient Phenomena in the Time Domain Using the Feature Selective Validation (FSV) Method. *Electromagnetic Compatibility, IEEE Transactions on*, 56(4):825–834, Aug 2014.

[63] C. Jeruchim. Techniques for Estimating the Bit Error Rate in the Simulation of Digital Communication Systems. *Selected Areas in Communications, IEEE Journal on*, 2(1):153–170, Jan 1984.

[64] C. Keller and K. Feser. Fast Emission Measurement in Time Domain. *Electromagnetic Compatibility, IEEE Transactions on*, 49(4):816–824, Nov 2007.

[65] Keysight Technologies. Advanced Design System (ADS). http://www.keysight.com/.

[66] K. Kilani, V. Degardin, P. Laly, and M. Lienard. Transmission on aircraft power line between an inverter and a motor: Impulsive noise characterization. In *Power Line Communications and Its Applications (ISPLC), 2011 IEEE International Symposium on*, pages 301–304, April 2011.

[67] A. Knobloch and H. Garbe. Critical review of converting spectral data into prospective bit error rates. In *Electromagnetic Compatibility, 2002. EMC 2002. IEEE International Symposium on*, volume 1, pages 173–178 vol.1, Aug 2002.

[68] T. Kowada, Y. Hayashi, K. Yamane, and T. Shinozuka. Interference on wide-band digital communication by disturbance in 2 GHz band. In *Electromagnetic Compatibility, 1999 International Symposium on*, pages 317–320, 1999.

[69] F. Krug and P. Russer. Ultra-fast broadband emi measurement in time domain using classical spectral estimation. In *Microwave Symposium Digest, 2002 IEEE MTT-S International*, volume 3, pages 2237–2240 vol.3, June 2002.

[70] Florian Krug, T. Hermann, D. Mueller, P. Russer, J. Waldmann, and M. Aidam. Strategies for precompliance measurements using the tdemi measurement system. In *Electromagnetic Compatibility, 2003 IEEE International Symposium on*, volume 2, pages 511–516 vol.2, Aug 2003.

[71] Florian Krug and P. Russer. Ultra-fast broadband emi measurement in time-domain using fft and periodogram. In *Electromagnetic Compatibility, 2002. EMC 2002. IEEE International Symposium on*, volume 2, pages 577–582 vol.2, Aug 2002.

[72] Florian Krug and P. Russer. Signal processing methods for time domain EMI measurements. In *Electromagnetic Compatibility, 2003. EMC '03. 2003 IEEE International Symposium on*, volume 2, pages 1289–1292 Vol.2, May 2003.

[73] Florian Krug and P. Russer. The time-domain electromagnetic interference measurement system. *Electromagnetic Compatibility, IEEE Transactions on*, 45(2):330–338, May 2003.

[74] Florian Krug and P. Russer. Quasi-peak detector model for a time-domain measurement system. *Electromagnetic Compatibility, IEEE Transactions on*, 47(2):320–326, May 2005.

[75] Lago-Fernández, J., and Salter, J. WHP 080 Modelling Impulsive Interference in DVB-T: Statistical Analysis, Test Waveforms and Receiver Performance. Technical Report April, Corporation, British Broadcasting, 2004.

[76] Jaeyoon Lee, Dongweon Yoon, and In Chul Im. General Expression for the Error Probability of Arbitrary Two-Dimensional Signaling with I/Q Amplitude and Phase Unbalances. In *Advanced Communication Technology, 2006.*

ICACT 2006. The 8th International Conference, volume 3, pages 1781–1784, Feb 2006.

[77] Frank Leferink, Ferran Silva, Johan Catrysse, Sven Batterman, Véronique Beauvois, and Anne Roch. Man-made noise in our living environments. *Radio Science Bulletin; International Union of Radio Science (URSI)*, 334:49–57, Sep 2010.

[78] M. Lienard, M.O. Carrion, V. Degardin, and P. Degauque. Modeling and Analysis of In-Vehicle Power Line Communication Channels. *Vehicular Technology, IEEE Transactions on*, 57(2):670–679, March 2008.

[79] S. Linder, J. Rantakokko, and P. Stenumgaard. A new approach for estimating the impact of pulsed interference on digital communication systems. In *Electromagnetic Compatibility, 2003. EMC '03. 2003 IEEE International Symposium on*, volume 2, pages 1047–1050 Vol.2, May 2003.

[80] S.E. Linder and J.G.J. Rantakokko. A new method for estimating the impact of interference on digital communication systems in intersystem interference analysis tools. In *Military Communications Conference, 2003. MILCOM '03. 2003 IEEE*, volume 2, pages 1149–1154 Vol.2, Oct 2003.

[81] Jr. Marple, S.L. Computing the discrete-time ldquo;analytic rdquo; signal via FFT. *Signal Processing, IEEE Transactions on*, 47(9):2600–2603, Sep 1999.

[82] A. Martin. The Feature Selective Validation (FSV) method. De Montfort University, 1999.

[83] MathWorks. Simulink. www.mathworks.com/products/simulink/.

[84] Y. Matsumoto. On the Relation Between the Amplitude Probability Distribution of Noise and Bit Error Probability. *Electromagnetic Compatibility, IEEE Transactions on*, 49(4):940–941, Nov 2007.

[85] Y. Matsumoto. Multi-frequency amplitude probability distribution measurement system and its application for electromagnetic interference analysis. In *General Assembly and Scientific Symposium, 2011 XXXth URSI*, pages 1–4, Aug 2011.

[86] Y. Matsumoto and K. Gotoh. Accuracy of Gaussian approximation applied to impulsive interference in OFDM reception. In *EMC Europe 2011 York*, pages 250–253, Sept 2011.

[87] Y. Matsumoto and K. Gotoh. An expression for maximum bit error probability using the amplitude probability distribution of an interfering signal and its application to emission requirements. *Electromagnetic Compatibility, IEEE Transactions on*, 55(5):983–986, Oct 2013.

[88] Y. Matsumoto and K. Gotoh. A method of defining emission limits including the gradient of an amplitude-probability-distribution curve. In *Electromagnetic Compatibility (EMC Europe), 2014 International Symposium on*, pages 895–900, Sept 2014.

[89] Y. Matsumoto, K. Gotoh, and K. Wiklundh. Band-limitation effect on statistical properties of class-A interference. In *Electromagnetic Compatibility - EMC Europe, 2008 International Symposium on*, pages 1–5, Sept 2008.

[90] Y. Matsumoto, I. Wu, K. Gotoh, and S. Ishigami. Measurement and modeling of electromagnetic noise from LED light bulbs. *Electromagnetic Compatibility Magazine, IEEE*, 2(4):58–66, th 2013.

[91] D. Middleton. Statistical-physical models of man-made and natural radio noise, Part I: First-order probability models of the Instantaneous Amplitude. Technical report, Office of Telecommunications, 1975.

[92] D. Middleton. Statistical-physical models of man-made and natural radio noise, Part II: First-order probability models of the envelope and phase. Technical report, Office of Telecommunications, 1976.

[93] D. Middleton. Canonical and Quasi-Canonical Probability Models of Class a Interference. *Electromagnetic Compatibility, IEEE Transactions on*, EMC-25(2):76–106, May 1983.

[94] E.K. Miller. *Time-Domain Measurements in Electromagnetics*. Van Nostrand Reinhold electrical/computer science and engineering series. Springer, 1986.

[95] Taketoshi Nakai. Automotive Noise Received with a Vertical Dipole Antenna Placed above And on the Ground. *Electromagnetic Compatibility, IEEE Transactions on*, EMC-27(3):119–125, Aug 1985.

[96] Taketoshi Nakai. Measurement and Analysis of Impulsive Noise from Bullet Trains. *Electromagnetic Compatibility, IEEE Transactions on*, 28(4):193–203, Nov 1986.

[97] Taketoshi Nakai and Z. Kawasaki. On Impulsive Noise from Shinkansen. *Electromagnetic Compatibility, IEEE Transactions on*, EMC-25(4):396–404, Nov 1983.

[98] T. Okazaki, Z. Kawasaki, and A. Hirata. Wideband characteristics of impulsive EM noise emitted from discharges and development of mathematical noise model. In *Electromagnetic Compatibility, 2005. EMC 2005. 2005 International Symposium on*, volume 2, pages 469–472 Vol. 2, Aug 2005.

[99] A. V. Oppenheim and R. W. Schafer. *Discrete-time signal processing*. Prentice Hall, 1989.

[100] H.S. Oranc. Ignition Noise Measurements in the VHF/UHF Bands. *Electromagnetic Compatibility, IEEE Transactions on*, EMC-17(2):54–64, May 1975.

[101] A. Orlandi, A.P. Duffy, B. Archambeault, G. Antonini, D.E. Coleby, and S. Connor. Feature selective validation (FSV) for validation of computational electromagnetics (CEM). part II- assessment of FSV performance. *Electromagnetic Compatibility, IEEE Transactions on*, 48(3):460–467, Aug 2006.

[102] R.E. Owen, W.R. Vincent, and W.E. Blair. Measurement of Impulsive Noise on Electric Distribution Systems. *Power Apparatus and Systems, IEEE Transactions on*, PAS-99(6):2433–2438, Nov 1980.

[103] J.D. Parsons and A.U.H. Sheikh. The characterization of impulsive noise and considerations for a noise-measuring receiver. *Radio and Electronic Engineer*, 49(9):467–476, September 1979.

[104] E. Perrin, C. Guiffaut, A. Reineix, and F. Tristant. Using a Design-of-Experiment Technique to Consider the Wire Harness Load Impedances in the FDTD Model of an Aircraft Struck by Lightning. *Electromagnetic Compatibility, IEEE Transactions on*, 55(4):747–753, Aug 2013.

[105] E. Perrin, F. Tristant, C. Guiffaut, F. Terrade, and A. Reineix. A 3D model to compute lightning and HIRF coupling effects on avionic equipment of an

aircraft. In *Aerospace EMC, 2012 Proceedings ESA Workshop on*, pages 1–5, May 2012.

[106] Florian Pfeiffer, Klaus Finkenzeller, and Erwin Biebl. Theoretical Limits of ISO/IEC 14443 type A RFID Eavesdropping Attacks. In *Smart Objects, Systems and Technologies (SmartSysTech), Proceedings of 2012 European Conference on*, pages 1–9, June 2012.

[107] The Sixth Framework Programme. RAILCOM Electromagnetic compatibility between rolling stock and rail-infrastructure encouraging European interoperability.

[108] D. Prost, F. Issac, T. Volpert, W. Quenum, and J.-P. Parmantier. Lightning-Induced Current Simulation Using RL Equivalent Circuit: Application to an Aircraft Subsystem Design. *Electromagnetic Compatibility, IEEE Transactions on*, 55(2):378–384, April 2013.

[109] Ferran Silva Ricardo Jauregui, Pere J Riu. Transient FDTD simulation validation. In *Electromagnetic Compatibility (EMC), 2010 IEEE International Symposium on*, pages 257–262, July 2010.

[110] M. Rice and B. Mazzeo. On the Superiority of the Negative Binomial Test Over the Binomial Test for Estimating the Bit Error Rate. *Communications, IEEE Transactions on*, 60(10):2971–2981, October 2012.

[111] P.J. Riu, R. Jauregui, F. Silva, and M. Fernandez. Transient Electromagnetic Field Computation in Automotive Environments using FDTD. In *Electromagnetic Compatibility, 2007. EMC 2007. IEEE International Symposium on*, pages 1–4, July 2007.

[112] F. Rouissi, V. Degardin, A. Ghazel, M. Lienard, and F. Gauthier. Impulsive Noise Modelling Using Markov Chains in Indoor - Environment - Comparison With Stochastic Model. In *Electronics, Circuits and Systems, 2005. ICECS 2005. 12th IEEE International Conference on*, pages 1–4, Dec 2005.

[113] F. Rouissi, V. Degardin, M. Lienard, and P. Degauque. Low amplitude impulsive noise in vehicular power line network. In *Intelligent Transport Systems Telecommunications,(ITST),2009 9th International Conference on*, pages 538–542, Oct 2009.

[114] F. Rouissi, F. Tlili, V. Degardin, A. Ghazel, and M. Lienard. Impulsive noise cancellation based on zero insertion technique for high bit rate power-line communication system. In *Telecommunications, 2009. ICT '09. International Conference on*, pages 276–280, May 2009.

[115] J.A. Russer, A. Frech, S. Braun, and P. Russer. Spatially resolved measurement of radiated electromagnetic interference for mapping of noise sources and ambient noise cancellation. In *Electromagnetics in Advanced Applications (ICEAA), 2012 International Conference on*, pages 547–550, Sept 2012.

[116] M.G. Sanchez, L. de Haro, M.C. Ramon, A. Mansilla, C.M. Ortega, and D. Oliver. Impulsive noise measurements and characterization in a UHF digital TV channel. *Electromagnetic Compatibility, IEEE Transactions on*, 41(2):124–136, May 1999.

[117] M.L. Schiff and P.J. Ready. Separation of CDMA spread spectrum signals. In *Tactical Communications Conference, 1994. Vol. 1. Digital Technology for the Tactical Communicator., Proceedings of the 1994*, pages 491–496, May 1994.

[118] Rohde & Schwarz. IQWizard Software - IQ Signal Measurement and Conversion. http://www.rohde-schwarz.com/.

[119] Rohde & Schwarz. WinIQSIM Simulation Software. http://www.rohde-schwarz.com/.

[120] ITU Radiocommunication Sector. REPORT ITU-R SM.2022-1: The effect on digital communications systems of interference from other modulation schemes, 2005.

[121] Qingshan Shan, I.A. Glover, R.C. Atkinson, S.A. Bhatti, I.E. Portugues, P.J. Moore, R. Rutherford, M. de Fatima Queiroz Vieira, A.M.N. Lima, and B.A. de Souza. Estimation of Impulsive Noise in an Electricity Substation. *Electromagnetic Compatibility, IEEE Transactions on*, 53(3):653–663, Aug 2011.

[122] R.A. Shepherd. Measurements of automobile ignition noise at HF. In *URSI Commission VIII, Boulder, Colo., Abstracts, USNCURSI, National Academy of Sciences, Washington, D.C.*, pages 105,, Aug 1973.

[123] R.A. Shepherd. Measurements of amplitude probability distributions and power of automobile ignition noise at HF. *Vehicular Technology, IEEE Transactions on*, 23(3):72–83, Aug 1974.

[124] Men Shuixian and Wang Guodong. The definition of APD limits for base-band digital modulation systems. In *Microwave, Antenna, Propagation and EMC Technologies for Wireless Communications, 2009 3rd IEEE International Symposium on*, pages 203–206, Oct 2009.

[125] H.H. Slim, C. Hoffmann, S. Braun, and P. Russer. A novel multichannel amplitude probability distribution for a time-domain EMI measurement system according to CISPR 16-1-1. In *EMC Europe 2011 York*, pages 22–25, Sept 2011.

[126] R. A. Southwick and R. B. Schulz. A method to evaluate the degradation effects of impulsive interference. In *in Int. Electromagnetic Compatibility Symp. Rec.I, EEE 73 CHO7 51-8 EMC*, June 1973.

[127] A . D. Spaulding and R. T. Disney. Man-Made Noise: Estimates for Business, Residential and Rural Areas. Technical report, Office of Telecommunications, 1976.

[128] A.D. Spaulding. Voice Communication System Performance in the Presence of Automotive Ignition Noise. *Electromagnetic Compatibility, IEEE Transactions on*, EMC-24(3):344–348, Aug 1982.

[129] SPEAG. SEMCAD X Matterhorn SOLUTIONS. Full-wave 3D electromagnetic simulation software. http://www.speag.com/products/semcad/intro/.

[130] M. Stecher. Weighting of interference according to its effect on digital communications services. In *Electromagnetic Compatibility, 1998. 1998 IEEE International Symposium on*, volume 1, pages 69–73 vol.1, Aug 1998.

[131] P.F. Stenumgaard. Using the root-mean-square detector for weighting of disturbances according to its effect on digital communication services. *Electromagnetic Compatibility, IEEE Transactions on*, 42(4):368–375, Nov 2000.

[132] P.F. Stenumgaard. A possible concept of how present radiated emission standards could be amended in order to protect digital communication services. *Electromagnetic Compatibility, IEEE Transactions on*, 46(4):635–640, Nov 2004.

[133] P.F. Stenumgaard. On Radiated Emission Limits for Pulsed Interference to Protect Modern Digital Wireless Communication Systems. *Electromagnetic Compatibility, IEEE Transactions on*, 49(4):931–936, Nov 2007.

[134] P.F. Stenumgaard and K.C. Wiklundh. An improved method to estimate the impact on digital radio receiver performance of radiated electromagnetic disturbances. *Electromagnetic Compatibility, IEEE Transactions on*, 42(2):233–239, May 2000.

[135] A. Sugiura. Formulation of normalized site attenuation in terms of antenna impedances. *Electromagnetic Compatibility, IEEE Transactions on*, 32(4):257–263, Nov 1990.

[136] The 3rd Generation Partnership Project. 3GPP TS 23.107: 3rd Generation Partnership Project; Technical Specification Group Services and System Aspects; Quality of Service (QoS) concept and architecture (Release 12). Technical report, 2014.

[137] Martin Tomlinson and M.N.A. Abu-Rgheff. The TAR decoder-a bandpass Viterbi/FFT decoder for convolutional encoded spread-spectrum signals. *Communications, IEEE Transactions on*, 44(11):1392–1398, Nov 1996.

[138] P. Torio and M.G. Sanchez. Novel procedure to determine statistical functions of impulsive noise. *Electromagnetic Compatibility, IEEE Transactions on*, 47(3):559–568, Aug 2005.

[139] M. Uchino, Y. Hayashi, T. Shinozuka, and R. Sato. Development of low-cost high-resolution APD measuring equipment. In *Electromagnetic Compatibility Proceedings, 1997 International Symposium on*, pages 253–256, May 1997.

[140] S. Verdaguer, M. Fernández, A. Vidal, and F. Silva. EMI receiver plus digitizer RF transient measurements. In *EMC York 2004 International Conference and Exhibition*, pages 635–640, July 2004.

[141] K. Wiklundh. Relation between the amplitude probability distribution of an interfering signal and its impact on digital radio receivers. *Electromagnetic Compatibility, IEEE Transactions on*, 48(3):537–544, Aug 2006.

[142] K. Wiklundh, K. Fors, and P. Stenumgaard. A measurement method of interfering signals to determine the radio communication performance. In

Electromagnetic Compatibility (EMC EUROPE), 2013 International Symposium on, pages 40–44, Sept 2013.

[143] K.C. Wiklundh. An Approach to Using Amplitude Probability Distribution for Emission Limits to Protect Digital Radio Receivers Using Error-Correction Codes. *Electromagnetic Compatibility, IEEE Transactions on*, 52(1):223–229, Feb 2010.

[144] Ifong Wu, H. Ohta, K. Gotoh, S. Ishigami, and Y. Matsumoto. Characteristics of Radiation Noise from an LED Lamp and Its Effect on the BER Performance of an OFDM System for DTTB. *Electromagnetic Compatibility, IEEE Transactions on*, 56(1):132–142, Feb 2014.

[145] Y. Yamanaka and T. Shinozuka. Measurement and estimation of BER degradation of PHS due to electromagnetic disturbance from microwave ovens. *Electronics and Communications in Japan*, 81(12):55–63, Dec 1998.

[146] P.N. Zakharov, A.F. Korolev, and A.P. Sukhorukov. On the necessity of information transmission channel characteristics consideration in wireless systems planning. In *Microwaves, Communications, Antennas and Electronics Systems, 2009. COMCAS 2009. IEEE International Conference on*, pages 1–9, Nov 2009.

[147] Jinbao Zhang, Yinghong Wen, Kesheng Zhou, Zhenhui Tan, and Yun Zhu. Research on statistical parameters of interference for digital radio. In *Antennas and Propagation in Wireless Communications (APWC), 2012 IEEE-APS Topical Conference on*, pages 1225–1228, Sept 2012.

[148] M. Zimmermann and K. Dostert. Analysis and modeling of impulsive noise in broad-band powerline communications. *Electromagnetic Compatibility, IEEE Transactions on*, 44(1):249–258, Feb 2002.

Publications

Journals & Magazines

[149] M. Pous and F. Silva. Full-Spectrum APD Measurement of Transient Interferences in Time Domain. *Electromagnetic Compatibility, IEEE Transactions on*, 56(6):1352–1360, Dec 2014. ISSN 0018-9375. doi: 10.1109/TEMC.2014.2352393.

[150] M. Pous and F. Silva. Prediction of the impact of transient disturbances in real-time digital wireless communication systems. *Electromagnetic Compatibility Magazine, IEEE*, 3(3):76–83, 3rd 2014. ISSN 2162-2264. doi: 10.1109/MEMC.2014.6924332.

[151] M. Pous, M. Azpúrua, and F. Silva. Measurement and Evaluation Techniques to Estimate the Degradation Produced to GSM System Interfered by Radiated Transients. Manuscript submitted for publication in *Electromagnetic Compatibility, IEEE Transactions on*, 2015.

[152] O. Ventosa, M. Pous, F. Silva, and R. Jauregui. Application of the Feature Selective Validation Method to Pattern Recognition. *Electromagnetic Compatibility, IEEE Transactions on*, 56(4):808–816, Aug 2014. ISSN 0018-9375. doi: 10.1109/TEMC.2013.2291494.

[153] S. Battermann, H. Garbe, F. Silva, M. Pous, V. Beauvois, K. Vantomme, J. Catrysse, J. Newbury, V. Degardin, M. Lienard, P. Degauque, I.D. Flintoft, A.D. Papatsoris, D.W. Welsh, and A.C. Marvin. Electromagnetic compatibility analysis of unstructured mains networks for high-speed data transmission: Part 2. *Science, Measurement Technology, IET*, 2(3):154–159, May 2008. ISSN 1751-8822. doi: 10.1049/iet-smt:20070056.

[154] S. Battermann, H. Garbe, F. Silva, M. Pous, V. Beauvois, K. Vantomme, J. Catrysse, J. Newbury, V. Degardin, M. Lienard, P. Degauque, I.D. Flintoft, A.D. Papatsoris, D.W. Welsh, and A.C. Marvin. Electromagnetic compatibility analysis of unstructured mains networks for high-speed data transmission: Part 1. *Science, Measurement Technology, IET*, 2(3):146–153, May 2008. ISSN 1751-8822. doi: 10.1049/iet-smt:20070055.

[155] M. A. Azpúrua, M. Pous, S. Çakir, M. Çetintaş, and F. Silva. Improving Time-Domain EMI measurements through Digital Signal Processing. Manuscript accepted for publication in *Electromagnetic Compatibility Magazine, IEEE*, 2015.

Conference Publications

[156] M. Pous, A. Atienza, and F. Silva. EMI radiated characterization of an hybrid bus. In *Electromagnetic Compatibility (EMC EUROPE), 2011 International Symposium on*, pages 208–213, Sept 2011.

[157] M. Pous and F. Silva. Co-simulation methodology to evaluate digital communication systems interfered by transients. In *Electromagnetic Compatibility (EMC EUROPE), 2013 International Symposium on*, pages 665–670, Sept 2013.

[158] M. Pous and F. Silva. APD radiated transient measurements produced by electric sparks employing time-domain captures. In *Electromagnetic Compatibility (EMC Europe), 2014 International Symposium on*, pages 813–817, Sept 2014. doi: 10.1109/EMCEurope.2014.6931016.

[159] M. Pous, M. Fernandez, and F. Silva. RFID system evaluation against radiated transient noise. In *EMC Europe 2010 9th International Symposium on EMC joint with 20th International Wroclaw Symposium on EMC*, pages 625–628, Sept 2010.

[160] Azpúrua M. Pous, M. and F. Silva. Radiated Transient Interferences Measurement Procedure To Evaluate Digital Communication Systems. Manuscript submitted for publication in *Joint IEEE International Symposium on Electromagnetic Compatibility and EMC Europe 2015*, 2015.

[161] G. Costa, M. Pous, A. Atienza, and F. Silva. Time-Domain Electromagnetic Interference Measurement System for intermittent disturbances. In *Electromagnetic Compatibility (EMC Europe), 2014 International Symposium on*, pages 833–837, Sept 2014. doi: 10.1109/EMCEurope.2014.6931019.

[162] R. Jauregui, M. Pous, Y. Vives, M. Fernandez, P.J. Riu, and F. Silva. Car windshield behavior transient analysis by FDTD. In *Electromagnetic Compatibility - EMC Europe, 2009 International Symposium on*, pages 1–4, June 2009. doi: 10.1109/EMCEUROPE.2009.5189718.

[163] R. Jauregui, M. Pous, M. Fernandez, P.J. Riu, and F. Silva. Validation of low-level, high-frequency transient fdtd simulation with radiated field measurements. In *Electromagnetic Compatibility - EMC Europe, 2008 International Symposium on*, pages 1–4, Sept 2008. doi: 10.1109/EMCEUROPE.2008.4786823.

[164] R. Jauregui, M. Pous, and F. Silva. Use of reference limits in the Feature Selective Validation (FSV) method. In *Electromagnetic Compatibility (EMC Europe), 2014 International Symposium on*, pages 1031–1036, Sept 2014. doi: 10.1109/EMCEurope.2014.6931054.

[165] D. Alonso, J. Rull, F. Silva, M. Pous, J. Coves, and R. Oriol. Measuring, modelling and correction actions for EMC assessment between high speed railway and medical equipment. In *Electrical Systems for Aircraft, Railway and Ship Propulsion (ESARS), 2010*, pages 1–5, Oct 2010. doi: 10.1109/ESARS.2010.5665252.

[166] R. Jauregui, M. Pous, M. Fernandez, and F. Silva. Transient perturbation analysis in digital radio. In *Electromagnetic Compatibility (EMC), 2010 IEEE International Symposium on*, pages 263–268, July 2010. doi: 10.1109/ISEMC.2010.5711282.

[167] I. Gil, R. Fernandez, M. Pous, and F. Silva. EMC filter based on complementary split-ring resonators for audio applications. In *EMC Compo 2009. Toulouse: 2009*, pages 1–4, November 2009.

[168] Azpúrua M., M. Pous, and F. Silva. A Measurement System for Radiated Transient Electromagnetic Interference Based on General Purpose Instruments. Manuscript submitted for publication in *Joint IEEE International Symposium on Electromagnetic Compatibility and EMC Europe 2015*, 2015.